Springer Series in Geomechanics and Geoengineering

Masanori Hamada

Engineering for Earthquake Disaster Mitigation

Springer

Springer Series in Geomechanics and Geoengineering

For further volumes:
http://www.springer.com/series/8069

About this Series

Geomechanics deals with the application of the principle of mechanics to geomaterials including experimental, analytical and numerical investigations into the mechanical, physical, hydraulic and thermal properties of geomaterials as multiphase media. Geoengineering covers a wide range of engineering disciplines related to geomaterials from traditional to emerging areas.

The objective of the book series is to publish monographs, handbooks, workshop proceedings and textbooks. The book series is intended to cover both the state-of-the-art and the recent developments in geomechanics and geoengineering. Besides researchers, the series provides valuable references for engineering practitioners and graduate students.

Masanori Hamada

Engineering for Earthquake Disaster Mitigation

Springer

Masanori Hamada
Waseda University
Tokyo, Japan

Original Japanese edition published by Maruzen Publishing Co., Ltd.
Giban Taishinkougaku (Geotechnical Earthquake Engineering)

ISSN 1866-8755 ISSN 1866-8763 (electronic)
ISBN 978-4-431-54891-1 ISBN 978-4-431-54892-8 (eBook)
DOI 10.1007/978-4-431-54892-8
Springer Tokyo Heidelberg New York Dordrecht London

Library of Congress Control Number: 2014933947

Printed on acid-free paper

Springer is part of Springer Science+Business Media (www.springer.com)

Preface

Over the last quarter of a century, Japan has experienced two major earthquake disasters: the 1995 Kobe earthquake and the 2011 Tohoku earthquake. Huge loss of human lives and vast damage to structures resulted from serious failure by scientists and engineers, including the author, endeavoring to mitigate natural disasters. The mistakes we made must not be repeated. Thoroughly and systemically, we must draw broad lessons from the two calamities and take steps to deal effectively with future earthquakes and tsunamis.

It is said that the large rupture between tectonic plates, which caused the 2011 earthquake, might have changed the stress condition of the Japanese archipelago. This, it is further assumed, may accelerate the triggering of earthquakes in the regions along the Nankai Trough, i.e., Tokai, Tonankai, and Nankai earthquakes, and the northern Tokyo Bay earthquake. Our urgent task is to reveal the vulnerability of the country and local communities to future natural hazards and to prepare accordingly.

For the reduction of the loss of human lives and property and for the creation of a safe society, we have to firstly regain the reliance of the people on science and technology related to natural disaster mitigation. Also essential are the endeavors of experts in the natural sciences and the humanities, all of whom must actively strive to advance interactive communication.

About 1 month after the 2011 Tohoku earthquake, as the chair of the Civil Engineering and Architectural Committee organized by the Science Council of Japan, I requested the presidents of 22 academic societies to organize a liaison committee for a multidisciplinary and comprehensive survey of lessons from the earthquake and tsunami disaster. What is needed from us is close cooperation and coordination of the academic societies to analyze the cause of the disaster, to contribute to restoration and reconstruction of the affected area, and to scientifically and technologically mitigate the destructive effects of future natural disasters.

During the last half-century, natural disasters, such as earthquakes, tsunamis, storms, and floods, have been increasing. Unfortunately, we the Japanese people painfully experienced the 2011 earthquake and tsunami disaster, but we learned many lessons from this disaster. We must share with the world the practical lessons

we have learned. In that endeavor, the national government, local governments, research organizations, universities, and NPOs must all, each at its own level, strive to move forward.

With the participation of many architects, civil engineers, and researchers in engineering fields, I organized a non-profit organization named "Engineers without Borders, Japan (EWBJ)" in 2000. It has provided technological assistance for developing measures to deal with natural disasters in Asian countries such as Indonesia, Pakistan, and Bangladesh with aid for the restoration and revitalization of communities and disaster-related education for children. The EWBJ continues to expand its endeavors for the creation of a safe and secure world.

After my university graduation in 1966, I worked for Taisei Corporation, then at Tokai University, and subsequently at Waseda University. I have continued in each organization to conduct research on practical work in the field of earthquake disaster-prevention engineering. With the aim of further contributing to the development of the earthquake engineering and its related fields, this book summarizes and generalizes what I have learned over the years.

In Chap. 1, I focused on the increase of natural disasters due to vulnerability of societies and global climate change in Japan as well as around the whole world, and analyzed the reasons of this increase. I have continuously conducted field surveys whenever an earthquake disaster occurred and have given advice and technical assistance for the reconstruction of the affected areas in the world. Sections 1.2 and 1.3 summarize the results of those field surveys.

The Great Kanto Earthquake in 1923 provided the impetus for development of earthquake-resistance design in Japan. The technology has developed, with lessons being drawn from each subsequent earthquake and infrastructures being reinforced. The principles and strategies of enhancement of earthquake resistance of societies, along with reinforcement technology of existing structures, are outlined in Chap. 2. At the same time, in order to make the content of the book more accessible to young readers, the essentials of the dynamic analysis method are explained.

Chapters 3 and 4 describe, respectively, the mechanisms of liquefaction and liquefaction-induced large ground displacement, along with their induced damage to various kinds of structures and lifeline facilities. Countermeasures to prevent damage of structures are also introduced. Chapter 4 focuses in particular on 11 examples of liquefaction-induced ground displacements and the damage during past earthquakes, both in Japan and abroad. The data are mostly drawn from the outcomes of U.S.–Japan joint research on liquefaction and its effects on lifeline systems.

Chapter 5 discusses the dynamic behaviors of underground structures by earthquake observations and numerical analyses of an underground tank, undersea tunnels, and a rock tunnel. Most of this research was done during my work at Taisei Corporation. The earthquake observations revealed that the deformation of underground structures was governed by the strain of the surrounding ground. Based on this finding, the response displacement method was proposed for the earthquake-resistant design for underground structures.

It has been predicted that an earthquake directly below the Tokyo area and large earthquakes along the Nankai Trough in the Pacific Ocean would cause serious damage to the central part of Japan. In Chap. 6, several issues which are increasing the danger of these earthquakes and the measures to reduce the damage are discussed.

It was Dr. S. Okamoto, Dr. K. Kubo, and Dr. C. Tamura, professor emeriti of the University of Tokyo, who first cleared the path that led me to become a scholar in the field of earthquake disaster prevention engineering. Prof. Okamoto guided me in how to conduct empirical research based on experimentation and observation. Prof. Kubo provided countless opportunities for me to conduct research into liquefied soil flow and lifeline earthquake engineering. Prof. Tamura always supported me in my research at University of Tokyo, even after graduation. Here I wish to express my deep thanks to these illustrious scholars.

Finally, in regard to the publication of this book, I extend my gratitude to colleagues at Taisei Corporation, Tokai University, and Waseda University with whom I have continued to work; to the associates who took part in surveys and research; and to the staff members of my laboratory who contributed to the compilation of this book. In particular, I am also indebted and grateful to research associate Dr. D. Guo and my graduate students I. Kato, N. Tonsho, and R. Nakamachi, as well as our laboratory secretaries R. Matsunaga and T. Nagata, for providing outstanding support in arranging the text and the various charts. Last but not least, I express my highest appreciation to my wife Noriko and my family for their deep understanding and support for my research work.

Tokyo, Japan Masanori Hamada
December 2013

Introduction

The Tohoku earthquake (Great East Japan Earthquake and Tsunami Disaster), with a magnitude of 9.0, struck the northeast region of Japan on March 11, 2011, even as this book was being written. It was the largest earthquake in Japanese seismic history. As a result of the destructive effects, including tsunami, ground motion, soil liquefaction, and slope failure, the toll of dead and missing was 18,641 as of October 31, 2012. Thus, it was the severest disaster over the last half-century in Japan.

Why was the scale of the calamity so severe, here in a developed nation said to be a leader in the development of measures to counteract seismic effects, a country whose researchers in the field, including the author, take considerable pride in their work? Without doubt, the ultimate answer lies in the failure to predict both the earthquake itself and the resulting tsunami. The Central Disaster Management Council (CDMC) of the Cabinet Office of the Japanese Government had predicted that in the Tohoku region a Miyagi Prefecture offshore earthquake had a 99 % probability of occurrence within the next 30 years. Nevertheless, the estimated magnitude was 7.5, whereas the energy generated by the actual quake was 180 times greater than the prediction.

Moreover, in addition to the CDMC report, the Headquarters for Earthquake Research Promotion of the Ministry of Education, Culture, Sports, Science and Technology issued the same figure for the Miyagi Prefecture offshore earthquake as well as predicting one more earthquake along the Japan Sea Trough with a magnitude of 7.7. It was said that even if two such earthquakes were to occur simultaneously, the magnitude would be 8.0. But the energy actually released was 32 times greater than predicted. In the prediction of the earthquakes in Japan along the Pacific Ocean, the possibility of earthquakes in the region along the Nankai Sea Trough, the Tokai, Tonankai and Nankai earthquakes drew much attention. Many seismologists focused on making predictions there, and considerable government funding for research was provided. It was assumed that these three earthquakes would occur simultaneously with a magnitude of 8.5.

However, the reality confounded us all, as the earthquake struck in an entirely different area. It is said that the 2011 tsunami was comparable to that caused by the

Jogan earthquake in 869 that struck similar areas in the Tohoku region. Prior to the 2011 Tohoku earthquake, the same sort of destructive earthquake and tsunami had been predicted by some seismologists for an area ranging from the entire Tohoku region to Ibaraki Prefecture. But this warning was not heeded in the strategies for earthquake disaster prevention. How to account for this failure? The overall lessons to be drawn are indispensable in our efforts to reduce the disaster of future earthquakes and tsunamis. Therefore, based on these lessons, national organizations and systems for earthquake and tsunami prediction must be fundamentally restructured.

In 2004 an earthquake with a magnitude of 9.1 occurred offshore of Sumatra Island in Indonesia. It induced a huge tsunami that affected the countries around the Indian Ocean, causing a catastrophe that attacked the lives of over 200,000 people. A month later, I visited Banda Aceh in the north end of Sumatra. There, the tsunami took the lives of more than 70,000 people, approximately one-fourth of the total population of the city.

As I surveyed the horrific aftermath of the disaster, I thought that even if such a tsunami were to strike Japan, the damage would not be on the same scale. I also assumed that an earthquake of such magnitude over 9 would not occur in Japan. However, I should have reminded myself that the offshore plate tectonics of Sumatra were very similar to those of the Pacific Coast of Japan. Furthermore, I should have paid attention to the fact that the plate structures in Japan were more complex and vulnerable than those in Sumatra, because four tectonic plates are colliding with one another in our country. We have come to the painful realization that we were naïve to assume that we were exempt from the threat of any earthquakes with a magnitude of 9 or more.

We made a similar mistake at the time of the 1995 Kobe earthquake (the Hanshin-Awage Great Earthquake Disaster). The earthquake with a moment magnitude of 7.2 was caused by faults near large cities such as Kobe and Nishinomiya and killed more than 6,400 people. One year before the Kobe earthquake, in 1994, the Northridge earthquake occurred in southern California and collapsed a large number of houses, other buildings, and freeway bridges. The Japan Society of Civil Engineers (JSCE) dispatched its members to the site of the damage. At the time, many researchers and engineers declared in press interviews that a similar disaster could not occur in Japan, since the highway bridges and buildings in Japan had enough earthquake resistance. One year later, the Kobe earthquake destroyed numerous bridges and buildings by strong ground motion induced by the nearby inland active faults. It became apparent that the earthquake resistance of various kinds of infrastructures was inadequate against strong ground motion by the earthquake. The Kobe earthquake made us realize that the assumed superiority of the earthquake resistance of structures in Japan was based on too much confidence without scientific bases.

In the Great East Japan Earthquake and Tsunami Disaster, big fires broke out in the petrochemical complexes in the ports of Sendai and Chiba. In the former case, a tank truck floated by the tsunami collided with the pipeline of the plant; in the latter case, 17 spherical tanks for storage of liquefied propane gas were collapsed by the

inertial forces exceeding those for the design. In Kesennuma in Miyagi Prefecture, a large number of marine fuel tanks was flowed outby the tsunami, and ignited fires. During previous earthquakes in Japan, oil refinery and petrochemical plants had been repeatedly damaged. In the 1964 Niigata earthquake, tanks of heavy oil were subjected to sloshing vibration as the result of long-period components of earthquake ground motion, resulting in a fire that continued for more than two weeks. Furthermore, in the 2003 Tokachi offshore earthquake, tanks of crude oil and naphtha in Tomakomai caught on fire and collapsed. Tank fires induced by long-period components of earthquake ground motion were also reported in the 1999 Kocaeli earthquake in Turkey and the Chi-Chi earthquake in Taiwan.

During the Great East Japan Earthquake and Tsunami Disaster, extensive soil liquefaction occurred in the artificial islands that had been reclaimed from Tokyo Bay and in the flood plain along large rivers, such as the Tone River and the Arakawa River. This resulted in substantial damage to houses and other buildings and to buried lifeline pipes. In the reclaimed lands around Tokyo Bay, it is reported that there are over 5,000 tanks for oil, high-pressure gas, and hazardous materials. Soil liquefaction and the resulting large ground displacements, long-period components of earthquake ground motion, and tsunami threaten the safety of industrial complexes and neighboring areas. There is every reason to fear that fires breaking out simultaneously along the waterfronts of Japanese major cities would engulf nearby residents and cause a natural disaster that Japan has never experienced before. Unfortunately, the industrial complexes are not adequately prepared to deal with disasters caused by earthquakes and tsunamis.

The Great East Japan Earthquake and Tsunami Disaster revealed the following lessons. One is the insufficiency of the strength of infrastructures against earthquakes and tsunamis, such as the collapse of tsunami-barrier walls; another is the inadequate preparedness for emergency response after the disaster, such as slow collection of the information on the disaster conditions and delay in the transport of rescue and aid matériel. The earthquake also raised another problem, namely, the huge number of refugees. As we confront the high probability of another major earthquake, we must expose the vulnerabilities of infrastructures and social systems and disclose those to the entire community in order to overcome them.

The accident at the Fukushima Daiichi nuclear power plant, triggered by the earthquake, is the most serious. The ultimate cause of the serious accident in Fukushima was the loss of the cooling function when the external and emergency power supplies were cut off by the impact of the tsunami. It is thought that the disastrous effects might have been reduced if adequate multiplex measures, in addition to the enforcement of strength of structures and facilities against earthquake and tsunami, had been in place. On December 16, 2011, the Japanese Government announced that efforts to achieve cold shutdown status had succeeded, but the plant remains in a highly difficult situation. While working in the construction industry, I was also engaged in the design of earthquake-resistant design of nuclear power plants. As a member of the Nuclear Reactor Security Inspection Committee of the Japanese Government, I also participated in the inspection committee on safety design against earthquakes. Nuclear power generation is

indeed said to be the fruition of the integration of diverse fields in science and engineering. It also has been stated that nuclear energy generation is possible as the culmination of success in scientific fields such as seismology and geology and in engineering fields such as nuclear engineering, civil engineering, architecture, and mechanical engineering. However, there was a major pitfall. Rather than being a case of integration of science and engineering, it may have been a hodgepodge of science and engineering. It often appeared to be that the evaluation of a nuclear plant's overall safety constituted nothing more than numbers added up from a motley assortment of different fields.

Since graduating from university in 1966, I have been engaged academically as well as practically in the engineering aspects of earthquake disaster prevention for over 47 years. During my employment in the construction business, I conducted research on the dynamic response of submerged tunnels, rock caverns, and underground tanks during earthquakes, and had experience in actual designs for improving the seismic resistance of infrastructures. I was also involved in an enhancement approach now known as the "response displacement method".

The Central Japan Sea earthquake of May 1983 occurred just as I had moved from the construction company to the Oceanography Faculty of Tokai University. My work in investigating the damage to gas pipes in the city of Noshiro in Akita Prefecture motivated me to conduct research on soil liquefaction-induced large ground displacements. At about the same time, research into ground displacements caused by liquefaction was being conducted in the United States by Prof. Thomas D. O'Rourke and his colleagues at Cornell University. Our simultaneous endeavors helped to bring about relevant U.S.–Japan collaborative research and international symposiums. The goal of our collaborative research was to clarify the causative mechanism of liquefied soil flow, to develop methods for predicting ground displacements, and to develop practical countermeasures against large ground displacements. Unfortunately, the 1995 Kobe earthquake occurred before the research efforts had come to fruition. In the artificial islands reclaimed from the sea in Kobe and its neighboring areas, houses and other buildings, bridges, quay walls, and lifeline facilities were seriously damaged. After the 1995 Kobe earthquake, the method of earthquake-resistant design of civil engineering structures was extensively revised. An ad-hoc committee on the improvement of earthquake resistance of structures was organized by the Japan Society of Civil Engineers (JSCE) and proposed a basic concept for earthquake-resistant design, in which structures should survive any strong ground motions without total collapse so as to save human lives. In order to realize this concept, the performance-based design was introduced against two levels of intensities of earthquake ground motion. The first level of earthquake ground motion has a moderate intensity with a probability of one or two occurrences during the lifetime of the structures, which has been used for design after the 1923 Kanto earthquake. The second level of earthquake ground motion has a low probability of occurrence but with high intensities, as observed in Kobe and its surrounding areas. JSCE recommended that all civil engineering structures should not totally collapse. As a member of the committee, I was involved in the JSCE committee to propose recommendations on

the earthquake resistance of infrastructures, and contributed to revision of the Basic Plan for Disaster Prevention by the CDMC (1995). Following the JSCE's proposals and the council's basic plan, revisions were made in the earthquake-resistant design codes for railway structures and various kinds of lifelines.

Earthquake disasters have been increasing worldwide, as can be seen in the 2011 earthquake in Japan and the 2010 earthquakes in Chile and Haiti. Besides earthquakes, there were flood and storm disasters, thought to be the result of global climate change. The increase in vulnerability of our society against natural hazards results from the sluggish preparedness of disaster-prevention infrastructures and the lack of risk and crisis management. The Japanese people have experienced many bitter hardships from the Tohoku earthquake, but these hard experiences can contribute to reducing natural disasters in the world. The lessons from the disaster must be utilized for the creation of a safer society against natural hazards in the future.

For the effective reduction of natural disasters, tripartite elements—governmental measures, people's cooperation among local communities, and self-support by individuals—are indispensable. All of the concerned experts and researchers in the field of natural disaster prevention must actively join in this tripartite activity. They can recommend national and local strategies for natural disaster prevention in regard to governmental activities. Their assistance and support to the preparation of the local disaster prevention plan, emergency response, recovery, and reconstruction are required in local communities. Contributions to the people for assessment and reinforcement of houses and land are also one of important roles of the experts and researchers in regard to self-support.

The task of mitigating the effects of natural disasters is not restricted to the fields of science such as seismology and geology, and engineering including civil engineering, building engineering, mechanical engineering, and nuclear engineering. To effectively confront the challenge, those working in the fields of sociology, economics, humanities, information science, and medical science must also be involved. We the researchers engaged in the field of natural disaster prevention should not allow ourselves to be confined within our own specialties. The creation of a much safer and more secure society against natural disasters by multilateral cooperation, nationally and internationally, can contribute to consoling the victims of the 2011 Great East Japan Earthquake and Tsunami Disaster.

Contents

Chapter 1
Recent Earthquake and Tsunami Disasters Worldwide

Abstract In recent years, the number of earthquake and tsunami disasters has been increasing globally. In addition to the earthquake and tsunami disasters, storm, flood, heavy rain and land sliding have been also increasing. Over the last quarter century, disasters with more than one thousand dead and missing occurred 60 times, and more than 1.2 million lives were lost in the world.

In this chapter, the damages by seven recent disastrous earthquakes and tsunami in the world, including the 2004 Sumatra offshore earthquake and the 2008 Wenchuan earthquake in China, as well as by nine Japanese earthquakes and tsunamis, including the 1995 Kobe earthquake and the 2011 Tohoku earthquake are introduced, and the lessons learned from these earthquake and tsunami disasters are discussed.

Keywords Disastrous earthquakes • Lessons from disasters • Natural disasters • Tsunamis

1.1 Increase in the Number of Earthquake and Tsunami Disasters Worldwide

In recent years, the number of earthquake and tsunami disasters has been increasing globally. Figure 1.1 shows 20 earthquake and tsunami disasters worldwide from 1995 to 2011 with more than 1,000 dead and missing; these disasters killed nearly 780,000 in total [1]. Over the last decade, huge earthquakes and tsunamis with more than 70,000 dead and missing have been frequent. These include the 2004 Indian Ocean earthquake and tsunami (over 304,000 dead and missing), the 2005 Northern Pakistan earthquake (over 75,000), the 2008 Wenchuan earthquake (over 69,000), and the 2010 Haiti earthquake (over 222,000). In addition, the 2011 Tohoku earthquake (Great East Japan earthquake and tsunami disaster) caused massive casualties, with 18,550 dead and missing (as of July 11, 2012). Disastrous earthquakes and tsunamis have mainly occurred in Asian countries.

M. Hamada, *Engineering for Earthquake Disaster Mitigation*,
Springer Series in Geomechanics and Geoengineering,
DOI 10.1007/978-4-431-54892-8_1, © Springer Japan 2014

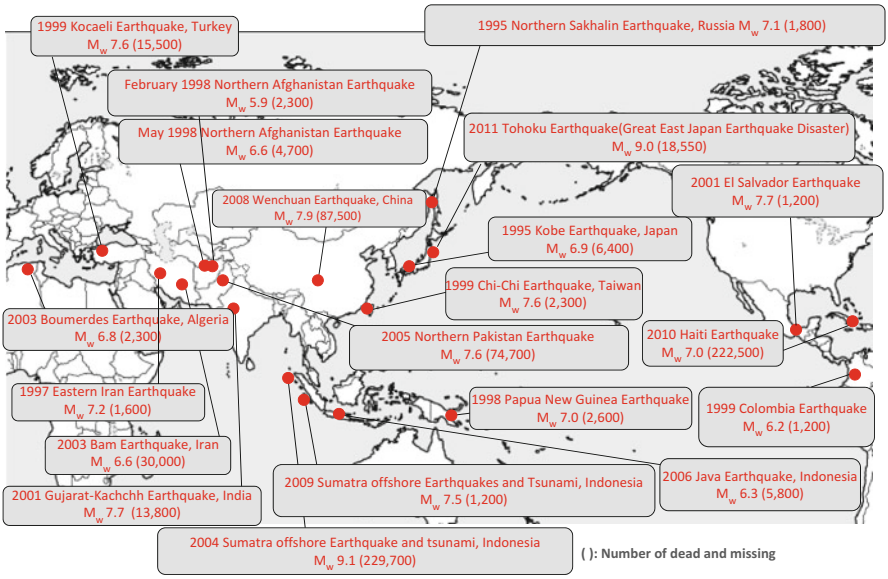

Fig. 1.1 Earthquake and tsunami disasters worldwide (1995–2011) (disasters with more than 1,000 dead and missing, *Mw* moment magnitude) [2]

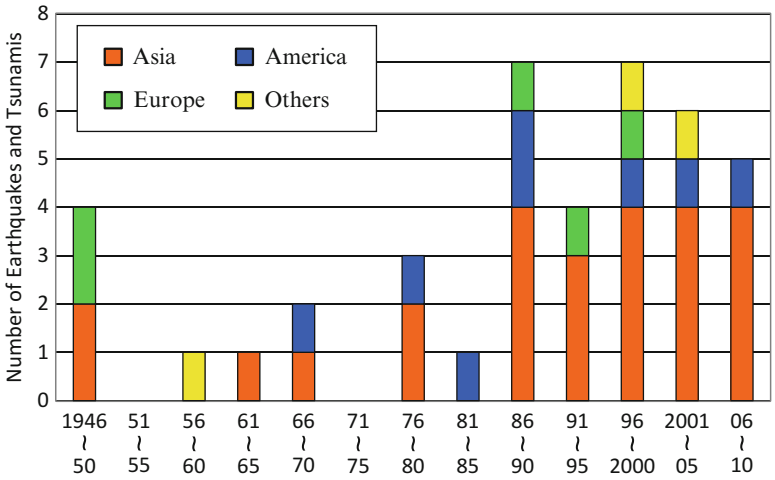

Fig. 1.2 Numbers and areas of earthquakes and tsunami disasters (1946–2010) (disasters with over 1,000 dead and missing for every 5 years) (white note of disaster prevention, Cabinet office, Government of Japan [1])

Statistics in Fig. 1.2 show the numbers and areas of earthquake and tsunami disasters with over 1,000 dead and missing, every 5 years from 1946 to 2010 [2, 3]. This indicates that the number of disasters rapidly increased in the last quarter century (from 1986 to present), and they concentrated in Asia. What caused this increase?

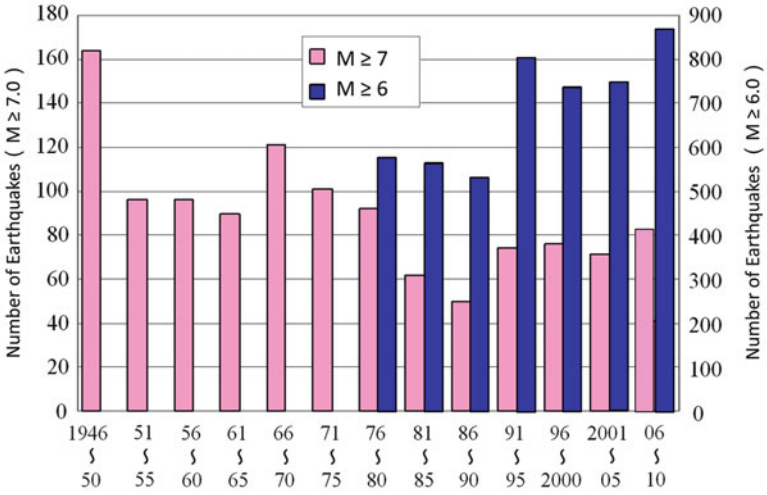

Fig. 1.3 Total number of earthquakes with moment magnitude (Mw) greater than 6 (1946–2010) (Japan Meteorological Agency and U.S. Geological Survey [2, 3])

Figure 1.3 shows the total number of earthquakes worldwide with moment magnitude (Mw) greater than 6.0. The number of earthquakes of magnitude 6.0 or greater has been increasing over the last 20 years, but the number of those of magnitude greater than 7.0, which can cause a larger number of fatalities, has been declining over 65 years. This trend does not coincide with the rapid increase of earthquake and tsunami disasters in Fig. 1.2.

What is the reason for the discrepancy between Figs. 1.2 and 1.3? Earthquakes and the tsunamis they induce are natural hazards or phenomena. The rapid increase in disasters shown in Fig. 1.2 is not proportional with the number of earthquakes. This means that human societies and social systems have become vulnerable to natural hazard. The reasons for this vulnerability are an increase of settlement in disaster-prone areas, excessive concentration of population in urban areas, a lack of disaster-preventive infrastructures and software measures, and inadequate preparations for emergency response. In addition, there is a deficiency of disaster-mitigation strategies against unprecedented natural phenomenon, as indicated by the 2011 Tohoku earthquake disaster.

Figure 1.4 shows regional ratios of natural disasters (e.g., earthquake, tsunami, storm, heavy rain, flood and landsliding), and dead and missing since 1986. According to Fig. 1.4a, disasters with more than 1,000 dead and missing over the last quarter century occurred 60 times, among which 42 were in Asian countries. Figure 1.4b shows more than 1.2 million dead or missing from these disasters, with about three quarters of this total in Asia. This indicates that reduction of natural disaster impacts in Asia is of great importance for creating a safer world.

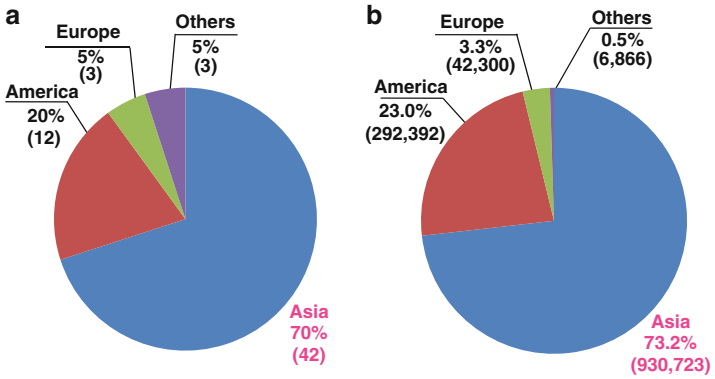

Fig. 1.4 Regional ratios of natural disasters, and dead and missing (1986–2011) (disasters with more than 1,000 dead and missing). (**a**) Regional ratio of natural disasters (total: 60). (**b**) Regional ratio of number of dead and missing (total: 1,272,281)

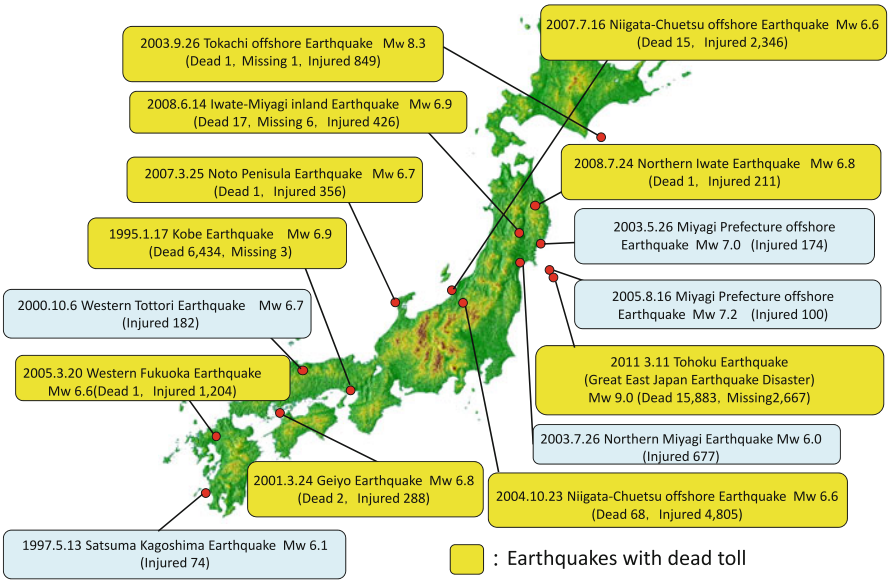

Fig. 1.5 Earthquakes and tsunamis in Japan (1995–2011, Cabinet office, Japanese Government [4]) (number of dead, missing and injured, *Mw* moment magnitude)

Figure 1.5 shows earthquakes and tsunamis in Japan since 1995 [4]. The 1995 Kobe (Great Hanshin-Awaji earthquake disaster) and 2011 Tohoku earthquakes; these two earthquakes caused the most catastrophic damage among earthquakes in Japan since the Great Kanto earthquake in 1923.

The Kobe earthquake destroyed various infrastructures, such as road and railway bridges, port and harbor structures, lifeline systems, and a huge number of buildings and houses by strong ground motions near an inland active fault. These motions largely exceeded the design motion. There were 6,434 fatalities, including those by illness in the aftermath. The earthquake raised various issues in need of resolution regarding future large earthquakes, such as tardy information gathering, delay in rescue operations, expansion of damage by the resultant fire, inadequacy of victim care after the disaster, and difficulties in achieving consensus from the people regarding reconstruction of the damaged areas.

Based on lessons learned from the Kobe earthquake, earthquake disaster prevention measures were thoroughly reviewed, including both hardware and software. Codes for earthquake-resistant design and guidelines for retrofitting of infrastructures, lifeline facilities, and public buildings were revised. However, the 2011 Tohoku earthquake again revealed the vulnerability of infrastructures to tsunamis, delays in information gathering, and shortcomings in social systems and emergency response.

The 2011 Tohoku earthquake, the largest earthquake ever in Japan, left numerous victims. From the northern Tohoku to northern Kanto regions, the tsunami height (seawater rise at the shoreline) reached a maximum of 14 m. The water invaded the coastline and a huge number of buildings and houses were washed away. 130,445 buildings were completely collapsed and 264,138 were partially destroyed, by the tsunami, earthquake ground motion, soil liquefaction and landslides (National Police Agency, August 1st, 2012).

The accident at the Fukushima No. 1 nuclear power plant was extremely serious. The plant lost all power sources for the nuclear reactor cooling system, resulting in catastrophic hydrogen explosions. A vast area from Tohoku to Kanto on the Japanese main island was largely contaminated by radioactive material. This critical situation is ongoing. Unfortunately, at the time of this writing, the Japanese government has not sought methods to deal with contaminated soil and water, or even with final debris disposal. The earthquake and tsunami also severely damaged lifeline systems, such as wastewater treatment plants, roads and railways along the coastline.

There have been many earthquakes over the past 16 years (1995–2011) in Japan, including the Kobe and Tohoku events, and these have raised new subject to be resolved. In 2003, the Tokachi offshore earthquake caused fires in tanks for storage of crude oil and naphtha in Tomakomai by sloshing vibration of the contents. This again emphasized the problem of so-called long-period component of ground motion. The 2004 Niigata-Chuetsu earthquake with its epicenter in hilly and mountainous areas triggered large landslides that dammed rivers and buried villages.

The 2007 Noto Peninsula earthquake and the 2007 Niigata-Chuetsu offshore earthquake raised a subject concerning ground motion for earthquake-resistant design of nuclear power plants. These two earthquakes were caused by faults near the power plants, whose existence had not been recognized during design and construction. Most notably, the 2007 Niigata-Chuetsu offshore earthquake

caused leakage of contaminated water from the Kashiwazaki-Kariwa nuclear power plant. Cooling water leaked from the spent nuclear fuel pool. Furthermore, there were more than 200 small and medium accidents at this plant, including a fire in an electric transformer. However, these did not lead to diffusion of large amounts of radioactive material as the 2011 Tohoku earthquake. Based on lessons from the Niigata-Chuetsu offshore earthquake, earthquake ground motion in the design of nuclear power plants was revised. Seismic safety of all such plants was verified, and numerous plant facilities and structures were reinforced against potential earthquakes in the future.

1.2 Recent Earthquakes and Tsunamis Worldwide and Their Lessons

1.2.1 1999 Kocaeli Earthquake, Turkey [5]

On August 17, 1999, the Kocaeli earthquake of Mw = 7.4 struck northwest Turkey. The epicenter was estimated at 40.77°N and 29.97°E, with hypocentral depth of 17 km (Ministry of Public Works, Turkey). There were nearly 16,000 dead, thousands missing, and at least 23,000 injured. About 20,000 houses were destroyed or partially damaged, and total economic loss exceeded 6.0 billion U.S. dollars.

Figure 1.6a shows counterclockwise rotation and horizontal movement of the Anatolian Plate, resulting from northward movement of the Arabian Plate and northeasterly motion of the African Plate (Rellinger et al. [6]). These plate movements generate the North Anatolian Fault Zone (NAFZ) with about 100 km length in the east–west direction. The Kocaeli earthquake was caused by the western part of the NAFZ from Düzce to Izmit (Fig. 1.6b), which consists of many right strike-slip fault segments. Figure 1.7 shows an example of a surface fault with about 3.6 right-strike-slip offset at Arifiye.

A bridge over a highway at Arifiye, constructed with pre-stressed concrete girders, collapsed due to fault offset. Figure 1.8 shows that the earthquake fault crossed the bridge axis at a 70-degree angle as the span expanded. The lateral offset of the fault was about 4 m. Water and gas pipes crossing earthquake faults were buckled and ruptured, as shown in Fig. 1.9.

Figure 1.10 depicts maximum horizontal accelerations observed at the ground surface from Istanbul to the source area. Maximum acceleration was 399 cm/s^2 at Adapazari, 245 cm/s^2 at Ambarli (130 km west of the epicenter), and 88 cm/s^2 at Istanbul Airport.

The Tüpraş petroleum refinery on the southern coast of the Gulf of Izmit in Kocaeli produces 270,000 m^3 oil, which is about one third of Turkey's annual oil production. Four tanks of 20–25 m diameter and two of 10 m diameter were destroyed by earthquake-induced fire (Fig. 1.11). All these tanks had floating

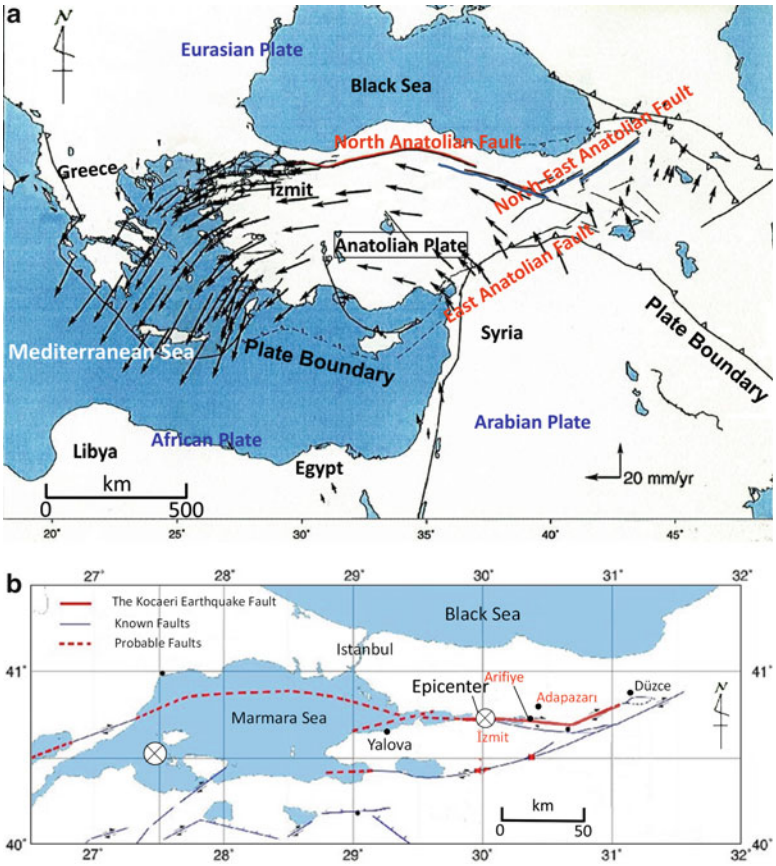

Fig. 1.6 Plate tectonics and active faults in Turkey and its surrounding area. (**a**) Plate tectonics and active faults in Turkey and its surrounding area (source: Rellinger 2006) [6]. (**b**) Active fault that caused the Kocaeli earthquake, Turkey

Fig. 1.7 Right-strike-slip fault offset (1999 Kocaeli Earthquake, Turkey, Arifiye)

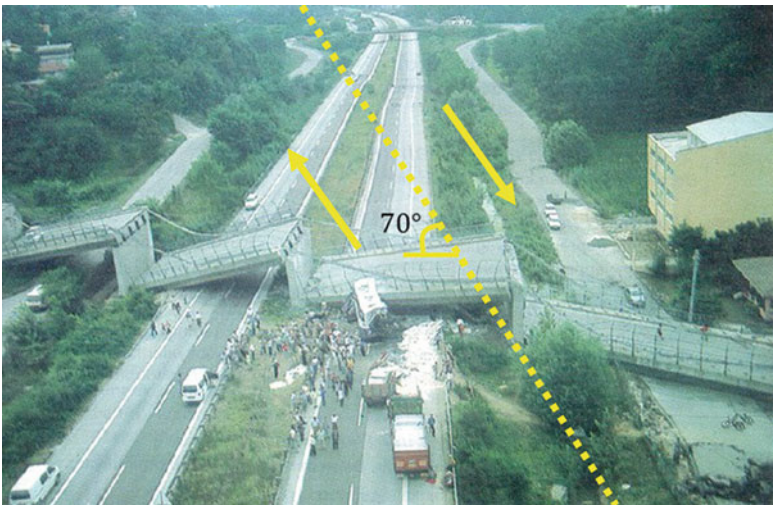

Fig. 1.8 Fall of bridge girders due to fault offset (1999 Kocaeli earthquake, Turkey, at Arifiye)

Fig. 1.9 Buckling of buried pipe due to earthquake fault offset (1999 Kocaeli earthquake, Turkey, at Arifiye)

roofs, and the fire was caused by sloshing vibration of the oil, due to the long-period component of earthquake ground motion. The natural period of sloshing vibration of a 20–25 m diameter tank is about 4–6 s. These periods were consistent with the dominant periods of the ground motion observed at Izmit. Buckling occurred on the sidewalls of fixed-roof tanks; there was no serious damage. It was reported that spherical tanks were undamaged.

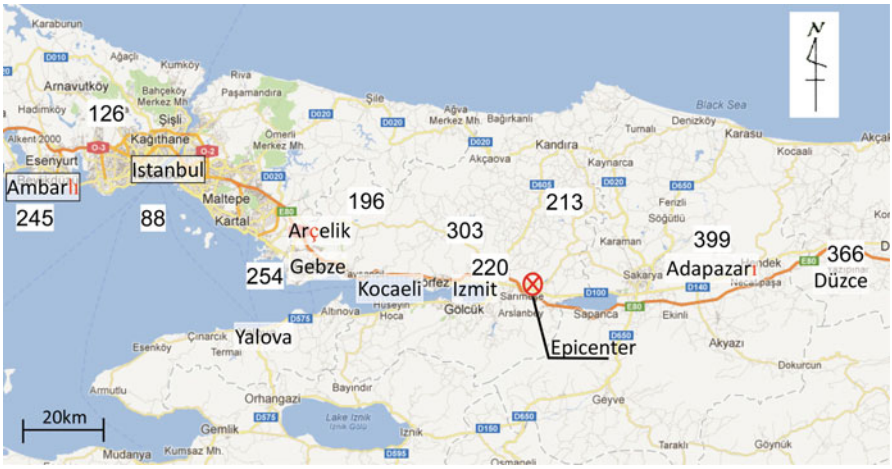

Fig. 1.10 Maximum horizontal accelerations at ground surface (cm/s^2) (source: Institute of earthquake engineering, Istanbul Technical University)

Fig. 1.11 Fire of tanks by long-period component of earthquake ground motion (1999 Kocaeli earthquake, Turkey, at Tüpraş oil refinary)

Liquefaction occurred over a large area between Adapazari to western Yalova, severely damaging buildings and buried pipes. The liquefaction and resultant large ground displacements around Lake Sapanca are described in detail in Chap. 4.

Damage from soil liquefaction at Adapazari was the most serious. About 1,000 buildings and houses were inclined and subsided. As one of examples, Fig. 1.12

Fig. 1.12 Collapse of a building due to soil liquefaction (1999 Kocaeli earthquake, Turkey, at Adapazarı)

shows collapse of a six story building. Furthermore, soil liquefaction extensively damaged buried lifeline pipes.

More than 20,000 buildings and houses were destroyed by ground motion and soil liquefaction. Most had infill brick walls in reinforced concrete (RC) frame structures. Causes of the damage to buildings were:

(i) Coincidence of the natural periods of 5–8-story buildings (severely damaged by the earthquake) with the predominant periods of observed earthquake ground motions
(ii) Poor-quality construction, such as the use of sea sand for concrete fine aggregate
(iii) Insufficient shear strength of first-floor columns
(iv) Collision of adjacent buildings
(v) Soil liquefaction of foundation ground

1.2.2 1999 Chi-Chi Earthquake, Taiwan [7]

The Chi-Chi earthquake of Mw = 7.3 occurred on September 21, 1999. The epicenter was at 23.85°N, 120.81°E, about 200 km southwest of Taipei, with hypocentral depth of about 6 km. The earthquake resulted in 2,386 people dead and missing, and damaged 12,000 buildings and houses, among which 6,000 totally collapsed. The earthquake also damaged infrastructures such as bridges, dams and port facilities, as well as water, electricity and gas lines. In addition, large-scale landslides buried several villages and killed many people.

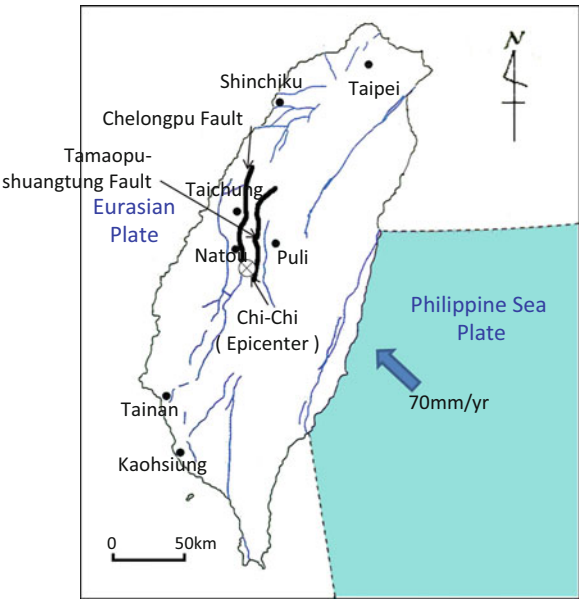

Fig. 1.13 Plate tectonics in Taiwan and active faults

Ten days after the earthquake, the Japan Society of Civil Engineers (JSCE) sent a reconnaissance team to survey the damage and recommend technical advices for restoration of damaged infrastructures such as road and railway, and lifelines. Based on a JSCE report, the earthquake mechanism, characteristics of ground motion, and damage outlines are described in the following.

The island of Taiwan lies on the boundary of the Eurasian and Philippine Sea plates, as shown in Fig. 1.13. The latter plate is subducting beneath the former at mean speed of 70 mm per year, and the plate movement forms many reverse faults, mostly in the north-south strike. The earthquake occurred along the active Chelongpu Fault, the length of which is estimated to be as long as 80 km.

Earthquake ground motions were recorded at more than 500 seismic stations during this earthquake. Maximum accelerations of 983 cm/s^2 in the horizontal and 335 cm/s^2 in the vertical were observed at the ground surface, 13.2 km west of the epicenter. The distribution of maximum east–west ground motion is shown in Fig. 1.14. This motion was slightly greater than that in the north-south component. The region with greater than 500 cm/s^2 accelerations extended approximately 45 km in the north-south and 10 km in east–west.

Many earthquake faults emerged at the ground surface. Figure 1.15 shows that Shin-Kang Dam was destroyed by a reverse fault. The dam was a concrete gravity-type of 25 m height and 357 m crest length, constructed in 1997 about 15 km north of Taichung for water supply. According to the Water Resources Agency of Taiwan, the dam was destroyed by a vertical differential displacement of 10 m, caused by the reverse fault. The left side of the dam was lifted 11 m and the right

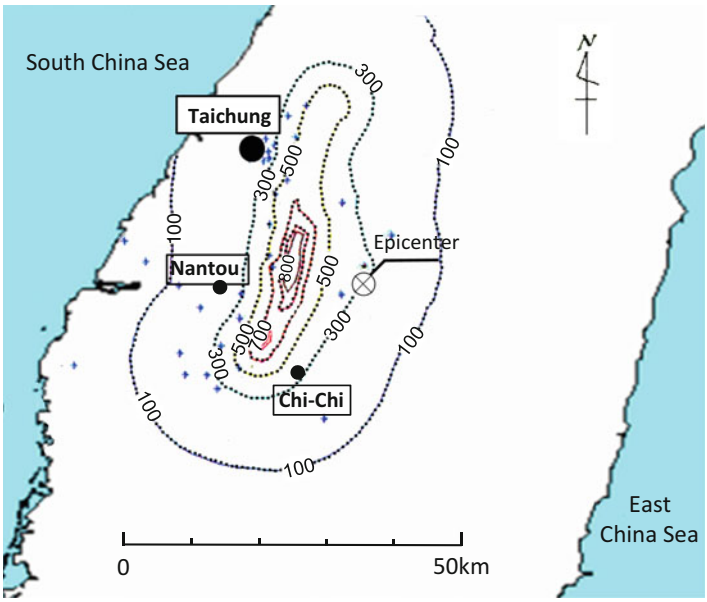

Fig. 1.14 Maximum horizontal accelerations at ground surface (1999 Chi-Chi earthquake, Taiwan, east-west component, cm/s^2)

Fig. 1.15 Destruction of Shin-Kang dam caused by the earthquake fault (1999 Chi-Chi earthquake, Taiwan)

Fig. 1.16 Earthquake fault on the playground of an elementary school (1999 Chi-Chi earthquake, Taiwan)

Fig. 1.17 Collapse of a bridge and water fall by earthquake fault offset (1999 Chi-Chi earthquake, Taiwan)

side 1 m. Figure 1.16 shows the earthquake fault that emerged on the playground of an elementary school, with a vertical gap about 2 m.

Among 754 highway bridges in the area affected by the earthquake, ten collapsed or were severely damaged, and another 30 were partially damaged but could be recovered. Causes of the bridge damage were:

(i) Offset displacements of the earthquake fault
(ii) Slope sliding
(iii) Strong earthquake ground motion in the epicentral area

Figure 1.17 shows a reverse fault emergence in the river and collapse of a concrete bridge. The fault offset formed a new waterfall in the river. Yi-Jiang Bridge in Fig. 1.18 is another example of a concrete bridge collapsed by fault movement. It was reported that vertical offset of the fault reached over 4 m at this location.

Fig. 1.18 Collapse of Yi-Jiang bridge crossing earthquake fault (1999 Chi-Chi earthquake, Taiwan)

Fig. 1.19 Buckling of a gas pipe by earthquake fault offset (1999 Chi-Chi earthquake, Taiwan)

Lifeline systems such as electricity, gas and water were severely damaged. The damage included:

(i) Ruptures of facilities of key stations such as electric substations by strong earthquake motion
(ii) Ruptures of buried pipes and tunnels by fault crossing
(iii) Collapse of electric transmission towers by slope sliding

Figure 1.19 shows buckling of a gas pipe with diameter 20.4 cm due to fault crossing, and Fig. 1.20 shows the destruction of air circuit breakers at an electric substation by strong earthquake motion and offset displacement of earthquake fault.

The Chi-Chi earthquake caused avalanches in western parts of the central mountain areas of Taiwan. Large-scale slope sliding was triggered in areas within about 60 km from the epicenter. Figure 1.21 shows an example of avalanches at Tsao-Ling. About three million cubic meters of mud slid into the Ching-Shoei

Fig. 1.20 Collapse of air circuit breakers by strong ground motion and earthquake fault offset (1999 Chi-Chi earthquake, Taiwan)

Fig. 1.21 Avalanches at Tsao-Ling (1999 Chi-Chi earthquake, Taiwan)

River from both banks, having buried villages. Most sliding occurred on soil slopes with cobbles.

In Nontou and Taichun prefectures, more than 12,000 buildings were damaged, half of which were perfectly destroyed. Most damaged buildings were RC structures on spread foundations. Causes of damage to the buildings were:

(i) Shear failures of RC columns
(ii) Ground subsidence and inclination due to lack of bearing capacity of the ground
(iii) Offset displacement caused by the earthquake fault
(iv) Poor quality of construction

Fig. 1.22 Collapse of reinforced concrete buildings caused by strong ground motion (1999 Chi-Chi earthquake, Taiwan)

Figure 1.22 shows an example of damaged buildings caused by shear failure of RC columns.

1.2.3 2001 Gujarat-Kachchh Earthquake, India [8]

The Gujarat-Kachchh earthquake with Mw = 7.7 occurred on January 26, 2001, about 20 km northeast of Bhuj in the Kachchh District of Gujarat State, western India (Fig. 1.23). The epicenter was at 23.40°N and 70.32°E, with hypocentral depth of about 17 km.

In this area, the Indo-Australian Plate is subducting beneath the Eurasian Plate, and there are active reverse faults in the west-east and northwest-southeast strikes as shown in Fig. 1.24 [9]. The Kachchh Mainland fault caused the earthquake. According to the Gujarat local government, the death toll reached about 13,800 and more than 166,000 people were injured. The quake destroyed about 370,000 houses, and left approximately 922,000 partially damaged buildings. Total property damage was estimated at 2.1 trillion rupees (about 6 billion U.S. dollars). In addition to the houses, infrastructures such as roads, port facilities, dams, and lifeline systems such as electricity, water and telecommunications were heavily damaged.

There was no clear evidence of the fault at the ground surface, based on an investigation done by JSCE. However, as shown in Fig. 1.25, several fissures

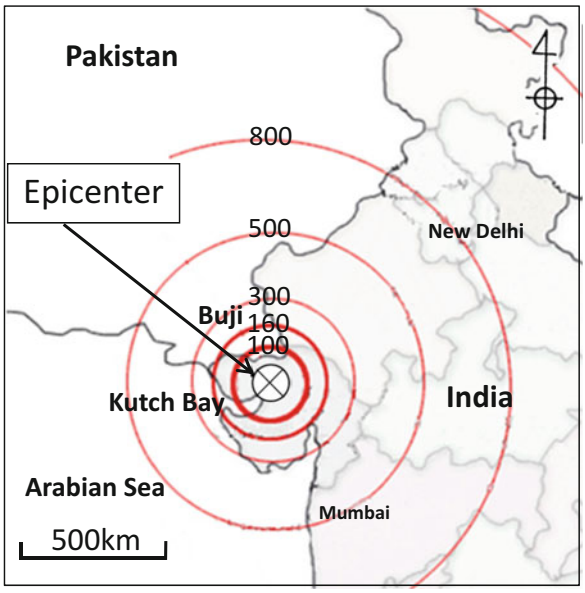

Fig. 1.23 Epicenter of 2001 Gujarat-Kachchh earthquake, India

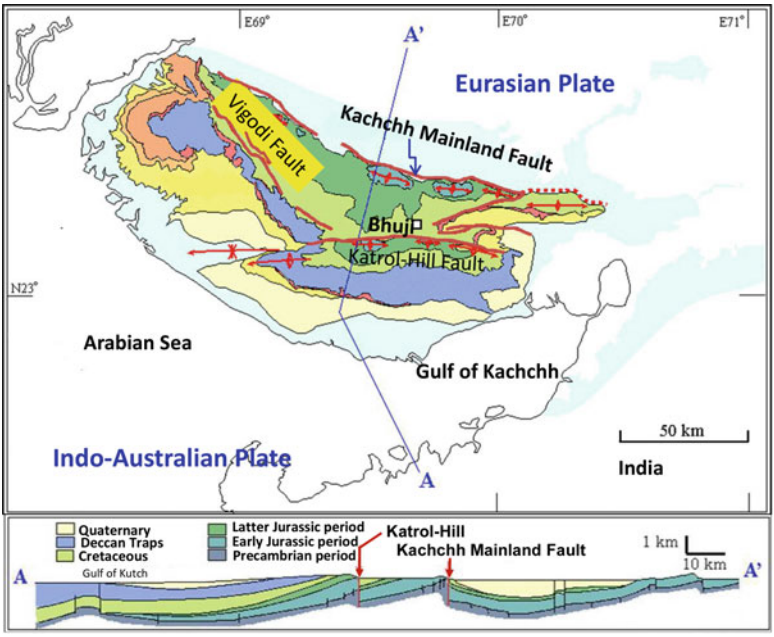

Fig. 1.24 Plate tectonics and active faults of 2001 Gujarat-Kachchh earthquake, India (source: Biswas [9])

Fig. 1.25 Ground surface fissures by the fault displacement (2001 Gujarat-Kachchh earthquake, India)

Fig. 1.26 Movement of bridge pier due to liquefied ground displacement (2001 Gujarat-Kachchh earthquake, India, at Hadakia bridge). (**a**) Movement of pier. (**b**) Soil liquefaction and surface break

appeared at the ground surface of a farm in east-west direction which was mostly parallel with Kachchh Mainland fault. This indicated that ground ruptures caused by fault displacement. Maximum ground acceleration was 110 cm/s^2, observed at a basement of a nine-story building at Ahmedabad, about 300 km from the epicenter.

Figure 1.26a shows the concrete pier of a bridge with total length 1,171 m and 30 spans crossing the Hadakia River, about 50 km from the epicenter. Due to horizontal displacement of liquefied ground in the river reservation, the foundations of bridge piers moved toward the river center. Ground surface break due to ground displacements was observed in a river channel, as shown in Fig. 1.26b. Horizontal movements of foundations and piers from liquefied ground flow were also reported in the 2003 Boumerdès earthquake, Algeria (Fig. 1.31).

The number of destroyed houses was about 370,000, most of which were constructed by soil bricks or so-called adobe. Whenever large earthquakes have occurred in developing countries, tremendous numbers of lives have been lost

Fig. 1.27 Collapse of Piloti-type concrete building (2001 Gujarat-Kachchh earthquake, India, at Ahmadabad)

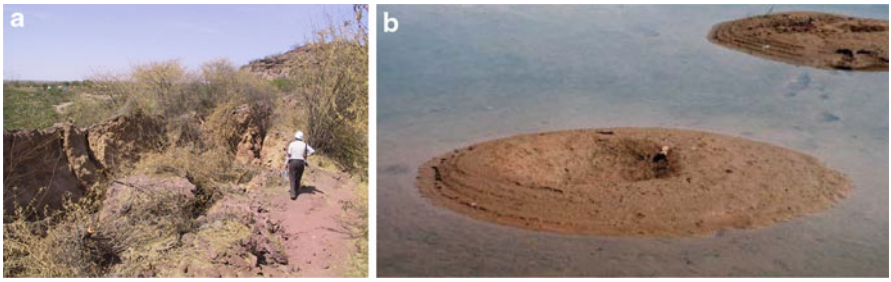

Fig. 1.28 Sliding of earth dam and sand volcanos at the foot (2001 Gujarat-Kachchh earthquake, India, at Changi dam). (**a**) Sliding and subsidence of the dam crest. (**b**) Sand volcanos at the foot of upstream slope

because of the collapse of houses with poor earthquake-resistance. Some researchers have developed low-cost and effective methods to improve earthquake resistance of these types of houses, but these methods were not widely adopted because associated financial problems were unresolved.

Many piloti-type buildings were severely damaged. Figure 1.27 shows a damaged concrete building in Ahmadabad. It was reported that the subsurface layer largely amplified earthquake motion, and the natural periods of the building coincided with the dominant period of ground motion. Power generation plants, oil refineries, and port facilities were also damaged.

There were many earth dams for water supply to local people and agriculture in the affected region. Figure 1.28a shows an example of damage to one such dam

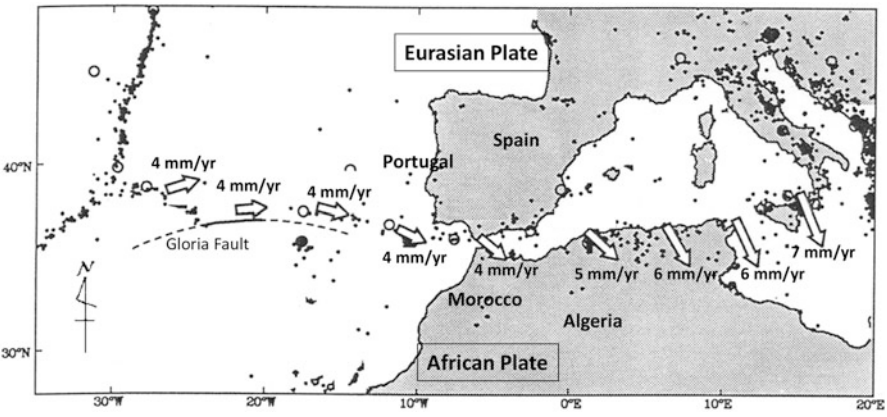

Fig. 1.29 Plate tectonics in northern Africa and Western Europe region

(Changi) with a height of 15 m. The slope slid downward from the dam top and the crown sank substantially. Near the foot of the upstream slope, sand volcanos and ground fissures were observed (Fig. 1.28b). Riverbed sediments that were not dredged during dam construction triggered soil liquefaction, and liquefied riverbed sediments initiated extensive sliding of the entire dam. However, because the earthquake occurred in the dry season and reservoir water levels were low, there was no disastrous flooding.

In the suburbs of large Japanese cities such as Tokyo, many small and medium size earth dams have been constructed for water supply. In most cases, because of a lack of consideration for soil liquefaction, liquefiable riverbed sediments were not removed. In addition, after dam construction, dense residential areas were sometimes developed nearby. The damage to Changi Dam by the Gujarat-Kachchh earthquake serves as a warning regarding the safety of such dams in heavily populated areas.

1.2.4 2003 Boumerdès Earthquake, Algeria [10]

An earthquake with Mw = 6.8 occurred on May 21, 2003 at Boumerdès, northern Algeria. The epicenter was at 36.8°N, 3.71°E, approximately 60 km east of the capital Algiers, with hypocentral depth of about 10 km.

It was reported that the earthquake was near the boundary of the African and the Eurasian plates. The latter plate (Fig. 1.29) is moving in an easterly and southeasterly direction about 4–6 mm per year. The Boumerdès earthquake was caused by

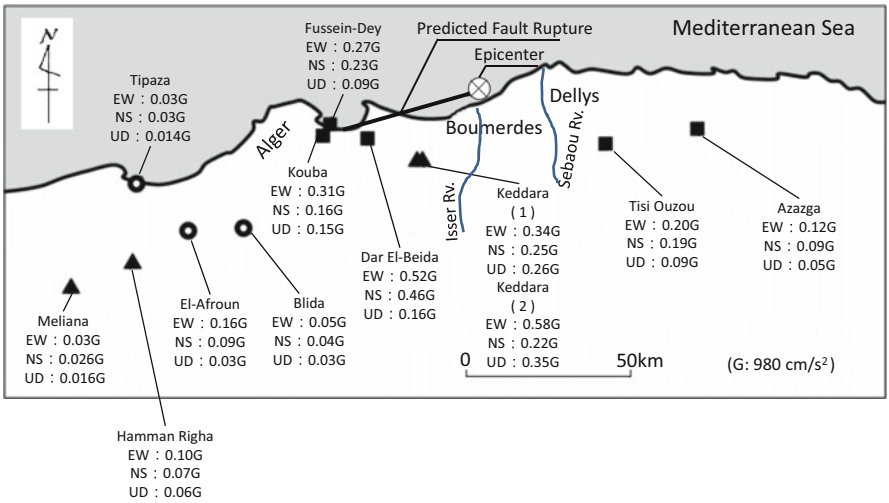

Fig. 1.30 Maximum accelerations at ground surface (2003 Boumerdès earthquake, Algeria, *G* gravity acceleration)

movement of a reverse fault with length about 40 km offshore from Boumerdès to the west, which was recognized after the event (Fig. 1.30).

Maximum ground accelerations caused by the earthquake are shown in Fig. 1.30. At Dar El Beida, 27 km from the epicenter, maximum ground surface acceleration reached 520 and 460 cm/s^2 in the east-west and north–south directions, respectively, and 157 cm/s^2 in the vertical.

Extensive soil liquefaction was caused, near the Isser and Sebaou rivers, about 5–10 km away from the epicenter. Figure 1.31a shows a pier foundation of the Isser River bridge, with length 454 m and 13 spans, that moved about 50 cm toward the river center due to ground flow caused by soil liquefaction; however, the girders did not fall. Figure 1.31b displays ground surface fissures with vertical differential settlements, caused by the ground flow from liquefaction.

There were 2,278 fatalities and 11,450 injuries. In the entire area affected by the earthquake, about 10,000 houses and buildings completely collapsed, which was about 10 % of the total number of houses and buildings. Causes of the damage to houses and buildings were:

(i) Low strength of column-beam connections
(ii) Lack of column shear strength
(iii) Collapse of the infill brick wall

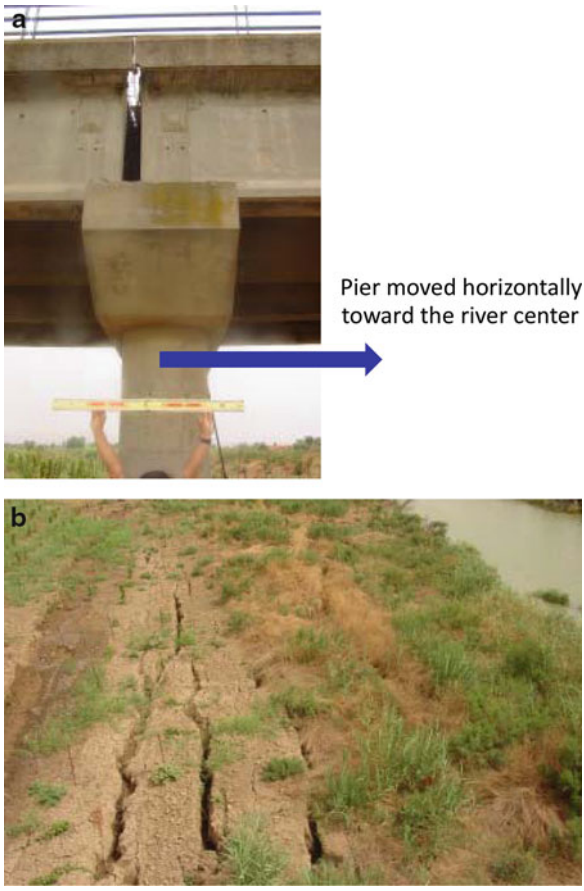

Fig. 1.31 Movement of a bridge pier due to liquefaction-induced ground displacement (2003 Boumerdès earthquake, Algeria, at Isser River). (**a**) Movement of a pier. (**b**) Surface fissures due to liquefied ground displacement

1.2.5 2004 Sumatra Offshore Earthquake and Tsunami, Indonesia

On December 26, 2004, there was a destructive earthquake of Mw = 9.1, with an epicenter off the west coast of Sumatra. This epicenter was at 3.3°N and 94.3°E, with hypocentral depth of about 30 km. A plate boundary about 1,000 km in length, from northwestern Sumatra to the Andaman-Nicobar Islands, ruptured. The earthquake source area is part of the extensive boundary between the Indo-Australian and Eurasian plates (Fig. 1.32). The former plate is subducting beneath the latter at an average rate of 50–60 mm per year, repeatedly generating earthquakes of magnitude 8–9 [11].

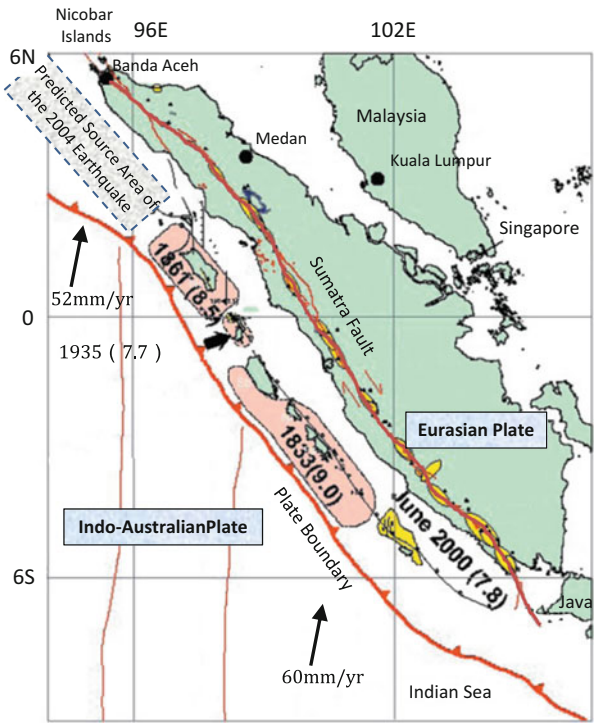

Fig. 1.32 Plate tectonics of west coast of Sumatra in Indonesia and active faults

The earthquake was an unprecedented natural disaster in recorded history, and generated the most destructive tsunami ever recorded. The tsunami caused waves as high as 20 m at its maximum along most coasts bordering the Indian Ocean. The total number of dead and missing was about 290,000 in 13 countries. Numbers of dead and missing people, and damaged houses in countries around the ocean are given in Fig. 1.33.

At Banda Aceh in the northern part of the island of Sumatra, the tsunami with wave height over 10 m completely destroyed and swept away numerous houses within about 2 km from the coastline, including reinforced concrete structures. Figure 1.34 shows Banda Aceh after this devastating tsunami.

However, Fig. 1.35 shows that some mosques near the coast survived from the tsunami without any structural damage. Because mosques in Islamic societies are the most important buildings, it was presumed that these were constructed with high strength. The tsunami passed through the prayer hall on the first floor of a piloti-type structure.

Figure 1.36 shows an example of a surviving concrete bridge in Banda Aceh. According to the testimony of residents, the tsunami flowed over the bridge, but no structural damage to pier or girder was found by the local government. Figure 1.36b shows that concrete shear stoppers were constructed on top of the piers to prevent

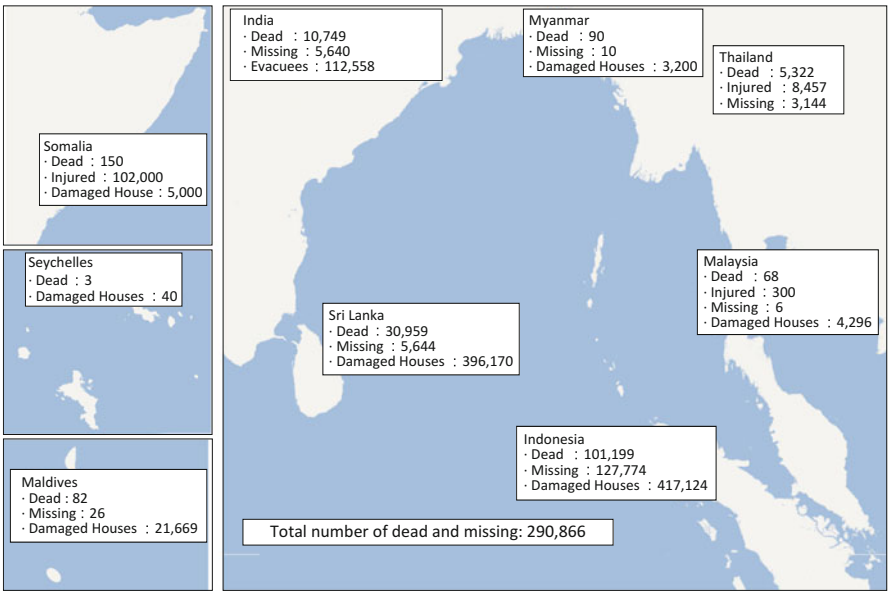

Fig. 1.33 Numbers of dead, missing, damaged houses and others (2004 Sumatra offshore earthquake and tsunami, Indonesia)

Fig. 1.34 Banda Aceh after the tsunami (2004 Sumatra offshore earthquake and tsunami)

Fig. 1.35 Mosque survived from the tsunami (2004 Sumatra offshore earthquake and tsunami, at Banda Aceh)

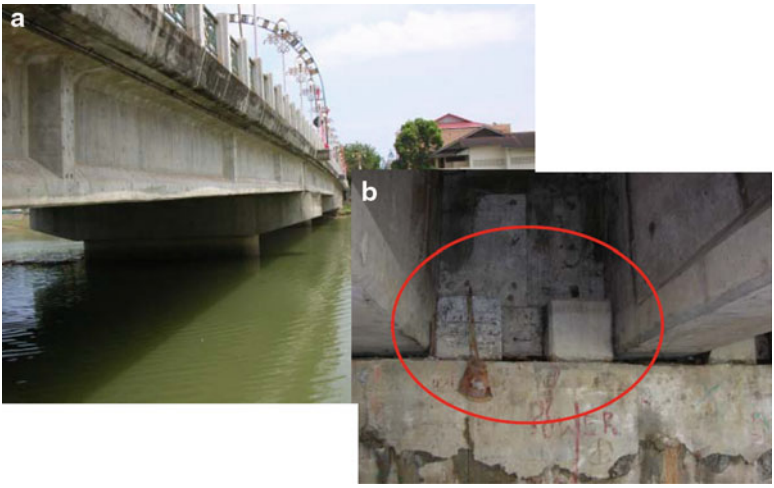

Fig. 1.36 Concrete bridge survived from the tsunami (2004 Sumatra offshore earthquake and tsunami at Banda Aceh) (**a**) Concrete bridge girder. (**b**) Concrete stopper for prevention of lateral movement of girders

movement of concrete girders by earthquake inertia force. These stoppers worked well to protect the bridge from the horizontal force of the tsunami.

By request of the United Nations (UN) authority in Aceh, the author conducted a specific investigation into damages along the west coast road from Banda Aceh to Meulaboh (length about 150 km), toward establishment of the plan for road

Fig. 1.37 Steel truss bridge washed down by the tsunami (2004 Sumatra offshore earthquake and tsunami, on the west coast of Sumatra)

reconstruction. Along this stretch, about 80 bridges were swept away; most were of a steel-truss type (Fig. 1.37). Embankments behind bridge abutments were washed away by the tsunami. It was assumed that the soft foundation ground was scoured by the tsunami.

The JSCE technical team recommended to the Indonesian government the following for road construction along the west coast of Sumatra:

(i) Bridge design considering tsunami external force (promotion of concrete bridge construction with shear stoppers)
(ii) Soil improvement of weak foundation ground to prevent tsunami scouring
(iii) Mangrove tree planting to attenuate tsunami wave force
(iv) Construction of a bypass route at an important section for preservation of traffic capability along the coast
(v) New routes in the mountains and measures for prevention of slope failures

Planting mangrove trees was implemented with the support of Japanese nonprofit organization OISCA (The Organization for Industrial, Spiritual and Cultural Advancement-International). It was reported that during the 2011 Tohoku earthquake, windbreak forests on the coastline reduced the tsunami force. Therefore, effects of these plantations should be studied as an anti-tsunami measure.

In an oil storage yard in the port of Krueng Raya, 25 km east of Banda Aceh, three tanks were floated by floodwater and were transported about 300 m from their original locations (Fig. 1.38). Three oil tanks of a cement factory on the west coast of Banda Aceh also floated, resulting in substantial oil leakage.

1.2.6 2005 Kashmir Earthquake, Pakistan [12]

The Kashmir earthquake of Mw = 7.6 occurred on October 8, 2005 in northern Pakistan, near the border with India. The epicenter was at 34.4°N and 73.5°E, and

Fig. 1.38 Floated and displaced oil tanks (2004 Sumatra offshore earthquake and tsunami, Indonesia)

hypocentral depth was 12 km. The number of dead and missing was more than 75,000, in both Pakistan and Indian-administered Kashmir.

Figure 1.39 indicates that the Indian continent has been moving northward 35–50 mm annually, and the Indo-Australian Plate is subducting beneath the Eurasian and Arabian plates. There are many active faults in this area, such as the Main Central Thrust (MCT) and Balakot-Bagh Fault (BBF). It was reported that the earthquake was caused by a reverse fault on this plate boundary.

Maximum ground acceleration in the north-south direction was 230 cm/s^2, measured at the basement of a two-story building in Abbottabad, about 100 km from the epicenter. In Muzaffarabad, the capital of Azad Jammu and Kashmir in Pakistan, and in Balakot, a huge number of houses collapsed by strong ground motion. Since the epicenter was in a mountainous area there were numerous slope failures which buried villages [13]. It was reported that slope failures concentrated on the hanging wall side of the reverse fault. The slope failure types were:

(i) Soil slope sliding
(ii) Weathered rock slope sliding
(iii) Toppling of rock masses

Figure 1.40 shows examples of each of the above.

1.2.7 2008 Wenchuan Earthquake, China [14, 15]

On May 12, 2008, the Wenchuan earthquake of Mw = 7.9 struck the western mountainous area of Sichuan Province, at the border of the Sichuan Basin and

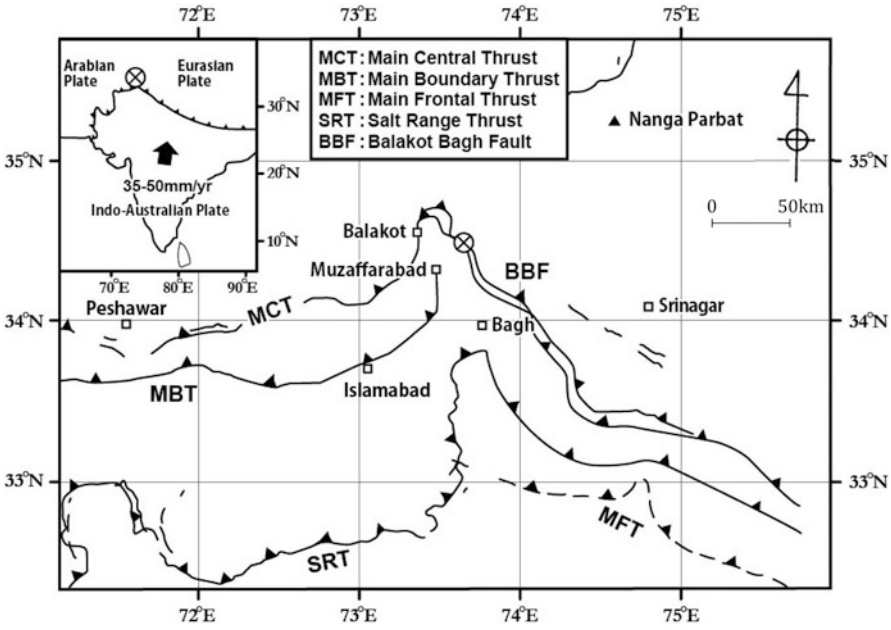

Fig. 1.39 Plate tectonic of Indo-Pakistan boundary and active faults (after the reference [11])

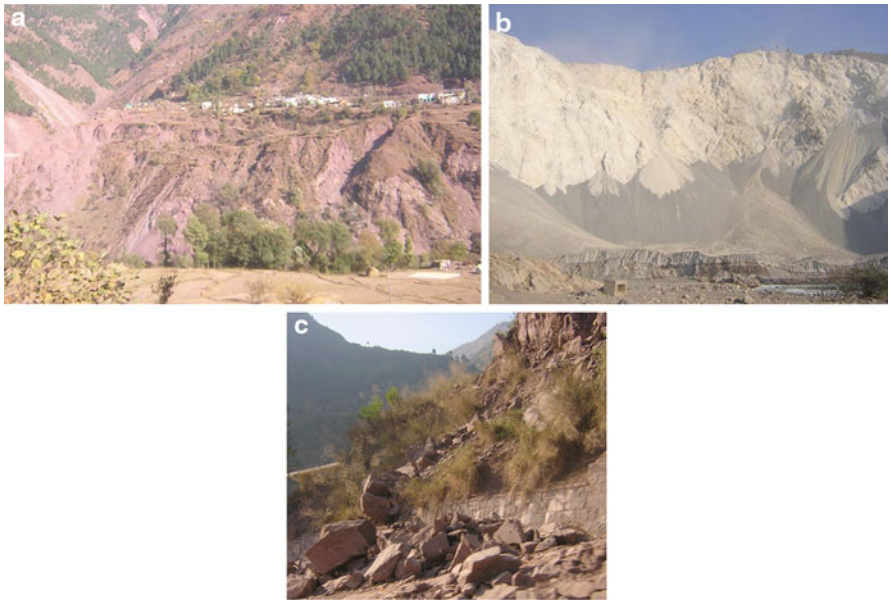

Fig. 1.40 Slope slidings (2005 Kashmir earthquake, Pakistan). (**a**) Soil slope sliding. (**b**) Weathered rock slope sliding. (**c**) Toppling of rock masses

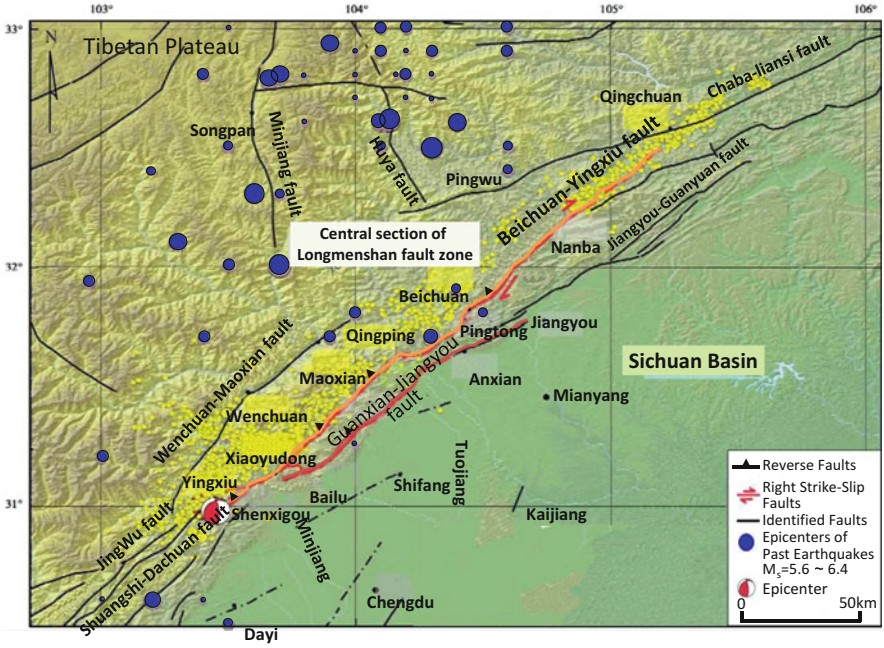

Fig. 1.41 Two active faults which caused 2008 Wenchuan earthquake (after Xu et al. [15])

Tibetan Plateau. The China Earthquake Administration estimated the epicenter at Yingxiu (31°N and 103.4°E), with focal depth 14 km.

The Wenchuan earthquake was caused by two reverse faults, Beichuan-Yingxiu and Guanxian-Jiangyou, which belong to the central and forward segments of the Longmenshan fault zone (Fig. 1.41). The length of the fault rupture was estimated as more than 300 km. This was the largest inland earthquake ever recorded. The Chinese Ministry of Civil Affairs announced that the earthquake left about 69,277 dead, 17,923 missing, 373,643 injured, and 5.3 million wrecked houses. The estimated direct economic loss exceeded 8.45 billion Yuan (approximately 1.36 billion U.S. dollars).

According to recent GPS measurement, the Indian continent is moving northward at an average speed of 20 ± 10 mm per year in this region (Fig. 1.42), resulting in uplift of the Tibetan Plateau. That plateau has been rotating in the clockwise direction and moving toward the Sichuan Basin at about 15 ± 7 mm per year.

Earthquake surface faults emerged along 240 km of the Beichuan-Yingxiu fault and 72 km along the Guanxian-Jiangyou fault. Another surface fault (Xiaoyudong) of length about 6 km emerged, connecting these two faults. A maximum vertical displacement of 6.2 m was observed along the Beichuan-Yingxiu fault, between Hongkou and Qingping. Furthermore, 5.3 m of maximum vertical displacement was observed at Qingping. Figure 1.43 displays surface faults at Bailu Central Elementary School. Fortunately, this school building survived although it was

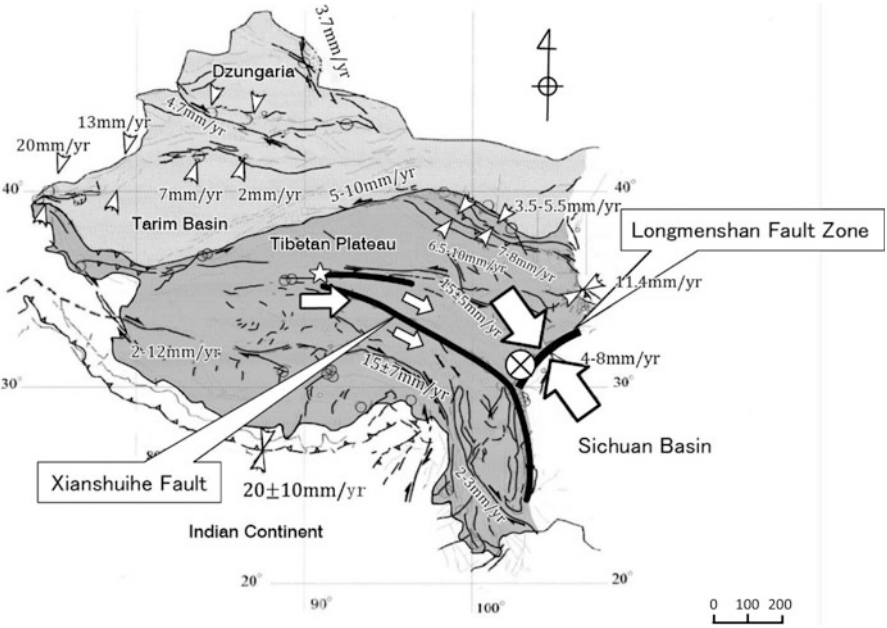

Fig. 1.42 Plate tectonics of Shichuan Basin and Tibetan Plateau

Fig. 1.43 Earthquake fault in Bailu central elementary school (2008 Wenchuan earthquake, China)

extremely close to the fault. However, a village directly atop an extension of this earthquake fault was completely ruined.

Figure 1.44 is a map of seismic intensity published by the China Earthquake Administration. The maximum intensity was XI on the Chinese Seismic Intensity (equivalent to XI of the Modified Mercalli Intensity, MMI), the maximum intensity ever recorded in the country. The area of intensity VI (corresponding to intensity VI

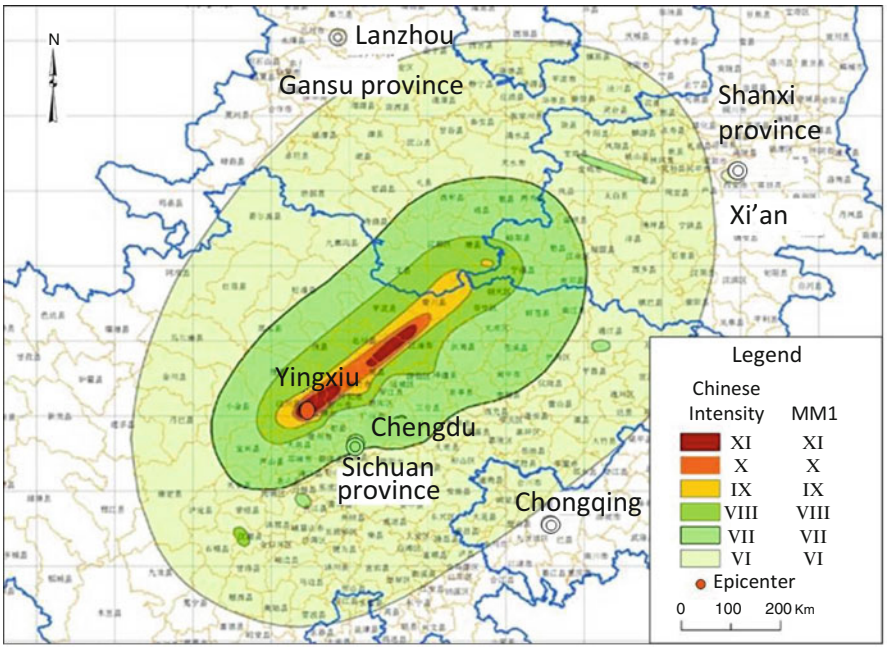

Fig. 1.44 Seismic intensities in source area (2008 Wenchuan earthquake, China) (source: China earthquake administration)

at MMI) was about 440,000 km^2, which covered Sichuan, as well as Gansu and Shanxi provinces in Northwest China.

Figure 1.45 shows that maximum ground acceleration in this earthquake was 957.7 cm/s^2 at Wolong in east-west component. The record clearly shows that ground motions were divided into two portions, resulting from two continuous ruptures of the Beichuan-Yingxiu and Guanxian-Jiangyou faults.

In the region near the epicenter, a number of buildings and civil engineering structures suffered heavy damage from strong ground motion. Tables 1.1 and 1.2 gives an overview of the damage. Severe damage concentrated around the source and ten neighboring prefectures and cities (Wenchuan, Beichuan, Mianzhu, Shifang, Qingchuan, Maoxian, Anxian, Dujiangyan, Pingwu, and Pengzhou). A large number of slope failures and massive landslides occurred, because the source of the earthquake was in a steep and weathered mountainous area. These landslides dammed river flows and created many lakes. Figure 1.46 shows the largest lake on Minjiang River, Tangjiashan quake lake, total landslide debris volume was 20.4 million m^3.

According to an investigation of damage to reinforced concrete buildings in Dujiangyan and Hanwang cities in the source area and environs, major causes of the damage to buildings were:

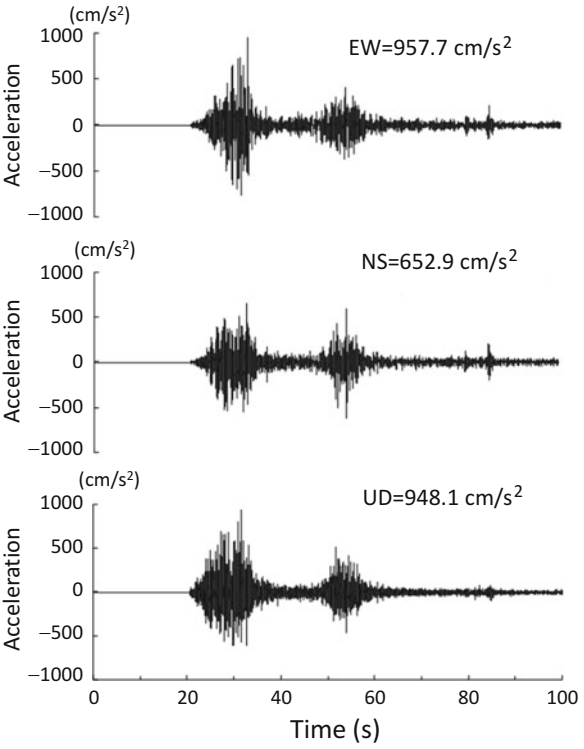

Fig. 1.45 Ground surface accelerations at Wolong (2008 Wenchuan earthquake, China)

Table 1.1 Damage to buildings and structures (2008 Wenchuan earthquake, China)

Building (F: frame structure, M: brick structure)		Damage rate (%)	Collapse rate (%)
Intensity IX	F	86.9	28.2
	M	99.5	29.3
VIII	F	68.6	3.8
	M	75.7	10.8
VII	F	17.7	0.3
	M	45.3	3.0
VI	F	7.7	0.0
	M	17.5	0.9

(i) Shear failure of columns
(ii) Destruction of column-beam joints
(iii) Collapse of brick walls between columns
(iv) Offset displacement by earthquake fault
(v) Slope sliding

Figure 1.47 shows building damage of types (i) and (ii).

Table 1.2 Damage to bridges, tunnels and dams

Bridge, tunnel, and dam		Total number	Damage number	Damage rate (%)	Collapse & total rupture	Collapse & total rupture rate (%)
Bridge	Expressway	607	576	94.9	69	11.4
	National road	1,163	1,081	92.9	191	16.4
	Total	1,770	1,659	93.6	260	14.7
Tunnel	Expressway	23	14	60.9	8	34.8
	National road	28	17	60.7	3	10.7
	Total	51	31	60.8	11	21.6
Dam	Sichuan province	6,678	1,996	29.9	69	1.0
	Shanxi province	1,036	126	12.2	0	0.0
	Gansu province	297	81	27.3	0	0.0
	Others	27,590	463	1.7	0	0.0
	Total	35,601	2,666	7.5	69	0.2

Fig. 1.46 A Quake lake caused by slope failure (2008 Wenchuan earthquake, China) (Institute of Mountain Hazards and Environment, Chinese Academy of Science (CAS), by Xiaogang Zhang)

In Sichuan Province, seven expressways, five national roads, and ten provincial roads were blocked. Total length of damaged road reached about 3,400 km. Most of these roads were aligned in mountainous areas, and many bridges and tunnels were constructed in unstable slopes. Because of strong earthquake motion in the source area and offset displacement by earthquake fault, a number of bridges and tunnels

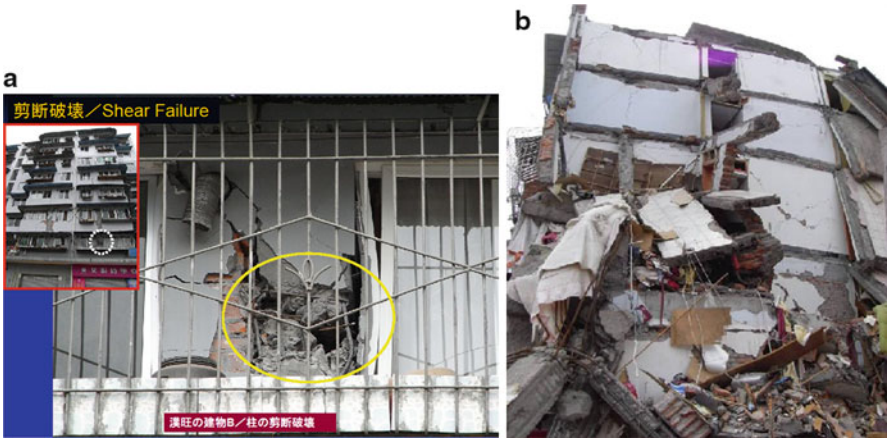

Fig. 1.47 Damage to buildings (2008 Wenchuan earthquake, China). (**a**) Shear failure of concrete column. (**b**) Destruction at joint between column and beam

were severely damaged. There were extensive slope failures along the roads. An 83-km long road connecting Dujiangyan-Yingxiu-Wenchuan was under construction, and its tunnels, bridges, and slopes were greatly affected. Between Wenchuan and Yingxiu, 22 of 43 bridges were damaged and 90 million m^3 of soil containing large rocks fell on the roads, resulting in obstacles to rapid recovery of transportation.

Many tunnels were also severely damaged. This damage was from compression failure of concrete lining at arch crowns, shear failure of sidewalls, and uplift of inverts. Because of this extensive damage to tunnels, recovery was extremely difficult to implement.

In Sichuan Province, 1,996 dams (about 30 % of the total 6,678) were damaged by the earthquake. Figure 1.48 shows Zipingpu, a rock-fill dam with impermeable concrete facing on upstream slope. This dam is on the Minjiang River, the footwall side of the Beichuan-Yingxiu fault and hanging wall side of the Guanxian-Jiangyou fault. The height and crest length of the dam are 156 and 664 m, respectively. The dam has multiple purposes, including water supply to the region and power generation of 76 million Kw.

Cracks in the concrete impermeable facing of the top of the upstream side and relative displacement of joints for the concrete casting were reported, resulting in water leakage. Maximum subsidence of the crest was approximately 1 m, and horizontal displacements in the downstream as well as axial directions were 20 and 22 cm, respectively.

In Sichuan Province, 3,619 slope failures, 5,899 landslides and 1,054 debris flows were caused by the earthquake. There were 34 landslide-caused dams with height 10 m or greater, and lakes with water volume greater than 100,000 m^3.

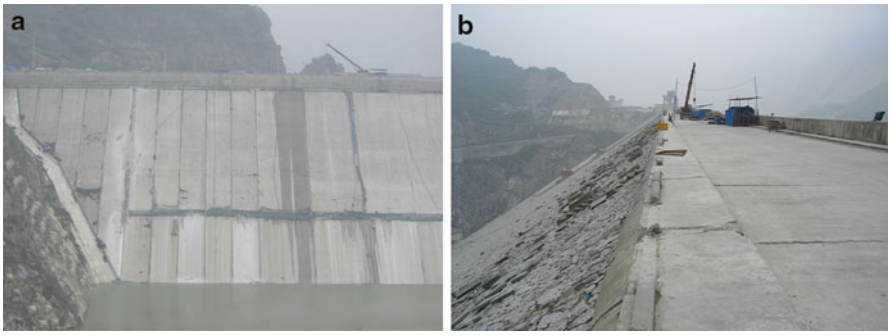

Fig. 1.48 Damage to Zipingpu dam (2008 Wenchuan earthquake, China, concrete facing dam, height: 156 m). (**a**) Damage to concrete facing. (**b**) Subsidence of the dam crest

Fig. 1.49 A large slope failure and buried villages (2008 Wenchuan earthquake, China, at Donghekou)

There were 23 locations where landslides killed more than 30 people. About 20,000 lives were lost in total. This represents approximately 30 % of the total dead and missing by the earthquake.

Figure 1.49 displays the long travel landslide at Donghekou in Qingchuan Prefecture, about 250 km from the epicenter. A large amount of soil of a million cubic meters collapsed from a 550-m-high mountaintop, spreading several kilometers. Four villages were buried by this landslide.

1.3 Recent Earthquakes and Tsunamis in Japan and Their Lessons

1.3.1 1993 Southwest Hokkaido Offshore Earthquake

On July 12, 1993, a Mw = 7.8 earthquake occurred in the Sea of Japan near the Oshima Peninsula of Hokkaido. The epicenter was at 42.47°N and 139.12°E, with hypocentral depth of about 34 km. Figure 1.50 shows that seismic intensity 5 on the Japan Meteorological Agency Intensity (JMAI), equivalent to seismic intensity VI–VII on the MMI, was recorded at Otaru, Suzu, Esashi and Fukaura. Intensity 4 (V on the MMI) was observed over a wide area. At the ground surface of the alluvial plane at Suzu on the peninsula, about 78 km from the epicenter, a maximum horizontal acceleration 216 cm/s^2 was observed.

This earthquake triggered a tsunami along the west coast of Hokkaido, including Okushiri Island. According to the Fire Defense Agency (FDA), the tsunami caused 203 deaths and 28 missing. Furthermore, Okushiri Island was also damaged by tsunami aftermath fire.

Figure 1.51 shows the tsunami run-up height and numbers of dead and missing on Okushiri Island. The maximum run-up height was 29 m in the southwestern part of the island. Figure 1.52 shows aerial photos of Aonae district, the southernmost

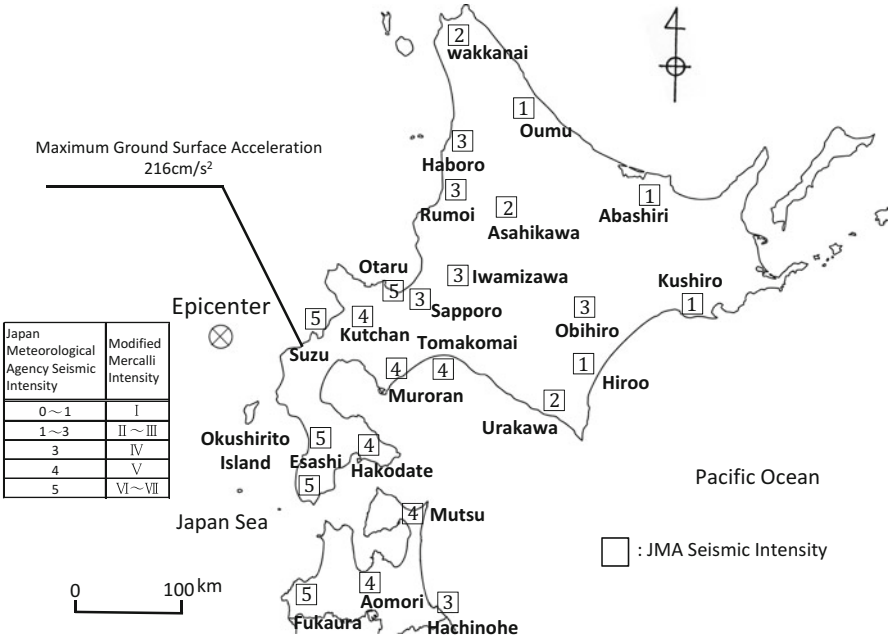

Fig. 1.50 Epicenter of 1993 Southwest Hokkaido offshore earthquake and seismic intensity (JMA)

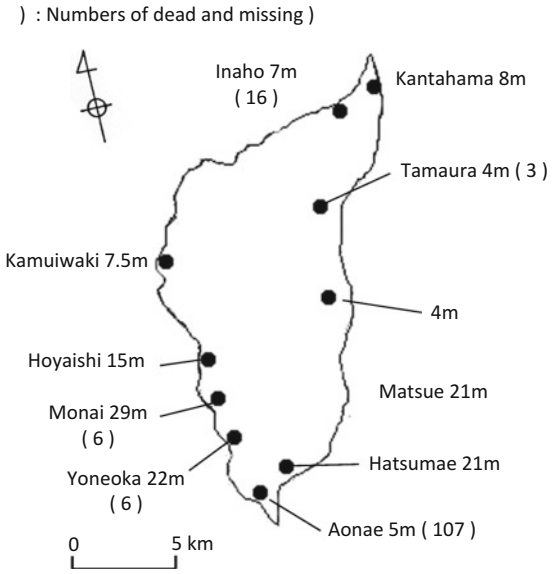

Fig. 1.51 Run-up height of the tsunami in Okushiri island (1993 Southwest Hokkaido offshore earthquake) (( ): Numbers of dead and missing)

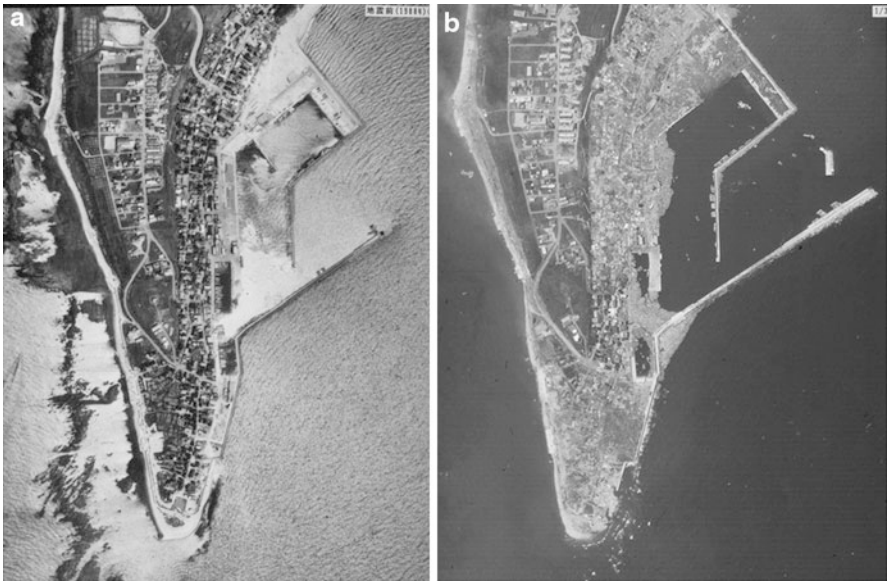

Fig. 1.52 Aerial photos of Aonae in Okushiri Island (1993 Southwest Hokkaido offshore earthquake). (**a**) Before the tsunami. (**b**) After the tsunami

Fig. 1.53 Shelter terrace constructed after the tsunami

part of the island, before and after the tsunami. According to testimonies from the residents, 4–5 min after the earthquake, the tsunami came from the west and passed to the east, traversing the entire cape area.

There was not enough time for evacuation, because many residents of Okushiri were fishermen who lived in lowlands along the coast. The high-speed tsunami spread over all lowlands of the island. Furthermore, it struck at 10 PM at night, making evacuation more difficult.

In the most severely damaged area of Okushiri Island, embankments of 3–5 m height were constructed behind the existing tide barrier wall after the tsunami. In addition, the area near the coast was made into a park and non-residential area, and residents were relocated to higher ground. Figure 1.53 shows a terrace for the tsunami evacuation shelter that was constructed nearby the coastline.

This earthquake caused extensive liquefaction over a wide area, from Oshima Peninsula to Hakodate. Roads, port structures, houses, and lifelines were seriously damaged. In particular, there was severe liquefaction on the alluvial lowland along the Shiribeshi-Toshibetsu River flowing through the town of Kitahiyama. Horizontal ground displacement caused by soil liquefaction nearly reached 2.0 m. This liquefaction-induced ground displacement is described in Sect. 4.1.6.

In the Hakodate port area with seismic intensity 4 (JMAI), liquefaction caused inclinations and horizontal displacements of coastal revetments, and subsidence of the pavement behind the revetment (Fig. 1.54). However, the quay wall in the western part of the port was not damaged by soil liquefaction, because the ground had been improved by a sand compaction pile method.

Fig. 1.54 Deformation and inclination of quay wall by steel sheet piles at Hakodate port (1993 Southwest Hokkaido offshore earthquake)

1.3.2 1993 Kushiro Offshore Earthquake [16]

A Mw = 7.8 earthquake occurred 13 km off the coast of Kushiro, Hokkaido, on January 15, 1993. The epicenter was at 42.51°N and 144.23°E, with hypocentral depth of about 107 km. This earthquake was caused by rupture of an active fault on the Pacific Ocean Plate. The Kushiro city office reported two dead, 478 severely injured, 6 completely destroyed buildings, and 1,538 partially damaged houses.

Figure 1.55 shows seismic intensities and maximum accelerations at ground surface in southern Hokkaido and the northern Tohoku region. Seismic intensity was 6 (JMAI), and maximum acceleration at the ground surface was 467 cm/s^2 in port of Kushiro. However, at the Kushiro Meteorological Observatory building, about 16 km from the epicenter, maximum acceleration reached 920 cm/s^2.

Soil liquefaction caused the uplift of manholes, subsidence and inclination of houses, ruptures of buried pipes, and others. Figure 1.56 shows a lifted sewage manhole caused by buoyancy of the liquefied soil. It was reported that sandy soil was used for backfill material after excavation and that the ground water level was high.

Furthermore, there was liquefaction-induced damage such as cracks, differential settlement of roads, and subsidence of pavement behind quay walls. However, some of quay walls survived without any damage, because the ground was improved by the sand compaction pile method [17]. Based on lessons of the 1983 Central Japan Sea earthquake, anti-liquefaction measures for port structures had been implemented. The ground was behind the quay wall improved by sand compaction pile method.

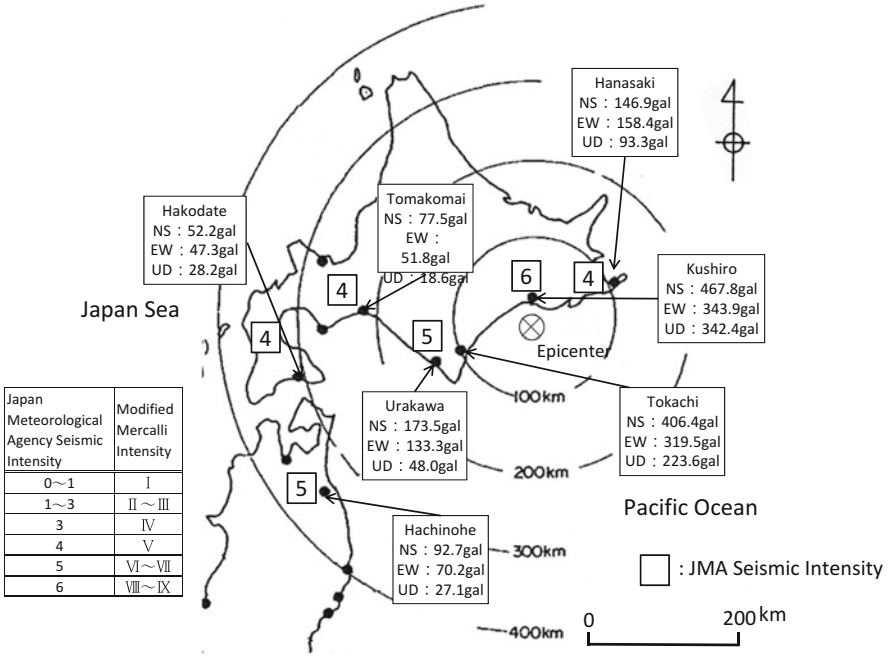

Japan Meteorological Agency Seismic Intensity	Modified Mercalli Intensity
0～1	Ⅰ
1～3	Ⅱ～Ⅲ
3	Ⅳ
4	Ⅴ
5	Ⅵ～Ⅶ
6	Ⅷ～Ⅸ

Fig. 1.55 1993 Kushiro offshore earthquake, seismic intensity and ground surface acceleration (cm/s^2)

Fig. 1.56 Uplift of a manhole by soil liquefaction (1993 Kushiro offshore earthquake)

Fig. 1.57 Slope failure in residential area (1993 Kushiro offshore earthquake)

Because the Kushiro earthquake was in January, the ground was frozen to about 1-m depth. The damage to buried pipes and buildings from liquefaction was likely reduced because of decreased displacement and acceleration at the frozen surface. Nevertheless, damage to residential houses was produced by landslides in hilly and mountainous areas (Fig. 1.57).

At the Kushiro Meteorological Observatory, a maximum acceleration of 920 cm/s^2 was recorded at the ground surface. Despite such strong ground motion, significantly greater than the design-level acceleration, there was relatively minor damage to buildings, port structures, roads, railways, and lifelines. This minor damage to structures against strong accelerations caused overconfidence among Japanese engineers and scientists regarding earthquake resistance of structures. Two years later, the 1995 Kobe earthquake revealed that this overconfidence had an inadequate scientific basis.

1.3.3 1995 Kobe (Hyogo-ken Nambu) Earthquake [18]

An earthquake of Mw = 7.2 with epicenter near the Akashi Strait in Hyogo Prefecture occurred on January 17, 1995. The epicenter was at 34.35.7°N and 135.02°E, with hypocentral depth of about 16 km. It was the first recorded occurrence of the highest intensity 7 on the JMAI (X or greater on the MMI). The disaster-stricken area had a long belt shape, about 1 km wide and 20 km long, from Kobe to Nishinomiya. According to Sekiguchi et al. [19], there were several active faults (Fig. 1.58), and it is assumed from analysis of ground motion records that these faults caused the earthquake. Seismic intensity was 7 in the cities of Kobe, Ashiya, Nishinomiya and Awaji, and 6 in nearby cities. Intensities 5 and 4 were widely observed (Fig. 1.59).

Earthquake ground motions were observed at many seismic stations near the epicenter. Figure 1.60 shows accelerations recorded at the ground surface of the Kobe Marine Meteorological Observatory and their acceleration response spectra.

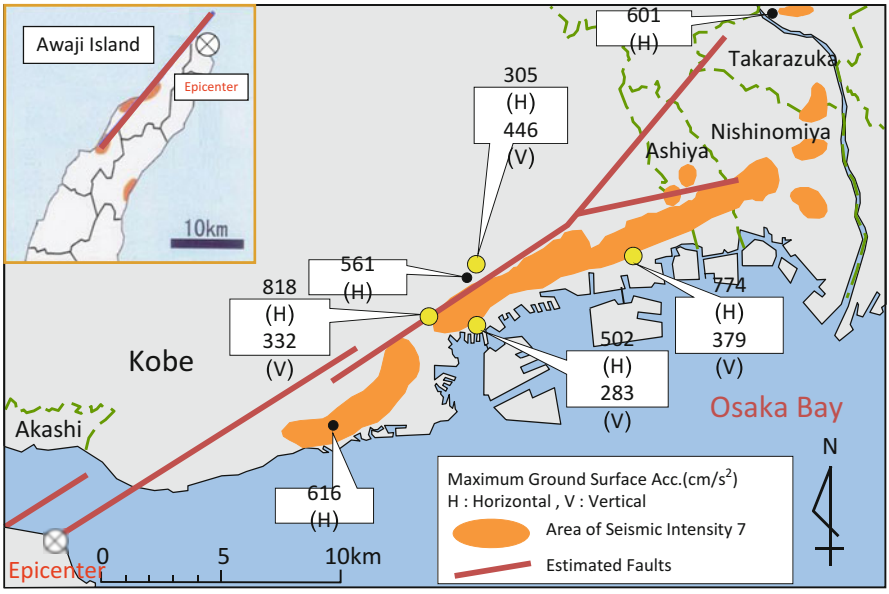

Fig. 1.58 Active faults which caused the 1995 Kobe earthquake and maximum accelerations at ground surface (faults: after Sekiguchi et al. [19])

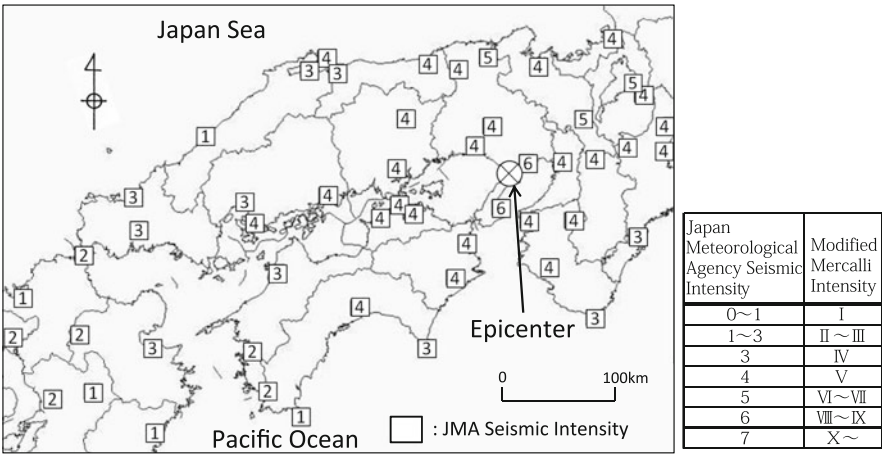

Japan Meteorological Agency Seismic Intensity	Modified Mercalli Intensity
0～1	Ⅰ
1～3	Ⅱ～Ⅲ
3	Ⅳ
4	Ⅴ
5	Ⅵ～Ⅶ
6	Ⅷ～Ⅸ
7	Ⅹ～

Fig. 1.59 Seismic intensities of the 1995 Kobe earthquake

The maximum north-south horizontal acceleration was about 820 cm/s^2. According to the acceleration response spectrum in Fig. 1.60b, motions with periods of 0.3–1.0 s were dominant. These components of ground motions had strong powers on the destruction of numerous structures.

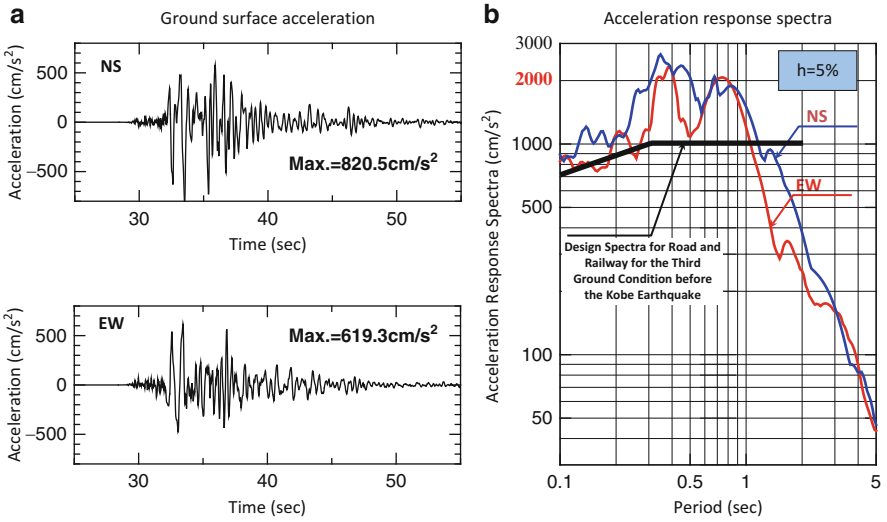

Fig. 1.60 Ground surface accelerations at Kobe marine meteorological observatory and their response spectra. (**a**) Ground surface acceleration. (**b**) Acceleration response spectra

A total of 6,432 lives were lost, including deaths from disease after the earthquake, and 43,792 injuries were reported (May 2006, the Fire Defence Agency). A total of 104,906 buildings were completely destroyed or burned down, which was the main cause of fatalities.

The Kobe earthquake raised the following issues for disaster prevention in highly urbanized areas, against earthquakes caused by nearby inland faults. The earthquake was caused by an approximately 40 km-long inland faults. Strong ground motion caused by these faults destroyed a number of buildings, infrastructures and lifelines in the urban area within 5–10 km from the faults. According to response spectra shown in Fig 1.60b, the response acceleration reached 2,000 cm/s^2 between 0.3–0.8 s. This was largely beyond the acceleration of 1000 cm/s^2 used in the design of road bridges and railway structures before the earthquake. The ground motion caused tremendous damage to buildings, roads, railways, subways, quay walls and tunnels (Fig. 1.61).

Around reclaimed seaside areas, soil liquefaction and flow of liquefied ground heavily damaged lifeline facilities and foundations of structures. Key stations such as water purification plants, wastewater treatment plants, electrical substations and buried pipelines were damaged.

Table 1.3 shows damage to lifeline systems and the time needed for function recovery. The number of households which experienced outages of water, city gas and electricity reached about 1.3 million, 860,000 and 260,000, respectively. More than 280,000 phone lines malfunctioned. Therefore, it took an extended time to recover. Waterworks required 70 days, the sewage system about 5 months, electricity

Fig. 1.61 Damage to building, road, railway, subway and tunnel (1995 Kobe earthquake, Japan). (**a**) Collapse of a building. (**b**) Shear failure of concrete pier of road bridge. (**c**) Shear failure of concrete column of railway bridge. (**d**) Shear failure of columns of subway. (**e**) Large inclination of quay wall. (**f**) Damage to a tunnel for water transmission

6 days, phone lines 14 days, and city gas 54 days. The malfunction of transportation systems and damage to lifelines caused a long period urban function paralysis.

In addition, the aftermath fire worsened the damage. Fires started at 261 points in Kobe and neighboring cities, having burnt an area about 830,000 km^2. Although exact reasons of fire ignition were not identified, it was probable that they were related to recovery of electricity supply. Fortunately, there were no fires by leakages of oil and petrochemical products from industrial complexes.

The Japanese government was criticized for not acting quickly enough to gather information about the situation in damaged areas and to save lives through rapid

Table 1.3 Damage to lifeline systems by the 1995 Kobe earthquake and function recovery time

	Functional disorder	Function recovery time (days)
Water	1,256,000 (cut off households)	70 (Kobe, Nishinomiya) 64 (Ashiya)
Sewage	198 km (length of damaged pipe)	Buried pipes: 140 Pumping station: 24 Sewage treatment plants: 5 months
Electricity	2,600,000 (blackout households)	6
Phone line	285,000 (malfunctional lines)	14
City gas	857,000 (cut off households)	54

response. For several hours after the earthquake, information on the devastated areas could be gathered only by the broadcast media and Self-Defense Force aircrafts. Government response was delayed by this lack of information.

Recovery and reconstruction work was confronted with many difficulties. These included traffic disturbances that caused long delays in transporting emergency goods and personnels, disposal of debris and rubble from destroyed buildings and houses, care for a huge number of refugees, and resident consensus on plans for reconstructing damaged areas.

Attention should be given to "hidden" disasters, which did not meet certain conditions during the earthquake. The following are two examples of such disasters. First was the derailment of trains caused by strong earthquake ground motion. Because the earthquake was in the early morning (5:46 AM), most trains including the Shinkansen (bullet train) were not running. According to the Railway Technical Research Institute [20], nine trains were halted at the time of the earthquake in the area of seismic intensity 7 (Fig. 1.62), eight of which were derailed. However, there were no fatal accidents because there were no passengers.

The second hidden disaster was that the earthquake did not trigger large fires in storage tanks of oil, petrochemical products and hazardous material in industrial complexes on artificial islands reclaimed from the sea. Figure 1.63 shows inclination of tank due to soil liquefaction in a reclaimed land of Kobe, but there was no collapse. The main reason of no serious damage was the short duration of ground motion of the earthquake, only 10–15 s. A longer duration of several 10 s–1 min would have caused greater inclination and possible collapse, resulting in a much more severe disaster. Oil spilled from collapsed tanks could have induced a large fire on the sea. The large inclination and subsidence of the tanks caused by soil liquefaction during the Kobe earthquake showed the importance of enhancement of earthquake resistance for industrial complexes in reclaimed areas around big cities such as Tokyo, Nagoya and Osaka.

The tremendous damage by the 1995 Kobe earthquake far exceeded predictions of Japanese engineers and scientists engaged in earthquake disaster prevention. However, in 1994, 1 year before the occurrence of the Kobe earthquake, highway bridges and houses were collapsed by the Northridge earthquake in U.S. A survey team from Japan, including the author, reported and annouced that "These kinds of

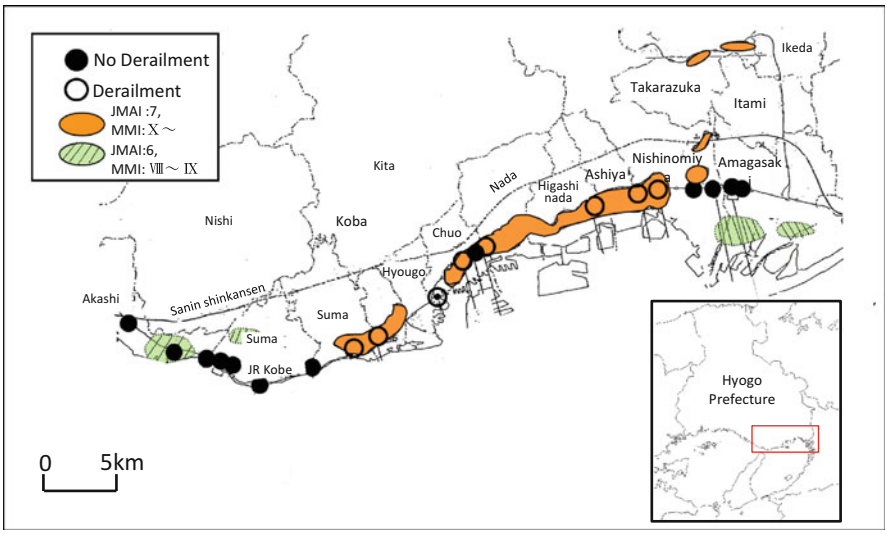

Fig. 1.62 Derailment of trains caused by 1995 Kobe earthquake (after Railway Technical Research Institute [20])

Fig. 1.63 Inclination and subsidence of tanks of petro-chemical products (1995 Kobe earthquake)

heavy damages to structures would not have been caused in Japan, because of high earthquake resistance of structures in our country." Unfortunately, the strong ground motion near the inland fault, which had not been considered in earthquake-resistant design, had sufficient power to destroy various types of infrastructures, houses, buildings and lifeline facilities.

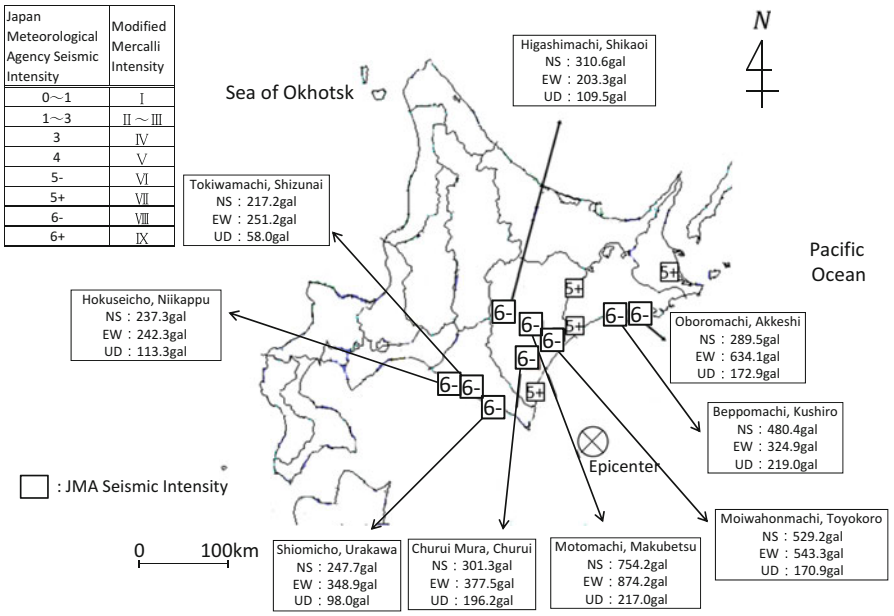

Fig. 1.64 2003 Tokachi offshore earthquake, seismic intensity and maximum ground surface acceleration (cm/s^2)

1.3.4 2003 Tokachi Offshore Earthquake

An earthquake with Mw = 8.0 occurred offshore of Tokachi in Hokkaido on September 26, 2003, with seismic intensity 6 lower in the nine towns of Tokachi (marked as "6−" in Fig. 1.64, equivalent to VIII on the MMI). According to the Japan Meteorological Agency, the epicenter was at 41.46°N and 144.2.64°E and hypocentral depth was about 42 km. This earthquake occurred between the North American and subducting Pacific Ocean plates, the epicenter was on the upper surface of the latter plate.

Figure 1.64 indicates that seismic intensity 6 lower (6−) was recorded over a large area from Niikappu to Akkeshi. Maximum acceleration was 874.2 cm/s^2, recorded by K-NET (Kyoshin network, National Research Institute of Earth Science and Disaster Prevention) at the ground surface of Makubetsu, about 150 km from the epicenter.

There was extensive soil liquefaction across a wide area of southern Hokkaido, from Sapporo to Kushiro. Liquefaction heavily damaged port facilities, embankments, buried pipes, and residential houses. Figure 1.65 illustrates sand boiling and an inclined house at Kiyota in Sapporo, about 300 km from the epicenter. This residential area was constructed on ground by reclamation from a valley.

There was a tsunami along the coast from the cities of Hakodate to Nemuro (Fig. 1.66). According to the Japan Meteorological Agency, maximum tsunami

Fig. 1.65 Sand boiling by soil liquefaction and an inclined house (2003 Tokachi offshore earthquake, at Sapporo)

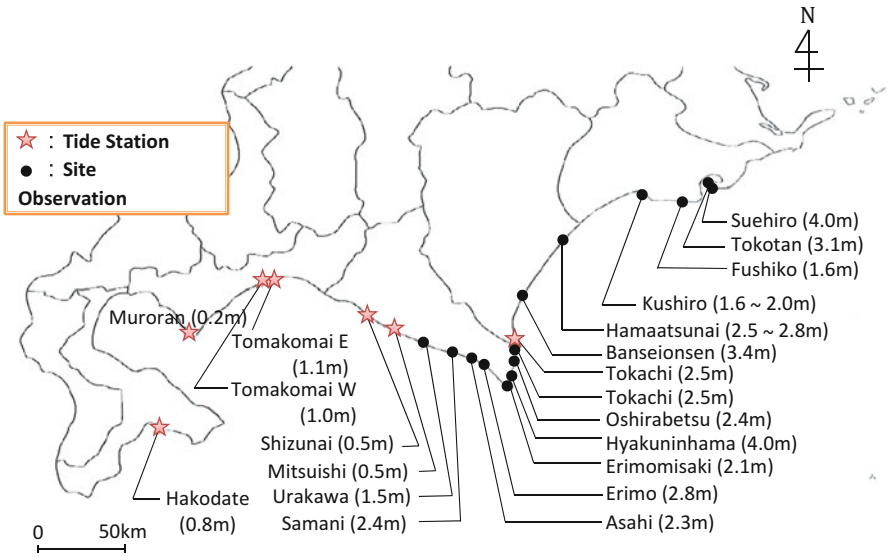

Fig. 1.66 Heights of the tsunami by 2003 Tokachi offshore earthquake (after Japan meteorological agency)

height (rise of seawater along the shoreline) was 4.0 m at Suehiro on Akkeshi Bay and Hyakuninhama on Cape Erimo.

There were no fatalities, but about 840 were injured from Ishikari to Nemuro. There were 1,250 totally or partially collapsed houses. Embankments and bridges of roads and railways, and lifelines were also damaged.

Two floating roof-type tanks of diameter about 40 m burnt down at an oil refinery in Tomakomai (Fig. 1.67). Long-period ground motions caused sloshing vibration of the contents of floating type of tank, which triggered the fires. Figure 1.68 shows accelerations at the ground surface and their velocity response spectra, which were recorded at Tomakomai and Hiroo. The epicenter was off

Fig. 1.67 Fire of oil tanks (2003 Tokachi offshore earthquake, at Tomakomai, after Kyodo Tsushin)

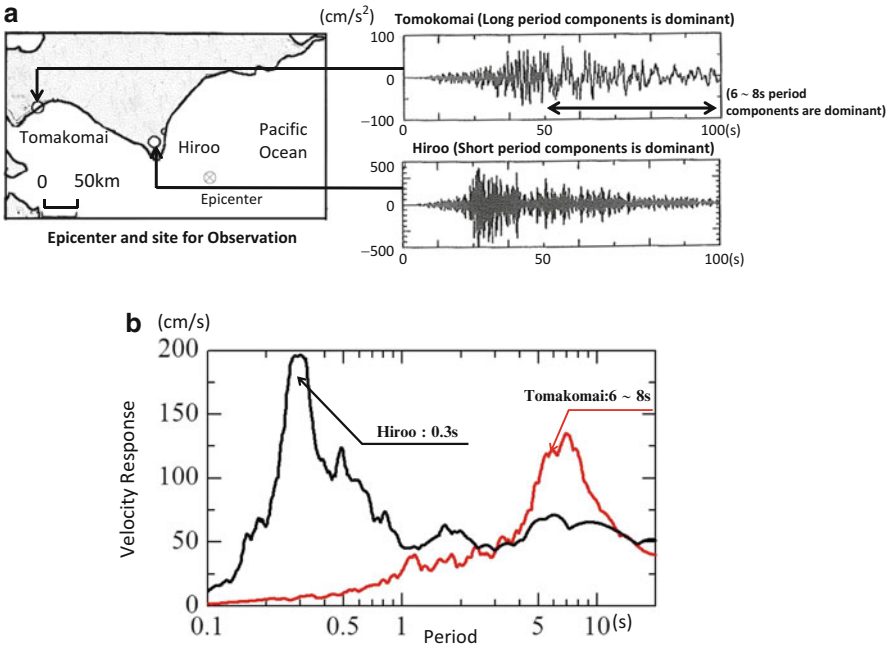

Fig. 1.68 Acceleration at a ground surface at Tomakomai and Hiroo (2003 Takachi offshore earthquake). (**a**) Ground surface acceleration. (**b**) Velocity response spectra of the observed ground motion

the Pacific coast of the Cape of Erimo, and distances to two observatories from the epicenter were about 100 and 250 km. The ground motion at Tomakomai contained long components with periods of 6–8 s. This was not observed in the record at Hiroo, where vibration component of 0.3 s was dominant. The difference of dominant periods resulted from different soil and geological conditions at these two locations. Hiroo is on hard soil, whereas Tomakomai is on soft sediments with thickness about 2 km. This thick sedimentary layer amplified the long-period component of ground motion.

The natural period of sloshing vibration of tank contents was estimated to be about 6–7 s based on Eq. (2.21) in Sect. 2.2.3, Fig. 1.68b shows that the estimated natural period was close to the dominant periods of acceleration observed at Tomakomai. This long-period ground motion induced sloshing vibration of contents in the tanks.

During many earthquakes worldwide, sloshing vibration of oil in large tanks, consequent overflow and fires have been reported. The 1964 Niigata earthquake caused fire in oil tanks, which continued for 2 weeks. As mentioned in Sect. 1.2.1, oil tanks fires were reported during the 1999 Kocaeli earthquake in Turkey.

Several methods have been proposed to prevent this sloshing vibration, but these could not be applied to actual tanks because of technical difficulties. Therefore, the following measures are recommended and required by the Fire Defense Agency to prevent fires at oil refinery and petrochemical plants:

(i) Decreasing volume of contents to avoid the overflow
(ii) Preparation of immediate fire fighting to prevent large fires
(iii) Reinforcement of floating roofs to avoid sinking into the contents

1.3.5 2004 Niigata-Chuetsu Earthquake

On October 23, 2004, the Niigata-Chuetsu earthquake of Mw = 6.8 occurred in central Niigata Prefecture. The epicenter was at 37.17°N and 138.8°E, with hypocentral depth of about 13 km.

According to "Active Faults in Japan, New Edition" [21], several active faults were identified in this area before this earthquake, such as the Nonomi-touge Fault Zone and Tokamachi Fault (Fig. 1.69). However, the epicenter of the Niigata-Chuetsu earthquake was between these two faults, and no active fault had been recognized directly beneath the epicenter. Another oversight of active faults was also reported for the Iwate-Miyagi inland earthquake (mentioned in Sect. 1.3.8). These oversights of active faults demonstrate the difficulty of defining exact locations of inland faults at high accuracy before earthquake occurrence.

Figure 1.70 shows seismic intensities. At Kawaguchi, the highest intensity 7 on the JMAI (equivalent to X or greater on the MMI) was observed. Intensities of 6 higher (shown as $\overline{6}$ in the figure) on the JMAI (IX on the MMI) were recorded in Ojiya, Yamakoshi-mura, and Oguni-cho. There was intensity 6 lower (6 in the figure) across a wide area of Niigata Prefecture.

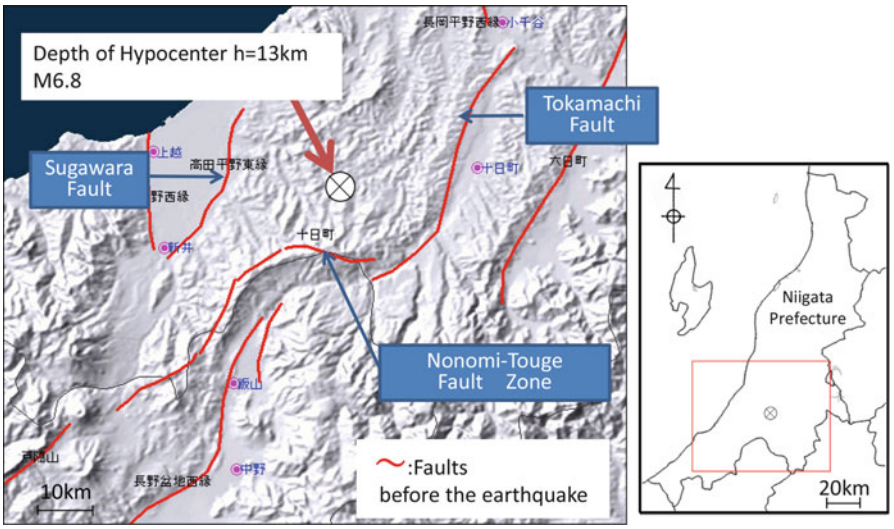

Fig. 1.69 Epicenter of 2004 Niigata-Chuetsu earthquake and active faults [22]

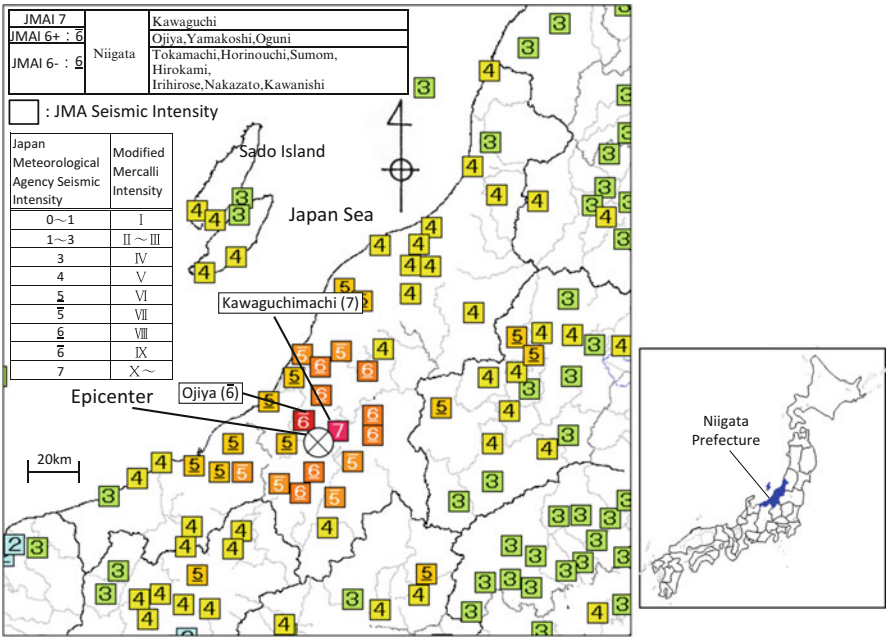

Fig. 1.70 Seismic intensity of 2004 Niigata-Chuetsu earthquake (JMAI)

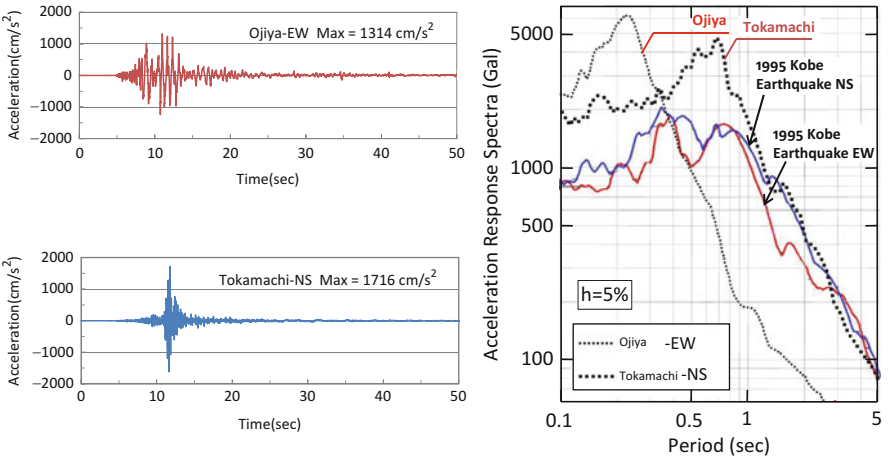

Fig. 1.71 Ground surface accelerations and response spectra at Ojiya and Tokamachi (2004 Niigata-Chuetsu earthquake)

Horizontal accelerations and their response spectra observed by K-NET at the Tokamachi and Ojiya seismic stations are shown in Fig. 1.71. The maximum accelerations (1,314 cm/s^2 at Ojiya and 1,716 at Tokamachi) greatly exceeded the maximum 820 cm/s^2 observed during the 1995 Kobe earthquake. Fortunately, compared with the Kobe earthquake, damage to buildings, houses and bridges was not so heavy, because earthquake ground motions with relatively short periods of 0.2–0.3 s were dominant (as recorded at Ojiya).

This earthquake caused 67 fatalities, including nine dead due to post-trauma stress, and 636 severe injuries. Because there were more than 825 aftershocks, most people could not stay in their damaged homes overnight, but in their cars at night during the cold season. These stressors affected people mentally and physically.

In addition to the human impacts, over 3,000 buildings and houses were destroyed and about 120,000 were partially damaged. Because of damage to buried lifeline pipes, the number of households without electricity, gas and water reached 280,000, 56,000 and 130,000, respectively.

Landslides were a major characteristic of the Niigata-Chuetsu earthquake. Areas impacted by the earthquake were in an active fold zone compressed by oceanic plate movement. Mountain slopes were weathered and vulnerable because of abundant groundwater. Strong ground motion caused many landslides. According to a report from the Ministry of Land, Infrastructure, Transport and Tourism, there were approximately 1,662 landslides totally with 70 million m^3 of debris, which dammed rivers and formed many lakes (Fig. 1.72). Imo River were blocked at 38 locations and maximum water volume of the quake lake reached 2.5 million m^3 (Fig. 1.73).

Another feature of this earthquake was that numerous manholes were lifted by soil liquefaction (Fig. 1.74a). Over 1,400 manholes were lifted in Ojiya, Nagaoka,

Fig. 1.72 Failures of weathered rock slope (2004 Niigata-Chuetsu earthquake)

Fig. 1.73 A quake lake by slope failures (2004 Niigata-Chuetsu earthquake)

and other areas. Figure 1.74b shows subsidence of the ground surface along sewage pipes, caused by liquefaction of backfilling soil.

Figure 1.75 shows the relationship between the rate of lifted sewage manholes (the ratio of the number of lifted manholes to the total number) and micro-

Fig. 1.74 Damage to buried sewage pipes (2004 Niigata-Chuetsu earthquake). (**a**) Uplift of a manhole by liquefaction of backfilling soil (at Nagaoko). (**b**) Subsidence of ground surface by liquefaction of backfilling soil (at Ojiya)

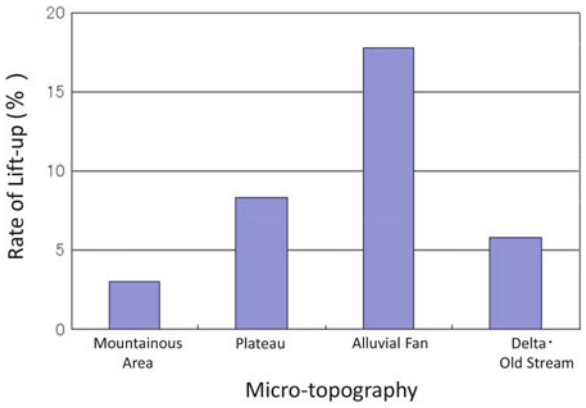

Fig. 1.75 Relationship between rate of lifted sewage manholes and micro-topographical condition (2004 Niigata-Chuetsu earthquake)

topographic conditions in Ojiya. The rate of lifted manholes was higher on the alluvial fan than those in the delta and old river streams. Generally, delta and old streams are considered to be more liquefiable than an alluvial fan, where gravel can release pore water pressure. The reason why many manholes lifted up in alluvial fan was that the sandy backfilling soil was liquefied (Fig. 1.76).

Since the earthquake, to prevent uplift of manholes by soil liquefaction, several measures have been developed and implemented. These include weighting of manholes by cast-metal blocks and hardening of backfill soil by cement milk mixing. Detailed methods are described in Sect. 3.3.3.

Figure 1.77 reveals that the rate of sewerage pipe damage (the ratio of damaged length to total length) was greater in mountainous regions and the delta and old streams than those in the alluvial fan and plateau. Damage to sewage pipes in the mountainous area was caused by landslides and slope failures of road embankments. The reason of high damage rate in delta and old streams was soil liquefaction.

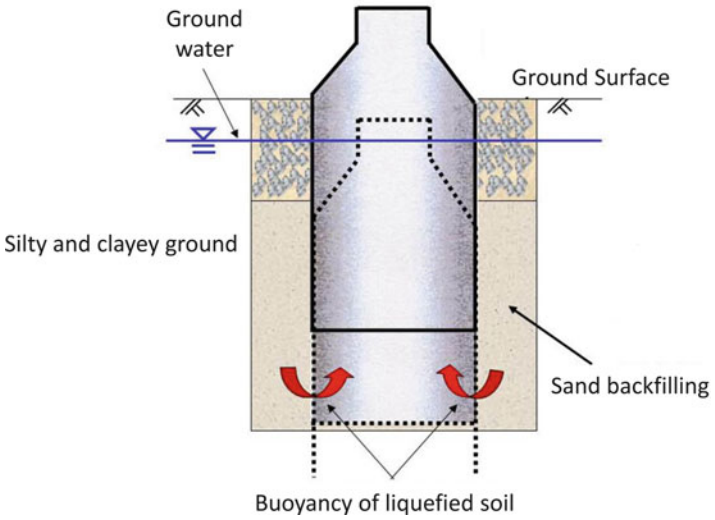

Fig. 1.76 Uplift of manholes by liquefaction of backfill soil

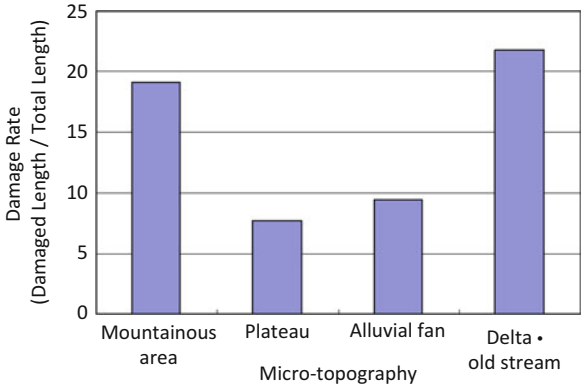

Fig. 1.77 Relationship between damage rate of buried sewage pipe and micro-topographical condition (2004 Niigata-Chuetsu earthquake)

Other notable damage was derailment of the Shinkansen (bullet train) (Fig. 1.78). The Shinkansen No. 325 from Tokyo to Niigata was derailed between Urasa and Nagaoka by strong earthquake motion. Fortunately, there were no deaths or injuries among the 151 passengers. The train was running on a viaduct of 8.82 m height. The viaduct was constructed on river terraces and alluvial lowlands. The earthquake motion was greatly amplified by the surface soil and viaduct. Seismic intensity at the ground surface in the area was 6 lower, JMAI (6 in Fig. 1.70). However, because of amplification of earthquake motion, intensity at the level of the rail increased to 7. As mentioned above, train derailment was also reported during the 1995 Kobe earthquake. Among nine trains in the area of seismic intensity 7, eight trains derailed.

Fig. 1.78 Derailment of Shinkansen due to strong ground motion (2004 Niigata-Chuetsu earthquake)

Enhancement of the safety of high-speed trains against strong ground motion by inland earthquakes directly beneath railways is one of the most important issues toward saving the lives of passengers. Trains with low centers of gravity and devices for safe stop are being developed.

Another issue raised by this earthquake is how to collect and transmit information about damage in isolated mountainous areas with aging populations, and how to recover the long-established culture and tradition of mountain villages.

1.3.6 2007 Noto Peninsula Earthquake [22]

On March 25, 2007, a Mw = 6.9 earthquake occurred offshore of Noto Peninsula. The epicenter was at 37.13°N, 136.41°E, with hypocentral depth of about 11 km. About 20 km of a right lateral reverse fault caused this earthquake (Fig. 1.79). Most of this fault segments are in the seabed, but some are in land. For construction of the Shika nuclear power plant, active faults in areas surrounding the plant were precisely investigated (including the sea), but the active fault that caused the earthquake was overlooked. Sonic exploration was used for investigation of undersea faults, but there were difficulties in clear identification of their existence. Noto Peninsula is in a relatively low seismic activity area in Japan, and the probability of seismic intensity 6 higher, JMAI within the subsequent 30 years had been estimated at 0.1 %. However, intensity 6 higher was observed at Wajima and Anamizu.

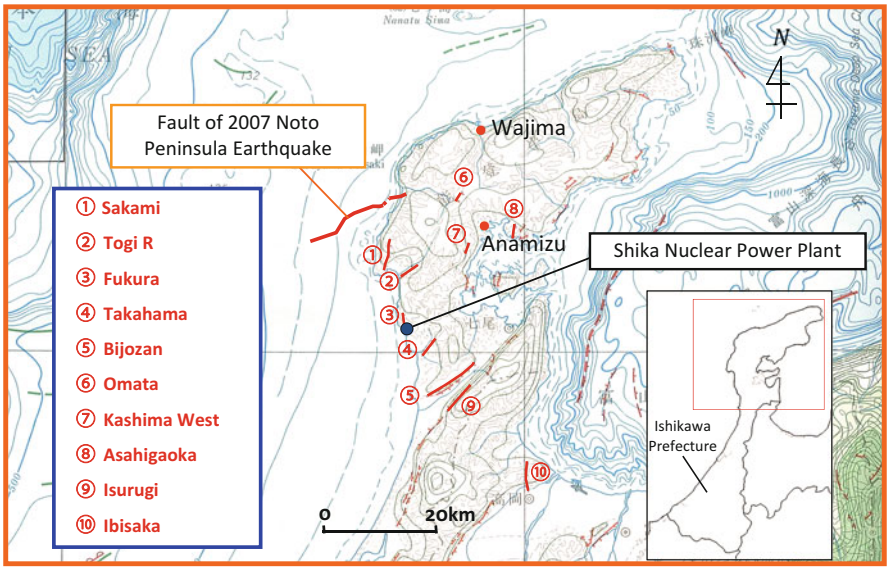

Fig. 1.79 Active faults along west coast of the Noto Peninsula (after the National Institute of Advanced Industrial Science and Technology (AIST))

Maximum acceleration at the ground surface recorded by K-NET in the town of Togi (about 7 km from the epicenter) was 846 cm/s^2 (Fig. 1.80). This acceleration was greater than the 820 cm/s^2 of the Kobe earthquake. Short period components of vibration less than 0.5 s were dominant in the Togi record. This is considered one reason that the degree of the damage to houses and buildings were both less than those of the Kobe earthquake.

One person was killed and 359 were injured. The numbers of totally collapsed or partially damaged houses and buildings were 638 and 13,553, respectively. This earthquake severely damaged road embankments, quay walls, and buried water and sewage pipes. Figure 1.81 shows a collapse of a highway road embankment crossing a valley.

There was also soil liquefaction in extensive areas. At the time of the earthquake, operation of the Shika nuclear power plant had been suspended for periodic inspection. Damage to nuclear facilities and structures was not reported.

1.3.7 2007 Niigata-Chuetsu Offshore Earthquake

On July 16, 2007, an earthquake of Mw = 6.8 occurred off the coast of Kashiwazaki in Niigata Prefecture. The epicenter was at 37°33′24″N, 138°36′30″E, with hypocentral depth of about 17 km. This earthquake was caused by a reverse fault with a compression axis in the southeast-northwest strike. Figure 1.82 shows seismic intensities (JMAI). Intensity 6 higher (6+) was recorded in the cities of Kashiwasaki

Japan Meteorological Agency Seismic Intensity	Modified Mercalli Intensity
0～1	Ⅰ
1～3	Ⅱ～Ⅲ
3	Ⅳ
4	Ⅴ
5–	Ⅵ
5+	Ⅶ
6–	Ⅷ
6+	Ⅸ

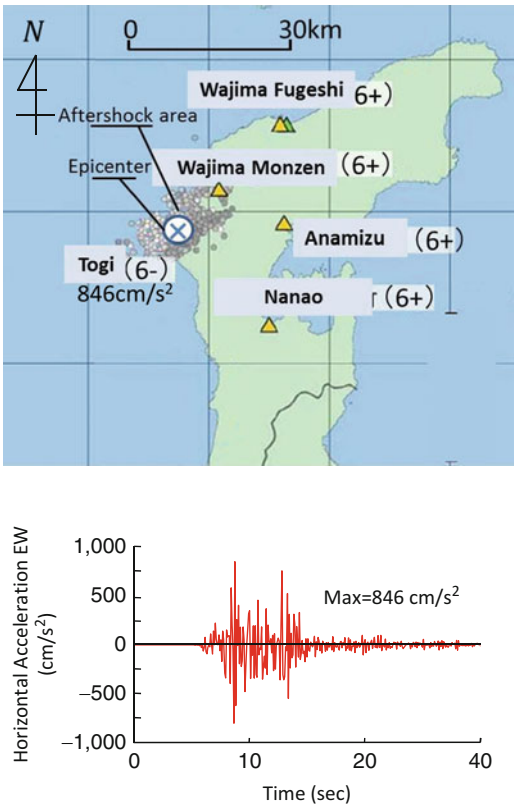

Fig. 1.80 Seismic intensity of 2007 Noto Peninsula earthquake and observed acceleration at Togi. (**a**) Seismi intensity. (**b**) Seismic intensity and horizontal acceleration observed at Togi K-NET

and Nagaoka in Niigata Prefecture and Iizuna-cho in Nagano Prefecture; 6 lower (6−) was measured in Ojiya. This earthquake caused 15 deaths, and 133 completely collapsed and 5,250 partially damaged houses. Because of heavy damage to lifeline systems, the numbers of households without electricity, gas and water were reported as 56,000, 3,400 and 60,000, respectively.

The earthquake raised public attention of seismic safety of nuclear power plants. Several heavy incidents were caused by the earthquake at the Kashiwazaki-Kariwa nuclear power plant, 17 km from the epicenter. These were an electric transformer fire, overflow of cooling water from used fuel storage tanks, derailment of crane, and soil liquefaction.

The earthquake was caused by an active fault unrecognized at the time of design and construction. Ground motion greatly exceeded the design motion. Figure 1.83 shows locations of active faults around the plant. Among these faults, the solid line

Fig. 1.81 Failure of embankment of a highway crossing vollay (2007 Noto Peninsula earthquake)

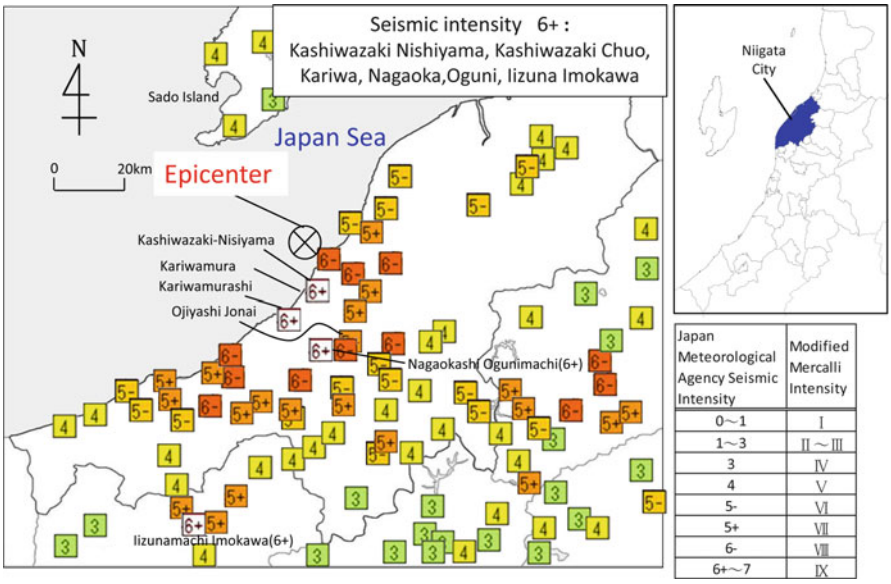

Fig. 1.82 Seismic intensity by 2007 Niigata-Chuetsu offshore earthquake (JMAI)

labeled "B" in the figure was recognized at the time of fault investigation, but was assessed to be "inactive." However, the Headquarters for Earthquake Research Promotion, Ministry of Education, Culture, Sports, Science and Technology (MEXT) reported that the earthquake was caused by rupture of the active fault including the dotted line in the figure, with length 27 km. For the design and

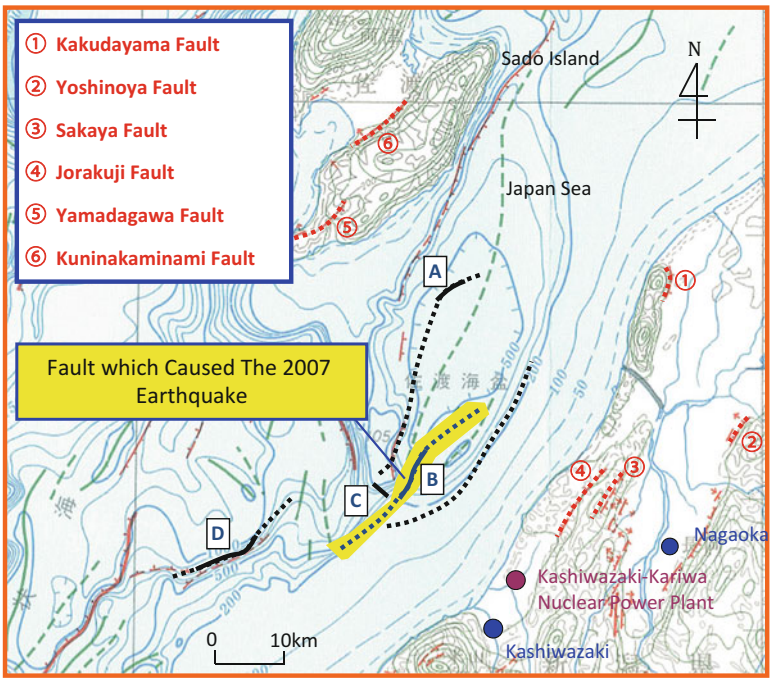

Fig. 1.83 Active faults in the neighborhood of the Kashiwazaki-Kariwa nuclear power plant

construction of nuclear power plants, extensive and careful investigation into active faults nearby the plants is conducted. However, this case reveals that it is difficult to detect all of the potentially influential faults.

Maximum horizontal acceleration of 680 cm/s^2 was observed at the basement of a reactor building. Figure 1.84 compares the acceleration response spectrum for the plant design with that of the observed ground motion. The observed motion was significantly larger than that for the design. Fortunately, there was no radioactive contamination accident. However, the failure to detect the active fault raised a serious question to determine the design ground motion for earthquake resistant design of nuclear power plants.

The earthquake also caused a fire in an electric transformer of the plant. The fire continued for several hours, because of inadequate firefighting systems and facilities. This harmed public confidence on the seismic safety of nuclear power plants. Figure 1.85a shows the plant fire and Fig. 1.85b illustrates the burned transformer. The direct cause of the fire was oil leaking from the transformer. There was a large differential settlement between the foundation of the transformer, which was supported by piles, and the mat foundation of a cable rack.

The utmost goal of earthquake-resistant design of nuclear power plants is to prevent radioactive contamination and leakage of nuclear materials by

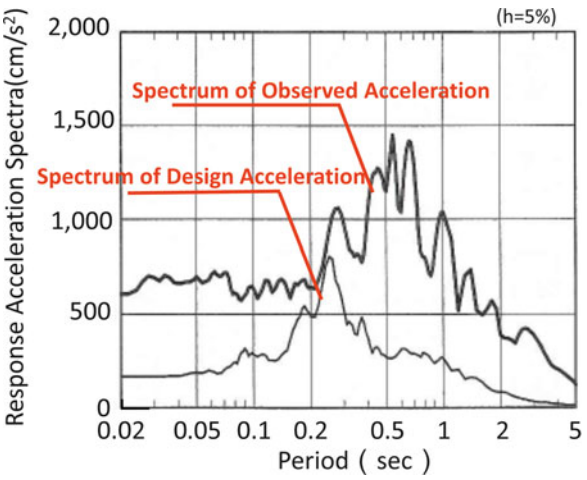

Fig. 1.84 Response spectrum of ground motion observed at the basement of nuclear reactor building and design spectrum (2007 Niigata-Chuetsu offshore earthquake)

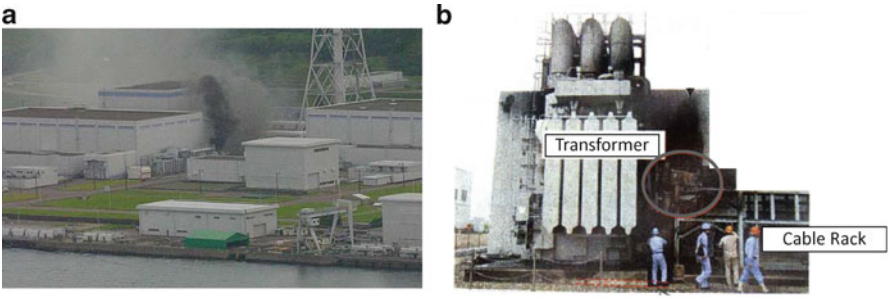

Fig. 1.85 Fire of an electric transformer at Kashiwazaki-Kariwa nuclear power plant (2007 Niigata-Chuetsu offshore earthquake). (**a**) Fire of electric transformer. (**b**) Differential subsidence of foundations between the electric transformer and cable rack

earthquakes. From this standpoint, the plant design satisfied the goal, but the differential settlement between two neighboring facilities led to the fire. This accident showed the necessity to revise the design method of so-called C-class structures, which were required to resist against earthquake ground motions of medium intensity.

The author surveyed damage to buried sewage pipes caused by the earthquake within approximately 40 km^2 of Kashiwazaki, over a total length of 112 km. Figure 1.86 shows the relationship between damage rate of buried pipes and manholes with micro-topographic conditions, categorized into natural levee, sand dune, alluvial plain, alluvial fan and terrace. The damage rate of the buried pipes is the ratio of the number of damaged sections between two neighboring manholes to the total number of sections. Seventy percent of the damage to sewage pipes was bending deformation caused by differential settlement of ground. Other damage

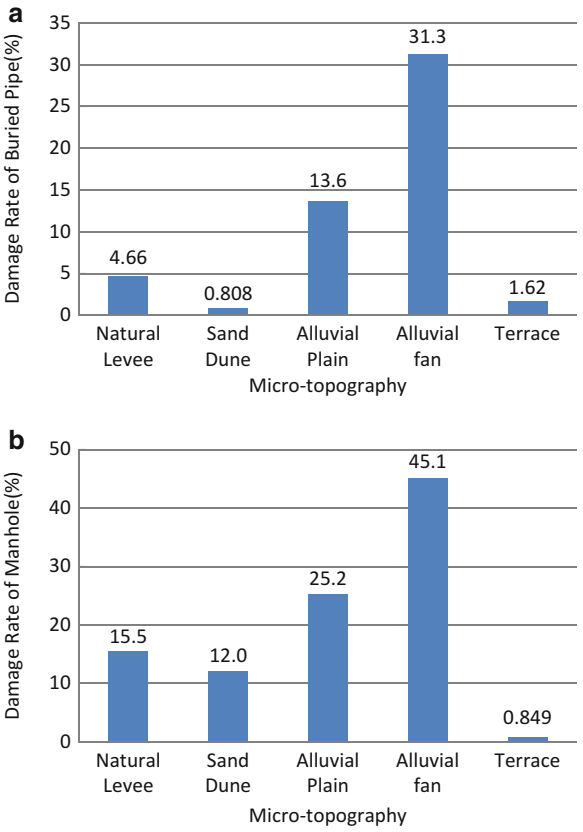

Fig. 1.86 Relationship between damage rate of buried sewage pipes and micro-topographical condition (2007 Niigata-Chuetsu offshore earthquake, Kashiwazaki). (**a**) Damage rate of buried sewage pipes and micro-topographical condition. (**b**) Damage rate of manholes and micro-topographical condition

was the rupture of joints and inverse gradient of pipes. Approximately 90 % of pipe material was polyvinyl chloride (PVC). Damages to manholes were uplift by soil liquefaction, rupture of manhole concrete, and water and soil inundation. The damage rate of buried pipes and manholes was higher on the alluvial fan and alluvial plain. The reason for this is liquefaction of backfilling soil.

Figure 1.87 shows the number of dead in each age group by the 2007 Niigata-Chuetsu offshore earthquake and the 2004 Niigata-Chuetsu earthquake. Larger number of dead over 60 years reveals that the area had an aging population and that the elderly were more vulnerable to the disaster.

1.3.8 2008 Iwate Miyagi Inland Earthquake

On June 14, 2008, an earthquake of $M_w = 6.9$ occurred in the mountainous region of southern Iwate Prefecture. The epicenter was at N39°01′ and E140°53′, with hypocentral depth of 8 km. Figure 1.88 depicts seismic intensities in Iwate, Akita

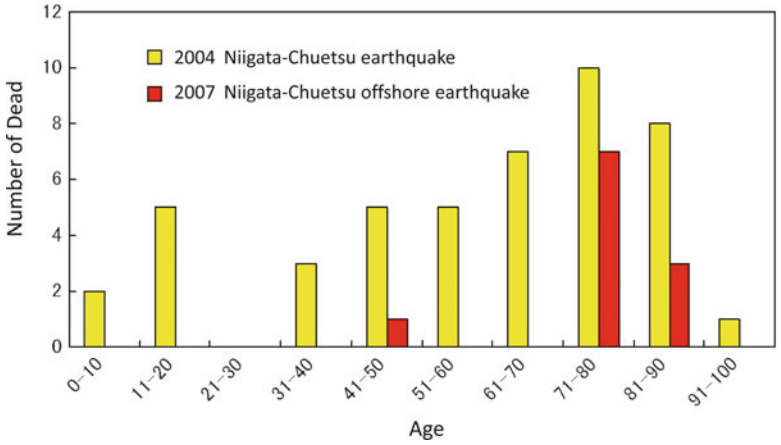

Fig. 1.87 Numbers of dead by 2004 Niigata-Chuetsu offshore earthquake and 2007 Niigata-Chuetsu offshore earthquake

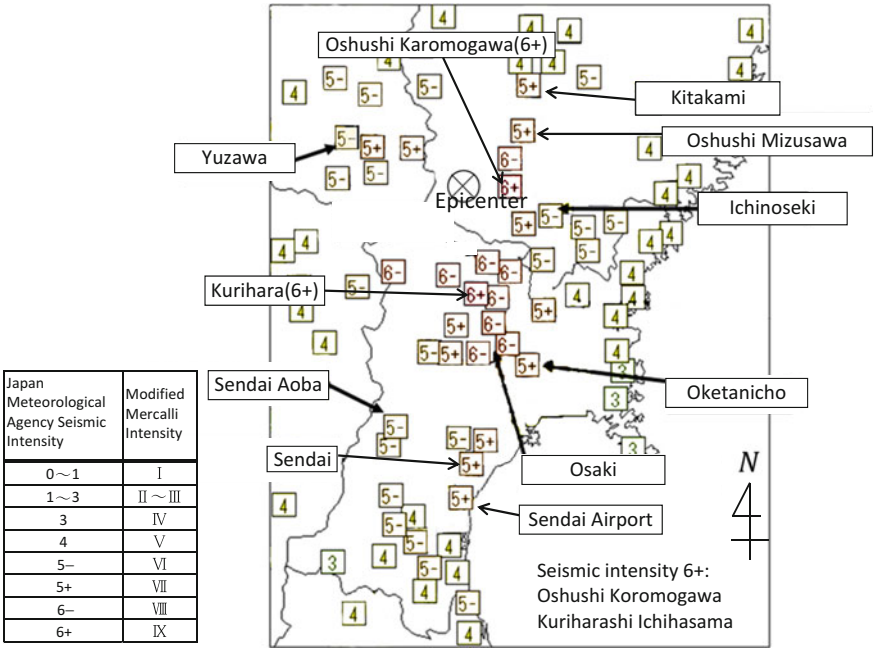

Japan Meteorological Agency Seismic Intensity	Modified Mercalli Intensity
0～1	Ⅰ
1～3	Ⅱ～Ⅲ
3	Ⅳ
4	Ⅴ
5–	Ⅵ
5+	Ⅶ
6–	Ⅷ
6+	Ⅸ

Fig. 1.88 Seismic intensity by 2008 Iwate-Miyagi inland earthquake

and Miyagi Prefectures. Intensity 6 higher (6+, JMAI) was recorded in the cities of Kurihara and Oshushi. Accelerations at the ground surface and underground were observed at many K-NET and KiK-net (Kiban-Kyoshin Net) points of the National Research Institute for Earth Science and Disaster Prevention. A maximum vertical

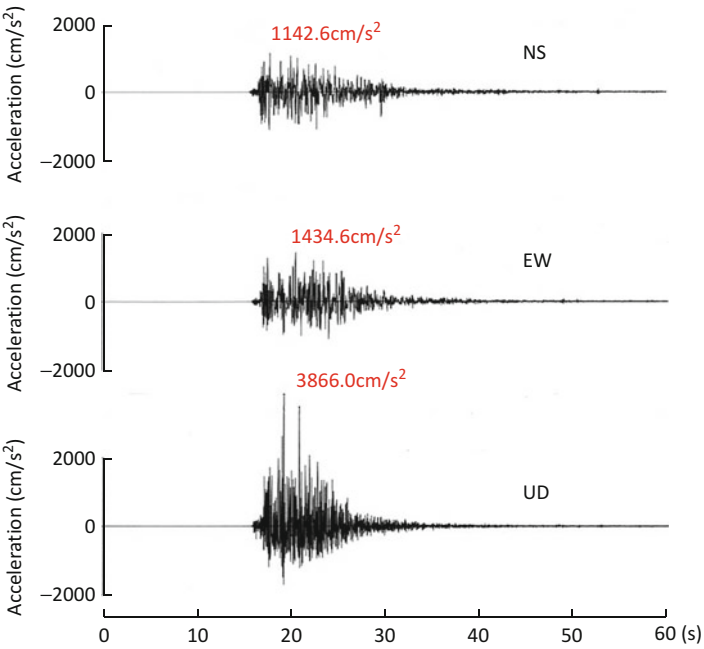

Fig. 1.89 Accelerations observed at ground surface in Ichinoseki (2008 Iwate-Miyagi inland earthquake)

acceleration of 3,866 cm/s^2 was recorded at an observation point in Ichinoseki, 21 km from the epicenter. Maximum horizontal acceleration there was 1,434 cm/s^2, much less than that in the vertical, as shown in Fig. 1.89. This might be a characteristic of inland earthquakes.

A seismological survey after the earthquake indicated that it was caused by a reverse fault, but its epicenter was not on any active fault identified prior to the event (Fig. 1.90) [21]. As in the case of the 2004 Niigata-Chuetsu earthquake, this shows the difficulty of predicting the exact locations of earthquakes caused by inland active faults.

The number of dead and missing was 23, and those of destroyed houses and partially damaged houses were 2,667. The epicenter was in a mountainous region, so there were many large-scale slope failures. Most of these failures were reported to concentrate on the hanging wall side of the reverse fault. Large amounts of landslide debris dammed river streams, creating lakes. There were also slope slides of road and railway embankments.

Figure 1.91 shows a huge slope sliding around Aratosawa reservoir, the largest caused by the earthquake. Total length and width of this sliding were 1,300 m and 900 m, respectively. Approximately 7 million m^3 of soil surged downward about 300 m. A ground surface of volcanic ash caused the large-scale slope slide.

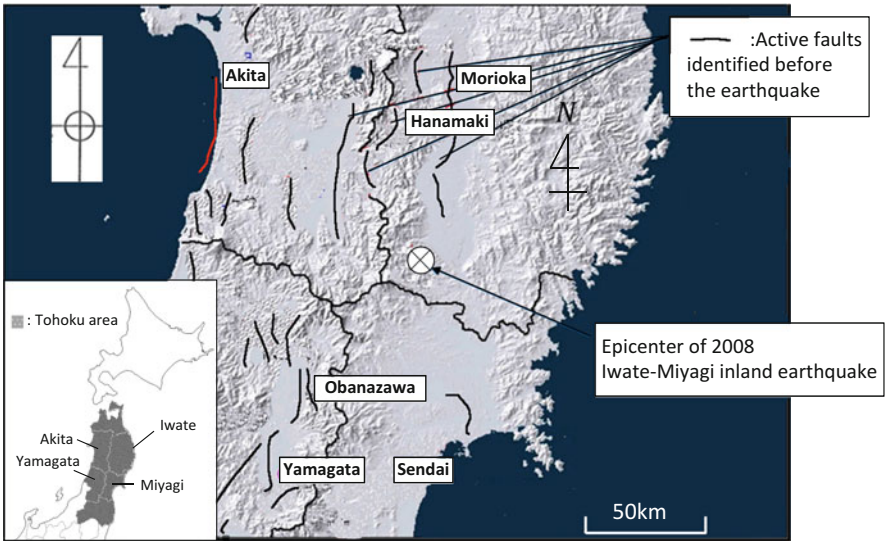

Fig. 1.90 Epicenter of 2008 Iwate-Miyagi inland earthquake and active faults in Tohoku area (after active faults in Japan [21])

Fig. 1.91 Large slope slide at Aratosawa dam lake, (2008 Iwate-Miyagi inland earthquake length: 1.3 km,width: 900 m, debris volume: 70×10^6 m^3)

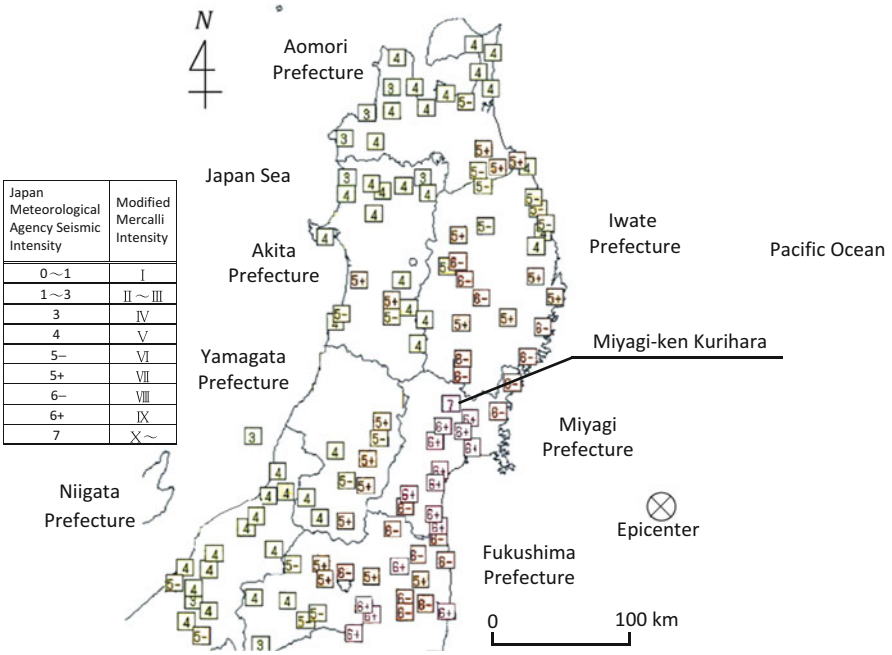

Japan Meteorological Agency Seismic Intensity	Modified Mercalli Intensity
0～1	Ⅰ
1～3	Ⅱ～Ⅲ
3	Ⅳ
4	Ⅴ
5–	Ⅵ
5+	Ⅶ
6–	Ⅷ
6+	Ⅸ
7	Ⅹ～

Fig. 1.92 Seismic intensity by 2011 Tohoku earthquake (JMAI)

1.3.9 2011 Tohoku Earthquake (Great East Japan Earthquake and Tsunami Disaster) [23–25]

At 2:46 PM on March 11, 2011, there was a gigantic earthquake of Mw = 9.0. Its source area was extensive, from offshore of Iwate Prefecture to that of Ibaraki Prefecture. The earthquake was on the boundary between the Pacific Ocean and North American plates. This was the largest recorded earthquake in Japanese history. The epicenter was at 38°10′N and 142°86′E, with hypocentral depth of 24 km. Seismic intensities 6− and 6+ were observed over a vast area in Tohoku region (Fig. 1.92), with intensity 7 in Kurihara in Miyagi Prefecture. Figure 1.93 shows the maximum acceleration observed by K-NET and KiK-net. At the ground surface of Tsukidate in Iwate Prefecture the maximum horizontal acceleration was 2,700 cm/s^2.

According to the National Police Agency, the number of the dead was 15,782, and that of the missing 2,769. The number of completely or partially destroyed houses and buildings was 395,822.

A huge tsunami triggered by the earthquake attacked large areas of the coast from the northern Tohoku region to the Shikoku region. Figure 1.94 shows that maximum wave height (about 13 m) was observed at the coast of Iwate Prefecture,

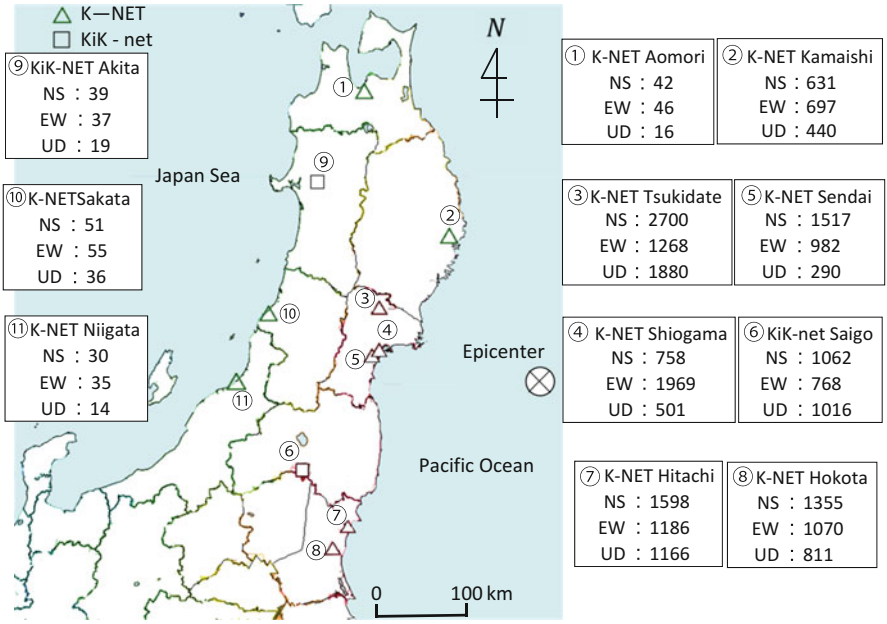

Fig. 1.93 Maximum accelerations at ground surface (2011 Tohoku earthquake, cm/s^2)

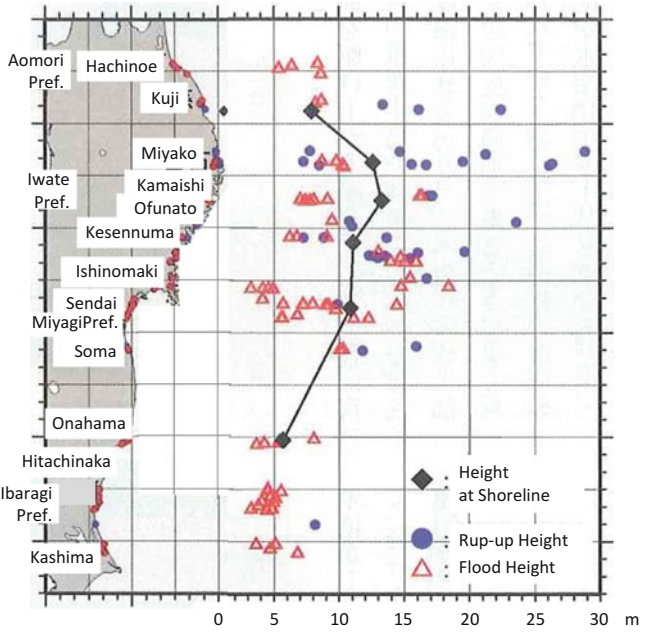

Fig. 1.94 Height of the tsunami (2011 Tohoku earthquake, after port, harbor and airport research institute)

Table 1.4 Rate of dead and missing of Kamaishi and Kesennuma

	Kamaishi	Kesennuma
Death/missing rate in the city	$\frac{1,091}{39,508} = 2.76\ \%$	$\frac{1,407}{74,247} = 1.90\ \%$
Children & students' death rate	$\frac{5}{3,244} = 0.15\ \%$	$\frac{12}{6,054} = 0.20\ \%$
Disaster education		
Basic concept	"Safety of the children"	"Disaster mitigation by self-act and help one another"
Tool for disaster education	Moving tsunami hazard map	Digital library of tsunami

and the run-up height reached about 30 m in the same area. Most of the dead and missing in the Tohoku region were attributed to this tsunami.

The Headquarters for Earthquake Research Promotion of MEXT had predicted that a mid-size earthquake of Mw = 7.5 would occur with 99 % probability in the next 30 years. The actual earthquake had 180 times greater energy than the predicted one. The headquater had predicted that in addition to the Mw = 7.5 earthquake, another of Mw = 7.7 would occur near the Japan Sea Trough. The headquater indicated that if these two earthquakes occurred simultaneously, their combined magnitude would be 8.0. The energy of the actual earthquake was still 32 times greater than that of these combined earthquakes.

Prior to the Tohoku earthquake, a group of Japanese seismologists pointed to the possibility of reoccurrence of the Jogan earthquake in 869. It was reported that a large tsunami caused by this earthquake had struck similar areas along the Pacific coast of Tohoku. However, these seismologists' opinions were not referred to national disaster mitigation strategies.

More than 16,000 lives were lost by the great tsunami. Direct causes and processes of this loss of life should be carefully examined. These should be related to the effectiveness of tsunami warning and its transmission, the density of and distance to evacuation shelter, evacuation behaviors of the dead and survivors, and efficiency of evacuation training and education.

The cities of Kamaishi and Kesennuma were good examples for demonstrating the effectiveness of disaster education and training. Both cities have been eagerly promoted disaster-prevention education and established evacuation systems, with aid from MEXT. Table 1.4 shows fatality ratios of the total population, as well as those of elementary school children and middle high school students in both cities. The ratio of dead and missing children and pupils is mostly less than 1/10 that of the entire population. Both cities had been repeatedly conducting disaster-prevention education and evacuation training for the children and pupils. The fatality ratios shown in Table 1.4 prove that the disaster-prevention instruction and evacuation training were effective to save lives.

Fig. 1.95 Five Story concrete building survived from the tsunami (2011 Tohoku earthquake, at Rikuzen-Takada)

The tsunami inflicted extensive damage on residential houses, buildings, and infrastructures such as roads, railways and lifelines. The accident at the Fukushima Daiichi Nuclear Power Plant is especially serious, and had never been experienced in Japan. All power systems for cooling the nuclear reactors and spent fuel were completely lost, causing a hydrogen explosions. This resulted in contamination by large amounts of radioactive materials, not only in Fukushima Prefecture, but also in large areas of the Kanto region. At the time of this writing, there is no certain prospect for containing this tragic accident.

Although many structures and facilities were destroyed by the tsunami, some structures surved. Figure 1.95 shows a survived five-story RC building, which located on the seashore of Rikuzen-Takada. No structural damage was found in the concrete superstructure and on concrete piles. The water level reached the fifth story and the tsunami passed through the building. Figure 1.96 shows survived viaduct for a road along the shore of Kamaishi. The tsunami reached the top of the concrete bridge piers, but no structural damage to the piers was reported.

In addition to the tsunami damage, the 2011 Tohoku earthquake triggered soil liquefaction across broad areas from the Tohoku to Kanto regions. Especially on artificial islands reclaimed from Tokyo Bay, there was extensive soil liquefaction. In Urayasu, located along Tokyo Bay in Chiba Prefecture, more than 5,000 houses and buildings inclined and subsided. Soil liquefaction also severely damaged lifeline facilities such as buried pipes and sewage manholes.

Fig. 1.96 A concrete viaduct for road survived from the tsunami (2011 Tohoku earthquake, at Kamaishi)

Using satellite and aerial photos of the reclaimed lands around Tokyo Bay taken before and after the earthquake, the author found traces of sand boils and identified locations of soil liquefaction. An example of sand boiling traces is shown in Fig. 1.97. Figure 1.97a is an aerial photo taken half year before the earthquake, and Fig. 1.97b shows the same area 20 days after the earthquake. On the surface within the circles, the traces of sand boiling can be seen. The sites of soil liquefaction surveyed by the aerial photos around the Tokyo Bay are summarized in Fig. 1.98. The result shows that most of the bay areas liquefied. Figure 1.99 shows a lifted sewage manhole in Urayasu, and sand and water boils in reclaimed land of Kawasaki.

The 2011 Tohoku earthquake also severely damaged industrial complexes atop reclaimed land around Tokyo Bay. Figure 1.100 shows the locations of 11 accidents caused by the earthquake. At an oil refinery plant in Ichihara, 17 LPG tanks exploded and burst into flames. It was reported that iron fragments from exploded tanks were scattered over residential areas about 6 km away. Furthermore, sinking of floating roofs into oil and oil leakage caused by sloshing vibration was also reported.

Along coastal areas of the Tohoku region, there were also accidents at petrochemical facilities (Fig. 1.101). In Kesennuma in Miyagi Prefecture, twenty two fuel tanks for fishing boats floated out to sea by the tsunami and ruptured. This generated large fires on the sea, which spread to residential areas on land.

Figure 1.102 shows the tsunami height around Tokyo Bay. The highest was 2.8 m at Kisarazu in Chiba Prefecture. The tsunami impact was not considered in

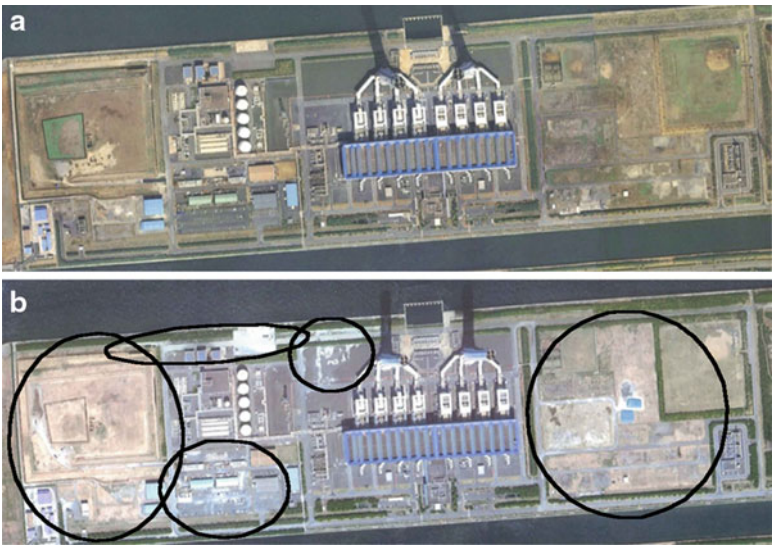

Fig. 1.97 Soil liquefaction in power plant around the Tokyo Bay (2011 Tohoku earthquake). (**a**) Before the earthquake (2009.10.16). (**b**) After the earthquake (2011.3.31) (identification of liquefaction traces by aerial photographs, *circles* show the traces of the sand boiling)

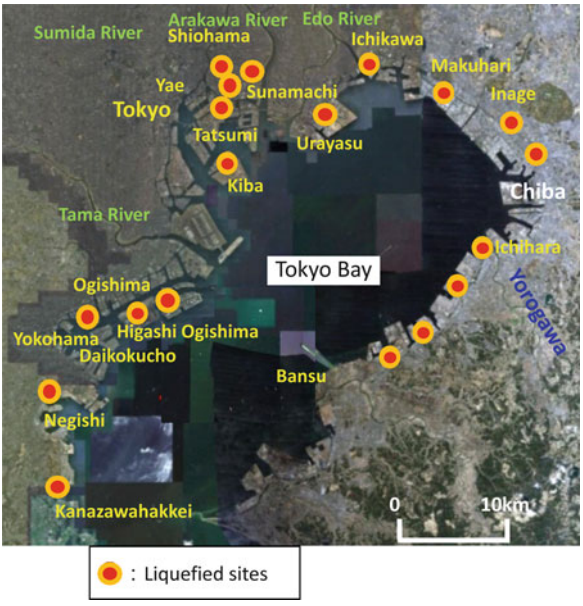

Fig. 1.98 Sites of soil liquefaction in reclaimed area around the Tokyo Bay (2011 Tohoku earthquake)

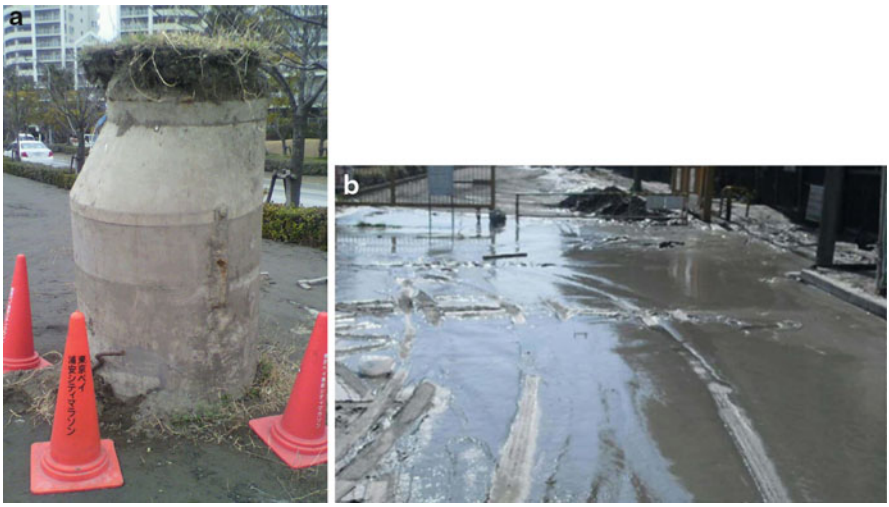

Fig. 1.99 Uplift of a manhole and sand boils (2011 Tohoku earthquake). (**a**) Uplift of a manhole (at Urayasu). (**b**) Sand and water boil (at Kawasaki)

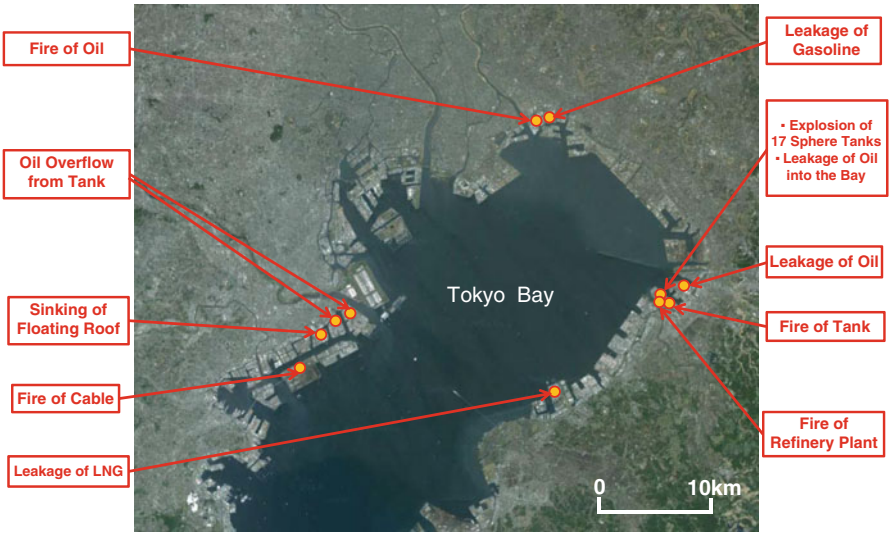

Fig. 1.100 Accidents in industrial complexes around the Tokyo Bay (2011 Tohoku earthquake)

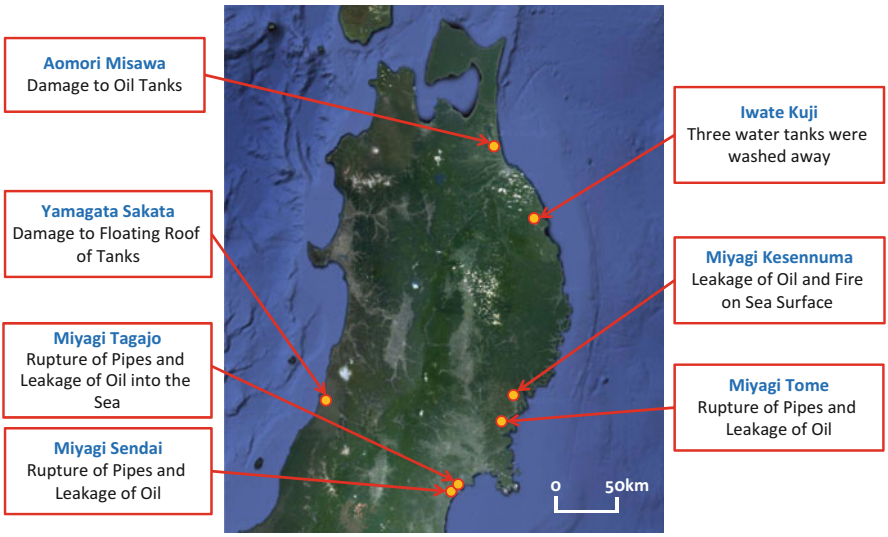

Fig. 1.101 Damage to oil petro-chemical facilities in Tohoku district (2011 Tohoku earthquake)

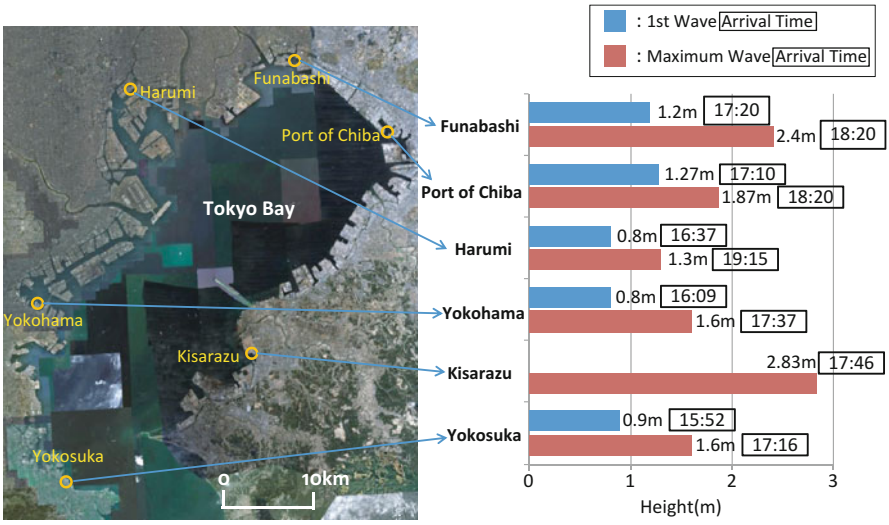

Fig. 1.102 Tsunami height and arrival time in the Tokyo Bay (2011 Tohoku earthquake)

the design and construction of industrial complexes around the bay. The tsunami damage from the Tohoku earthquake has raised a heavy issue how to protect industrial complexes around the bay areas of big cities, such as Tokyo, Osaka and the others against the future tsunamis.

References

1. Cabinet Office of Japanese Government (2010) While note of disaster prevention (in Japanese)
2. Home Page of Japan Metrological Agency. http://www.jma.go.jp/jma/index.html
3. Home Page of United States Geological Survey. http://www.usgs.gov/
4. Cabinet Office of Japanese Government (2011) Disaster management in Japan
5. Japan Society of Civil Engineers (JSCE) (1999) The 1999 Kocaeri earthquake, Turkey. Earthquake damage investigation series 5
6. Rellinger R et al (2006) GPS constraints on continental deformation in the AFRICA-Arabia-Eurasia continental collision zone and implications for the dynamics of plate interactions. J Geophys Res 111:B054111
7. JSCE (1999) The 1999 Chi-Chi earthquake, Taiwan. Earthquake damage investigation series 6
8. JSCE (2001) The 2001 Kachchh earthquake Gujarat state, India. Earthquake damage investigation series 7
9. Biswas SK (1987) Regional tectonic framework, structure and evolution of the western marginal basin of India. Technophysics 135:307–327
10. Japan Association of Earthquake Engineering (JAEE), JSCE, Architectural Institute of Japan (AIJ), Japan Geological Society (JGS) (2004) Boumerdes earthquake, The 21st May
11. Hirata K, Satake K, Tanioka Y, Kuragano T, Hasegawa Y, Hayashi Y, Hamada M (2006) The 2004 India Ocean tsunami, source model from satellite altimetry. Earth Planets Space 58:195–201
12. JSCE, AIJ (2005) Joint investigation/technical support team for resonation and reconstruction of the affected areas by the Pakistan earthquake on Oct 8
13. Ulrich K et al (2008) GIS-based landslide susceptibility mapping for the 2005 Kashmir earthquake region. Geomorphology 101:631–642
14. Hamada M, Wu X (2009) The Wenchuan earthquake, its caused damage, recovery and reconstruction. Earthquake J 47:27–31 (in Japanese)
15. Xu X et al (2009) Seismic reverse and oblique: slip surface faulting generated by the 2008 Mw 7.9 Wenchuan earthquake, China. Geology 37(6):515–629
16. JSCE (1993) Report on 1993 Kushiro offshore earthquake and its caused damage. Earthquake damage investigation series 7 (in Japanese)
17. Iai S et al (1994) Effectiveness of soil improvement on Quay walls during 1993 Kushiro offshore earthquake. In: 9th Japan earthquake symposium on earthquake engineering, pp 757–762 (in Japanese)
18. JSCE, AIJ, JGS, Japan Society of Mechanical Engineers (JSME), Seismological Society of Japan (SSJ) (1999) Report on the Hanshin-Awaji earthquake disaster (in Japanese)
19. Sekiguchi H et al (1996) Determination of the location of faulting beneath during the 1995 Hyogoken-Nanbu earthquake from near-source particle motion. Geophys Res Lett 23(4): 387–390
20. Railway Technical Research Institute (1996) Damage to railway facilities by repent on the 1995 Kobe earthquake, special vol 4 (in Japanese)
21. The Research Group for Active Faults of Japan (1991) Active faults in Japan, revised edition. University of Tokyo, Tokyo
22. JSCE (2007) Report on the 2007 Noto Peninsula earthquake and its caused damage (in Japanese)
23. AIJ (2012) Preliminary reconnaissance report of the 2011 Tohoku-Chiho Taiheiyo-Oki earthquake
24. Kashimura S, Hayashi S, Gokon H (2013) Lessons from the 2011 Tohoku earthquake tsunami disaster. J Disast Res 8(4):549–559
25. Tomita T (2013) The 2011 off the Pacific coast of Tohoku earthquake tsunami. J Disast Res 8(4):594–604

Chapter 2
Earthquake-Resistant Design and Reinforcement

Abstract For the methods of earthquake resistant design of structures, firstly the seismic coefficient method and the modified seismic coefficient method in which the response spectra are used, are explained, and the development of the design methods against soil liquefaction as well as long period components of earthquake ground motion are introduced.

The new concept for earthquake resistant design against two levels of ground motion, and the revisions of the design codes and standards after the 1995 Kobe earthquake are described. Furthermore, theory on S-wave propagation and the characteristics on the response of the surface ground, amplification of ground motion and dominant period are explained. The mass-spring model is explained to solve the dynamic response of surface ground.

In addition, the design procedure of nuclear power plant and tsunami-resistant measures after the 2011 Tohoku earthquake are introduced. Furthermore, technologies of reinforcement of existing structures are introduced.

Keywords Earthquake-resistant design • Mass-spring model • Nuclear power plant • Response spectrum • Seismic wave propagation • Tsunami

2.1 Beginning of Earthquake-Resistant Design in Japan

2.1.1 Earthquake Engineering and Seismology

The difference between earthquake engineering and seismology might be difficult to understand for non-professional people outside these fields. Characteristics of active faults that cause earthquakes and propagation of seismic waves in the earth crust are investigated in seismology, and are illustrated in Fig. 2.1. One of the major objectives of seismology is earthquake prediction. As seen in the 2011 Tohoku earthquake (Great East Japan Earthquake and Tsunami Disaster), seismology was completely unable to predict an earthquake of $M_{JMA} = 9.0$ (magnitude on the

M. Hamada, *Engineering for Earthquake Disaster Mitigation*,
Springer Series in Geomechanics and Geoengineering,
DOI 10.1007/978-4-431-54892-8_2, © Springer Japan 2014

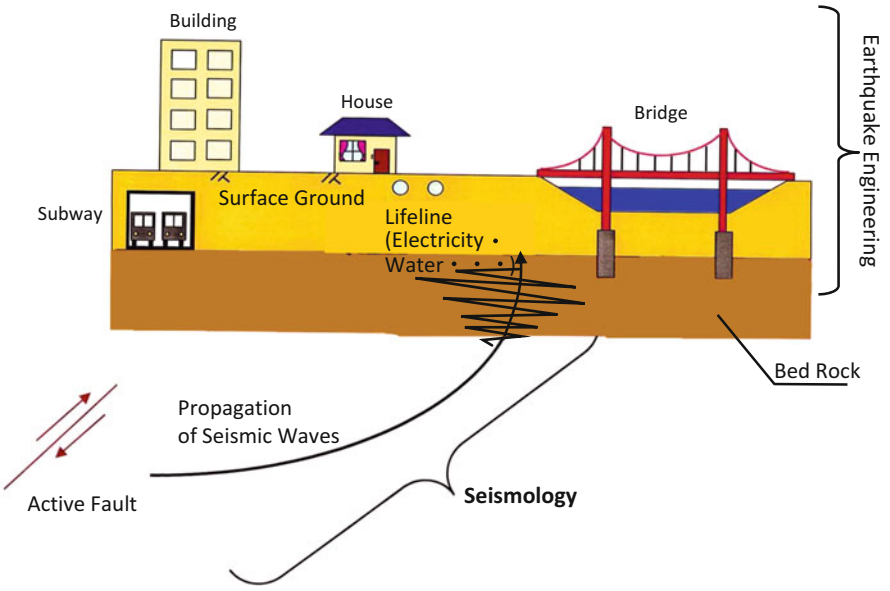

Fig. 2.1 Earthquake engineering and seismology

Japan Metrological Agency scale). Therefore, whether earthquake prediction will be able to significantly contribute to mitigation of earthquake disasters in the next several decades is very questionable, because problems may persist. A thorough examination of the failure of prediction of the 2011 Tohoku earthquake are indispensable. Without this endeavor, there should be no expectation of new developments in earthquake prediction in our country. Furthermore, it is very important to explain to people that short-period earthquake prediction from 1 day to several weeks before an earthquake will be impossible.

The purpose of earthquake engineering is to analyze the response of structures such as buildings, bridges and surface ground to earthquake motions, and ensure their safety. The ultimate goal of this engineering is to create safer and more secure societies, based on the design and construction of structures.

Originally, the seismology discipline was developed by scientific researchers engaged in studies such as geophysics. In contrast, earthquake engineering is peopled by civil engineering, mechanical engineering, geological engineering, and related fields.

In the scientific field, researchers are asked to make predictions of earthquake probability and severity. In the engineering field, researchers are tasked with preventing loss of life and property by ensuring the safety of structures during future earthquakes and the tsunamis they induce. If both seismologic science and earthquake engineering execute their individual obligations and collaborative roles, a safe and risk-free society in the face of earthquakes and tsunamis would be achieved. However, it is a matter of regret that the activities of both fields have never been fully in cooperation, and that this was one of the principal causes of the great disaster of the Tohoku earthquake and tsunami.

Fig. 2.2 Damage to modernistic buildings by 1923 Kanto earthquake (home page of the National Science Museum)

2.1.2 Beginning of Earthquake-Resistant Design: Seismic Coefficient Method

Attention has been paid to earthquake-resistance of structures such as buildings and bridges, particularly since the 1923 Kanto earthquake (Great Kanto Earthquake Disaster), More than 576,000 houses and buildings were destroyed and burnt by the earthquake. Because of fires after the earthquake, there were more than 140,000 dead and missing. This earthquake has been regarded as the most serious calamity in modern history in Japan. Modernistic buildings constructed by European and American technologies during the Meiji Era (1868–1912) were greatly damaged in this event, as shown by Fig. 2.2.

In 1917, 6 years before the Great Kanto earthquake, Sano had proposed so-called seismic coefficient method to enhance the earthquake resistance of structures [1]. Figure 2.3 explains the concept of this method, where inertia force caused by earthquake motion is taken into the consideration for the design of structures, with addition of the self weight W. The inertia force H acting horizontally on the structures is obtained by W multiplied by horizontal seismic intensity coefficient K_H. That is, H is set to several tens of percent of W to examine building stability and the stress on individual members of buildings.

$$H = K_H \cdot W \tag{2.1}$$

One of subjects to apply the seismic coefficient method to actual design, is how to determine the horizontal seismic intensity coefficient. At the beginning of the adoption of this methods, about 10 % of the structure weight W, namely $K_H \fallingdotseq 0.1$,

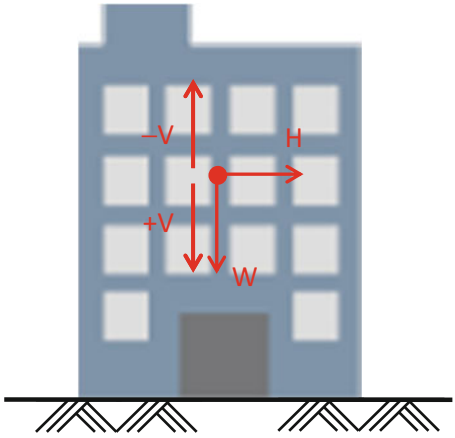

Fig. 2.3 Earthquake resistant design by the seismic coefficient method

was considered as the horizontal force. However, importance of the structures, impact of destruction of structures and other influential factors on society came to be considered later. Thus, larger values coefficient of seismic intensity gradually came to be adopted. Current horizontal seismic intensity coefficients in Japan are roughly shown below.

Ordinary buildings/bridges ≒ 0.2
Oil and petrochemical products ≒ 0.3 to 0.6
Dams ≒ 0.15
Port and harbor facilities ≒ 0.15 to 0.20
Nuclear power structures = 0.2 ∼ 0.6

As shown above, the seismic coefficient greatly depends on the type of structure. This is because characteristics of the dynamic response to earthquake motions and the importance of structures are, as stated above, under consideration.

The horizontal force H is the inertia force caused by an earthquake that acts on structures, therefore can be expressed as,

$$H = \alpha_m \cdot M \tag{2.2}$$

where α_m is the maximum horizontal acceleration on the structures by earthquake ground motion, and M is their mass. Eq. (2.2) can be rewritten as

$$H = \frac{\alpha_m}{g} \cdot M \cdot g \tag{2.3}$$

where g is gravitational acceleration (980 cm/s^2) and $M \cdot g$ the weight W of the structures. From Eqs. (2.1) and (2.3), the following can be obtained:

$$K_H = \frac{\alpha_m}{g} \tag{2.4}$$

that is, horizontal seismic intensity coefficient K_H is the ratio of the horizontal maximum acceleration acting on the structures to gravitational acceleration.

In addition to the horizontal force, earthquake-resistant design is often done with consideration of the inertia force V caused by acceleration in the vertical direction:

$$V = \pm K_V \cdot W \tag{2.5}$$

With respect to stability of structures and stress of members, the vertical force is acted in danger side direction, i.e., upward or downward. For the seismic coefficient intensity in the vertical, approximately 1/2 the horizontal seismic intensity coefficient is often used. K_V is called the vertical seismic intensity coefficient. In some cases, coefficients K_H and K_V are called engineering-oriented seismic intensity, for distinguishing them from the JMA seismic intensity and MMI (Modified Mercalli Intensity).

In earthquake-resistant design by the seismic coefficient method, the seismic forces are constantly acted in same direction. This implies that a static external force is considered. The inertia force by earthquake motion is dynamic, repetitively changing its direction with time. Comparing with the design in which repetitive loading is considered, design by a static external force in one direction generally has a superfluity of earthquake resistance of structures. Exact evaluations of such superfluity of structures designed with static seismic force compared with the repetitive load vary with dynamic characteristics and the failure process of structures. Large shaking-table tests and numerical analysis have been conducted to clarify the behavior of that failure process, toward evaluating the superfluity. However, it is generally difficult to pursue the failure process using an experimental model of reduced scale, because the similitude requirement is not satisfied because of strong non-linearity between external force and structural deformation in the failure process. Full-size (same size as actual structures) models are needed. Therefore, a three-dimensional and actual-size experimental facility (E-Defence) was constructed in Miki, Hyogo Prefecture after the 1995 Kobe earthquake [2]. The facility has a large shaking table with loading capacity 1,200 tf. With the aid of this facility, failure experiments have been conducted for reinforced concrete buildings, and pile foundations. Thus, research on the failure process is underway.

2.1.3 *Modified Seismic Coefficient Method*

When natural periods of structures are close to dominant periods of earthquake ground motion, dynamic response of those structures is amplified. However, the inertia force by the seismic coefficient method is always constant without any relationship to the amplification of response acceleration.

A modified seismic coefficient method is proposed to solve this limitation. Seismic intensity coefficient is required to change with the natural period of structures. Figure 2.4 depicts the K_H in *Specifications for Highway Bridges and*

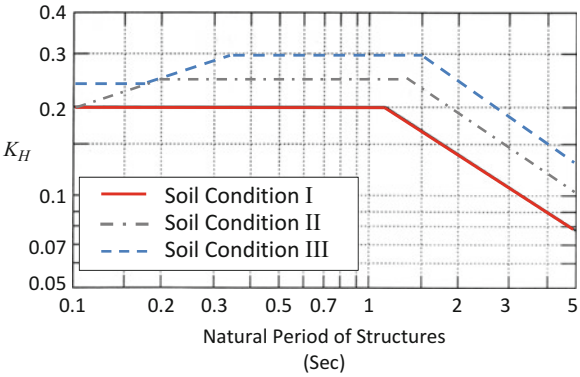

Fig. 2.4 Seismic coefficients K_H for modified seismic coefficient method (Specification for Highway Bridges and Explanation, Part *V*, Seismic Design [3])

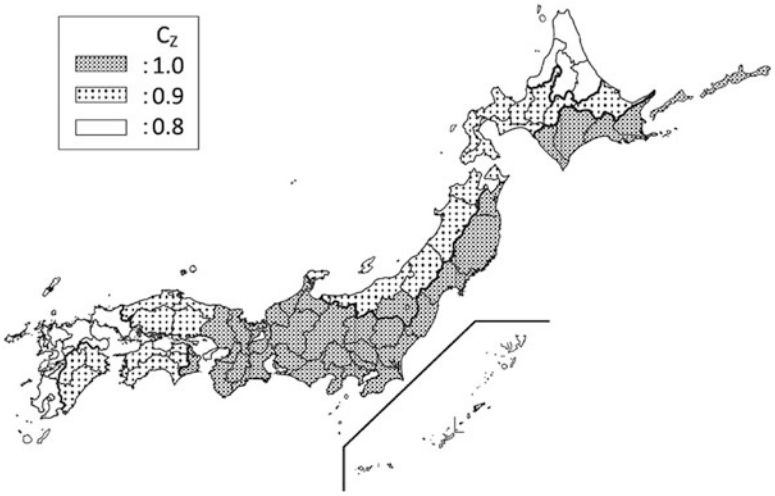

Fig. 2.5 Regional coefficients for modification of seismic coefficient (Specification for Road Bridges and Explanation, *V* earthquake resistant design [3])

Explanation Part V, Seismic Design [3]. The horizontal axis indicates the natural period of structures, and K_H is determined by natural periods of structures and soil condition (I to III). The horizontal force H on the structures can be obtained from

$$H = C_Z \cdot K_H \cdot W \tag{2.6}$$

where C_z is the regional coefficient; values of 0.8–1.0 were adopted (Fig. 2.5) according to regional seismic activities. Figure 2.4 indicates that K_H is relatively large for periods between 0.3 s and 1.5 s under the soil condition III. This follows from the fact that earthquake ground motions are generally dominant in these periods.

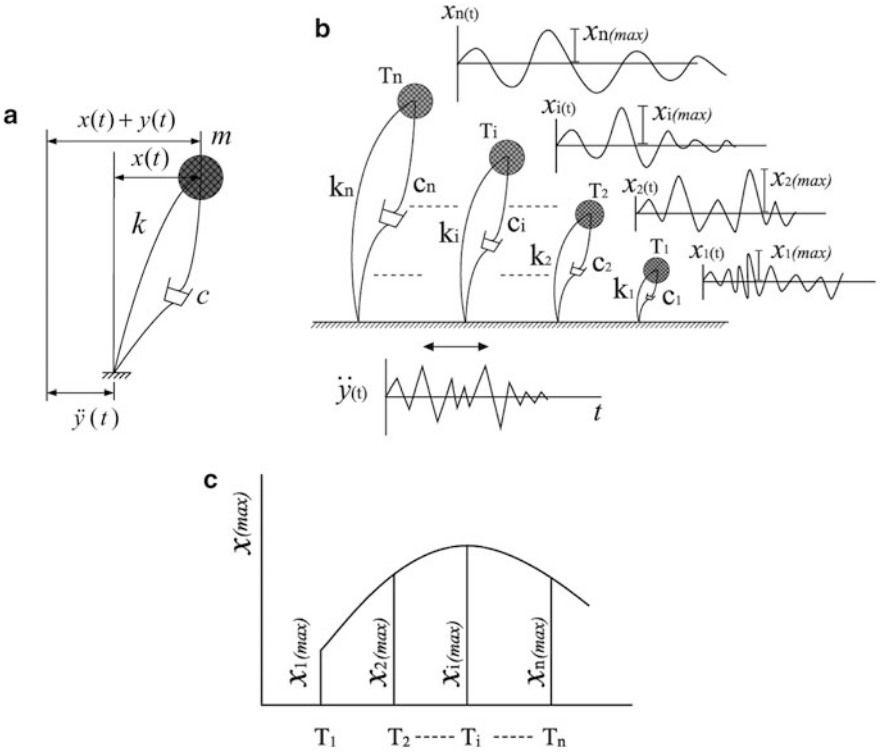

Fig. 2.6 Calculation of response spectra. (**a**) Dynamic response of single mass-spring-damper model. (**b**) Maximum displacements response of each mass-spring-damper model. (**c**) Displacement response spectra

Soil conditions I to III are determined based on the natural period of the surface ground. Type III represents soft soil such as alluvial plain and reclaimed land, whereas type I indicates hard soil such as diluvial ground and bedrock. Type II specifies soil intermediate to types I and III. Figure 2.4 is termed a response spectrum, and is calculated by the method described below.

2.1.4 Response Spectra

As displayed in Fig. 2.6a, the vibration equation of one-mass-spring-damper model can be expressed as

$$\ddot{x}(t) + 2\omega_0 h\dot{x}(t) + \omega_c^2 x(t) = -\ddot{y}(t) \tag{2.7}$$

where $x(t)$ is displacement of one mass (relative displacement from the fixed point of the spring). $\dot{x}(t)$ and $\ddot{x}(t)$ are velocity and acceleration of the mass, respectively.

ω_0 is the circular natural frequency of the one-mass-spring-damper model and h is the critical damping constant. They can be written as follows:

$$\omega_0 = \sqrt{\frac{m}{k}}$$
$$h = \frac{c}{2\omega_0 m} \tag{2.8}$$

where m and k are the mass and spring constants, respectively, and c is the viscous damping coefficient.

The solution of Eq. (2.7), relative displacement $x(t)$ relative velocity $\dot{x}(t)$, and absolute acceleration $\ddot{x}(t) + \ddot{y}(t)$ of the one-mass-spring-damper model can be obtained as follows:

$$x(t) = -\frac{1}{\omega_0\sqrt{1-h^2}}\int_0^t \exp[-\omega_0 h(t-\tau)] \cdot \sin\omega_0\sqrt{1-h^2}(t-\tau)\cdot\ddot{y}(\tau)d\tau \tag{2.9}$$

$$\dot{x}(t) = -\int_0^t \exp[-\omega_0 h(t-\tau)]\cdot \left\{\cos\omega_0\sqrt{1-h^2}(t-\tau) - \frac{h}{\sqrt{1-h^2}}\sin\omega_0\sqrt{1-h^2}(t-\tau)\right\}\ddot{y}(\tau)d\tau \tag{2.10}$$

$$\ddot{x}(t) + \ddot{y}(t) = \omega_0\frac{1-2h^2}{\sqrt{1-h^2}}\int_0^t \exp[-\omega_0 h(t-\tau)] \cdot \sin\omega_0\sqrt{1-h^2}(t-\tau)\cdot\ddot{y}(\tau)d\tau + 2\omega_0 h\int_0^t \exp[-\omega_0 h(t-\tau)]\cos\omega_0\sqrt{1-h^2}(t-\tau)\cdot\ddot{y}(\tau)d\tau + \ddot{y}(t) \tag{2.11}$$

By taking the maximum value irrespective of time t of the relative displacement, relative velocity and absolute acceleration, the response spectra S_D, S_V, and S_a are as follows:

$$S_D = |x(t)|_{\max} \tag{2.12}$$

$$S_V = |\dot{x}(t)|_{\max} \tag{2.13}$$

$$S_A = |\ddot{x}(t) + \ddot{y}(t)|_{\max} \tag{2.14}$$

Generally, h is much smaller than 1.0 for ordinary structures, hence, the response spectra S_D and S_V can be rewritten as

$$S_D = \frac{1}{\omega_0}\left|\int_0^t e^{-\omega_0 h(t-\tau)} \cdot \sin\omega_0(t-\tau)\cdot\ddot{y}(\tau)d\tau\right|_{\max} \tag{2.15}$$

$$S_V = \left| \int_0^t e^{-\omega_0 h(t-\tau)} \cos \omega_0 (t-\tau) \cdot \ddot{y}(\tau) d\tau \right|_{\max} \tag{2.16}$$

The input acceleration $\ddot{y}(t)$ in Eq. (2.11) can be neglected, because its influence on the maximum value of the absolute acceleration $\ddot{x}(t) + \ddot{y}(t)$ is limited. The following can be obtained:

$$S_A = \omega_0 \left| \int_0^t e^{-\omega_0 h(t-\tau)} \cdot \sin \omega_0 (t-\tau) \cdot \ddot{y}(\tau) d\tau \right|_{\max} \tag{2.17}$$

If the earthquake ground motion $y(\tau)$ in Eqs. (2.15), (2.16) and (2.17) are sufficiently long, the influence of the difference obtained by multiplying it by either sin $\omega_0(t - \tau)$ or cos $\omega_0(t - \tau)$ becomes negligible, and the following equations are obtained:

$$S_D \fallingdotseq \frac{1}{\omega_0} \cdot S_V \tag{2.18}$$

$$S_A \fallingdotseq \omega_0 \cdot S_V \tag{2.19}$$

That is, all the response spectra can be defined if the displacement, velocity, or acceleration spectrum is obtained. When the time history of the input acceleration $\ddot{y}(t)$ is given, the maximum displacement $|x(t)|_{\max}$ of each one-mass-spring-damper model with different natural circular frequency ω_0 (natural period $T = 2\pi/\omega_0$) under a constant critical damping constant h, can be obtained as shown in Fig. 2.6b. Figure 2.6c is the displacement response spectrum where the values of the maximum displacement of each mass-spring-damper model are plotted with the natural periods of the models $T_1 \sim T_n$ in the horizontal axis. Generally, the response spectra is given at $h = 0.05$ (5 %) for ordinary structures. For sloshing vibration of the contents of large storage tanks (referred to Sect. 2.2.3), $h \fallingdotseq 0.5$ % is usually used. This is because damping of the sloshing vibration, e.g., that of crude oil in large tanks, is very small.

As a method for analyzing dominant periods in an earthquake ground motion of random time history, the Fourier spectrum is generally used. However, the aforementioned response spectrum can also depict dominant components of earthquake ground motions. The response spectra have more engineering-oriented information.

Figure 2.7a shows an example of horizontal accelerations at the ground surface and their response spectra at K-NET [2] in Sendai during the 2011 Tohoku earthquake. The maximum accelerations were 1,517 and 982 cm/s^2 in the north–south and east–west directions, respectively. The response acceleration in the north–south direction exceeded 2,000 cm/s^2 between 0.5 and 0.8 s as shown in Fig. 2.7b. This demonstrates that the earthquake ground motion was dominant in these periods, and that dynamic responses of structures with these natural periods are amplified.

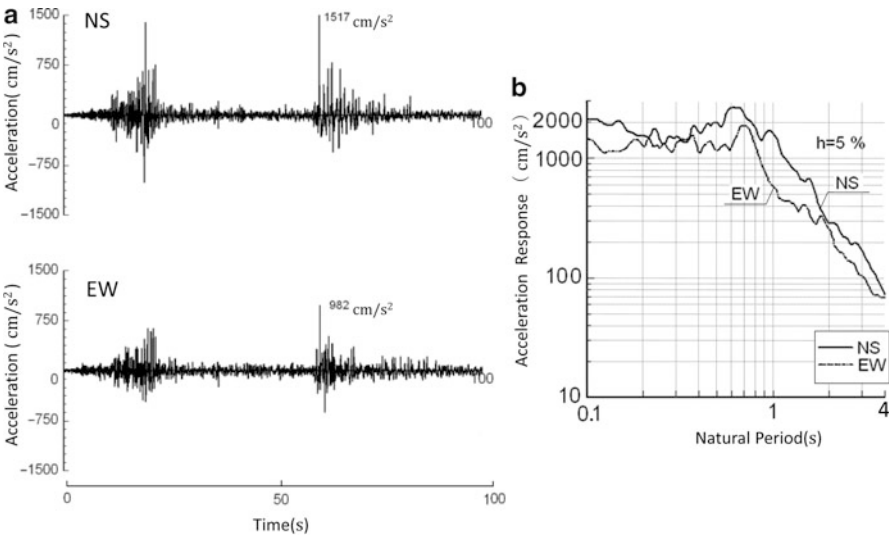

Fig. 2.7 Ground acceleration and acceleration response spectra (2011 Tohoku earthquake at Sendai K-NET). (**a**) Accelerations observed at the ground surface. (**b**) Acceleration response spectra

2.2 Development of Earthquake-Resistant Design

The seismic coefficient method was proposed in 1917, followed by a modified seismic coefficient method. The latter method, in which the seismic coefficient is changed according to natural periods of structures, has been widely used in earthquake-resistant design. However, earthquake-resistant design methods have been repeatedly revised, based on knowledge and experience from past earthquake damage.

2.2.1 Earthquake-Resistant Design Against Soil Liquefaction

In the 1964 Niigata earthquake, liquefaction of sandy ground was firstly recognized from an engineering perspective. Sand and ground water boils were observed within wide areas along the Shinano and Agano rivers in Niigata, and many structures subsided and inclined. Figure 2.8a shows a three-story reinforced concrete building steeply inclined by soil liquefaction. The building was constructed on a mat foundation. As addressed in Sect. 4.1.3, girders of the Showa Bridge fell into the river because of large ground displacement caused by the flow of liquefied soil (Fig. 4.19). Many underground structures such as purification tanks and sewage manholes were lifted by the buoyancy of liquefied soil (Fig. 2.8b).

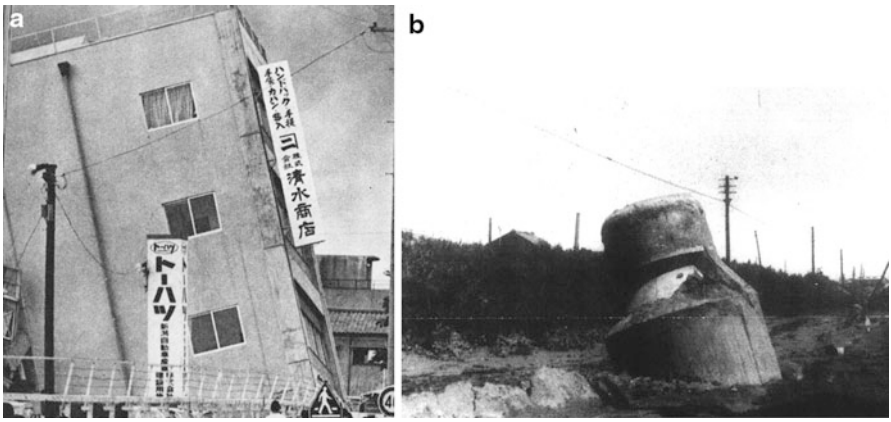

Fig. 2.8 Liquefaction-caused damage (1964 Niigata earthquake). (**a**) Inclination and subsidence of a three-story RC building. (**b**) Uplift of sewage manhole

At the time it was difficult for scientists and engineers to satisfactorily explain the mechanism of soil liquefaction and its damage to structures. They thought that a kind of "quick sand phenomenon", in which sand loses strength because of vibration, occured. However, a report on the Niigata earthquake by the Japan Society of Civil Engineers (JSCE) [4] called the phenomenon over the entire region of Niigata as "sand flow" or "ground flow." From this description, it can be imagined that a large amount of sand moved horizontally.

From the 1964 Niigata earthquake and subsequent earthquakes, the following have been explained as damage from soil liquefaction:

(i) Inclination and subsidence by loss of bearing capacity of the ground
(ii) Uplift of underground structures by buoyancy of liquefied soil
(iii) Collapse of earth structures such as embankments and levees by loss of strength of soil
(iv) Collapse and inclination of quay walls and retaining walls by increase of earth pressure

With these types of liquefaction-induced damage as motivation, methods for estimation of liquefaction potential and various countermeasures against soil liquefaction were developed for practical use.

After the 1983 Central Japan Sea earthquake, ground displacements caused by the flow of liquefied soil were first measured. In addition, ground displacement caused by the 1964 Niigata earthquake was measured anew. Furthermore, the relationship between damage to foundation piles and buried pipes, and measured ground displacements was investigated. Japan–U.S. cooperative research was done to clarify the mechanism of large ground displacements by liquefied soil flow, and

to develop countermeasures against such displacements. Despite these efforts, liquefaction-induced large ground displacements were again caused in reclaimed lands during the 1995 Kobe earthquake, inflicting damage to bridges, buildings and lifeline facilities.

With consideration of such damage, studies for earthquake-resistant designs and countermeasures against liquefaction-induced large ground displacements were promoted. Descriptions of countermeasures and estimation of ground displacement are provided in Chaps. 3 and 4, respectively.

2.2.2 *Lifeline Earthquake Engineering*

"Lifeline" was originally a maritime word meaning "life-saving rope" or "life preserver." In the context of protecting human life by constructing the environment for daily life in populated cities, the word is used as a comprehensive expression of systems for maintaining city function. In an earthquake engineering conference in the United States in 1975, "Lifeline Earthquake Engineering" was proposed. With this as motivation, water, sewage, electric power, gas, telecommunication, and others came to be called lifeline systems [5].

Lifeline systems are generally classified based on the services they supply:

(1) Water supply and purification systems—water, sewage, and river facilities (intake and discharge of water)
(2) Energy systems—electric power, city gas, and local cooling/warming
(3) Information and communication systems—telephone, information and broadcast facilities
(4) Transportation systems—roads, railroads, ports, airports

In the 1978 Miyagi offshore earthquake, there was serious damage to buried pipes of lifeline systems, such as water, sewage and gas in residential areas in the hills of suburban Sendai. The main cause of damage to those pipes was differential vertical ground displacements between zones reclaimed from valleys and those developed by excavation of ridges. After the earthquake, research for strengthening earthquake resistance of buried pipes was promoted. In 1982, *Standard for Earthquake Resistant Design of High Pressure Gas* [6] was compiled by the Japan Gas Association. In this standard, methods for earthquake-resistant design of buried pipes against ground surface fissures and differential settlement of ground were taken into the consideration.

The 1985 Kobe earthquake inflicted unprecedented damage to urban lifeline systems in the Kobe and Osaka districts. The summary of the damage to various lifeline systems, and recovery days are shown in Table 1.3 of Sect. 1.3. Details of damage to water and sewage systems and recovery days are shown in Tables 2.1 and 2.2.

Table 2.1 Damage to water systems by the 1955 Kobe earthquake and days for recovery

City	Number of households in suspension of supply (rate)	Direct money loss (Yen)	Days for recovery	Mainly damaged facilities
Kobe	650,000 (100 %)	31,570,000	70	Purification plants Transmission pipes Distribution pipes Buildings
Nishinomiya	157,000 (95 %)	4,580,000	70	Reservoir Transmission pipes Distribution Pipes
Amagasaki	193,000 (100 %)	308,000	14	Transmission pipes Distribution pipes
Ashiya	33,400	1,474,000	64	Purification plants Tunnels
Hyogo prefecture	1,265,730	55,759,000		

Table 2.2 Damage to sewage systems by the 1955 Kobe earthquake and days for recovery

City	Total length of pipes (m)	Damaged length (m) (rate)	Direct economic loss (Yen)	Mainly damaged facilities and days for recovery
Kobe	3,315,392	73,005 (2.2 %)	51,425,972	Waste water treatment plants and pumping stations by strong ground motion and soil liquefaction
Amagasaki	1,019,290	45,583 (4.4 %)	1,562,431	Days for recovery Pipes: 140 days (Kobe) Waste water treatment plants: 5 months
Nishinomiya	916,900	32,088 (3.4%)	11,963,615	
Ashiya	215,400	28,548 (13.3 %)	6,155,764	
Takarazuka	531,800	8,597 (1.6 %)	1,504,239	
Hyogo prefecture	7,491,982	198,510 (2.6 %)	73,456,585	

For water supply to Kobe, Nishinomiya and Ashiya cities, it took about 70 days to recover from damage to purification plants, distribution and transmission pipes, and others. Most notably, the city water works office in Kobe, on the 5th floor of the city hall, collapsed by the earthquake (Fig. 1.61a). Thus, documents regarding facilities and buried pipes were unusable, greatly hindering restoration work.

The water conveyance tunnel in Ashiya (Fig. 1.61f) was damaged. This may be attributed to strong earthquake ground motion near the active fault and shallow depth of the tunnel.

Major causes of damage to sewage facilities are strong earthquake ground motion and soil liquefaction. Liquefaction at the Higashinada wastewater treatment plant was particularly severe. The ground moved toward the canal about 3 m, and foundation piles of the administration building and sewage treatment plants were ruptured and the buildings inclined. This caused the recovery to take about 5 months. Details of the damage to the waste water treatment plant will be given in Sect. 4.1.4.

Causes of damage to the lifeline systems were as follows:

(i) Extensive soil liquefaction and large ground displacement by liquefied soil flow in the reclaimed land damaged key stations, such as wastewater treatment plants, purification plants, and buried pipes.
(ii) There were large numbers of decayed and old pipes of low strength.
(iii) Earthquake ground motion far exceeded the design level.

Reasons for the very long recovery time were as follows:

(i) The database of buried pipes was inadequate, and it took much time to detect pipe damage.
(ii) Transportation of equipment/personnel was hindered due to traffic congestion.
(iii) Recovery work was entangled with that on other lifeline systems.

After the 1995 Kobe earthquake, there were comprehensive revisions of earthquake-resistant design codes for water, sewage, city gas, electricity, and telecommunication. In these revisions, earthquake ground motion for the design was greatly increased. Concurrently, the effect of liquefaction-induced large ground displacement came to be considered. Furthermore, support systems for restoration of lifelines among municipalities were nationwide established.

In the 2004 Niigata-Chuetsu offshore earthquake, more than 1,400 sewage manholes were lifted in Nagaoka, Ojiya and other cities. This was mainly attributed to the liquefaction of backfilling soil around the manholes. Therefore, various countermeasures have been developed and applied, namely, compaction of backfilling soil, gravel and rock filling, and hardening of soil by cement milk. Furthermore, several countermeasures against soil liquefaction of existing manholes were developed. Details are described in Sect. 3.3.3.

Numerous waste water treatment plants and pumping stations were severely damaged by the tsunami of the 2011 Tohoku earthquake. Because of loss of power sources by tsunami inundation, inflow of floating objects to the sedimentation basins, and flowing-out of machineries, sewage treatment functions were stopped for a long period. For this reason, the *Fundamental Concept for Promoting Anti-Tsunami Measures* was established by the "Committee for Anti-Earthquake and Tsunami Measure of Sewage System". Details are described in Sect. 2.8. Furthermore, there were another kinds of sewage pipelines damage such as horizontal differential displacement of concrete ring elements of manholes, pullout of sewage pipes connecting manholes, and inflow of liquefied soil. An example of liquefied soil flow into a manhole is shown in Fig. 2.9.

Fig. 2.9 Liquefied soil flow into a manhole (2011 Tohoku earthquake)

2.2.3 Earthquake-Resistant Design Against Long-Period Ground Motion

The 2003 Tokachi offshore earthquake caused fires of crude oil and naphtha tanks of an oil refinery in Tomakomai (Fig. 1.67). Long-period earthquake ground motion triggered sloshing vibration of the contents of floating roof-type tanks. It is also assumed that fire broke out from collision of metal fragments of the tanks. Tank fires by long-period component of earthquake motions have been caused in earthquakes greater than mid–scale, such as the 1964 Niigata and 1999 Kocaeli (Turkey) earthquakes. A large number of floating-roof type tanks have been constructed in oil and chemical industrial complexes in Japan. Around Tokyo Bay, the number of such tanks exceeds 600. Several methods to suppress the sloshing vibration of tank contents have been proposed, but none have been practically used to control vibration of content in tanks with diameters of several tens of meters. Moreover, for tanks that have already been constructed, it is difficult to install devices to suppress the sloshing vibration.

Given such difficulty, the following countermeasures are taken for preventing fires from the sloshing in the floating roof-type tanks:

(i) Reinforcement of floating roofs by double deck structures
(ii) Reinforcement of barrier walls for outflow of oil against soil liquefaction
(iii) Installation of equipments and preparations for rapid firefighting

After the 2003 Tokachi offshore earthquake, design codes for oil tanks, petrochemical products, and high-pressure gas were updated. The height of liquid rise W_h induced long-period ground motion can be expressed as follows [7]:

$$W_h = \frac{R}{g} \cdot 0.837 \left(\frac{2\pi}{T_S} \right) \cdot S_V \tag{2.20}$$

Here, R indicates the radius of the tank (in m), and g is the acceleration of graviation (9.8 m/s^2). T_S is the first natural period of the sloshing vibration of tank contents, which is

$$T_s = 2\pi\sqrt{\left(\frac{R}{1.84g}\right)\coth\left(3.68\frac{H}{D}\right)} \tag{2.21}$$

Here, H is depth of the contents (in m).

S_V (m/s) is the velocity response spectrum from long-period ground motion, which is

$$S_V = S_{V0} \cdot \nu_5 \tag{2.22}$$

S_{V0} is the standard velocity response spectrum, and is shown in Fig. 2.10a for four areas in Japan. ν_5 is a coefficient reflecting the likelihood of long-period earthquake ground motion, which is shown for several areas with major oil refinery complexes in Fig. 2.10b. The response spectra were attained by observation of long-period earthquake ground motions and by a survey of deep soil conditions.

The volume of overflowing liquid ΔV of tank contents can be obtained from

$$\Delta V = \pi R^2 \cdot \frac{\alpha \cdot \delta_h (R - r_0)\theta_0}{R} \tag{2.23}$$

δ_h (in m) in this equation is the height of overflow (Fig. 2.11) [7]. This can be determined from the difference between the height of liquid rise W_h and the original depth of content surface from the top of the sidewall H_c (in m). θ_0 is an angle allowing the sloshing wave height to equal H_c. r_0 denotes the horizontal distance from the tank center to the intersection of the sloshed oil surface with the horizontal plane at the level of the sidewall top. α is a coefficient expressing the control effect on the sloshing vibration of the floating roof, and is generally taken as 0.4023.

2.3 Performance-Based Earthquake-Resistant Design Against Two Levels of Earthquake Ground Motion

2.3.1 JSCE Recommendation for Earthquake-Resistant Design and Reinforcement of Existing Structures

The 1995 Kobe earthquake killed more than 6,000 people and destroyed various types of infrastructures such as roads, railways, ports and lifelines. The response acceleration of earthquake ground motion in Kobe (Fig. 1.60) reached approximately 2,000 cm/s^2 in the period range from 0.3 to 1.0 s. The acceleration greatly

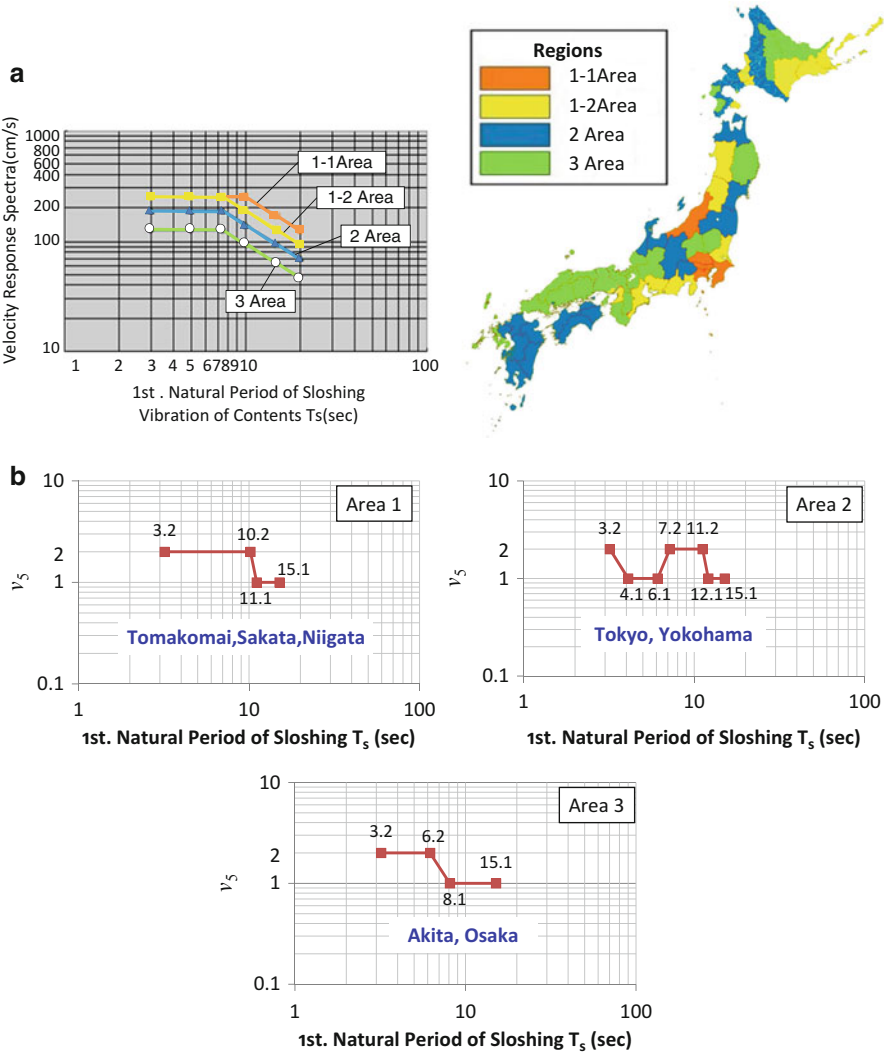

Fig. 2.10 Velocity response spectra for estimation of sloshing wave height of tank content (S_{v0}) [8]. (**a**) Velocity response spectra (critical damping constant h = 0.5 %). (**b**) Regional coefficients based on likelihood of occurrence of long period ground motion

exceeded the 1,000 cm/s^2 that had been used for earthquake-resistant design of road bridges and railway facilities prior to the earthquake, in which plastic deformation of structures was considered.

In response to the severe damage to numerous structures from the Kobe earthquake, the JSCE "Ad Hoc Committee of Basic Principles for Earthquake-Resistant Design and Reinforcement of Existing Structures" recommended the

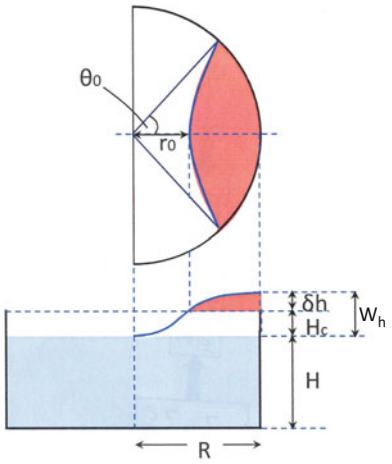

$$\Delta V = \pi R^2 \cdot \frac{\alpha \cdot \delta_h (R - r_0)\theta_0}{R}$$

ΔV : Total Volume of Overflow
R : Radius of Tank
α : Control Coefficient(Floating Roof Tank : 0.4023)
δ_h : Height of Overflow
H_C : Depth of Content Surface from Top of Side Wall
r_0 : Horizontal Distance between Tank Center and The Intersection of Sloshed Oil Surface with Horizontal Plane
θ_0 : Angle Allowing Sloshing Wave Height to Equal H_C
W_h : Wave height of Sloshing

Fig. 2.11 Sloshing vibration of contents of circular tanks by long period ground motion [8]

following fundamental policies for earthquake-resistant design and reinforcement of existing structures [8].

(i) Two levels of earthquake ground motions should be considered in earthquake-resistant design. Level 1 earthquake ground motion has a probability of occurrence of once or twice during structure's lifetime. Level 2 earthquake ground motion has low probability of occurrence, but strong shaking such as observed around Kobe during the 1995 earthquake.
(ii) Structures should be designed to satisfy requisite performances during and after the earthquakes assumed in the design. Those performances are determined by considering the probabilities of occurrence of level 1 and 2 earthquake ground motions, plus effects on human lives, rescue operations, restoration and reconstruction works. The most important point for earthquake resistant design of structures from requisite performance against level 2 earthquake ground motion is to prevent structures from total collapses for saving human lives. This design method is called performance-based design. This concept is applied for the earthquake-resistant design of all civil engineering structures, including earth structures such as embankments, river levees and dams.

The recommendation by JSCE is based on the most important lesson learned from the 1995 Kobe earthquake. That is to save lives, even when structures encounter strong ground motion as in the Kobe earthquake. The JSCE recommendation was incorporated in one of the national policies on earthquake-resistance of structures. In the *Basic Plan for Disaster Prevention* published by the Cabinet Office, Government of Japan, the following were declared in Chap. 1 ("Creation of Safe Nation and Community against Future Earthquakes") [9].

(i) Two types of earthquake ground motions should be considered for the design of structures. The first is motion with a probability of occurrence once or twice during the structure lifetime. The second is strong motion caused by inland earthquakes or huge earthquakes along sea troughs, which have comparatively low probabilities of occurrence.
(ii) Structures shall be designed with the fundamental objective that human lives not be lost to strong earthquake ground motion, and that post-earthquake rescue operations and regional economic activities not be seriously affected.

Given the concept of earthquake resistance of structures in the *Basic Plan for Disaster Prevention* as fundamental policy for their earthquake-resistant design after the Kobe earthquake, the following standards and codes were revised.

- *Specifications for Highway Bridges, and Explanation Part V Seismic Desig*n *(1996)* , Japan Road Association [3]
- *Guidelines for Earthquake-resistant Measures for Sewage Facilities and Explanation (1997)*, Japan Sewage Works Association
- *Basic Principles of Seismic Design and Construction for Water Supply Facilitie*s (1997), Japan Water Works Association [10]
- *Guidelines for Earthquake-resistant Design of High Pressure Gas Facilities (1997)*, The High Pressure Gas Safety Institute of Japan
- *Seismic Design for Railway Structures and Commentary (1999)*, Railway Technical Research Institute [11]
- *Technical Standards and Commentaries for Port and Harbor Facilities (1999)*, Bureau of The Ports of Harbor, Ministry of Transport [12]
- *Guidelines for Earthquake-resistant Design of High Pressure Gas (2000)*, The Japan Gas Association
- *Guidelines for Earthquake-resistant Design of Gas Facilities (2001)*, The Japan Gas Association
- *Guidelines for Earthquake-resistant Design of High Pressure Gas Facilities against Liquefaction (2001)*, The Japan Gas Association

The concept of performance based design against two levels of ground motion is illustrated in Fig. 2.12 [12]. Figure 2.12a shows an example of relationship between seismic force and displacement at the top of a concrete bridge pier. As seismic force increases, cracks appear in the concrete, and further increase of the force results in yielding of reinforced steel bars. After that, the pier collapses via maximum load. Design should not allow residual deformation during level 1 earthquake ground motion, although cracks in the concrete will remain after the earthquake. In this case, nearly the same earthquake resistance should be guaranteed after the earthquake, without any repair. For level 2 earthquake ground motion, the design is aimed at recovery of function and prevention of collapse. Function of the pier should be recovered, for an example, in 2 or 3 weeks, even with damage to the upper structure and foundation. Assessment of the earthquake-resistant performance of the piers (Fig. 2.12c) is made based upon the extent of damage to superstructures and the foundation, along with the residual displacement.

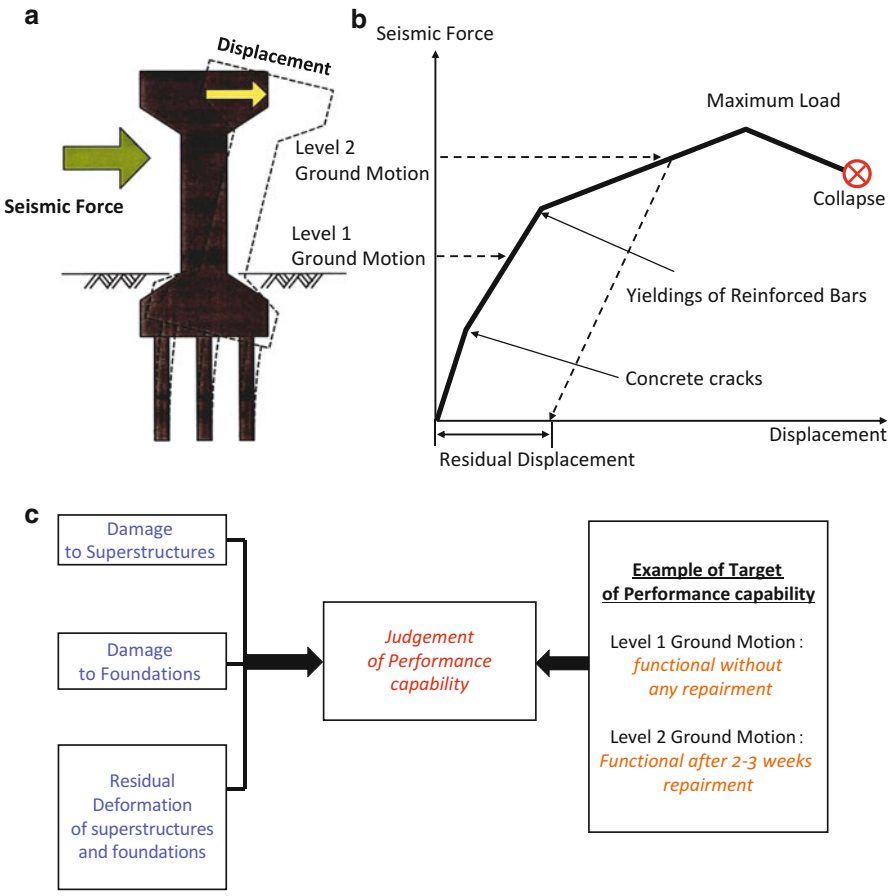

Fig. 2.12 Performance-based design against two-levels of earthquake ground motion. (**a**) Seismic force on reinforced concrete Pier and displacement. (**b**) Relationship between seismic force and displacement. (**c**) Judgment of performance capability

2.3.2 Setting of the Two Levels of Ground Motion

For performance-based design against the two levels of earthquake ground motion, it is necessary to determine those levels. The ground motion used in earthquake-resistant design before the 1995 Kobe earthquake is adopted, as level 1 ground motion in most of the design codes.

For level 2 motion, two methods are available. The first is to directly deduce earthquake ground motion by investigating active faults near the construction site of structures that will affect their seismic safety. In this case, the ground motion is calculated by numerical analyses based on the fault failure process and seismic wave propagation toward the site. In the second method, a standard ground motion

is determined based on ground motions observed during past earthquakes. The design ground motions are attained by modification of the standard ground motion, depending on the seismic activity in the region.

In the first method, it is sometimes difficult to avoid overlooking active faults. Furthermore, various parameters governing the failure process of faults are required for calculating earthquake ground motion, but it is not easy to determine these parameters from fault surveys.

In most cases of the second method, the maximum ground motion observed during past earthquakes is used as the design motion. However, that maximum ground motion is occasionally exceeded in subsequent earthquakes. Every time a new higher ground motion is recorded, the design ground motion should be revised. In the 2004 Niigata-Chuetsu offshore earthquake and 2008 Iwate-Miyagi inland earthquake, maximum accelerations greatly exceeded that in the 1995 Kobe earthquake (Figs. 1.71 and 1.89). For this reason, a new concept of exceedence probability was introduced for earthquake-resistant design of buried water and sewage pipes and facilities of key stations, such as water purification plant and waste water treatment plant.

In the design codes revised after the Kobe earthquake, two types of earthquakes were considered to induce level 2 ground motion. Type 1 are earthquakes near the plate boundary in the Pacific Ocean with magnitude of 8 or more. These earthquakes have been already considered in the design of highway bridges and railway facilities before the Kobe event. Type 2 are earthquakes caused by inland faults with magnitude in the 7 class, which was not considered before the Kobe earthquake.

In the "*Specification for Highway Bridges and Explanation, Part V, Seismic Design*," revised in 1996, response spectra were shown for each type (1 and 2) of earthquake, as shown in Fig. 2.13 [3]. In these figures, soil conditions I and III refer to hard and soft soil, respectively, as mentioned in Sect. 2.1.3. In type 1 earthquakes, spectra for ground condition III are higher than that for soil condition I. However, in type 2 earthquakes, spectra for soil condition I are higher than for soil condition III. This is because non-linearity of soft soil increases against the strong earthquake ground motion near inland faults, and decrease of the response at the ground surface is considered.

In the standards of railway structures [11], a flowchart as shown in Fig. 2.14 is recommended for determination of level 2 ground motion. In this flowchart, whether inland active faults existence is firstly investigated. Second, if it is determined that such faults do not exist, the standard spectrum I by plate-boundary earthquakes is used, with adjustment for epicentral distance. If it is ascertained that inland active faults exist and determination of the parameters of fault failure is possible, design ground motion is directly determined by numerical analysis(Spectrum III). When identification of those parameters is impossible, standard spectrum II, which is made based on ground motions observed during past earthquakes caused by inland faults, is adjusted by the regional seismic activity. When the existence and locations of inland faults are unknown, the standard spectrum II is adjusted by the regional seismic activity.

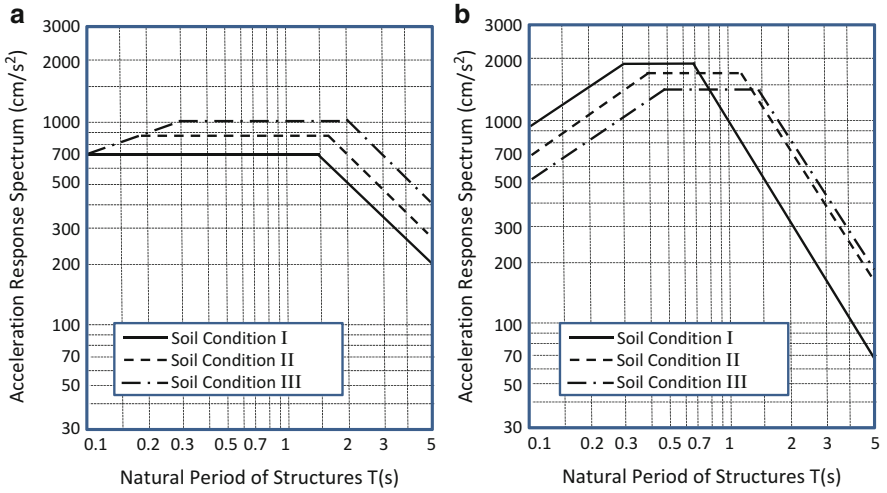

Fig. 2.13 Design spectra of level 2 earthquake ground motions for design of road bridges [3]. (**a**) Acceleration response spectra of type 1 earthquake ground motion. (**b**) Acceleration response spectra of type 2 earthquake ground motion

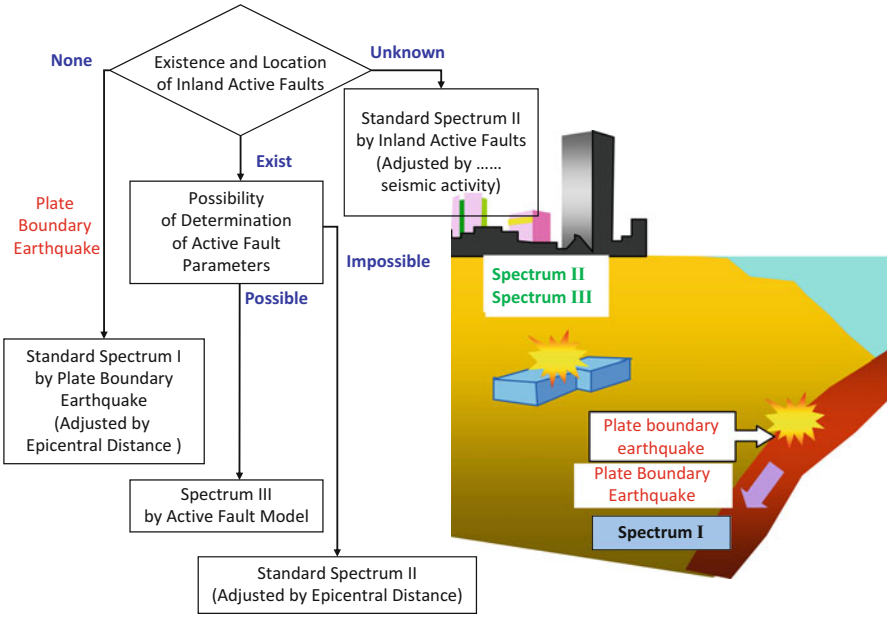

Fig. 2.14 Flow of setting of level-2 earthquake ground motion for railway structures [12]

2.4 Dynamic Response of Ground

2.4.1 Amplification of Earthquake Motion at Ground Surface and Dominant Periods

Figure 2.15 shows horizontal accelerations observed in reclaimed land around Tokyo Bay during the 2011 Tohoku earthquake and their Fourier spectra. As depicted in Fig. 2.15a, the ground at the observation point is composed of filled soil to −13 m elevation and alternating layers of sand and clay including gravel to −42 m. Layers deeper than −42 m are hard gravel or sand layers with N values exceeding 50, which can be regarded as bedrock. S-wave velocities of the ground above the bedrock are 160–240 m/s. Earthquake ground motion was observed at the ground surface and at depths −22 and −53 m from the ground surface in the hard gravel layer. Figure 2.15b shows that acceleration at the ground surface was much greater than those in the ground, and it is understood that the earthquake motion was amplified. Fourier spectra of the acceleration in Fig. 2.15c show that the earthquake motion was amplified in the frequency domain from 0.8 to 1.6 Hz. Amplification of the earthquake motion at 1.2 (1/s) was especially significant; this frequency is recognized as the natural period of the surface ground. The above findings reveal that earthquake motion at the ground surface had two characteristics: (i) amplification, and (ii) dominant vibration at specific frequencies.

2.4.2 Seismic Waves and Propagation

Seismic waves consist of body waves, which are P (primary) and S (Secondary) waves, and surface waves, which are Rayleigh and Love waves (Fig. 2.16). P and S-waves directly propagate in the earth crust and soil from the fault to the ground surface. The Rayleigh and Love waves, which are generated after the body (P and S) waves reach the surface, propagate along the surface.

Vibration by S-wave is a major constituent of earthquake ground motion, and oscillates structures such as bridges, dams, low- and medium-rise buildings. This is because the dominant periods of an S-wave are mostly shorter than 1 s, and coincide with natural periods of these structures.

The Rayleigh and Love waves generally have a long-period vibration component of several seconds. This component of vibration is amplified by the deep structure of ground, and induces sloshing vibration of oil in large tanks. These waves also affect earthquake resistance of high-rise buildings and long-span bridges. An example of tank fires from sloshing vibration caused by long-period components of earthquake ground motion is given in Section 1.3.4. The earthquake-resistant design of tanks against long-period ground motion was treated in Sect. 2.2.3.

Consider an S-wave propagating through homogeneous surface ground in a vertical direction (Fig. 2.17a). The wave equation of S-wave propagation can be obtained by considering the equilibrium of forces on soil segments at depth $z = z$.

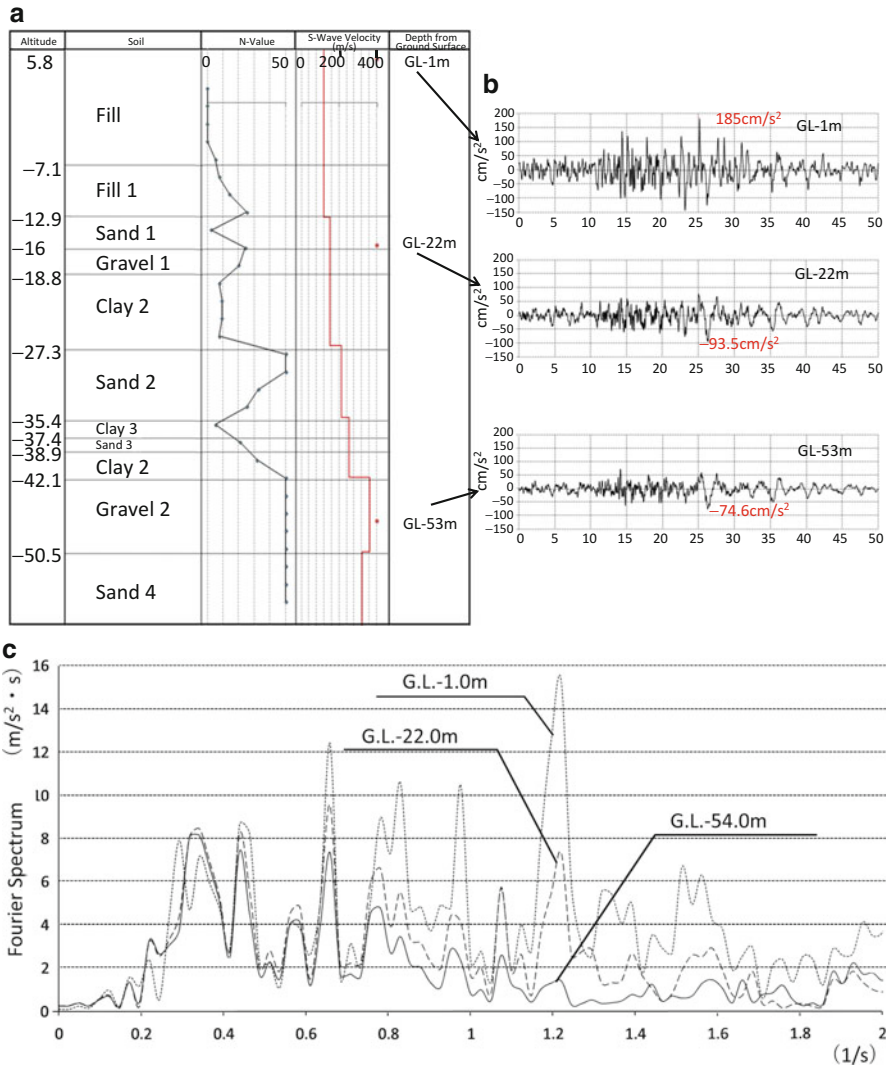

Fig. 2.15 Earthquake ground motion observed in artificial land reclaimed from the Tokyo Bay (2011 Tohoku earthquake). (**a**) Soil condition. (**b**) Observed ground motion. (**c**) Fourier spectra of observed ground acceleration

The equilibrium equation can be written as

$$\left(\tau + \frac{\partial \tau}{\partial z} dz\right) A - \tau A - \rho A dz \frac{\partial^2 U}{\partial t^2} = 0 \tag{2.24}$$

Here, U (t, z) is ground displacement in the horizontal direction induced by S-wave propagation, and is a function of time t and vertical coordinate z. A and dz

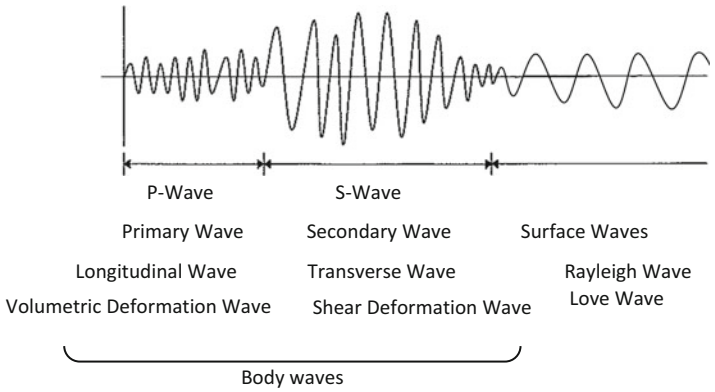

Fig. 2.16 Seismic waves

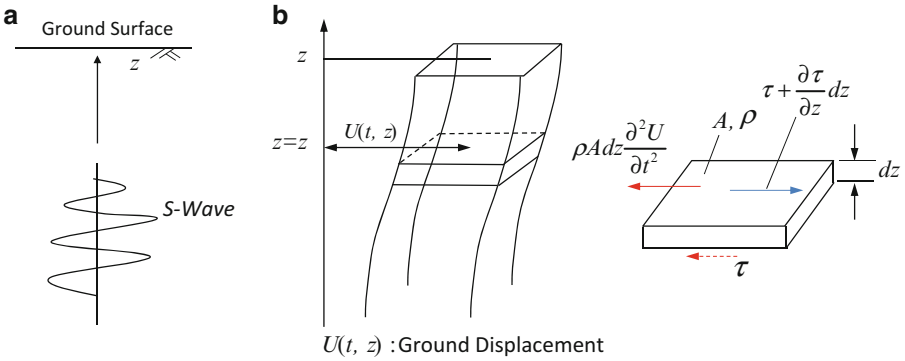

Fig. 2.17 Propagation of S-wave and wave equation. (**a**) Propagation of S-wave. (**b**) Force equilibrium of a soil segment

are area and thickness of the soil segment, and ρ is soil density. τ is the shear stress on the segment, and is expressed below using shear strain $\partial U/\partial z$.

$$\tau = G\frac{\partial U}{\partial z} \tag{2.25}$$

Here, G is the shear elastic modulus of the soil.
Assuming that G is constant, the following is obtained:

$$\frac{\partial^2 U}{\partial t^2} - {\nu_s}^2 \frac{\partial^2 U}{\partial z^2} = 0 \tag{2.26}$$

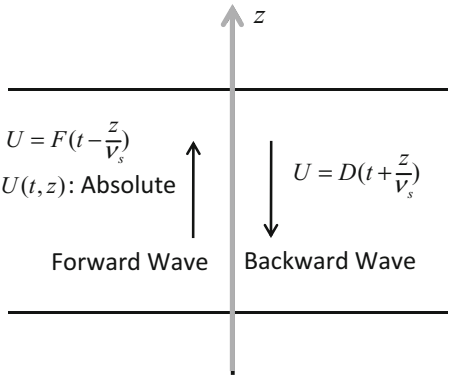

Fig. 2.18 Forward and backward waves

where ν_s is

$$\nu_s = \sqrt{\frac{G}{\rho}} \tag{2.27}$$

This indicates the propagation speed (called phase velocity).
A general solution satisfying Eq. (2.26) is shown below:

$$U(t,z) = F\left(t - \frac{z}{\nu_s}\right) \tag{2.28}$$

$$U(t,z) = D\left(t + \frac{z}{\nu_s}\right) \tag{2.29}$$

These two solutions show the waves propagating in plus and minus directions on the z axis, respectively. The wave represented by Eq. (2.28) is propagating in the plus direction and is called the forward wave. The wave represented by Eq. (2.29) is propagating in the minus direction, and is called the backward wave (Fig. 2.18).

Figure 2.19 depicts the response of surface ground with thickness H when bedrock motion $y(t)$ is input. Absolute displacement of the ground $U(t, z)$ is the sum of relative displacement $u(t, z)$ from the bedrock and displacement of the bedrock $y(t)$.

$$U(t,z) = u(t,z) + y(t) \tag{2.30}$$

Therefore, Eq. (2.26) is rewritten as

$$\frac{\partial^2 u}{\partial t^2} - {\nu_s}^2 \frac{\partial^2 u}{\partial z^2} = -\frac{d^2 y}{dt^2} \tag{2.31}$$

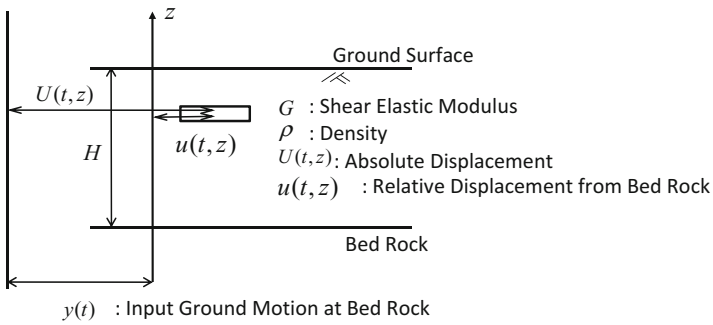

Fig. 2.19 Dynamic response of surface ground

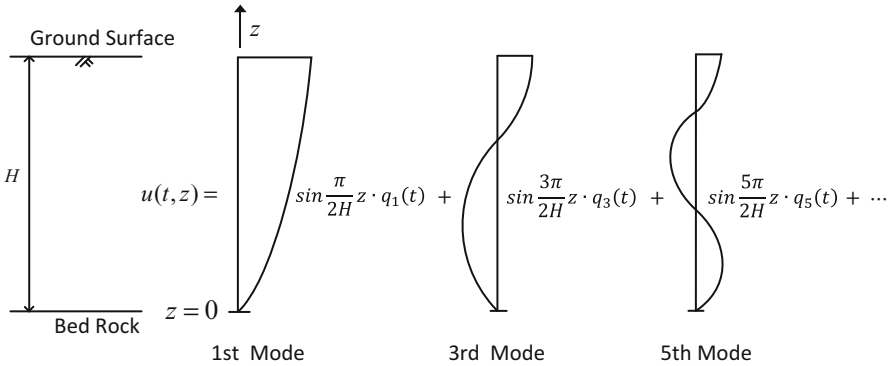

Fig. 2.20 Natural vibration modes

Equation (2.31) can be solved as below. The solution $u(t, z)$ is

$$u(t,z) = \sum_{i=1,3,5\cdots}^{\infty} q_i(t) \cdot \sin \frac{i\pi}{2H} z \tag{2.32}$$

In the above equation, $\sin \frac{i\pi}{2H} z$ is the ith vibration mode as illustrated in Fig. 2.20. Any vibration mode satisfies the boundary condition that the displacement $u(t, z)$ is zero at $z = 0$, and shear stress and shear strain are zero at $z = H$ (at the ground surface). $q_i(t)$ is the time function of the ith vibration.

By substituting Eq. (2.32) into Eq. (2.31), the following can be obtained:

$$\sum_{i=1,3,5\cdots}^{\infty} \ddot{q}_i(t) \cdot \sin \frac{i\pi}{2H} z + {v_s}^2 \sum_{i=1,3,5\cdots} \left(\frac{i\pi}{2H}\right)^2 q_i(t) \cdot \sin \frac{i\pi}{2H} z = -\frac{d^2 y}{dt^2} \tag{2.33}$$

By multiplying $\sin\frac{j\pi}{2H}z$ with the above equation and integrating from $z = 0$ to $2H$, the following can be attained by orthogonality of the trigonometric function, after replacing i with j:

$$\ddot{q}_i(t) + \omega_i^2 q_i(t) = -\frac{4}{i\pi}\frac{d^2y}{dt^2} \tag{2.34}$$

In the above equation, ω_i is the natural circular frequency of the ith vibration mode, as obtained below:

$$\omega_i = \frac{i\nu_s\pi}{2H} \qquad i = 1, 3, 5\cdots \tag{2.35}$$

The natural period of the ith vibration mode, T_i can be obtained from

$$T_i = \frac{4H}{i\nu_s} \qquad i = 1, 3, 5\cdots \tag{2.36}$$

Here, $i = 1$, that is, the first natural period $T_1 = 4H/\nu_s$ often appears as the dominant period of recorded earthquake ground motions. Because the soil has damping, the following is obtained by considering the damping term with respect to Eq. (2.34):

$$\ddot{q}_i(t) + 2\omega_i h_i \dot{q}_i(t) + \omega_i^2 q_i(t) = -\frac{4}{i\pi}\frac{d^2y}{dt^2} \tag{2.37}$$

Here, h_i is the critical damping constant regarding the ith vibration mode.

If the surface ground is composed by multiple soil layers of variable elastic shear modulus and density (Fig. 2.21a), the following simplified two methods are proposed for calculation of the natural periods of the surface ground:

$$T = \frac{4\sum_{i=1}^{n} H_i}{\overline{\nu}_s} \tag{2.38}$$

Here, $\overline{\nu}_s$ can be obtained as a mean of S-wave velocity, weighted by thickness of each soil layer.

$$\overline{\nu}_s = \frac{\sum_{i=1}^{n} H_i\nu_{si}}{\sum_{i=1}^{n} H_i} \tag{2.39}$$

Here, T is the natural period of the surface ground and H_i is thickness of the ith layer.

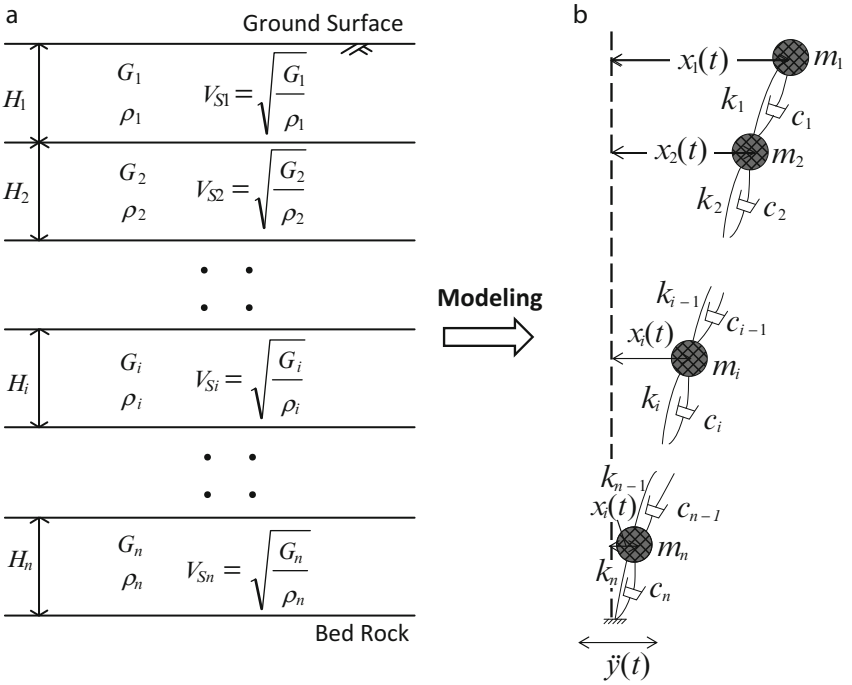

Fig. 2.21 Surface ground with multi-soil layers and mass-spring-damper model. (**a**) Surface ground with multi-soil layer. (**b**) Mass-spring-damper model

ν_{si} is S-wave velocity of ith soil layer, and is obtained by

$$\nu_{si} = \sqrt{\frac{G_i}{\rho_i}} \tag{2.40}$$

Here, G_i and ρ_i are shear elastic modulus and density, respectively.

The following equation is also a simple method for determining the natural period of the surface ground:

$$T = \sum_{i=1}^{n} \frac{4H_i}{\nu_{si}} \tag{2.41}$$

In "Specification for Highway Bridges and Explanation, Part V, Seismic Design," [3], a method to determine soil condition type by a characteristic value T_G representing the natural period of the surface ground is proposed. The ground condition is classified into the following groups:

soil condition I: T_G<0.2 s
soil condition II: 0.2 s < T_G < 0.6 s
soil condition III: 0.6 s < T_G

2.4.3 Dynamic Analysis by the Mass-Spring-Damper Model

Supported by the advancement of computing capacity since the 1970s, dynamic response analysis methods of structures and ground have been developed for use in earthquake-resistant design. Figure 2.21b shows multi-masses-springs-dampers model of surface ground composed by multiple soil layers. The vibration equation of this model can be generally expressed as follows:

$$\begin{bmatrix} m_1 & & & \\ & m_2 & 0 & \\ & 0 & & \\ & & & m_n \end{bmatrix} \begin{Bmatrix} \ddot{x}_1(t) \\ \ddot{x}_2(t) \\ \\ \ddot{x}_n(t) \end{Bmatrix} + \begin{bmatrix} c_1 & -c_1 & & \\ -c_1 & c_1 + c_2 & 0 & \\ & 0 & & \\ & & & c_{n-1} + c_n \end{bmatrix} \begin{Bmatrix} \dot{x}_1(t) \\ \dot{x}_2(t) \\ \\ \dot{x}_n(t) \end{Bmatrix}$$
$$+ \begin{bmatrix} k_1 & -k_1 & & \\ -k_1 & k_1 + k_2 & 0 & \\ & 0 & & \\ & & & k_{n-1} + k_n \end{bmatrix} \begin{Bmatrix} x_1(t) \\ x_2(t) \\ \\ x_n(t) \end{Bmatrix} = \begin{bmatrix} m_1 & & & \\ & m_2 & 0 & \\ & 0 & & \\ & & & m_n \end{bmatrix} \begin{Bmatrix} 1 \\ 1 \\ \\ 1 \end{Bmatrix} \ddot{y}(t) \tag{2.42}$$

In the above equation, $x_i(t)$, $\dot{x}_i(t)$, and $\ddot{x}_i(t)$ are relative displacement, relative velocity, and relative acceleration of the ith mass from the bedrock, and $\ddot{y}(t)$ represents the input acceleration on the bedrock. m_i is mass of the ith mass point, c_i, and k_i are viscous damping coefficient and spring constant that link the mass point i and mass point i + 1, respectively. Constants of m_i and k_i can be obtained as follows:

$$\begin{aligned} m_i &= \frac{1}{2}(\rho_{i-1}H_i + \rho_i H_i) \cdot A \\ k_i &= \frac{G_i A}{H_i} \end{aligned} \tag{2.43}$$

Here, A is area of the soil column, and usually takes as unit, and G_i and H_i is the elastic shear modulus and the thickness of ith layer.

c_i is the viscous damping constant between the ith mass and (i + 1)th mass. This coefficient usually is presumed proportional to the mass m_i or the spring constant k_i.

The matrixes $\boldsymbol{M}$, $\boldsymbol{C}$, $\boldsymbol{K}$ and the vector $\boldsymbol{X}$ are defined as follows,

$$\boldsymbol{M} = \begin{bmatrix} m_1 & & & & \\ & m_2 & & 0 & \\ & & \ddots & & \\ & & & m_i & \\ & 0 & & & \ddots \\ & & & & & m_n \end{bmatrix} \quad \boldsymbol{C} = \begin{bmatrix} c_1 & -c_1 & & & & \\ -c_1 & c_1 + c_2 & & & 0 & \\ & & \ddots & & & \\ & & & \ddots & & \\ & 0 & & & \ddots & \\ & & & & & c_{n-1} + c_n \end{bmatrix}$$

$$\boldsymbol{K} = \begin{bmatrix} k_1 & -k_1 & & & \\ -k_1 & k_1 + k_2 & & 0 & \\ & & \ddots & & \\ & & & \ddots & \\ & 0 & & & \ddots \\ & & & & & k_{n-1} + k_n \end{bmatrix} \quad \boldsymbol{X} = \begin{Bmatrix} x_1 \\ x_2 \\ \vdots \\ x_n \end{Bmatrix} \tag{2.44}$$

Equation (2.45) can be obtained:

$$\boldsymbol{M} \cdot \ddot{\boldsymbol{X}} + \boldsymbol{C} \cdot \dot{\boldsymbol{X}} + \boldsymbol{K} \cdot \boldsymbol{X} = -\boldsymbol{M} \cdot \boldsymbol{1} \cdot \ddot{y}(t) \quad \boldsymbol{1} = \begin{Bmatrix} 1 \\ 1 \\ \vdots \\ 1 \end{Bmatrix} \tag{2.45}$$

With respect to Eq. (2.45), $\boldsymbol{M}$, $\boldsymbol{C}$, and $\boldsymbol{K}$ are mass, damping and stiffness matrices, respectively. In addition, $\ddot{\boldsymbol{X}}$, $\dot{\boldsymbol{X}}$ and $\boldsymbol{X}$ are acceleration, velocity, and displacement vectors, respectively. $\boldsymbol{1}$ is the vector whose elements are all 1.

The following three methods are used to solve Eq. (2.45) under a given input acceleration $\ddot{y}(t)$ at the bedrock: (i) Direct integration in time domain; (ii) Integration in frequency domain by Fourier transformation; and (iii) Modal analysis.

For an analysis in which nonlinear characteristics of the material property of the soil or structures are considered, the direct integration in time domain is generally used.

2.4.3.1 Direct Integration in Time Domain

Under the condition in which $\boldsymbol{X}(t_{j-1})$ and $\boldsymbol{X}(t_j)$ are given at $t = t_{j-1}$ and $t = t_j$, $\boldsymbol{X}(t_{j+1})$ can be obtained by the following procedure (Fig. 2.22). For a constant time interval Δt, the velocity vector $\dot{\boldsymbol{X}}(t_j)$ can be expressed as

$$\dot{\boldsymbol{X}}(t_j) = \left[\boldsymbol{X}(t_{j+1}) - \boldsymbol{X}(t_j)\right]/\Delta t \tag{2.46}$$

Likewise, the acceleration vector $\ddot{\boldsymbol{X}}(t_j)$ is

$$\ddot{\boldsymbol{X}}(t_j) = \left[\boldsymbol{X}(t_{j+1}) + \boldsymbol{X}(t_{j-1}) - 2\boldsymbol{X}(t_j)\right]/\Delta t^2 \tag{2.47}$$

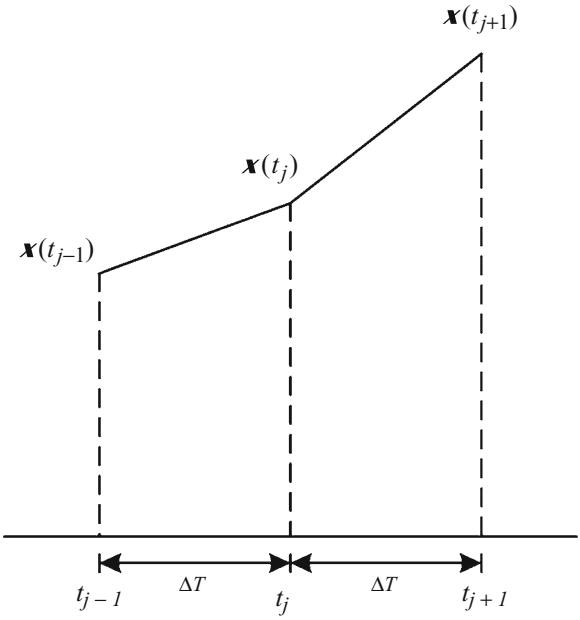

Fig. 2.22 Solution of vibration equation by direct integration method

By substituting Eqs. (2.46) and (2.47) into Eq. (2.44), the following is obtained:

$$\begin{aligned}\boldsymbol{M}\cdot\lfloor\boldsymbol{X}(t_{j+1})+\boldsymbol{X}(t_{j-1})-2\boldsymbol{X}(t_j)\rfloor/\Delta t^2+\boldsymbol{C}\cdot\lfloor\boldsymbol{X}(t_{j+1})-\boldsymbol{X}(t_j)\rfloor/\Delta t\\+\boldsymbol{K}\cdot\boldsymbol{X}(t_j)=-\boldsymbol{M}\cdot\boldsymbol{1}\cdot\ddot{y}(t_j)\end{aligned}\tag{2.48}$$

When $\boldsymbol{X}(t_{j-1})$, $\boldsymbol{X}(t_j)$, and input acceleration $\ddot{y}(t_j)$ at time of t_j are given, $\boldsymbol{X}(t_{j+1})$ can be attained. Repeating this procedure, the time history of $\boldsymbol{X}(t)$ is acquired.

2.4.3.2 Integration in Frequency Domain by Fourier Transformation

Fourier transformation $X_i(\omega)$ of the ith element $x_i(t)$ of the displacement vector $\boldsymbol{X}(t)$ is

$$X_i(\omega)=\int_{-\infty}^{\infty}x_i(t)\cdot e^{-i\omega t}\cdot d\omega\tag{2.49}$$

It therefore follows that Fourier transformation $\boldsymbol{X}_F(\omega)$ of the displacement vector $\boldsymbol{X}(t)$ becomes

$$\boldsymbol{X}_F(\omega)=\begin{Bmatrix}X_1(\omega)\\X_2(\omega)\\\vdots\\X_n(\omega)\end{Bmatrix}\tag{2.50}$$

Fourier transformation of the velocity vector $\dot{\boldsymbol{X}}(t_j)$ and acceleration vector $\ddot{\boldsymbol{X}}(t_j)$ are expressed as

$$-i\omega \boldsymbol{X}_F(\omega) \tag{2.51}$$
$$-\omega^2 \boldsymbol{X}_F(\omega)$$

Therefore, Fourier transformation of Eq. (2.45) can be done as

$$-\omega^2 \boldsymbol{M} \cdot \boldsymbol{X}_F(\omega) - i\omega \cdot \boldsymbol{C} \cdot \boldsymbol{X}_F(\omega) + \boldsymbol{K} \cdot \boldsymbol{X}_F(\omega) = -\boldsymbol{M} \cdot \boldsymbol{1} \cdot Y(\omega) \tag{2.52}$$

Here, $Y(\omega)$ is Fourier transformation of the input acceleration $\ddot{y}(t)$
From Eq. (2.52), the following can be obtained:

$$\boldsymbol{X}_F(\omega) = \left[\omega^2 \boldsymbol{M} + i\omega \cdot \boldsymbol{C} - \boldsymbol{K}\right]^{-1} \cdot \boldsymbol{M} \cdot \boldsymbol{1} \cdot Y(\omega) \tag{2.53}$$

Here, x_i(t) is displacement of ith element of vector $\boldsymbol{X}(t)$, which can be attained by inverse transformation $X_i(\omega)$, as shown below:

$$x_i(t) = \frac{1}{2\pi} \int_{-\infty}^{\infty} X_i(\omega) \cdot e^{i\omega t} \cdot d\omega \tag{2.54}$$

2.4.3.3 Modal Analysis

The equation of free vibration in which both the damping term and input motion $y(t)$ are zero, can be written from Eq. (2.45), as follows.

$$\boldsymbol{M} \cdot \ddot{\boldsymbol{x}} + \boldsymbol{K} \cdot \boldsymbol{x} = \boldsymbol{0} \tag{2.55}$$

Here $\boldsymbol{0}$ is a vector, all elements of which are zero.
When the displacement vector $\boldsymbol{x}(t)$ is written as

$$\boldsymbol{x} = \boldsymbol{X} \cdot e^{iwt} \tag{2.56}$$

the following is obtained:

$$-\omega^2 \cdot \boldsymbol{M} \cdot \boldsymbol{X} + \boldsymbol{K} \cdot \boldsymbol{X} = \boldsymbol{0} \tag{2.57}$$

where $\boldsymbol{X}$ expresses the vibration mode of the free vibration, and ω is circular frequency. Eq. (2.57) is rewritten as

$$\omega^2 \cdot \boldsymbol{X} = \boldsymbol{M}^{-1} \boldsymbol{K} \cdot \boldsymbol{X} \tag{2.58}$$

Thus, this becomes the eigenvalue problem of matrix $\boldsymbol{M}^{-1}\boldsymbol{K}$.

Different n values of ω satisfying Eq. (2.58) are attained, and vector $\boldsymbol{X}$ (vibration mode) is obtained as shown below.

$$\begin{array}{llll} 1st & \text{vibration} & \omega_1 & X_{11}, X_{21} \ldots\ldots\ldots\ldots X_{\mathrm{n}1} \\ ith & \text{vibration} & \omega_{\mathrm{i}} & X_{1i}, X_{2i} \ldots\ldots\ldots\ldots X_{ni} \\ \mathrm{n}th & \text{vibration} & \omega_{\mathrm{n}} & X_{1n}, X_{2n} \ldots\ldots\ldots\ldots X_{nn} \end{array} \tag{2.59}$$

In the above equation, X_{ji} expresses the vibration mode value of the jth mass of the ith vibration. The ith vibration mode is

$$\boldsymbol{X}_i = \begin{Bmatrix} X_{1i} \\ X_{2i} \\ \vdots \\ X_{ni} \end{Bmatrix} \tag{2.60}$$

$\boldsymbol{X}_i$ satisfies the following equation:

$$-\omega_i^2 \cdot \boldsymbol{M} \cdot \boldsymbol{X}_i + \boldsymbol{K} \cdot \boldsymbol{X}_i = \boldsymbol{0} \tag{2.61}$$

Likewise, the jth vibration mode $\boldsymbol{X}_j$ satisfies the following:

$$-\omega_j^2 \cdot \boldsymbol{M} \cdot \boldsymbol{X}_j + \boldsymbol{K} \cdot \boldsymbol{X}_j = \boldsymbol{0} \tag{2.62}$$

By multiplying Eq. (2.61) by the transpose vector $\boldsymbol{X}_j^T$ and Eq. (2.62) by transpose vector $\boldsymbol{X}_i^T$ the following is obtained:

$$-\omega_i^2 \boldsymbol{X}_j^T \cdot \boldsymbol{M} \cdot \boldsymbol{X}_i + \boldsymbol{X}_j^T \cdot \boldsymbol{K} \cdot \boldsymbol{X}_i = \boldsymbol{0} \tag{2.63}$$

$$-\omega_i^2 \boldsymbol{X}_i^T \cdot \boldsymbol{M} \cdot \boldsymbol{X}_j + \boldsymbol{X}_i^T \cdot \boldsymbol{K} \cdot \boldsymbol{X}_j = \boldsymbol{0} \tag{2.64}$$

where each of $\boldsymbol{X}_j^T \cdot \boldsymbol{K} \cdot \boldsymbol{X}_i$ and $\boldsymbol{X}_i^T \cdot \boldsymbol{K} \cdot \boldsymbol{X}_j$ is scalar. Therefore, the following are attained:

$$\left(\boldsymbol{X}_j^T \cdot \boldsymbol{K} \cdot \boldsymbol{X}_i\right)^T = \boldsymbol{X}_j^T \cdot \boldsymbol{K} \cdot \boldsymbol{X}_i \tag{2.65}$$

$$\boldsymbol{X}_i^T \cdot \boldsymbol{K}^T \cdot \boldsymbol{X}_j = \boldsymbol{X}_j^T \cdot \boldsymbol{K} \cdot \boldsymbol{X}_i \tag{2.66}$$

Because stiffness matrix $\boldsymbol{K}$ is symmetric,

$$\boldsymbol{X}_i^T \cdot \boldsymbol{K} \cdot \boldsymbol{X}_j = \boldsymbol{X}_j^T \cdot \boldsymbol{K} \cdot \boldsymbol{X}_i \tag{2.67}$$

Likewise, because mass matrix $\boldsymbol{M}$ is diagonal, the following is obtained:

$$\boldsymbol{X}_i^T \cdot \boldsymbol{M} \cdot \boldsymbol{X}_j = \boldsymbol{X}_j^T \cdot \boldsymbol{M} \cdot \boldsymbol{X}_i \tag{2.68}$$

Subtracting Eq. (2.64) from Eq. (2.63) produces

$$\left(\omega_j^2 - \omega_i^2\right) \cdot \boldsymbol{X}_j^T \cdot \boldsymbol{M} \cdot \boldsymbol{X}_i = 0 \tag{2.69}$$

where $\omega_i \neq \omega_j$; that is, if i≠j, the following is obtained:

$$\boldsymbol{X}_j^T \cdot \boldsymbol{M} \cdot \boldsymbol{X}_i = 0 \tag{2.70}$$

This is called orthogonal condition of the vibration mode. Likewise, we obtain

$$\boldsymbol{X}_j^T \cdot \boldsymbol{K} \cdot \boldsymbol{X}_i = 0 \tag{2.71}$$

The modal analysis method solves a partial differentiation equation using orthogonal condition among the vibration modes. The solution of Eq. (2.45) is

$$[\boldsymbol{X}] = [\,\boldsymbol{X}_1 \quad \boldsymbol{X}_2 \ldots \boldsymbol{X}_i \ldots \boldsymbol{X}_n\,] \cdot \begin{Bmatrix} q_1(t) \\ q_2(t) \\ \vdots \\ q_i(t) \\ \vdots \\ q_n(t) \end{Bmatrix} \tag{2.72}$$

where $\boldsymbol{X}_i$ is the ith vibration mode, and $q_i(t)$ is a time function relating to the ith vibration. Suppose that damping matrix $\boldsymbol{C}$ is proportional for mass matrix $\boldsymbol{M}$ or stiffness matrix $\boldsymbol{K}$. By substituting Eq. (2.72) into Eq. (2.45) and by orthogonal condition of the vibration mode mentioned above, the following is obtained.

$$\ddot{q}_i + 2\omega_i h_i \dot{q}_i + \omega_i^2 q_i = -\frac{\boldsymbol{X}_i^T \cdot \boldsymbol{M} \cdot \boldsymbol{1}}{\boldsymbol{X}_i^T \cdot \boldsymbol{M} \cdot \boldsymbol{X}_i} \ddot{y}(t) \tag{2.73}$$

In the above equation, h_i is the critical damping constant regarding the ith vibration. Provided the damping matrix $\boldsymbol{C}$ is given, the critical damping constant can be calculated. However, h_i corresponding to each vibration mode is directly determined in all general cases. Using masses m_1 to m_n of the individual mass, the right side of Eq. (2.73) is

$$-\frac{\boldsymbol{X}_i^T \cdot \boldsymbol{M} \cdot \boldsymbol{1}}{\boldsymbol{X}_i^T \cdot \boldsymbol{M} \cdot \boldsymbol{X}_i} \ddot{y}(t) = -\frac{\sum_{j=1}^{n} m_j X_{ji}}{\sum_{j=1}^{n} m_j X_{ji}^2} \ddot{y}(t) \tag{2.74}$$

The fraction on the right side is called a excitation function of the vibration mode. A vibration mode with larger excitation function has greater influence on vibration of the mass-spring –damper model. Eq. (2.73) is the same as that of the dynamic response of the single mass-spring-damper model shown in Eq. (2.7). Provided the input earthquake motion $\ddot{y}(t)$ is given, the time history of $q_i(t)$ can be attained. Furthermore, substituting $q_i(t)$ of Eq. (2.73) into Eq. (2.72) makes it possible for vector $\boldsymbol{X}(t)$ of the time history of response displacement to be calculated.

2.5 Seismic Reinforcement

The Japan Society of Civil Engineers (JSCE) recommended the followings with respect to seismic diagnosis and reinforcement of existing civil engineering structures after the 1995 Kobe earthquake. The first recommendation stated "Keeping the experience of disaster caused by the Kobe earthquake in mind, seismic diagnosis of existing structures shall be promoted in order of importance, and necessary reinforcement shall be rapidly promoted" [8]. The second recommendation states "The aim of seismic reinforcement shall be the same as that of newly built structures, and studies and development concerning seismic diagnosis and reinforcement technology shall be promoted."

The third recommendation of the Japan Institute of Architecture (AIJ) also indicates the "...importance of development of technologies for diagnosis and reinforcement of historical buildings and existing structures that do not satisfy the current standard of earthquake resistance. AIJ also indicates the necessity of investment and social alignment for retrofitting." Furthermore, the *Basic Disaster Prevention Plan* [9], revised in July 1995, states that "Enhancement of earthquake resistance of major infrastructures based on damage assessment should be dealt with as an important subject in the future."

Based on these recommendations, earthquake-resistant reinforcement has been carried out on infrastructures such as bridges, subways, quay walls, road and railway embankments, and with various types of lifelines. In this section, this reinforcement is described mainly with respect to civil engineering structures. Reinforcement of ground and foundations against soil liquefaction and liquefaction-induced ground displacements are introduced in Sects. 3.3 and 4.4.

2.5.1 Seismic Reinforcement of Concrete Piers

Considering the destruction of concrete piers by the 1995 Kobe earthquake, earthquake-resistant reinforcement of about 16,000 piers of road bridges, railway viaducts, subways and other structures was executed after the earthquake. Reinforcement of concrete piers was done by steel plate jacketing (Fig. 2.23a) or new

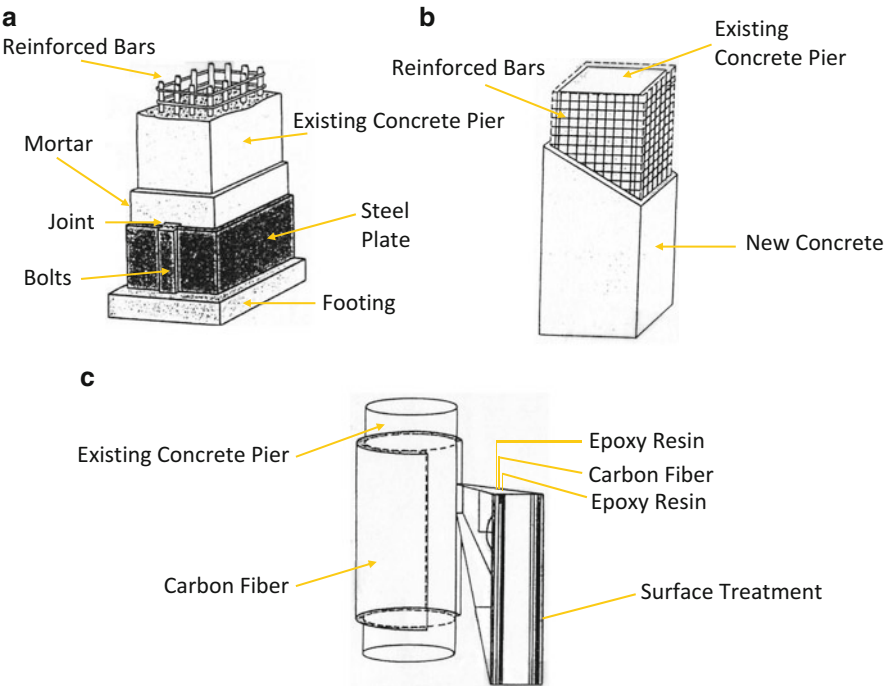

Fig. 2.23 Reinforcement of concrete piers. (**a**) Steel plate jacketing. (**b**) New concrete casting. (**c**) Carbon fiber facing

concrete casting (Fig. 2.23b). Examples of the reinforcement of viaducts of the Shinkansen (new trunk line), center columns of a subway, and piers of an express highway are shown in Fig. 2.24. Shear failures of subway center columns resulted in total collapse in Kobe. Therefore, about 3,000 concrete subway columns were reinforced in big cities, such as Tokyo and Osaka. In addition to the above-mentioned two methods, reinforcement by aramid and carbon fibers (Fig. 2.23c), and PC steel bars have been adopted. Furthermore, for rigid-frame piers, methods to construct shear walls between the piers and methods using dampers have been developed. The effectiveness of concrete pier reinforcement by steel jacketing was examined by model tests. It was confirmed that both strength and ductility of reinforced piers increased.

2.5.2 Seismic Reinforcement of Earth Dams

Niteko Reservoir dam in Nishinomiya slid and sank significantly in the 1995 Kobe earthquake (Fig. 2.25). N-values of the dam body and foundation ground were less than 10, and circular slip was caused by strong earthquake motion near the

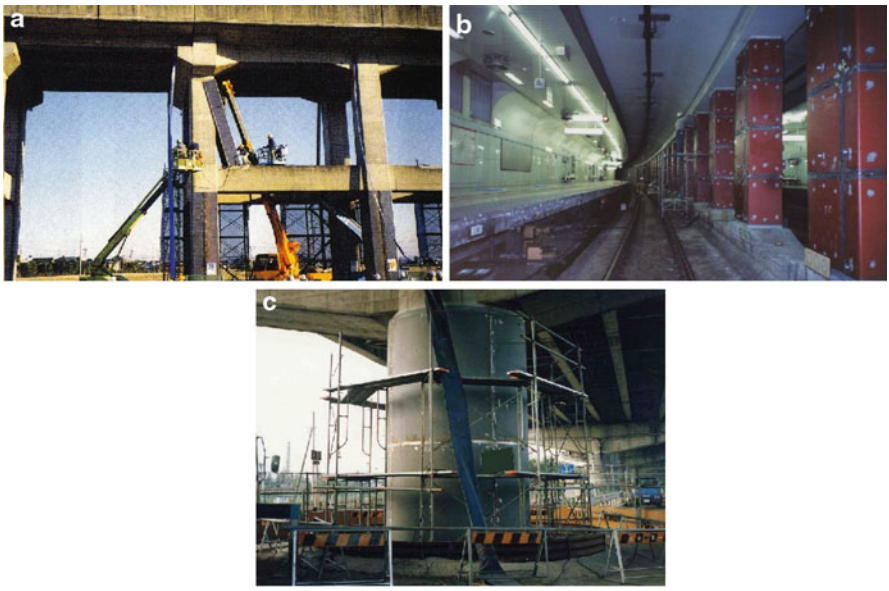

Fig. 2.24 Seismic reinforcement of concrete structures (by steel jacketing). (**a**) Concrete viaduct of shinkansen (*new trunk line*). (**b**) Center concrete column of subway station. (**c**) Concrete bridge pier of a express way

Fig. 2.25 Slide and sinkage of Niteko earth dam (1995 Kobe earthquake)

active fault. The dam was located in a densely populated area and had height approximately 15 m. Fortunately, the water level of the reservoir at the time of the earthquake was low, so there was no flooding.

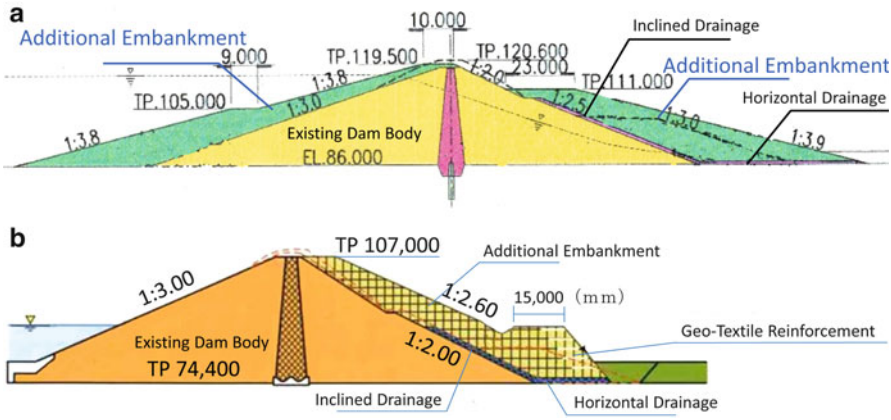

Fig. 2.26 Reinforcement of earth dams (Tokyo bureau of waterworks). (**a**) Yamaguchi reservoir (additional embankment). (**b**) Murayama reservoir (additional embankment and geo-textile reinforcement)

Motivated by such damage to the dam, the Tokyo Bureau of Waterworks conducted seismic reinforcement of two earth dams, at Yamaguchi (Sayama Lake) and Murayama (Tama Lake) reservoirs by methods illustrated in Fig. 2.26 [13]. The heights of Yamaguchi and Murayama dams are 34.6and 32.6 m, respectively. When dam construction began, surrounding areas were forested, but residential areas have been gradually developed. In particular, the downstream area had been rapidly populated. Therefore, dam safety should be ensured to protect life and property of people against level 2 earthquake ground motion that is predicted to be caused by nearby faults.

Each dam was reinforced by additional embankments on their surfaces to enhance safety against surface sliding. As illustrated in Fig. 2.26a, embankments were added on both upstream and downstream sides of Yamaguchi dam. Embankments were added on the downstream surface of Murayama dam. Furthermore, a method to reinforce the end of a slope with geotextiles was used (Fig. 2.26b), because the end of the embankment abuts parkland. The added embankment increases effective stress of the dam and thereby ensure the safety against slope sliding failure.

2.6 Measures Against Surface Earthquake Faults

There are more than 2,000 active faults in Japan. With particular regard to the 98 fault belts with relatively high activity, the Headquarters for Earthquake Research Promotion of the Ministry of Education, Culture, Sports, Science and Technology (MEXT) is engaged in a continuous survey of this fault belts. An active fault in the earth crust whose failure emerges at the surface is called a surface

Table 2.3 Earthquake faults (1981–1995)

Year	Earthquake	Faults	Fault offset	
			V: vertical (m)	H: horizontal (m)
1981	Nobi	Neodani	4.0	6.0
1896	Rikuu	Senya faults	3.5	–
1923	Kanto	Enmaiji	1.9	1.2
1925	Tajima	Tai	1.0	–
1927	Northern-Tango	Atomura	0.5	3.0
1930	Northern-Izu	Tanna	1.8	3.5
1938	Kussharo	Kussharo	0.9	2.6
1943	Tottori	Shikano	0.5	1.5
1945	Mikawa	Fukamizu	2.0	1.3
1948	Fukui	Fukui	0.7	2.0
1978	Izu Oshima offshore	Inatori-Omineyama	0.36	1.15
1995	Kobe	Nojima	1.6	1.8

earthquake fault or simply an earthquake fault. Examples of earthquake faults in Japan over 130 years are shown in Table 2.3. Among these, the 1891 Nobi earthquake caused the greatest surface fault. The Neodani Fault appeared on the surface, producing a 6.0 m offset in the horizontal and 4.0 m in the vertical. In the 1995 Kobe earthquake, the fault offset at Hokutan in Awaji Island was 1.8 m in the horizontal and 1.6 m in the vertical. Globally, many earthquake faults have appeared at the ground surface, destroying structures. In the 1999 Kocaeli (Turkey) earthquake, concrete girders of a bridge crossing an earthquake fault collapsed (Sect. 1.2.1). In the 1999 Chi-Chi earthquake, Taiwan, a concrete dam of height 25 m was destroyed by a 10 m differential displacement in the vertical direction from a reverse fault (Sect. 1.2.2). Fortunately, there are no known examples of direct damage to important structures by surface earthquake faults in Japan.

However, in the 1930 Northern-Izu earthquake (Table 2.3), faults crossed Tanna tunnel of the Tokaido Railway Line, which was under construction. The tunnel excavation face was completely lost. Furthermore, in the 1978 Off-Izu Oshima earthquake, the Inatori-Omineyama Fault crossed Inatori Tunnel, destroying the lining. It was reported that a large amount of soil entered the tunnel. The rail was lifted 50 cm, and meandered about 50 cm in the horizontal [14].

What measures should be taken to protect important structures against earthquake faults? Definitive countermeasures are exceedingly difficult but few have been realized. An example of such countermeasures for earthquake faults is Fuji River Bridge of the Tokaido Shinkansen (new trunk line). Near the Fuji River is Iriyamase Fault, with a high activity degree. Based on the supposition that this fault will move during the predicted Tokai earthquake, the effect on the bridge was examined. By surmising the amount of fault movement, damage to the truss bridge members was numerically analyzed. Based on this analysis, the top of a pier was expanded to prevent girders from falling (Fig. 2.27a). Together with this, preparatory members of the bridge and shoes that are presumed susceptible to be damaged

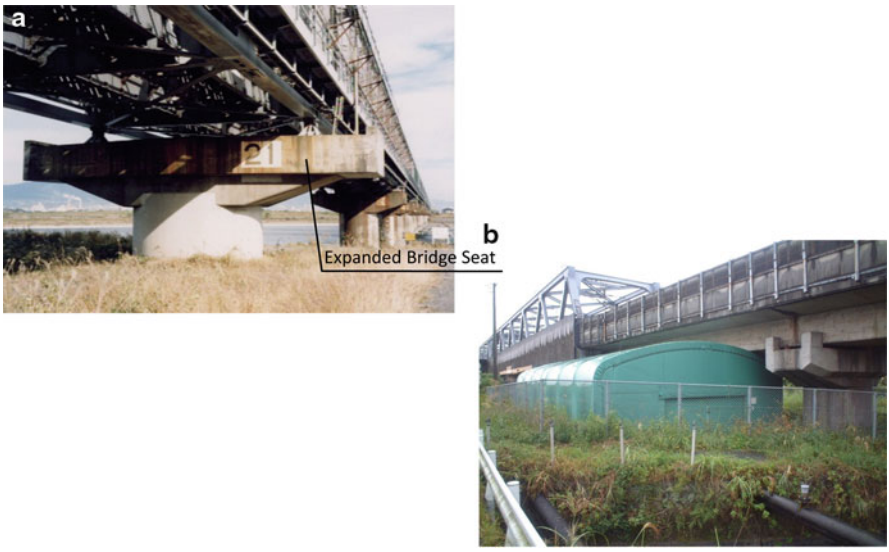

Fig. 2.27 Measures for Tokaido shinkansen against surface earthquake fault. (**a**) Expansion of bridge seat for prevention of girders' falling. (**b**) Storage of preparatory members of the truss bridge

were fabricated and kept in a hangar near the bridge (Fig. 2.27b). These measures are not aimed at operational safety of the high-speed train, but are intended for early recovery. It is difficult to ensure operational safety against earthquake faults directly beneath high-speed train like the Shinkansen. Particularly, safety is threatened wherever earthquake faults cross a tunnel.

Here is one more example of countermeasures for the Shinkansen against earthquake faults [15]. In construction of a viaduct of the platform of New-Kobe station of the Sanyo Shinkansen, an earthquake fault was found during excavation of foundation ground (Fig. 2.28). Through geologic survey, earthquake fault offset was shown to have exceeded 70 cm in the vertical during the last 10,000 years or so. To deal with the fault offset in the future, movable shoes were installed between the platform deck and viaduct. Furthermore, the floor slab of the platform and columns were connected by hinges. These countermeasures are intended to absorb vertical offset of the earthquake fault and rotational deformation. However, this cannot guarantee operational safety of the Shinkansen.

There are several examples of countermeasures to protect structures against surface earthquake faults in the world. One of the water supply sources of East Bay Municipal Utility District (EBMUD) in Oakland, USA, is Pardee Reservoir to the west of the city (Fig. 2.29a). A trunk line connects the reservoir with Oakland, which is crossed by the Hayward Fault in the Claremont Tunnel (Fig. 2.29b). Therefore, flexible pipes were used in the tunnel and shutdown valves were installed at its exits. Furthermore, temporary hoses were prepared for emergency water supply and stored in the neighborhood. In addition to these measures, EBMUD constructed a new trunk line, the South Trunk Line (Fig. 2.29a), to form a loop network for the water supply.

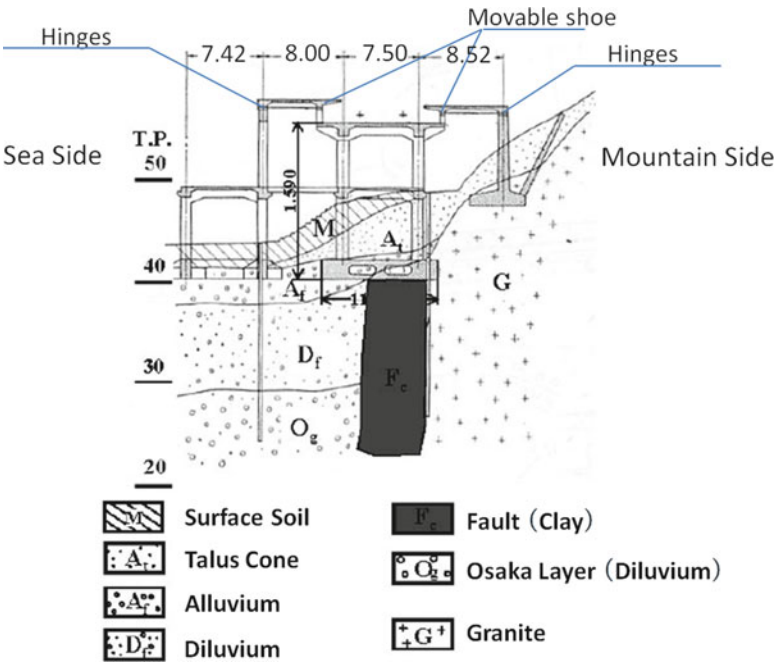

Fig. 2.28 Measures for new Kobe station of Sanyo shinkansen against earthquake faults [15]

These countermeasures are only possible when the location of the earthquake fault can be identified with high reliability. If surface ground is composed of thick soil, it is difficult to identify locations of earthquake faults in the bedrock.

Another example of countermeasures against earthquake faults is the case of Clyde Dam in the South Island of New Zealand, shown in Fig. 2.30, which is gravity-type concrete dam with a height of 102 m. Waterproof slip joints were installed in the dam body along the vertical direction. This joint can absorb 2 m fault offset in the horizontal and 1 m in the vertical [16].

2.7 Earthquake-Resistant Design of Nuclear Power Plants

2.7.1 Accident at the Fukushima Daiichi Nuclear Plant

The plan and concrete methods to end the serious accident at the Fukushima Daiichi Nuclear Power Plant are not yet decided at the time of this writing, but contamination by radioactive materials spread not only through Fukushima Prefecture but also over wide areas of Tohoku and Kanto regions. It is believed that it will take several 10 years to terminate this disaster.

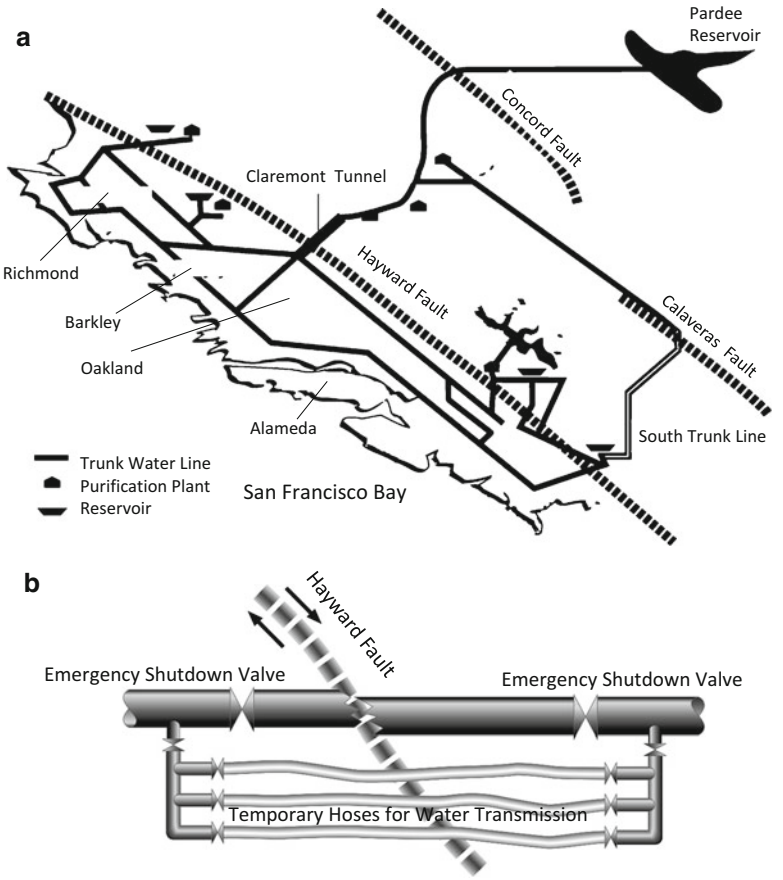

Fig. 2.29 Measure by EBMUD (East Bay Municipal Utility District) against earthquake fault. (**a**) Reinforcement of water transmission network by construction of south trunk line. (**b**) Emergency shutdown valves and temporary hoses

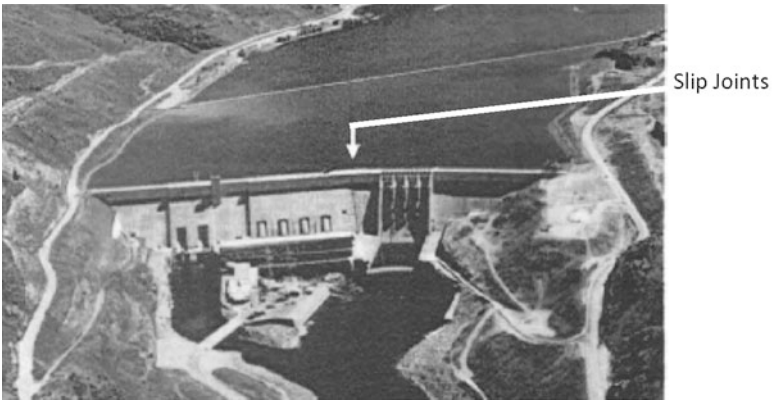

Fig. 2.30 Clyde dam with slip joints for absorbing of faults offset (height: 102 m, concrete dam)

Ensuring nuclear power plant safety in an emergency requires the following three major procedures [17].

(i) Ceasing the nuclear reaction
(ii) Cooling nuclear fuels to a cryogenic state
(iii) Confining radioactive materials in the nuclear reactor

Nuclear reaction at the Fukushima Daiichi Nuclear Power Plant was successfully halted by control-bar insertion in all reactors (Nos. 1 through 4) but all electric (including emergency) power sources were lost, triggering a hydrogen explosion. Thus, a large amount of radioactive material was emitted and dispersed. Concurrently, a large amount of contaminated water entered the sea, increasing the danger of contamination to fish and shellfish. A temporary cooling system for the nuclear reactor and fuel was constructed, in which radio active contamination of the water from the reactor was lowered and was returned to the reactor.

It is no exaggeration to say that the origin of the serious accident at the 1st Fukushima Nuclear Power Plant was due to the failure of tsunami prediction and countermeasures. It remains to be seen whether public confidence in atomic power can be restored for the continuance of nuclear power generation. To restore this confidence, it is necessary to fully comprehend why the prediction of tsunami height in the plant design was failed. Extensive examination of expected tsunamis is mandatory for the design of nuclear power plants. Taking necessary tsunami-resistant countermeasures during this examination is urgently required.

To maintain nuclear power generation in Japan, it is critical to have the concurrence of the public. To accomplish this, understandable explanations of the accident causes and exact information on tsunami-resistant countermeasures are essential.

In recent years, nuclear power generation has been promoted in underdeveloped countries, including in Asia. However, serious accidents have widespread and substantial effects. Safety of nuclear power plants against earthquakes and tsunamis must be inspected according to standards of individual countries and International Atomic Energy Agency (IAEA) guidelines. Japan, which unfortunately experienced the accident at the 1st Fukushima plant, is required to contribute to the improvement of earthquake and tsunami resistance of nuclear power plants based on its experience.

The author has long participated in inspecting earthquake resistance of nuclear power plants, as a member of the Nuclear Reactor Safety Inspection Committee of Japan. He has also taught earthquake-resistant engineering of nuclear facilities in a nuclear engineering course at a joint graduate school of Waseda University and Tokyo City University. The present state and problematic issues of earthquake-resistant design of nuclear power plants are introduced in this session.

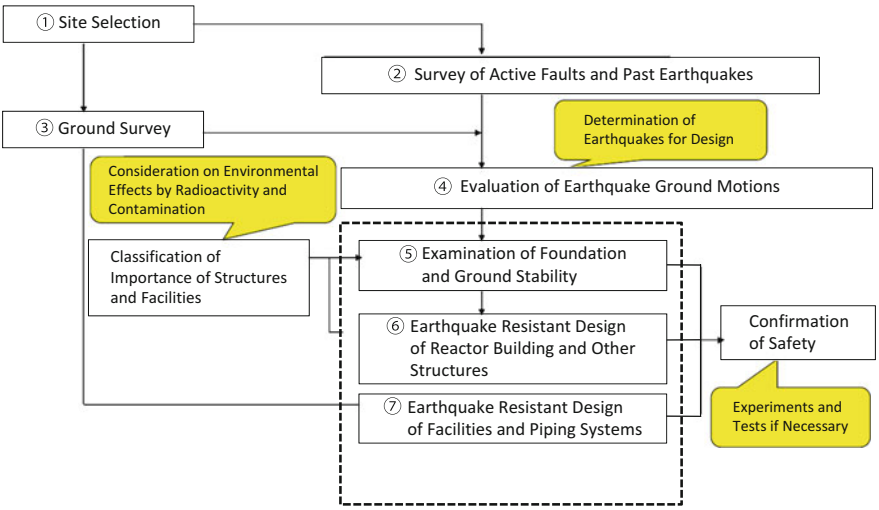

Fig. 2.31 Flow of earthquake resistant design of nuclear power plant

2.7.2 Flowchart of Earthquake-Resistant Design of Nuclear Power Plants and Surveys of Active Faults

A flowchart of the earthquake-resistant design of nuclear power plants is given in Fig. 2.31. In that chart, a survey of active faults and past earthquakes is required over a wide region to determine ground motions for the design. Referring to the literature about active faults in the plant surroundings, those faults affecting seismic safety of the plant are selected. In the next stage, lineament survey by air photos, outcrop observation, geologic survey by elastic and sound waves, and trench excavation are carried out. For geologic and soil conditions of the seabed near the plant, investigation is done mainly by sonic prospecting.

Nevertheless, it is generally difficult to detect all active faults that substantially affect seismic safety of the nuclear plant during the design stage. As mentioned in Sect. 1.3.5 and 1.3.8, active faults which caused the 2004 Niigata-Chuetsu and 2008 Iwate-Miyagi Inland earthquakes have not been recognized prion to earthquake occurrence.

Surveying active faults in sea regions is more difficult than on land, causing frequent misjudgment or oversight of such faults. The 2007 Niigata-Chuetsu offshore earthquake caused accidents such as electric transformer fire, overflow of cooling water from spent fuel tanks, and others. As illustrated in Fig. 1.84, earthquake ground motion observed on a reactor-building basement greatly exceeded the design motion. These facts impugn the reliability of active fault surveys for determining earthquake ground motions in the design.

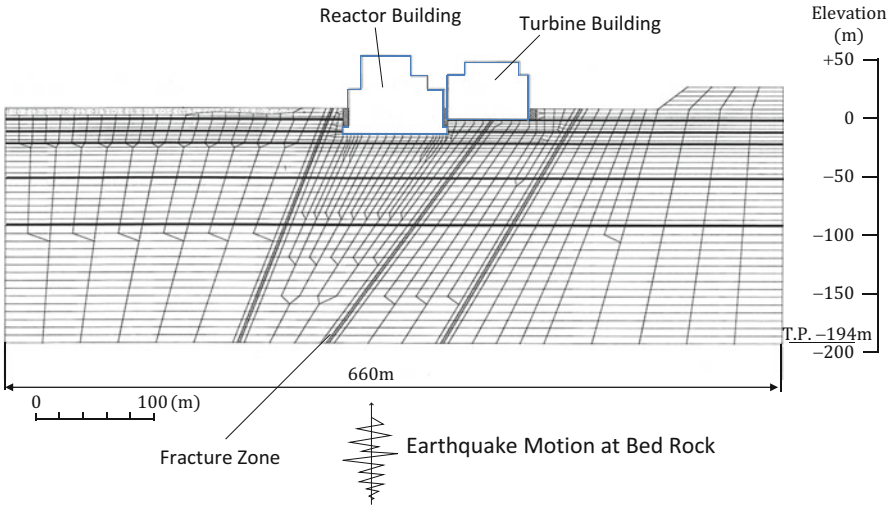

Fig. 2.32 Finite element model for dynamic analysis of foundation ground and building of nuclear power plant

Similar findings were reported in the 2007 Noto Peninsula earthquake. In design and construction of the Shika Nuclear Power Plant, active faults were identified (Fig. 1.79). However, the active fault that caused the earthquake was overlooked, but was identified after the event. Such oversight for two nuclear power plants highlights the difficulty of active fault surveys, particularly in sea regions.

2.7.3 Earthquake-Resistant Design of Structures, Facilities and Foundation Ground [17]

After selecting the active fault in earthquake-resistant design of the plant, earthquake motion on the bedrock is evaluated based on the magnitude of the fault, distance from the fault to the plant, and properties of the bedrock. Using the earthquake ground motion, the bedrock stability is examined with a finite element model (Fig. 2.32), in which fissures and weak seams are also modeled. The stiffness and strength of rock and weak seams are surveyed by in-situ and laboratory tests.

In the next stage, the dynamic response of structures such as reactor buildings is simulated, using bedrock motion as an input wave. Based on the simulation result, structure safety is examined and dynamic response of each floor of the structures is calculated for the design of facilities and piping on the floor.

For nuclear power plants, intake ducts for emergency cooling water, which allow the nuclear reactor to be submerged during serious accidents, are constructed.

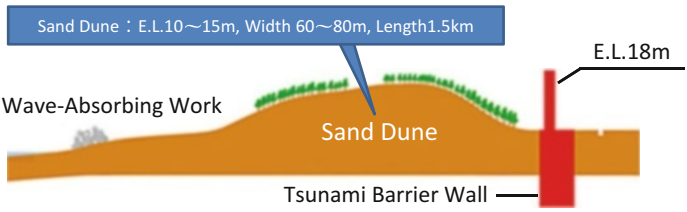

Fig. 2.33 Construction of tsunami barrier wall (Hamaoka nuclear power plant)

The intake ducts generally have a concrete box section, and steel pipes to take in water are installed inside the ducts. Earthquake-resistant design of these ducts is done by the response displacement method described in Sect. 5.6.

There are often slopes on the backsides of nuclear power plants. Nuclear reactor and turbine buildings locate on flat land constructed by excavation, leaving these slopes. In earthquake-resistant design of plants, it is necessary to examine slope stability and, in the worst case, the effect of the downward collapse of soil on the safety of these buildings.

2.7.4 Measures Against Tsunamis

The safety of nuclear power plants against tsunamis is examined with the following constraints:

(i) No seawater flows into the site, even at high tide. That is, the height of the site is higher than that of full tide plus the assumed tsunami height.
(ii) Even if the sea surface is lowered during the receding water stage of a tsunami, water intake should be ensured. However, if this intake becomes impossible, cooling water should be ensured by its storage in pits and tanks.
(iii) Seabed scouring or soil accretion around the intake gate by a tsunami should be prevented.

The accident at the Fukushima Daiichi Nuclear Power Plant was caused by the first requirement not being satisfied. Although it is critical to determine the anticipated height of tsunamis at nuclear power plants nationwide, it is also important to maintain cooling system functions. For this, emergency power functions should be secured. Countermeasures, such as a stock of spare power generators at high elevations or in watertight chambers, should be taken for post-disaster operation.

At Hamaoka Nuclear Plant in Shizuoka Prefecture, tsunami barrier walls of height above sea level 18 m and 1.6 km length were constructed along the coast (Fig. 2.33). These are for protection against a tsunami caused by an earthquake that has been predicted along the Nankai sea trough. Figure 2.34 shows the tsunami

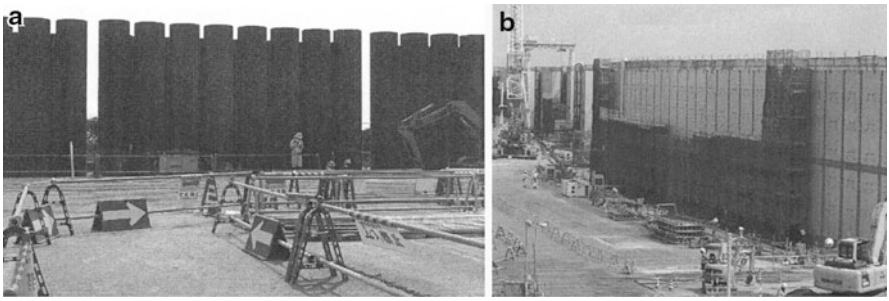

Fig. 2.34 Tsunami barrier wall of Hamaoka nuclear power plant. (**a**) Steel pipe wall. (**b**) Steel box wall

barrier walls under construction, which use continuous steel piles and steel box frames. Construction of such walls is being planned for another nuclear plants. However, the problem for wall design is the tsunami height. Geologic and seismic surveys by the Central Council for Disaster Prevention indicate that tsunamis of several tens of meters height may impact the sea coast along the Nankai Sea trough. In addition to hardware measures including construction of tsunami barrier walls, software measures should be sought to avoid serious accidents. These would maintain electric power source systems for cooling, even if tsunami water overtops barrier walls and flows into the site.

2.8 Countermeasures for Sewage Facilities Against Tsunamis

In the 2011 Tohoku earthquake, wastewater treatment plants and pumping stations of sewage systems were subjected to severe damage across a wide region, from the Tohoku to the Kanto. Among these plants within an area 100 m from the coast, 90 % lost all function. Furthermore, with tsunami inundation height greater than 3.0 m, all wastewater treatment function ceased. To deal with such damage to sewage systems from tsunamis, the Technical Committee for Earthquake and Tsunami Restraint Sewage Systems proposed a basic concept for design and countermeasures of sewage facilities against tsunamis [18]. In this proposal, prevention of wastewater backflow, pumping, and disinfection were designated as mandatory functions. Functions of sedimentation and sludge treatment should be rapidly recovered, although temporary interruptions were allowed. Facilities with the mandatory functions should be located above inundation water levels, or be protected by walls of height greater than those levels (Fig. 2.35). For facilities whose functions should be rapidly recovered, water protection structures are required.

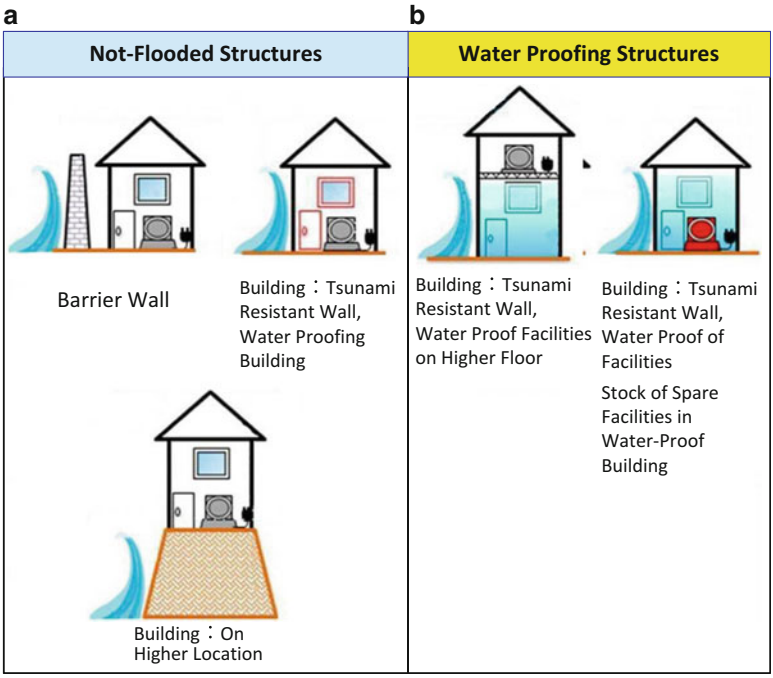

Fig. 2.35 Measures for sewage system against tsunami. (**a**) Measures for preservation of function. (**b**) Measures for quick recovery of function

When sewage facilities are severely damaged by earthquake ground motion or tsunami, the impact on the public is severe. There is the possibility for a secondary disaster, such as the spread of disease. All of treatment plants and pumping stations are built on sites near coasts. Therefore, both hardware and software measures should be implemented. The latter include the security of emergency electric power sources and evacuation system for the staffs.

References

1. Sano R (1917) Theory of earthquake resistant structures of houses, Association for Earthquake Disaster Prevention
2. National Research Institute for Earth Science and Disaster Prevention Home Page. http://www.bosai.go.jp/e/
3. Japan Road Association (1996/2002) Specifications for highway bridges, and explanation, Part V Seismic design. Japan Society of Civil Engineers (JSCE) (2000) Earthquake resistant codes in Japan, 1996 Seismic design specifications of highway bridges
4. JSCE (1965) Report on the 1964 Niigata earthquake and the caused damage (in Japanese)
5. Duke CM, Moran DF (1975) Guideline for evolution of lifeline earthquake engineering. In: Proceedings of the US national conference on earthquake engineering

6. Japan Gas Association (1982) Standards for earthquake resistant design of high pressure gas (in Japanese)
7. Nishi H, et al. Calculation of overflow volume of oil due to sloshing vibration, Journal of Pressure Technology, no. 46, vol. 5, pp 276–284 (in Japanese)
8. JSCE (1996) Proposal on earthquake resistant for civil engineering structures
9. Cabinet Office of the Japanese Government (1995) Basic disaster prevention plan (in Japanese)
10. Japan Water Works Association (1997) Basic principles of seismic design and construction for water supply facilities/JSCE (2000) Earthquake resistant codes in Japan
11. Railway Technical Research Institute (1999) Seismic design for railway structures and commentary. Seismic design of railway structures/JSCE (2000) Earthquake resistant design codes in Japan
12. Bureau of the Ports and Harbors, Ministry of Transport (1999) Technical standards and commentaries for port and harbor facilities earthquake resistant design of port facilities/ JSCE (2000) Earthquake resistant design codes in Japan
13. Tokyo Bureau of Waterworks (1212) Report on seismic reinforcement of Murayama Reservoir Dam (in Japanese)
14. Hakuno M, Fujino Y, Katada T (1978) Report on the 1978 Izu-shima offshore earthquake and it's caused damage. Bulletin of Seismology Institute University of Tokyo, vol 53 pp 1101–1133 (in Japanese)
15. Morishige R (1970) Special construction works of the Sanyo Shinkansen. Report on design of railway structures (in Japanese)
16. Hatton JW, Forster PF, Thomson R (1991) The influence of foundation conditions on the design of Clyde Dam Trans. 17 ICOLD (17th international commission on large dams), vol 66
17. Nuclear Safely Committee (2006) Safely guidelines for earthquake resistant design of nuclear power plant (in Japanese)
18. Technical Committee for Earthquake and Tsunami Resistant Sewage Systems (1212) Japan Sewage Works Association. Basic concept for design and countermeasures of sewage facilities against tsunamis (in Japanese)

Chapter 3
Soil Liquefaction and Countermeasures

Abstract The mechanism of soil liquefaction caused by earthquake ground motion and the soil conditions for the occurrence of liquefaction is explained. Liquefaction-induced damages to structures during past earthquakes, such as subsidence and inclination of buildings and bridges, uplift of underground structures, collapse of quaywalls and embankment are introduced. The methods of estimation of liquefaction potential based on topographical and geographical conditions, in-situ soil test, laboratory tests and dynamic response analysis of surface ground are mentioned. Furthermore, two ways for reduction of liquefaction-caused damages of buildings, residential houses and embankment against soil liquefaction are introduced. One is how to prevent the occurrence of soil liquefaction and another is how to protect the structures against soil liquefaction. Finally, the construction methods for restoration of houses and buildings inclined and subsided by liquefaction are explained.

Keywords Countermeasures against liquefaction • Damage to structures due to liquefaction • Liquefaction potential • Restoration of damaged structures • Soil liquefaction

3.1 Mechanism of Soil Liquefaction and Its Damage

3.1.1 Mechanism of Soil Liquefaction

Figure 3.1 shows a baseball field in Noshiro of Akita Prefecture just after the 1983 central Japan Sea earthquake, which caused widespread soil liquefaction [1]. The figure captures the moment of the seismically triggered "sand boil." Figure 3.2, was taken in the suburb of Dagupan after the 1990 Luzon Islands earthquake in the Philippines, showing a sand volcano of several meters in diameter, with sand and

M. Hamada, *Engineering for Earthquake Disaster Mitigation*,
Springer Series in Geomechanics and Geoengineering,
DOI 10.1007/978-4-431-54892-8_3, © Springer Japan 2014

Fig. 3.1 Sand and water boiling due to soil liquefaction (1983 Central Japan Sea earthquake) [1]

Fig. 3.2 A large sand volcano (1990 Luzon earthquake, Philippines) [2] (the diameter of sand volcano was about 5 m and sand spread about 15 m in radial direction)

water spreading outward concentrically [2]. According to local residents on the scene, the sand surged as high as the tops of telephone poles. Although this may have been exaggerated because of the state of agitation of these witnesses, the fact that an enormous volume of sand and water boiled out of the ground is indisputable.

The mechanism of soil liquefaction and the reason for the sand and water boiling can be understood as follows. As indicated schematically in Fig. 3.3, water completely fills the pores between sand grains, attaining a saturation condition. Prior to an earthquake, sand grains are coalesced and support both the weight of soil and structures on or in the ground. During earthquake ground motion, however, the sand grains lose their contacts to each other. The state like a liquid mixed with sand grains and pore water is called liquefaction.

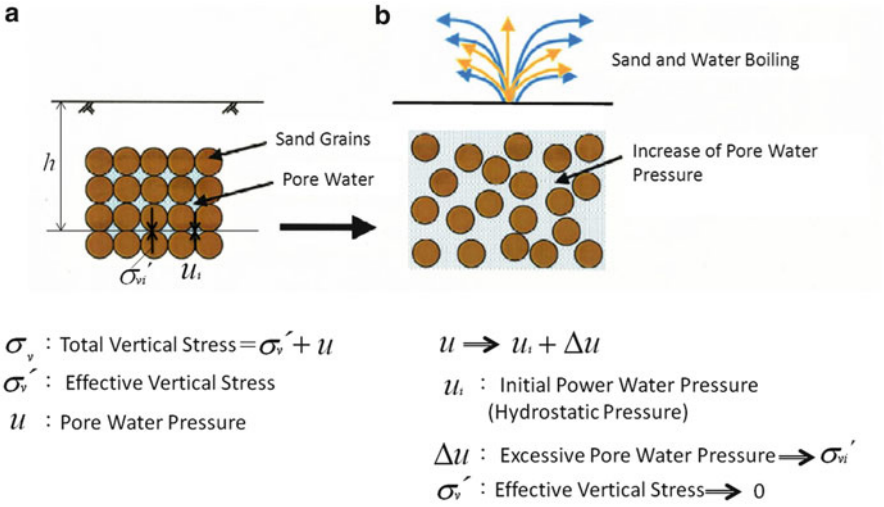

Fig. 3.3 Mechanism of occurrence of soil liquefaction. (**a**) Before liquefaction. (**b**) After liquefaction

The phenomenon can be understood as follows. As Fig. 3.3 demonstrates, the total vertical stress at depth h is

$$\sigma_V = \gamma_S \cdot h \tag{3.1}$$

Here, γ_S represents the saturated unit weight (unit weight of the mixture of soil and water) and h is the depth from the ground surface to the estimated point of soil stress. To simplify the explanation, we assume the groundwater level to be the ground surface, that is all of the ground is in a state of complete saturation.

The total vertical stress σ_V is a sum total of the effective vertical stress σ_V' carried by the sand grains, and the pore water pressure u.

$$\sigma_V = \sigma_V' + u \tag{3.2}$$

By earthquake ground motions, the pore water pressure u increases:

$$u = u_i + \Delta u \tag{3.3}$$

u_i represents the initial pore water pressure and Δu the excess pore water pressure. As Eq. (3.1) shows, σ_V does not change even during liquefaction, because saturated unit weight γ_S is constant. Thus, σ_V' decreases with the increase of pore water pressure. Ultimately, σ_V' will be reduced to zero with complete liquefaction, and Δu will be equal to σ_V'. At that stage, sand grains lose their contacts and the ground behaves as a liquid mixed with sand and groundwater. This results, as explained later, in considerable damage to structures. The pore water pressure proportionally

Fig. 3.4 Gravels boiled out of ground due to liquefaction (1995 Kobe earthquake)

increases with progress of the liquefaction, so ground water moves upward to ground surface. When the ground is relatively weak and there are openings between building foundations and surrounding ground, the sand and water spouts out.

Soil is classified according to grain size. The largest is gravel, from 2 to 75 mm in diameter. Next is sand from 0.07 to 2 mm, followed by silt and clay, consisting of a so-called fine fraction that is smaller than sand. Silt grains measure 0.005–0.075 mm, and clay less than 0.005 mm. When soil mostly consists of sand, it is likely to undergo liquefaction. However, when silt and clay are a major soil component, liquefaction is not likely to occur. The permeability of gravels can reduce pore water pressure and prevent soil liquefaction. However, during the 1995 Kobe earthquake, gravels of weathered granite liquefied. Figure 3.4 shows spouts on the ground surface of a gravel and soil mixture, which have pushed off a sewage manhole cover. Liquefaction of the soil with gravel was caused by the strong ground motions during the Kobe earthquake. Therefore, as explained below, liquefaction potential of soil with gravel was taken into the consideration in revisions to specifications of highway bridges [3].

With fine fractions of silt and clay, soil becomes cohesive, making it resistant to liquefaction. For example, during the 2011 Tohoku earthquake, some areas of Urayasu in Chiba Prefecture around the Tokyo Bay, experienced severe liquefaction, whereas in other areas liquefaction was not substantial. It is assumed that this difference was caused by a quantitative variation in amount of the fine fractions. Most of the land in Urayasu was reclaimed, mainly by dredging soil from the seabed, but some areas were reclaimed using mountain soil. The latter soil generally contains small-grained silt and clay and is not as susceptible to liquefaction. In soil dredged from the seabed, fine fractions such as silt and clay were transported large distances by seawater from the exits of dredging hoses and deposits, and the coarse fractions such as the sand deposits around the exits of hoses. Therefore, the severity of soil liquefaction is variable in the same land reclaimed from the sea.

Conditions for the occurrence of soil liquefaction can be summarized as follows:

(i) Sandy ground, i.e., soil containing a high percentage of sand
(ii) A high groundwater level, i.e., saturated soil
(iii) Loosely accumulated sandy ground

These conditions apply to lands reclaimed from sea, lake and marsh, and lowland along rivers, delta, old stream, and flood plain. In contrast, liquefaction is much less likely in mountain, plateau and hilly areas. The latter areas, however, may be susceptible if there are small rivers with loose sand sedimentation beside them.

Research also suggests that the susceptibility of artificial land to liquefaction is related to time. It is believed that if soil contains silt and clay, sand grains strongly connect over years because of chemical elements within them, thereby creating resistance. In fact, a survey of liquefaction in lands reclaimed from Tokyo Bay after the 2011 Tohoku earthquake indicates that older lands were less affected by soil liquefaction than newer ones.

3.1.2 Damage Caused by Liquefaction

Liquefaction came to be recognized from an engineering standpoint in the aftermath of the 1964 Niigata earthquake. However, there had been reports on the phenomenon, including spouting of sand and water from sand volcanoes and ground fissures during past earthquakes before the Niigata earthquake. Soil liquefaction as a fluid-like behavior causes damage as described below.

(i) Subsidence, inclination, and collapse of structures from a reduction in bearing capacity of the ground:due to soil liquefaction, the ground behaves as a mixture of the sand and water. Normally, sand grains are tightly clustered, providing supportive force to weight of structures and the ground itself. Soil liquefaction largely decreases the bearing capacity and thus causes subsidence, inclination and collapse of structures.

Figure 3.5a shows a building collapsed by the 1999 Kocaeli earthquake in Turkey [4], and Fig. 3.5b the inclination and subsidence of petro-chemical product tanks by the 1995 Kobe earthquake.

(ii) Uplift of underground structures due to buoyancy of liquefied soil:the unit weight of liquefied soil is roughly 16–20 KN/m^3 (1.6–2.0 tf/m^2). The apparent unit weight, considering inner open spaces, of inground structures such as sewage manholes and purification tanks, generally becomes less than that of liquefied soil. This causes the uplift of such structures due to soil liquefaction. Figure 3.6 shows the uplift of: (a) a water purification tank during the 1964 Niigata earthquake, and (b) a manhole during the 1923 Kushiro offshore earthquake. The purification tank in (a) is seen pushing up cars in a parking lot on the ground surface. In the 2004 Niigata-Chuetsu earthquake, more than 1,400 sewage manholes were lifted, in the cities of Nakaoka and Ojiya.

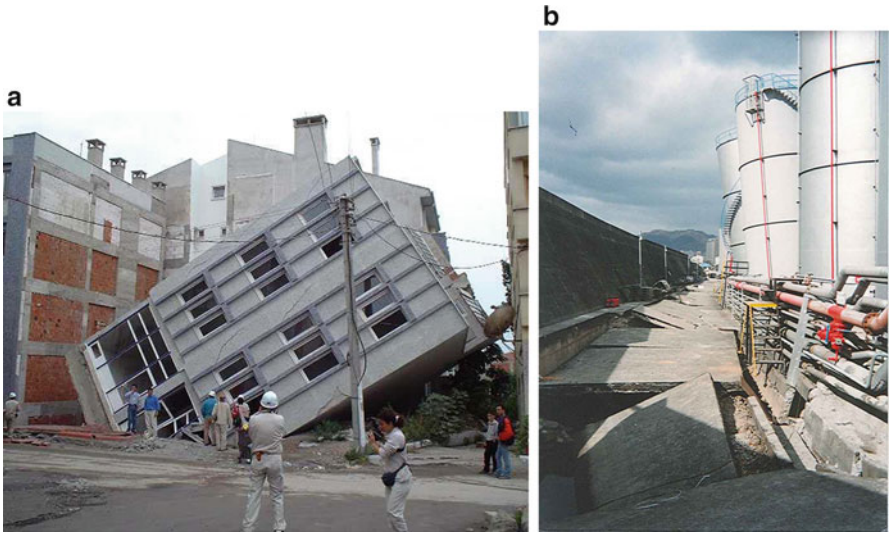

Fig. 3.5 Collapse and inclination of structures due to soil liquefaction. (**a**) Collapse of a building (1999 Kocaeli earthquake, Turkey) [3]. (**b**) Inclination of storage tanks for petro-chemical product (1995 Kobe earthquake)

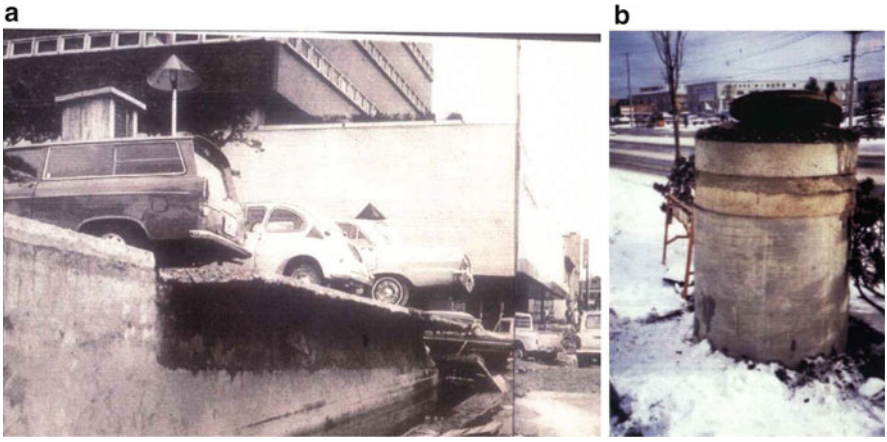

Fig. 3.6 Uplift of underground structures due to buoyancy of liquefied Soil. (**a**) Uplift of purification tank (1964 Niigata earthquake). (**b**) Uplift of sewage manhole (1993 Kushiro offshore earthquake)

Liquefaction occurred mainly in backfill soil, which buried manholes. Since then compaction, hardening and drainage methods have been developed and applied to the practice. This will be discussed in detail in Sect. 3.3.

(iii) Damage to earth structures: soil liquefaction causes large-scale deformation, slide and subsidence in earth structures, such as roads and railway

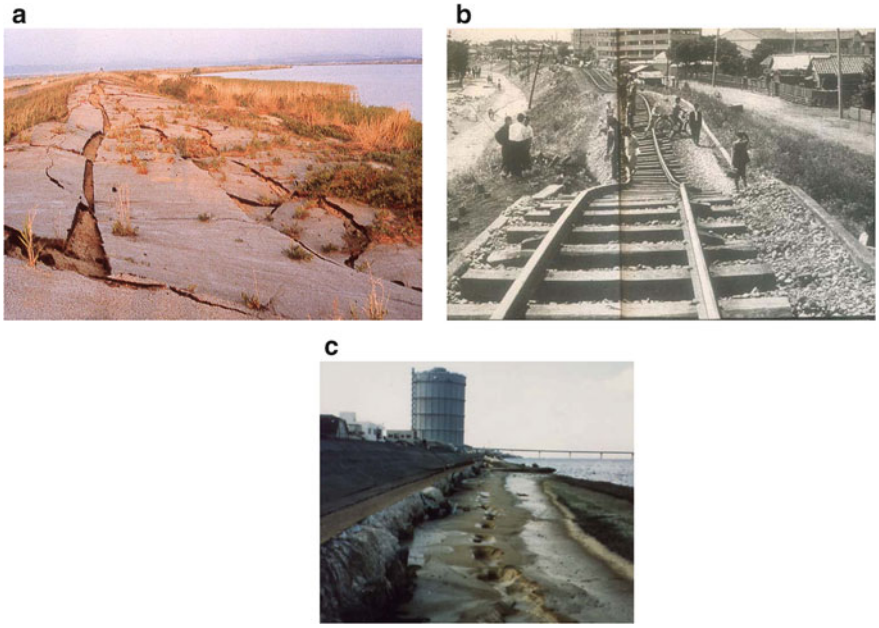

Fig. 3.7 Damage to earth structures. (**a**) Sliding and subsidence of polder dike (1983 Central Japan sea earthquake). (**b**) Sliding and subsidence of railway embankment (1964 Niigata earthquake). (**c**) Sliding of Yodo River levee (1995 Kobe earthquake)

embankments, dikes, levees and earth dams. In general, greater use of sandy soil than of silt and clay makes construction works easy. Figure 3.7a shows damage to the Hachirogata polder dike by the 1983 central Japan Sea earthquake. The embankment was constructed with sand and faced with waterproofing asphalt. Both of the foundation ground and the dike underwent liquefaction, resulting in significant sliding and subsidence. Figure 3.7b shows damage to a railway embankment by the 1964 Niigata earthquake.

Figure 3.7c shows sliding failure of a levee along the Yodo River during the 1995 Kobe earthquake. Sand boilings are seen on the slid slope, due to soil liquefaction. The levee slipped toward the river, but fortunately the river water level at the time of the earthquake was low, so flooding from the levee sliding was avoided. If the water level had been high, lives in the area would have been affected seriously. Liquefaction-induced damage to road and railway embankments threatens transport, thereby hampering conveyance of personals and good for emergency response, and delaying restoration and reconstruction. The repeated damages to embankments and levees by soil liquefaction has led to development and application of preventive measures as explained in Sect. 3.3.5.

(iv) Damage to coastal revetments and retaining walls from increase of earth pressure:coastal revetments and retaining walls are designed to withstand

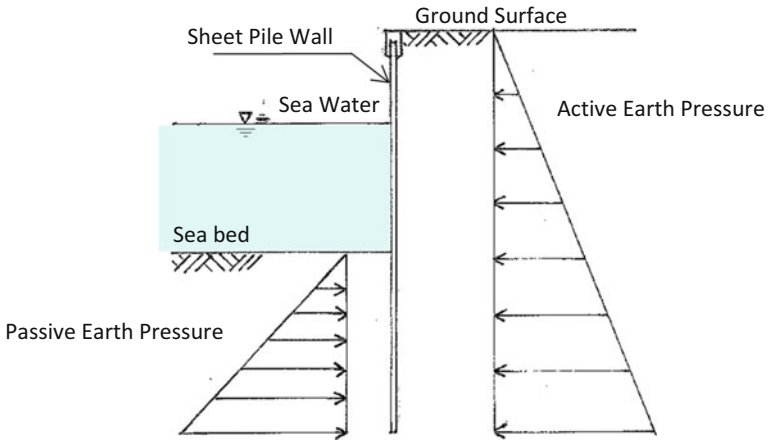

Fig. 3.8 External forces for design of sheet pile wall

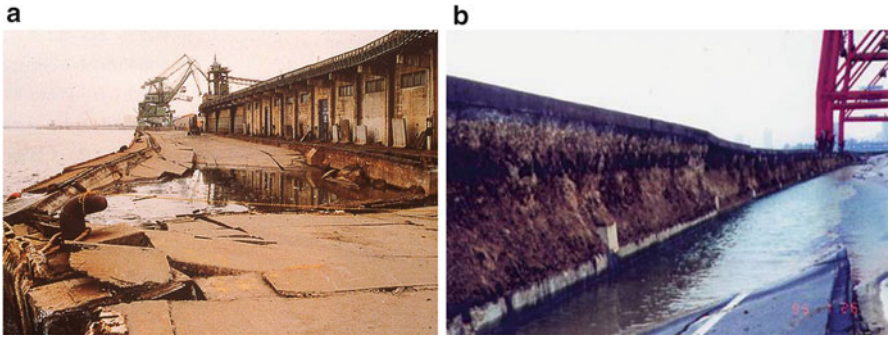

Fig. 3.9 Damage to coastal revetments due to soil liquefaction. (**a**) Inclination and subsidence of sheet pile wall (1983 Central Japan Sea earthquake). (**b**) Large movement of concrete caisson quay wall and ground subsidence (1995 Kobe earthquake)

earth pressure. Taking a sheet-pile type wall as an example, active earth pressure from land and passive earth pressure from the seabed are used as the external forces on the wall in its design, as shown in Fig. 3.8. The active earth pressure coefficient, i.e., the ratio of horizontal pressure to vertical stress of the soil, varies with seismic force. However, even under strong earthquake motion, the passive earth pressure coefficient is much less than 1.0. But if the ground behind the wall is entirely liquefied, the earth pressure equals the vertical stress and the earth pressure coefficient nears 1.0. This exceeds earth pressure in the design. Therefore, quay walls and retaining walls have been damaged due to soil liquefaction in past earthquakes.

Figure 3.9 shows (a) inclination and subsidence of a steel sheet-pile wall in the port of Akita, caused by the 1983 Central Japan Sea earthquake; (b) damage to a

caisson-type coastal revetment in Rokko-Island from the 1995 Kobe earthquake. Soil liquefaction of the foundation ground of the concrete caissons reduced bearing capacity, and liquefaction of backfill soil behind the caissons increased earth pressure, resulting in a maximum 5-m horizontal movement and large subsidence of the ground.

The 1983 central Japan Sea earthquake promoted to develop effective countermeasures for quay walls against soil liquefaction. Such countermeasures have been taken for major ports in Japan. The quay walls of these ports, reinforced against earthquakes, play a vital role in ensuring sea transport of emergency goods and personnel in the aftermath of future earthquake disasters.

Since the 1964 Niigata earthquake, engineers and scientists have become keenly aware of the four types of damage caused by soil liquefaction, as mentioned above. Countermeasures against soil liquefaction have been developed and implemented. These countermeasures are introduced in Sect. 3.3.

3.2 Estimation of Liquefaction Potential

3.2.1 Estimation of Potential

Methods for the estimation of liquefaction potential can be selected from the following three approaches, according to the importance of structures, areas of estimation, and soil survey precision:

(i) Method by topographical and geological conditions
(ii) Method based on soil exploration (e.g., N-value and grain-size distribution)
(iii) Detailed method based on liquefaction vulnerability tests in laboratory and dynamic response analysis of the ground

The first method is used when estimation of liquefaction potential is needed over wide areas, for example, buried pipelines of lifeline systems. The third method is used for the design of structures with a high importance, such as high-rise buildings and long-span bridges. The second method has been adopted in *Specifications of Highway Bridges* [3], *Building Foundation Standards* [5], *and Earthquake Resistant Design of Port Facilities* [6].

In the first method, liquefaction potential is categorized into the following groups, depending on geology and geography.

High-potential area of liquefaction (A): Current and old river channel, alluvial plain, lands reclaimed from sea, river, swamp and valley, lowland between sand dune.

Medium-potential area of liquefaction (B): All ground not fitting the description of either (A) or (C).

Low-potential area of liquefaction (C): Plateau, hill, mountain, and alluvial fan.

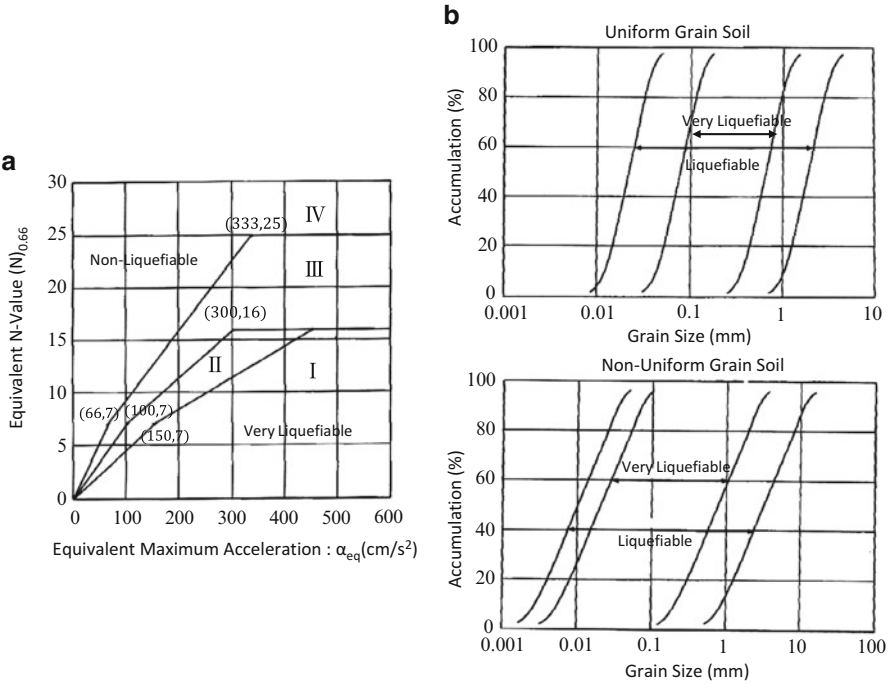

Fig. 3.10 Estimation of liquefaction potential (Coastal Development Technical Research Center [7]. (**a**) Method by critical N-Value. (**b**) Method by grain size distribution

Although alluvial fan is included in (C), liquefaction occurred with a mixture of pebbly and decomposed granite soil during the 1995 Kobe earthquake (Fig. 3.4). Thus, the liquefaction potential of alluvial fan must be qualified with consideration of soil contents.

Method (ii) includes two approaches as illustrated in *Handbook for Liquefaction and Measures in Reclaimed Land* [7], published by the Coastal Development Technical Research Center. Figure 3.10a shows the relationship between maximum acceleration at the ground surface and N-value for the estimation of liquefaction potential, and Fig. 3.10b shows the method for estimation by grain-size distribution.

Equivalent N-value $(N)_{0.66}$ of Fig. 3.10a can be obtained by modifying N-value measured from the standard penetration test, by the effective vertical stress σ'_V.

$$(N)_{0.66} = \frac{N - 1.828\left(\sigma'_V - 0.66\right)}{0.399\left(\sigma'_V - 0.66\right) + 1} \tag{3.4}$$

where:

$(N)_{0.66}$: the equivalent N-value,
N: the N-value from standard penetration test,
σ'_V: effective vertical stress of soil (kgf/cm^2).

Equivalent maximum acceleration α_{eq} in Fig. 3.10a can be obtained as

$$\alpha_{eq} = 0.7 \times \frac{\tau_{\max}}{\sigma_V'} \times g \tag{3.5}$$

where g is gravitational acceleration (980 cm/s^2). The constant 0.7 is for calculation of mean acceleration of the soil above the point for estimation of liquefaction potential. $\tau_{\max}$ is maximum shear stress in the soil, as determined by dynamic response analysis of the ground. It can be alternatively to estimate α_{eq} as 70 % of the maximum acceleration at the ground surface.

The method shown in Fig. 3.10b uses the soil grain-size distribution. Liquefaction potential of soil with a relatively uniform distribution is determined by the upper figure, and soil with relatively non-uniform grain-size by the lower figure.

In *Specification of Highway Bridges* [3] and *Building Foundation Standards* [5], the liquefaction resistant ratio F_L is used to estimate whether the ground is liquefiable or not. The F_L value is the ratio of soil strength against liquefaction R (called the dynamic shear strength ratio) to earthquake-induced load L (called shear stress ratio).

$$F_L = \frac{R}{L} \tag{3.6}$$

According to specifications for highway bridges, R is

$$R = C_w R_L \tag{3.7}$$

Here, the cyclic triaxial strength ratio R_L , corresponding to soil properties, is as follows.

(i) Alluvial soil

$$R_L = \begin{cases} 0.0882 \times \sqrt{(N_a/1.7)} & (N_a < 14) \\ 0.0882 \times \sqrt{(N_a/1.7)} + 1.6 \times 10^{-6} \cdot (N_a - 14)^{4.5} & (N_a \geq 14) \end{cases} \tag{3.8}$$

(ii) Reclaimed soil

$$R_L = \begin{cases} 0.0882 \times \sqrt{(N_a/1.7)} - 0.05 & (N_a < 14) \\ 0.0882 \times \sqrt{(N_a/1.7)} + 1.6 \times 10^{-6} \cdot (N_a - 14)^{4.5} - 0.05 & (N_a \geq 14) \end{cases} \tag{3.9}$$

The modified N-value, N_a is estimated as follows:

(i) Sandy soil

$$
\begin{aligned}
&N_a = c_1 \cdot N_1 + c_2 \\
&N_1 = 170 \cdot N / \left(\sigma_V^{'} + 70\right) \\
&c_1 = \begin{cases} 1 & (0\% \le F_C < 10\%) \\ (F_C + 40)/50 & \left(10\% \le F_C < 60\%\right) \\ F_C/20 - 1 & (60\% \le F_C) \end{cases} \\
&c_2 = \begin{cases} 0 & (0\% \le F_C < 10\%) \\ (F_C - 10)/18 & (10\% \le F_C) \end{cases}
\end{aligned} \tag{3.10}
$$

(ii) Gravel soil

$$N_a = [1 - 0.36\log_{10}(D_{50}/2)] \cdot N_1 \tag{3.11}$$

Here,

R_L: Cyclic triaxial compression strength ratio
N: N value from standard penetration test
N_1: Modified N-value equivalent at effective stress 100 kN/m^2
N_a: Modified N-value according to the influence of particle size
c_1, c_2: Coefficients determined by fine fraction ratio
F_C: Fine content ratio (%) (Percentage of weight of soil under 75 μm)
D_{50}: Average grain size (mm)

The coefficient in Eq. (3.7) C_w is determined of the types of earthquakes

For type 1 ground motion (sea trough earthquake, Sect. 2.3.2):

$$C_w = 1.0 \tag{3.12}$$

For type 2 ground motion (inland earthquakes):

$$C_w = \begin{cases} 1.0 & (R_L \le 0.1) \\ 3.3R_L + 0.67 & (0.1 < R_L \le 0.4) \\ 2.0 & (0.4 < R_L) \end{cases} \tag{3.13}$$

Shear stress ratio L is

$$L = r_d \cdot k_{hgL} \cdot \frac{\sigma_V}{\sigma_V^{'}} \tag{3.14}$$

Here, r_d is the reduction coefficient of shear stress at depth z ($= 1 - 0.15z$, where z is depth from the ground surface, in m)

k_{hgL}: Horizontal seismic intensity coefficient used for estimation of liquefaction potential, obtained as a product of k_{hgL0} as shown in Table 3.1 by regional coefficients shown in Fig. 2.5 (Chap. 2).

Table 3.1 Seismic intensity coefficients $K_{hgLO,}$ for evaluation of liquefaction potential

Classification of ground condition	Level 1 ground motion	Level 2 ground motion (type I)	Level 2 ground motion (type II)
I	0.12	0.50	0.80
II	0.15	0.45	0.70
III	0.18	0.40	0.70

Type I: inland earthquakes
Type II: sea trough earthquakes

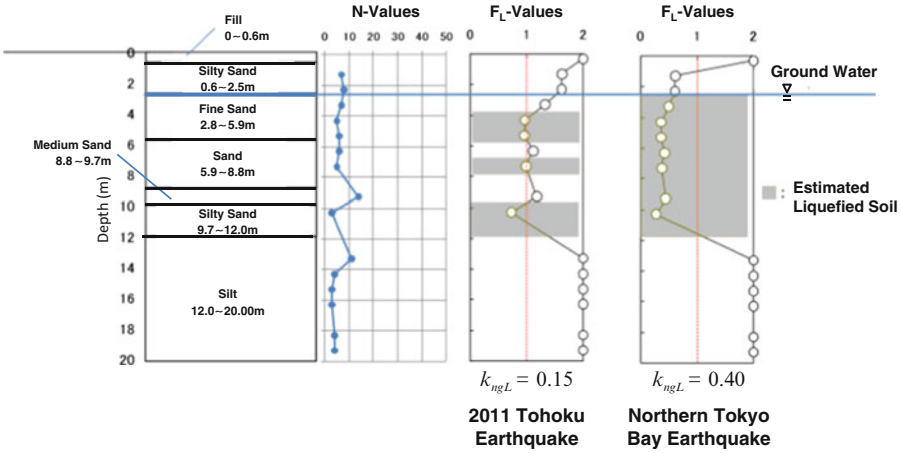

Fig. 3.11 Evaluation of liquefaction potential in Urayasu (2011 Tohoku earthquake and Northern Tokyo Bay earthquake)

Figure 3.11 depicts estimation of F_L at a location in Urayasu in Chiba Prefecture, which was severely damaged by the 2011 Tohoku earthquake, using the method of the specifications of highway bridges. The value of F_L was estimated versus two earthquake ground motions. One is the motion observed in Urayasu during the Tohoku earthquake and the other is the predicted motion of the northern Tokyo Bay earthquake. It was found that thickness of the liquefied layer is about 5 m in the Tohoku earthquake, but increases substantially to 9 m in the Tokyo Bay earthquake. F_L would be less than 0.5 and the degree of liquefaction in areas reclaimed from the bay would be severe. Measures must be taken to reduce damage to residential houses and buildings, as well as buried pipes of lifeline systems, such as water, sewage and electricity.

3.2.2 Liquefaction Hazard Map

In many prefectures and cities, liquefaction hazard maps have been made and distributed to the public, using simple topographical and geological methods, in conjunction with the methods based on N-value and grain-size distribution from

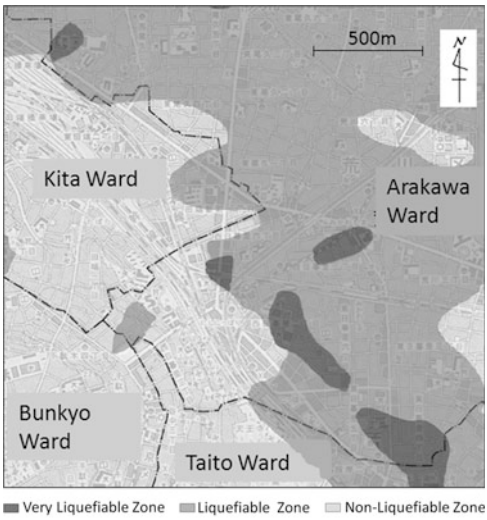

Fig. 3.12 Liquefaction potential map (Tokyo metropolitan government) [8]

soil surveys, described in Sect. 3.2.1. Figure 3.12 is an example of liquefaction hazard maps compiled by Tokyo Metropolitan government [8]. Liquefaction potential is divided into three categories: very liquefiable, liquefiable, and non-liquefiable. In most cases, the maps cover an extensive area, based on limited borehole data. To conduct highly reliable evaluations, detailed boring surveys at construction sites and tests of liquefaction strength of soil are required. For an example, the results from cone penetration tests, where a metallic screw is inserted into the ground, are used to measure soil strength. The most common is the Swedish cone penetration test, which is a low-cost method used for the estimation of liquefaction potential of residential houses.

3.3 Countermeasures Against Soil Liquefaction

3.3.1 Measures for Prevention of Soil Liquefaction

The followings are two ways to reduce the damage caused by soil liquefaction;

(i) Prevention of occurrence of soil liquefaction
(ii) Reinforcement of foundations of structures for resisting soil liquefaction

In this session, the first method which attempts to change the ground to "non-liquefiable" category is introduced. As explained above, conditions of occurrence of soil liquefaction are that the soil consists of loose sand and is saturated with

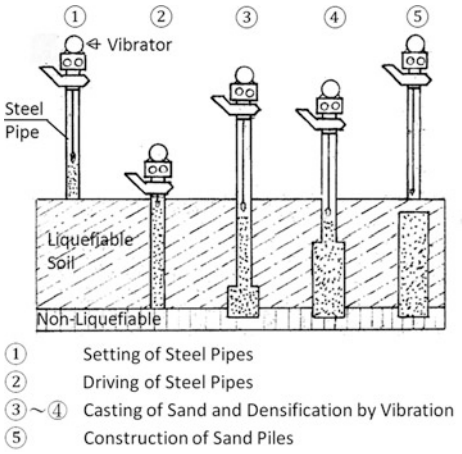

Fig. 3.13 Sand compaction pile method

groundwater. The essential idea to prevent occurrence of liquefaction is elimination of one of these conditions. There are three conceivable approaches:

(i) Densification of loose sand, so soil resists liquefaction
(ii) Lowering the groundwater level, so soil becomes unsaturated
(iii) Drainage of ground water to reduce excessive pore water pressure

As the first method (i), the vibro-flotation, sand compaction pile, and dynamic consolidation methods have been applied. The sand compaction pile method is illustrated by Fig. 3.13. First, steel pipes are driven into the ground and sand is cast into the pipes. By vibrating the pipes, liquefaction-resistant dense sand columns are constructed in the ground. This method has been widely used in Japan. It has been reported that prior to construction of Tokyo Disneyland, ground improvements were conducted using the sand compaction pile method. It was consequently unaffected by liquefaction from the 2011 Tohoku earthquake. The sand compaction pile method allows ground improvement to depths of 10–20 m.

Figure 3.14 shows that the dynamic consolidation method by dropping a weight from air to ground surface, hardening that ground by the impact. This is a simple and inexpensive method, but it is effective to just a shallow depth of 3–4 m, and is therefore ineffective in the case of liquefaction at a greater depth.

There is another approach for hardening of ground, illustrated in Fig. 3.15. It is called grouting method, whereby cement or chemical materials are grouted into the ground to harden the soil. There is also the deep mixing method, whereby hardening materials and soil are churned and mixed in the ground. This is being often used for reinforcement of existing seawalls. Because it hardens the seabed in front of seawalls, the method is effective in increasing resistance against large seawall movement and collapse. While these methods have the advantage that tremors do not occur during construction, they also pose problems. These include environmental issues, such as chemical pollution of underground water. Furthermore, it is sometimes difficult

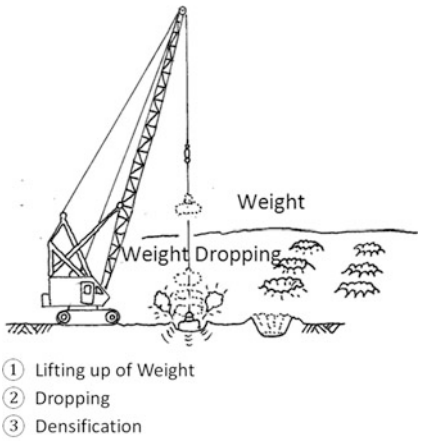

Fig. 3.14 Dynamic densification method

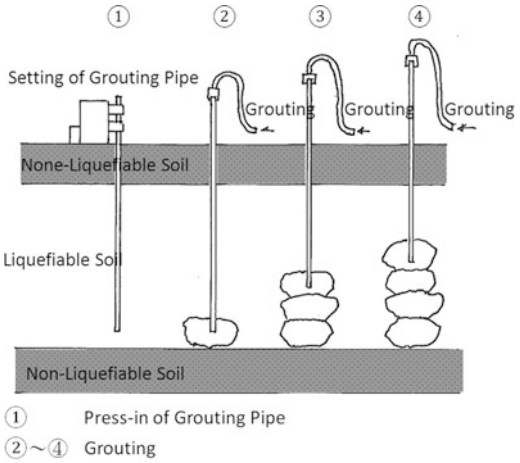

Fig. 3.15 Grouting method

to verify the actual functional situation underground following the procedures. To determine which of the above methods should be implemented, various factors must be considered, including depth of liquefiable soil, liquefaction potential of soil before improvement, type of structures, cost, and environmental impact.

The second method (ii), lowering the water level, is effective in converting saturated to non-saturated soil; it increases resistance against liquefaction by thickening the non-liquefiable surface soil above ground water level, and also increases the vertical effective stress of soil below the water level. Figure 3.16 shows an example dewatering method. In reclaimed land in Kawasaki, a tank yard has been surrounded by a flexible cut-off wall and water level within the yard was lowered. However, a problem of this method is differential settlement of

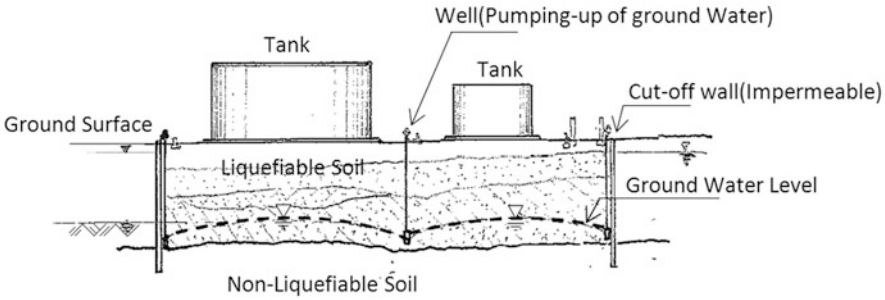

Fig. 3.16 Dewatering method

Fig. 3.17 Gravel drain method

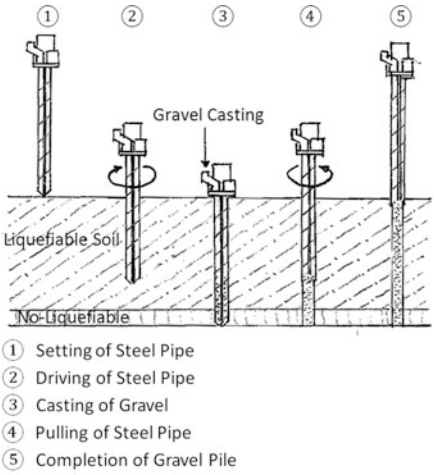

ground, caused by groundwater lowering and the need to continuously maintain the water at a low level.

The third method (iii), reducing excessive pore water pressure, is represented by the gravel drain method shown in Fig. 3.17. In this method, the ground around gravel drains is not much improved, but pore water flows swiftly through those drains and is released. This effectively shortens the time in which pore water pressure is high. Problems remain to be resolved, including drain clogging and ground subsidence. In addition to using gravel for drainage, it is used to refill the ground around underground structures. Figure 3.18 shows a gravel drain for an electric cable duct. Gravel columns are constructed below the duct and the surrounding area is filled by gravel, preventing a rise in pore water pressure and subsequent liquefaction.

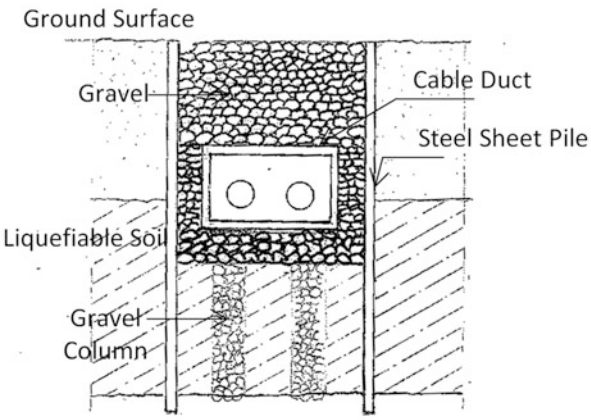

Fig. 3.18 Gravel backfill method for electrical cable duct

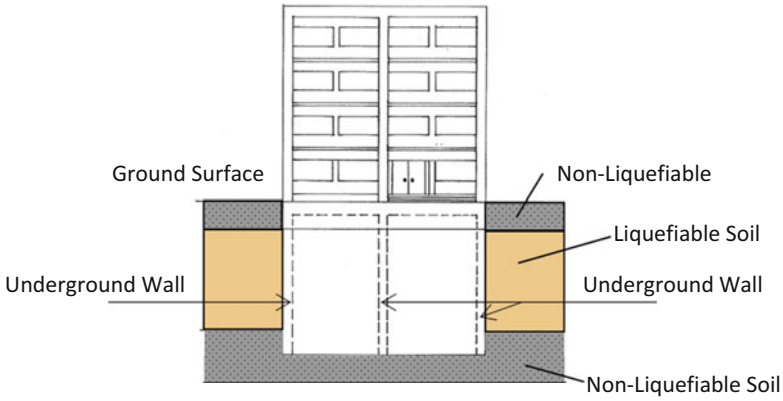

Fig. 3.19 Underground wall method

3.3.2 Reinforcement of Foundations of Structures for Resisting Soil Liquefaction

Underground walls and pile foundations have been constructed to protect buildings against soil liquefaction. Figure 3.19 illustrates a method using underground walls. A similar method is displayed in Fig. 3.20, in which steel sheet pile walls surrounding the tank foundations can protect tanks from subsidence and inclination by preventing the flow of liquefied soil in the horizontal direction. This method may also be applicable to existing structures. However, in that case, vibration and noise by construction works may affect neighboring structures and residents. Therefore, instead of driving piles, press-in methods have been adopted for construction of the steel sheet pile walls [9].

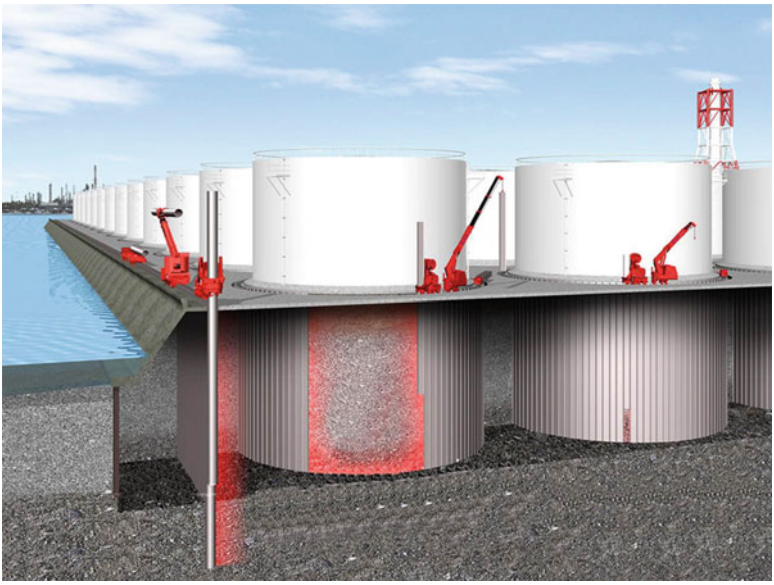

Fig. 3.20 Steel sheet pile wall method (after Japan Press-in Association) [9]

A huge number of houses have suffered subsidence and inclination from soil liquefaction during earthquakes. For residential houses, there is a problem of substantial construction cost for driving long piles into deep farm ground. One method to lessen house damage by liquefaction is the use of concrete spread foundations with gravel layer. Figure 3.21 is a photo taken after the 1993 Kushiro offshore earthquake, which shows a manhole lifted by soil liquefaction next to an undamaged house. Contrarily sand boils were observed in the neighborhood. It was reported that this house had a concrete mat foundation underlain by a gravel layer. It is believed that the gravel layer dissipated pore water pressure and the spread foundation prevented the structural damage of the house.

Figure 3.22 illustrates a countermeasure in which steel sheet piles are used to construct shallow walls around house basements, for preventing the flow of liquefiable soil in the horizontal direction under the house, thereby reducing settlement and inclination.

Figure 3.23a shows a 1/20 scale model of a two-story house. Shaking table tests were conducted under 1-g and centrifuge conditions to examine effectiveness of ground walls for the reduction of house settlement and inclination. The horizontal axis of Fig. 3.23b is the ratio of the length of the sheet-pile wall to liquefiable soil thickness. The vertical axis is the ratio of inclination of the model houses with the sheet-pile wall to that without a wall. If there are sheet-pile walls with length one-third the liquefiable soil thickness, inclination is reduced by about one-fifth to one-third that without the wall. Because spaces between neighboring houses are usually very narrow, it is often impossible to use large-scale construction machines. Adoption of lightweight and short sheet piles can facilitate construction in such space, at low cost.

Fig. 3.21 A non-damaged house against soil liquefaction (1993 Tokachi offshore earthquake)

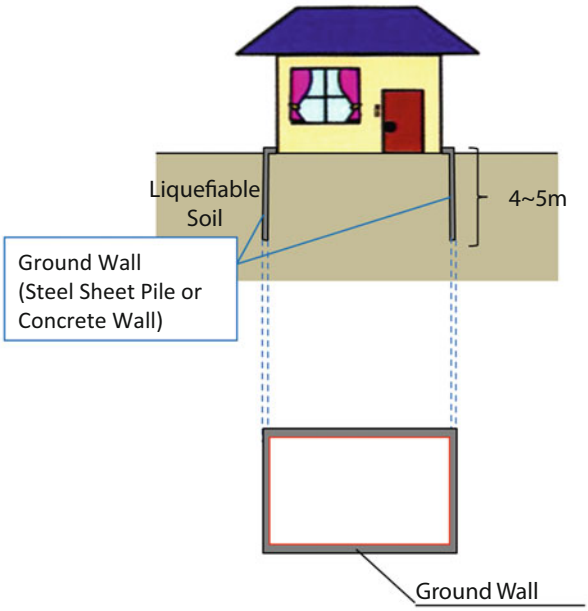

Fig. 3.22 Countermeasures of houses against liquefaction by shallow ground wall

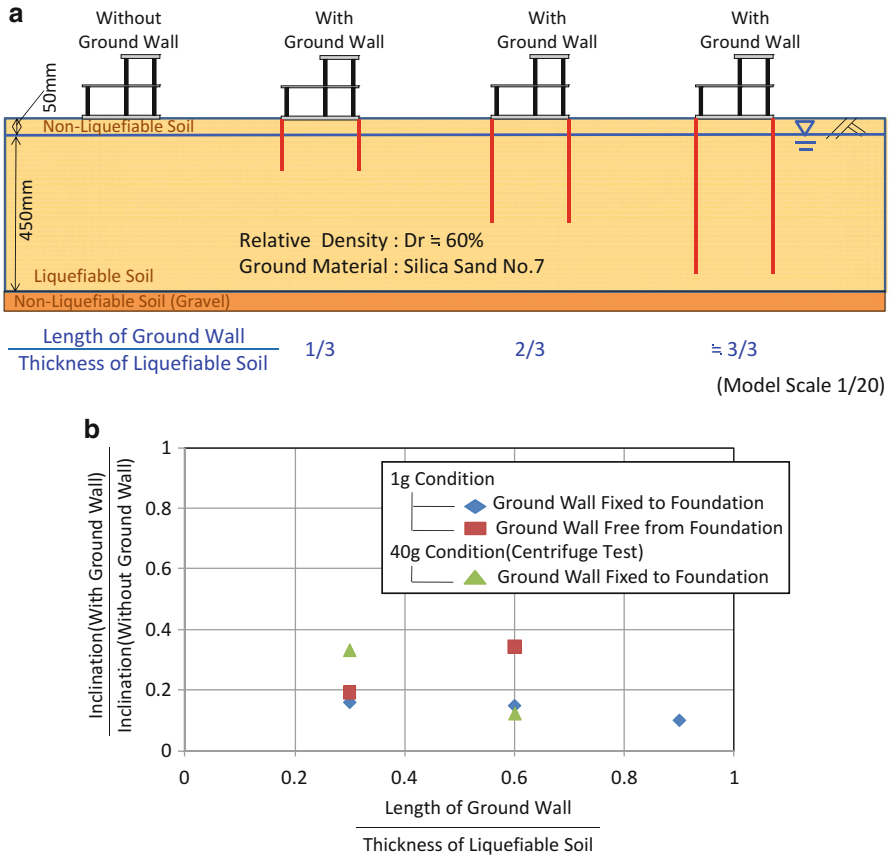

Fig. 3.23 Shaking table test on effectiveness of ground wall to reduce inclination of houses. (**a**) Test model of ground and ground wall. (**b**) Effectiveness of wall on reduction of inclination

Regarding the effects liquefaction on houses and low-rise buildings, the use of wooden piles from timber harvested in culled forests has been promoted. This idea was motivated in a survey of damage to reinforced concrete buildings from the 1964 Niigata earthquake. At that time, foundations for such buildings were wood piles, concrete piles, and mat foundations. Figure 3.24 shows that concrete buildings with mat foundations had high rates of damage compared with those with wooden or concrete piles. Moreover, the damage rate to buildings with wooden pile foundations is similar to that for buildings with concrete pile foundations. As noted in Sect. 4.2, it was reported that many concrete piles driven into firm ground were ruptured by the flow of liquefied soil. However, wood piles that did not reach firm ground were undamaged, because they were flexible enough to adapt ground deformation.

Regarding the use of wood piles, it is necessary to the determine the length of piles. The author tested a model at 1/20 scale under 1-g condition, to examine the effect of wood pile length in relation to liquefiable soil thickness as shown in Fig. 3.25a.

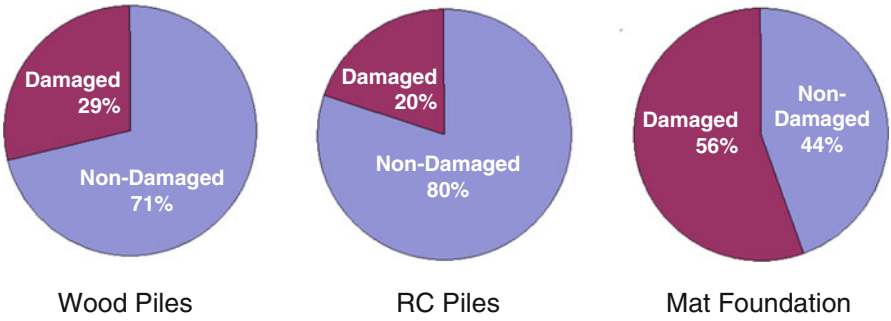

Fig. 3.24 Damage rate of concrete buildings with different types of foundations in Niigata city (1964 Niigata earthquake)

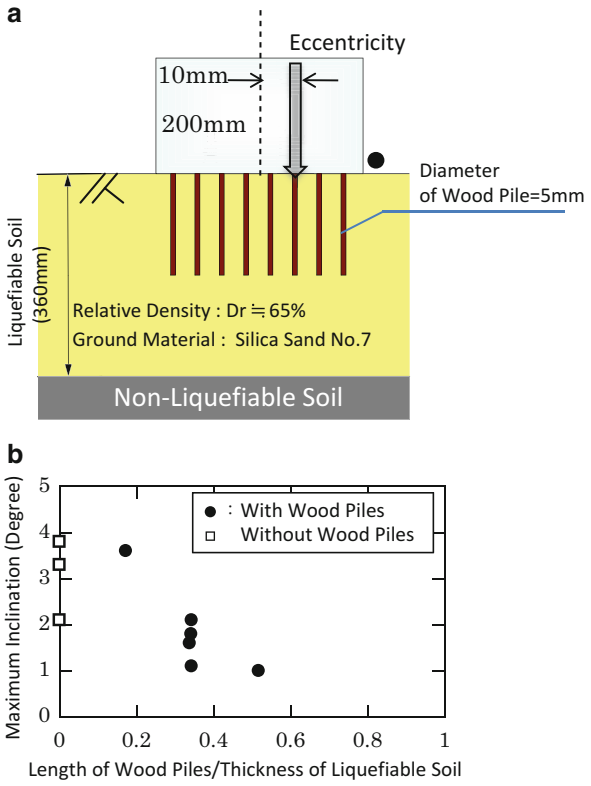

Fig. 3.25 Shaking table test on effectiveness of wood piles to reduce inclination of houses (pile interval: 5D, *D* diameter). (**a**) Model of wood piles and ground (scale: 1/20, interval of pile driving: 5D, *D* diameter of pile). (**b**) Effectiveness of wood piles for reduction of inclination

The horizontal axis in Fig. 3.25b shows the ratio of wood pile length to liquefiable soil thickness, and the vertical axis represents inclination of the model house. The interval for driving the piles was five times the pile diameter of 10 cm on the prototype scale. When the wood pipe length is one-half the liquefiable soil thickness, house inclination can be greatly reduced. Even in the case of the 1995 Kobe earthquake, maximum thickness of the liquefied soil was 10–12 m, wood piles measuring half that length (5–6 m) could be made from culled timbers. It would be necessary, however, to make appropriate judgments regarding pile driving interval and length.

3.3.3 *Countermeasures of Manholes Against Soil Liquefaction*

Following the 2004 Niigata-Chuetsu earthquake, downtown areas of cities including Nagaoka and Ojiya in Niigata Prefecture had more than 1,400 sewage manholes lifted by soil liquefaction. The resulting malfunction of the sewage system profoundly affected the lives of citizens and disrupted traffic, thereby greatly interfering with post-quake rescue efforts. In response to such damage, measures to prevent lifting have been developed and implemented, involving reinforcement of existing manholes. The following methods were developed [10].

(i) Use of backfill soil that is not liquefiable. After manhole construction, surrounding soil is hardened by careful compaction and hardening, thereby preventing liquefaction. The backfill soil is hardened by mixing soil with cement.
(ii) Increasing weight. Heavy materials such as crushed rock, metal clumps, and concrete blocks are installed inside or outside manholes, thereby resisting the buoyancy of liquefied soil (Fig. 3.26a illustrates one example of weighing by gravels).
(iii) Dissipating pore water pressure. Pipes and other devices are inserted in the ground from the inside of manholes, so that ground water drains into manholes and pore water pressure is dissipated (Fig. 3.26b).
(iv) Anchors. Steel cable or piles are inserted into firm ground (non-liquefiable soil layer), providing an anchor (Fig. 3.26c).

3.3.4 *Restoring Inclined and Subsided Houses*

During the 2011 Tohoku earthquake, many houses in areas such as Urayasu in Chiba Prefecture around the Tokyo Bay were subjected to subsidence and inclination by soil liquefaction. An inclination greater than 1/100 is a cause of human distress. When the inclination increases to 1.5/100 or more, the discomfort becomes difficult to endure, and is associated with long-term health damage. Thus, swift construction efforts must be made to restore houses that have suffered damage beyond a certain limit. The following construction methods for restoration of subsided and inclined houses have been developed and applied.

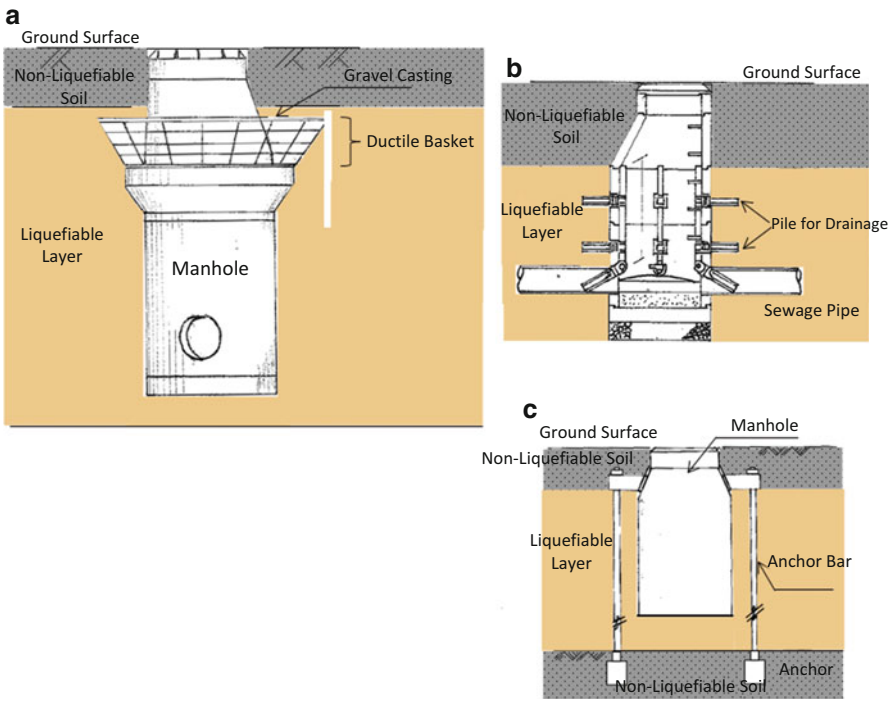

Fig. 3.26 Countermeasures for prevention of lifting of manholes against soil liquefaction. (**a**) Increase of weight. (**b**) Dissipation of pore water pressure. (**c**) Earth anchor

(i) Grouting method. An inclined house is raised to horizontal, using pressure from materials such as mortar or chemical liquids like urethane foam (Fig. 3.27a).
(ii) Underpinning method. Piles are driven or pressed-in into firm ground and houses are jacked up to horizontal (Fig. 3.27b).
(iii) Jack-up method. Grouting material such as mortar is first inserted in the ground, with steel plates installed on the ground surface. The counterforce provided by the jacks elevates the houses to horizontal (Fig. 3.27c).
(iv) Push-up method. Concrete foundations and wooden houses are separated, and only the houses are jacked-up horizontally. Additional columns are installed in the space between the house and concrete foundation (Fig. 3.27d).

Among the four methods, three methods [all except (ii)] involve the use of pressure to lift up houses. It must be ascertained that the foundations and ground can withstand additional stress caused by the pressure. Ground subject to liquefaction is often soft and weak, unable to provide adequate support for buildings. Moreover, concrete foundations are often insufficiently reinforced by steel bars. In such cases, the push-up method (iv), shown in Fig. 3.27d, can provide a safe and economical solution to restore houses without changing stress of the ground or the

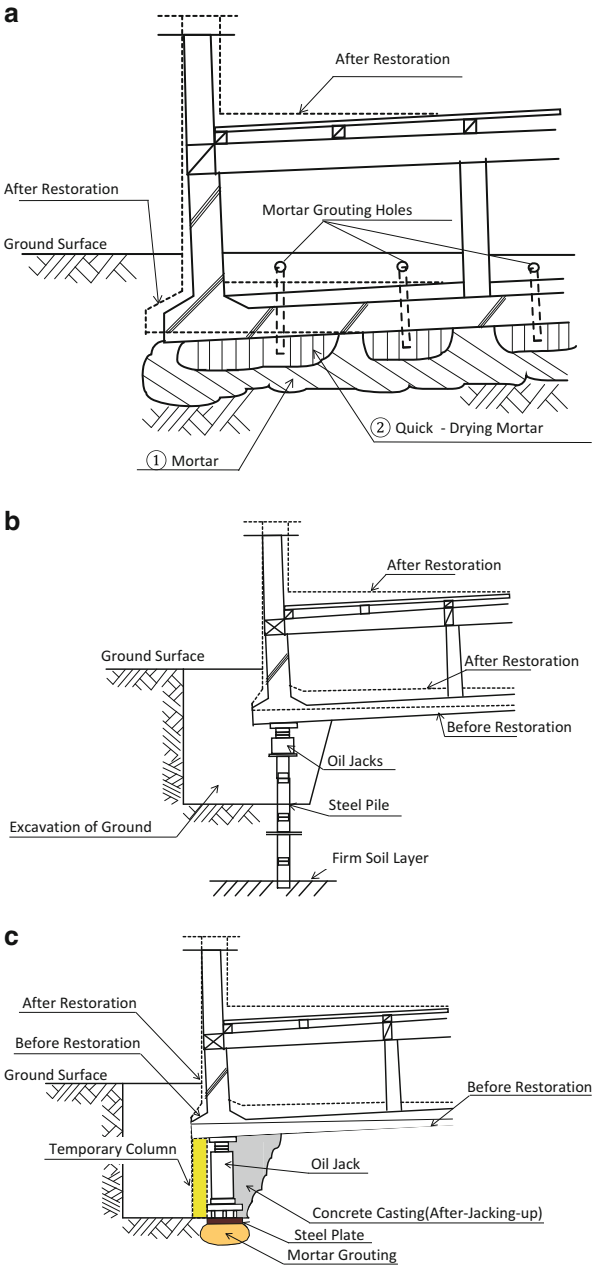

Fig. 3.27 Restoration of inclination and subsidence of houses from soil liquefaction. (**a**) Grouting method. (**b**) Underpinning method. (**c**) Jack-up method. (**d**) Push-up method

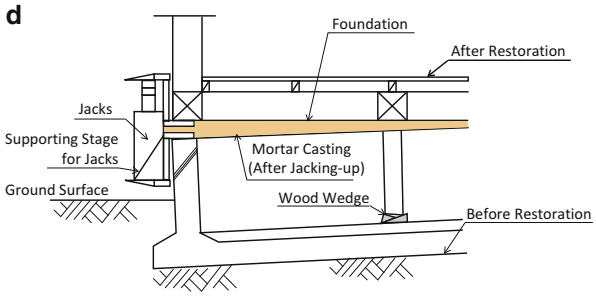

Fig. 3.27 (continued)

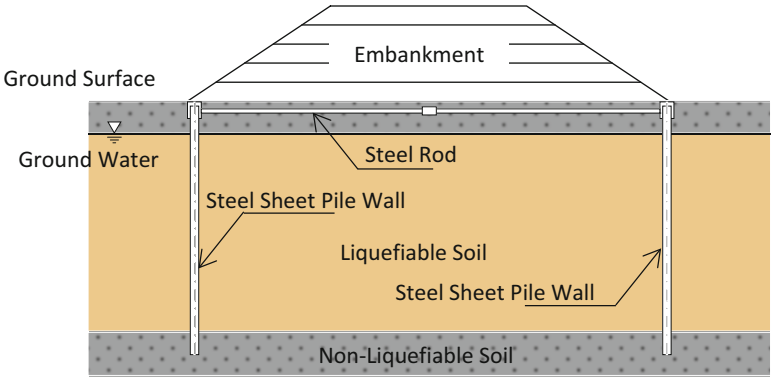

Fig. 3.28 Reinforcement of embankments by sheet pile wall

concrete foundation. Furthermore, the total weight in the jack-up can be reduced, because only wooden houses are lifted up. This method can reduce cost and increase the safety of construction.

3.3.5 Measures Against Soil Liquefaction for Embankments and Levees

Road and railway embankments have been damaged by soil liquefaction during earthquakes. Measures to lessen the potential for embankment sliding and settlement are particularly important to increase the safety and reliability of high-speed trains, such as the Shinkansen.

Cement grouting in liquefiable soil under embankments and driving sheet-pile walls (Fig. 3.28) to prevent liquefiable soil flow have been applied as measures against soil liquefaction for embankments. In addition, wood piles with relatively short lengths of culled timber are being used for improvement of foundation ground

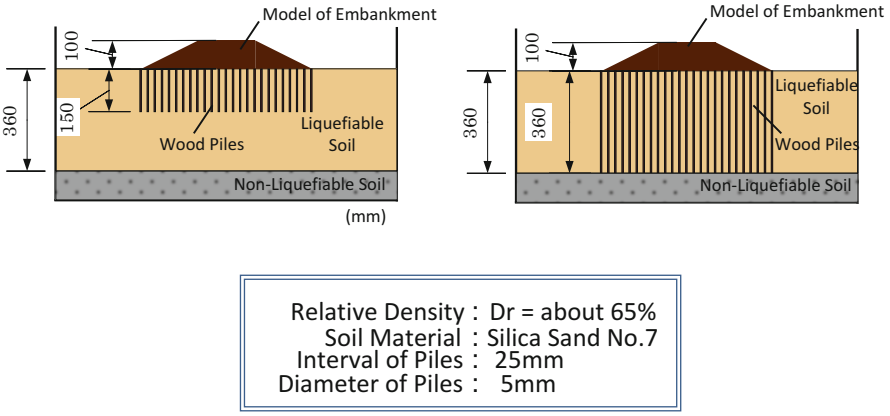

Fig. 3.29 Shaking table test of wood piles to prevent sliding and subsidence of embankment due to soil liquefaction (under 1-g condition)

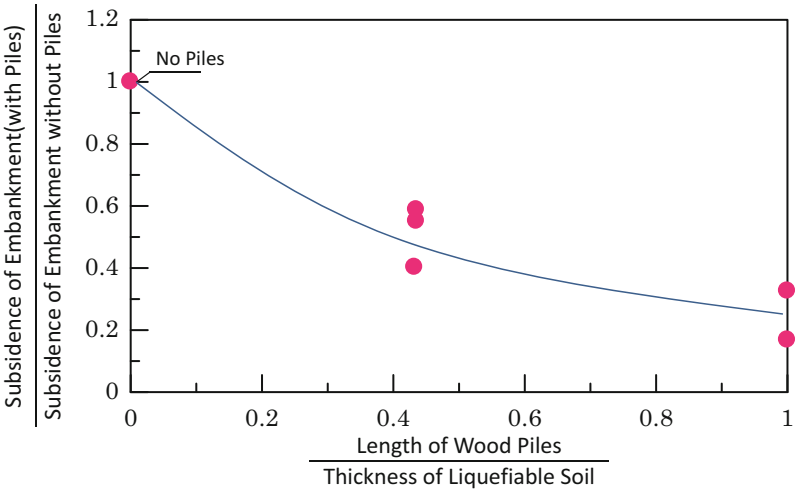

Fig. 3.30 Effect of wood piles length on reduction of subsidence of embankments

of embankments, for reducing liquefaction-caused sliding and subsidence. As indicated in Fig. 3.29, the author conducted a shaking table test under 1-g condition to verify the effect of wood piles to prevent slope sliding and subsidence. Results of the experiment are shown in Fig. 3.30. The horizontal axis indicates the ratio of wood pile length to liquefiable soil thickness. The vertical axis shows the ratio of subsidence of the crest of the embankment with wood piles to one without wood piles. It was ascertained that wood piles driven halfway into the liquefiable soil zone caused about 40 % reduction of embankment settlement. The availability of nearby timber, including culled forest sources, offers a low-cost and effective countermeasure against subsidence caused by soil liquefaction.

References

1. Noshiro City Office (1984) Report of the 1983 Central Japan Sea earthquake and its caused damage (in Japanese)
2. Association for Development for Earthquake Prediction (1991) Report of the 1990 Luzon Islands earthquake, the Philippines and its caused damage (in Japanses)
3. Japan Road Association (1996) Specifications for highway bridges, and explanations, Part V seismic design/JSCE (2000), Earthquake resistant design codes in Japan
4. Japan Society of Civil Engineers (JSCE) (1999) The 1999 Kocaeli earthquake, Turkey. Earthquake damage investigation serious, No.5
5. Architectural Institute of Japan (AIJ) (2001) Guidelines for building foundation standards (in Japanese)
6. Bureau of The Port and Harbors, Ministry of Transport (2000) Earthquake resistant design of port facilities/JSCE (2000), Earthquake resistant design in Japan
7. Coastal Development Technical Research Center (1997) Handbook for liquefaction and measured in reclaimed land (in Japanese)
8. Home page of Tokyo Metropolitan Government. http://doboku.metro.tokyo.jp/start/03-jyouhou/ekijyouka/index.htm
9. Home page of Japan Press-Inn Association. http://www.atsunyu.gr.jp/
10. Japan Association for New Technology Development of Sewage System (2008) Measures for prevention of lifting of sewage manholes (in Japanese)

Chapter 4
Liquefaction-Induced Ground Displacements: Damage and Countermeasures

Abstract Liquefaction-induced large ground displacements and their caused damage to buried lifeline facilities and foundations of structures during past worldwide earthquakes, such as the 1964 Niigata, 1971 San Fernando and 1999 Kocaeri, Turkey earthquakes, are introduced. The mechanism of the flow of liquefied soil, resulting in large ground displacements is discussed by case studies and experiments, and the methods to estimate the magnitude of the ground displacements are explained. Earthquake-resistant design methods of buried pipes and bridge foundations against liquefaction and liquefaction-related ground displacements, which were adopted in the design codes after the 1995 Kobe earthquake, are described. Furthermore, countermeasures and seismic reinforcement of quay walls and foundations of existing structures are introduced.

Keywords Buried pipes • Countermeasures against liquefaction and ground displacement • Earthquake resistant design • Foundations • Liquefaction • Liquefaction-induced ground displacement

4.1 Case Studies on Liquefaction-Induced Ground Displacements and Resulting Damage

4.1.1 Initiation of Research on Liquefaction-Induced Ground Displacements

The following four kinds of damage to structures caused by soil liquefaction during past earthquakes, such as the 1964 Niigata earthquake and 1983 Central Japan Sea earthquake, were introduced in Sect. 3.1.2: (i) subsidence and inclination of structures due to loss of bearing capacity of the ground; (ii) uplift of underground structures due to buoyancy of liquefied soil; (iii) damage to earth structures such

M. Hamada, *Engineering for Earthquake Disaster Mitigation*,
Springer Series in Geomechanics and Geoengineering,
DOI 10.1007/978-4-431-54892-8_4, © Springer Japan 2014

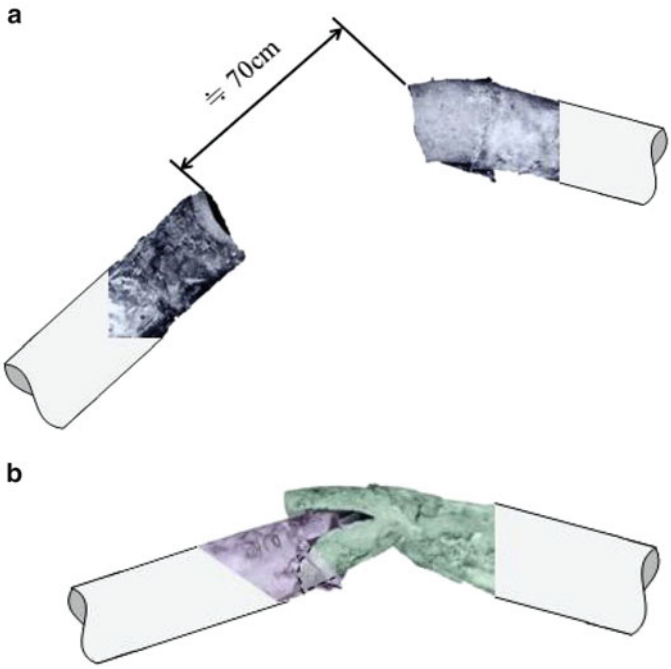

Fig. 4.1 Ruptures of buried gas pipes (1983 Central Japan Sea earthquake, at Noshiro in Akita prefecture). (**a**) Separation of ruptured sections at 45-degree bend. (**b**) Biting of ruptured pipes

as embankments and earth dams; and (iv) damage to coastal revetments and retaining walls due to increased earth pressure. However, the Central Japan Sea earthquake revealed another kind of damage by soil liquefaction.

Figure 4.1 shows damage to buried gas pipes caused by the 1983 Central Japan Sea earthquake in Noshiro of Akita Prefecture. Figure 4.1a shows that a welded section forming a 45° angle was ruptured and the two broken sections were separated by about 70 cm. Figure 4.1b shows that two broken sections bit into each other. It is highly improbable that these ruptures were caused only by dynamic ground motion of the earthquake, because the displacement magnitude of ground motions generally ranges from centimeters to decimeters.

To investigate the cause of these pipe ruptures, ground failures such as fissures and subsidence, and damage to structures such as houses in the liquefied area were surveyed. Figure 4.2 reveals examples of fissures at the ground surface that were observed over a broad area of Noshiro. It was inferred that there were large ground displacements in the horizontal direction. Figure 4.3 illustrates separation of a concrete-brick wall, which also showed a trace of horizontal ground displacements. These ground fissures and brick wall gap suggest that breakage of the pipes was not caused by cyclic ground displacements, but by monotonic ones. The damage to the pipes and traces of horizontal ground movement motivated research on liquefaction-induced ground displacements and their induced damage.

Fig. 4.2 Surface fissures by horizontal ground displacements (1983 Central Japan Sea earthquake). (**a**) Surface fissure and sand volcano in a park. (**b**) Surface fissure in a residential area

Aerial photos taken before and after the 1983 Central Japan Sea and 1964 Niigata earthquakes, and the other past earthquakes were used to measure liquefaction-induced ground displacements. It was shown that the ground had displaced by about 5 m in Noshiro and over 10 m in Niigata. Damage to foundation piles and buried pipes was also analyzed in relation to the ground displacements. About the same time as research on this subject began in Japan, similar research was being launched in the U.S. By using ground photos, horizontal displacements of reclaimed ground caused by the 1906 San Francisco earthquake were measured. Based on earthquake-caused distortion of the city's grid-like roads, it was found that the maximum displacement reached over 2 m.

Joint research efforts conducted simultaneously in Japan and the U.S. contributed to the investigation into the mechanism of large ground displacements and to the development of countermeasures. Eight U.S.–Japan workshops were held for exchanging scientific findings and promoting cooperative researches. The goal of these cooperative studies was to establish design methods for structural foundations and buried pipes, and to develop countermeasures against large ground displacements. However, the 1995 Kobe earthquake caused extensive liquefaction and consequent large ground displacements, primarily in the reclaimed lands of Kobe and surrounding cities, resulting in serious damage to foundations of buildings and bridges, port and harbor structures, and lifelines.

Fig. 4.3 Horizontal separation and vertical gap of a brick wall (1983 Central Japan Sea earthquake)

4.1.2 1983 Central Japan Sea Earthquake [1, 2]

Using aerial photos of Noshiro taken before and after the earthquake, liquefaction-induced ground displacements were measured. These were estimated as differences between pre-and post-earthquake three-dimensional coordinates of targets on the ground surface, such as manhole covers and corners of roadside ditches. Figure 4.4 are photos taken in Maeyama area in southern Noshiro. The accuracy of aerial survey depends on the reduction scale of the photos. In this case, measurement errors were estimated within ±16 cm in the horizontal and ±20 cm in the vertical (Table 4.1). These survey errors do not affect the reliability of the measurements, because the magnitude of measured displacements reached several meters.

Figure 4.5 shows one example of the measured displacements around Maeyama, where is a sand dune at an altitude of 20 m and has been developed for a residential area. It was found that a large area of about 300 m length in north–south as well east–west directions radially displaced downward from the top of the sand dune. Ground displacements were particularly predominant on the northern slope of the sand dune, reaching a maximum of about 5 m. The figure also shows ground fissures at the surface with vertical gaps, as surveyed by a research group from Akita University. The ground displaced down the slope, resulting in fissures with vertical gaps in the upper region of the slope, owing to tensile strains in the ground.

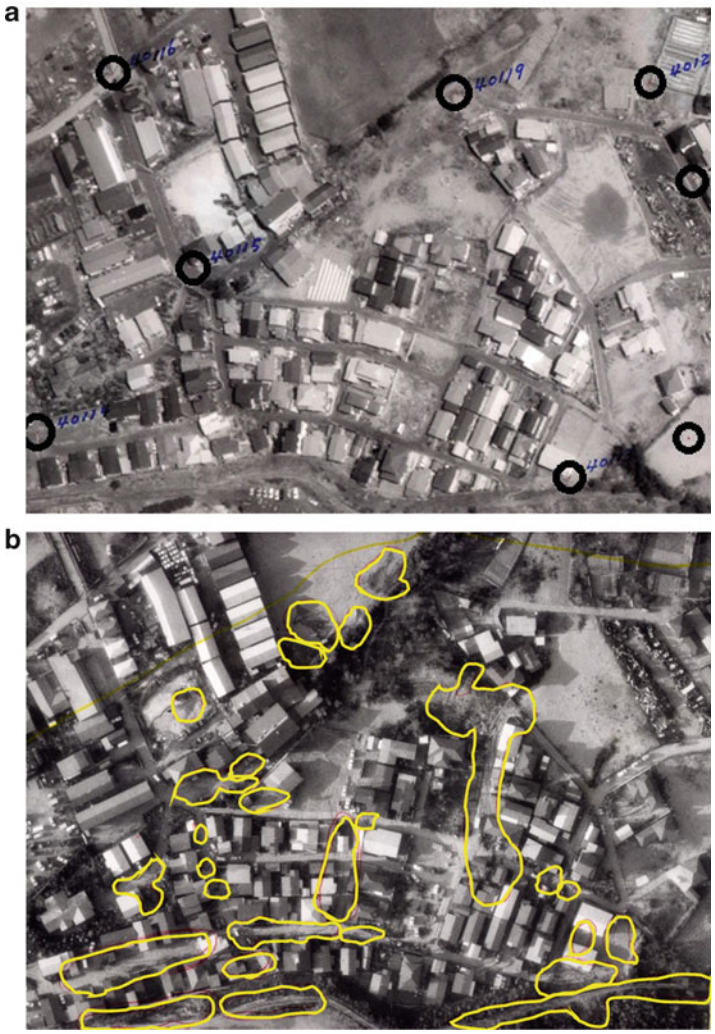

Fig. 4.4 Aerial photos of Maeyama area in Noshiro before and after the 1983 Central Japan Sea earthquake. (**a**) Two years before the earthquake (1981) *open black circle*: Targets for measurement on ground surface (cover of manholes, etc.). (**b**)Two days after the earthquake (1983) *Yellow ellipse*: Areas of sand boils

Table 4.1 Accuracy of ground displacement measurement

	Before earthquake	After earthqkae
Number of control points	21	5
Accuracy of aerial survey (m)	±0.08 (horizontal) ±0.16 (vertical)	±0.14 (horizontal) ±0.12 (vertical)
Accuracy of ground displacement measurement (m)	$\pm\sqrt{(0.16)^2+(0.12)^2}=\pm 0.20$ (vertical)	

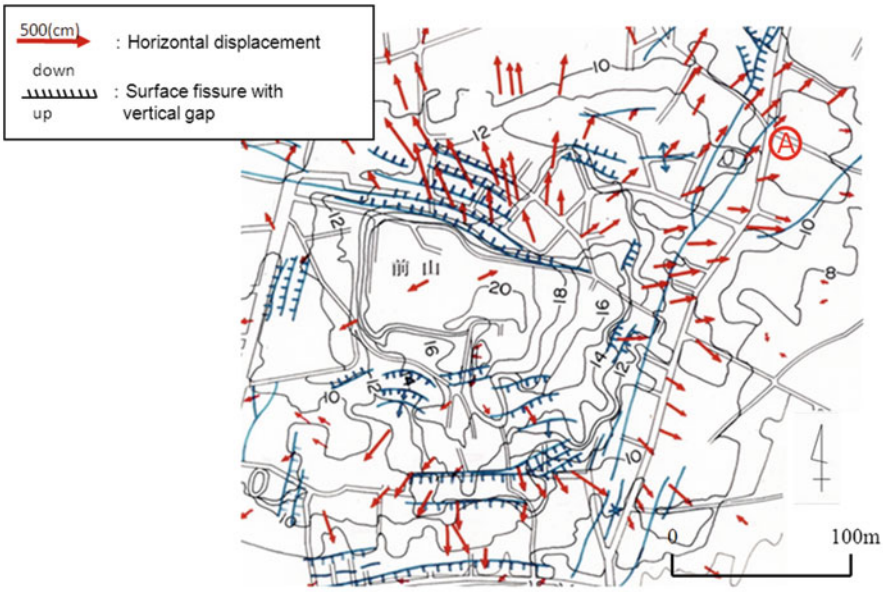

Fig. 4.5 Ground displacements and fissures in Maeyama area of Noshiro (the *number* shows altitude of ground surface)

To study the cause-and-effect relationship regarding the gas pipe rupture shown in Fig. 4.1a, ground displacements near the ruptured pipe were measured in detail. The circled "A" in Fig. 4.5 marks where the pipe was broken and separated into two sections, about 70 cm apart in Fig. 4.1a. A more precise measurement of horizontal ground displacement is given in Fig. 4.6. The vectors indicate the direction and the magnitude of the horizontal displacements, in centimeters. The ground displaced outward from the original line of the pipe by some 2–3 m, causing tensile forces the pipe. These induced a large bending moment at the bend point of the pipe. The concentration of stresses by the tensile force and bending moment ruptured the pipe, and two separated pipes moved with the ground displacements, as shown in Fig. 4.7.

In Noshiro, liquefaction-induced ground displacements caused further damage to lifelines. Figure 4.8 portrays damage to a buried telephone cable, intrusion of buried pipes into a manhole, and buckling of the cable. The damage occurred between two manholes. Figure 4.9 shows horizontal displacements at the ground surface, as measured by aerial photos. It is seen that the ground around manhole M2 displaced 1.2–1.6 m mostly in the direction of the cable axis, whereas the ground around manhole M1 displaced at right angles to the axis. Compressive strain with magnitude about 0.4 % in the axial direction, which was calculated from the measured displacements, was induced in the ground. This compressive strain of the ground caused buckling of the cable and intrusion of the pipes into the manhole.

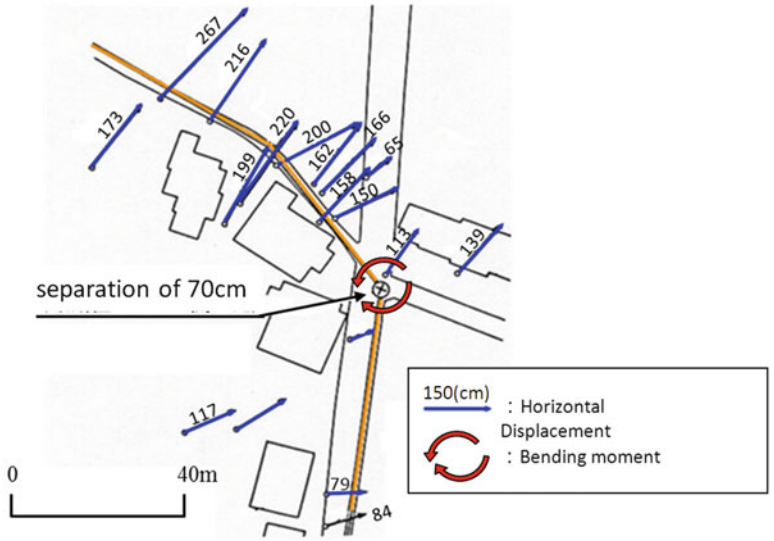

Fig. 4.6 Ground surface displacements in horizontal direction nearby the ruptured gas pipe

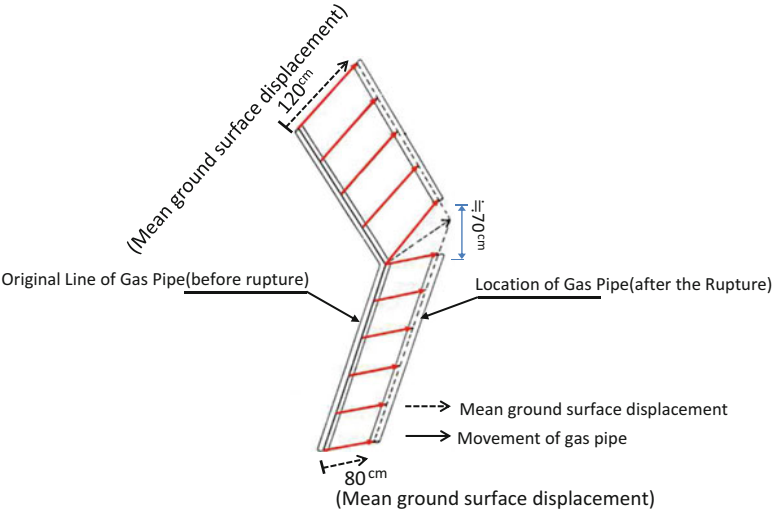

Fig. 4.7 Separation and movement of ruptured pipe

Figure 4.10 shows a rare event caused by ground strain. The figure comes from a report on the Central Japan Sea earthquake by the Noshiro city government [3]. The title of the photo is "Tree Split by Liquefaction". The boiled sand around the tree is an evidence of the soil liquefaction. However, it is not clear how soil liquefaction could cause splitting of the tree.

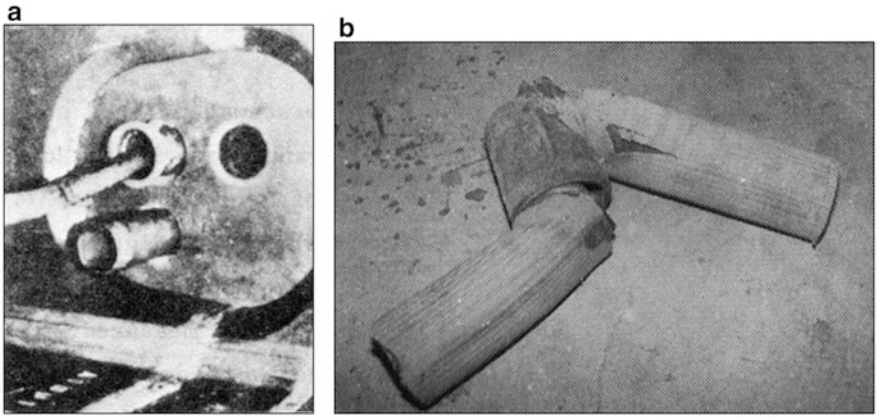

Fig. 4.8 Intrusion of buried telephone pipes into a manhole and buckling of cable (1983 Central Japan Sea earthquake). (**a**) Intrusion of pipes into a manhole. (**b**) Bucking of a cable

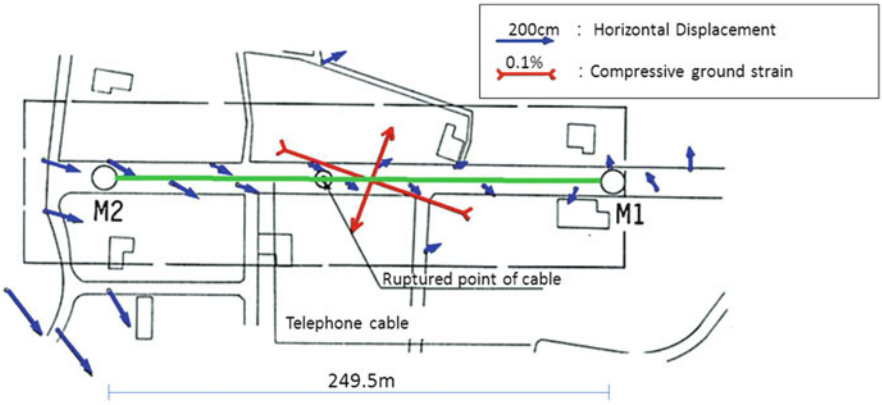

Fig. 4.9 Ground surface displacements in horizontal direction and ground strain

Figure 4.11 shows horizontal ground displacements measured near the split tree and ground strain calculated from the displacements. A tensile strain of approximately 2 % was caused at the location of the tree. It was presumed that this large tensile strain first tore the root of the tree, and the split propagated to the trunk.

Figure 4.12 shows ground displacements of an area in northern Noshiro, where was 800 m long and 600 m wide. The maximum displacement reached over 4 m in a north-northeast direction. The soil condition, estimation of liquefaction and ground surface displacements along the Section A–A' in Fig. 4.12 are shown in Fig. 4.13. The ground surface inclined slightly at an average gradient less than 0.5 %.

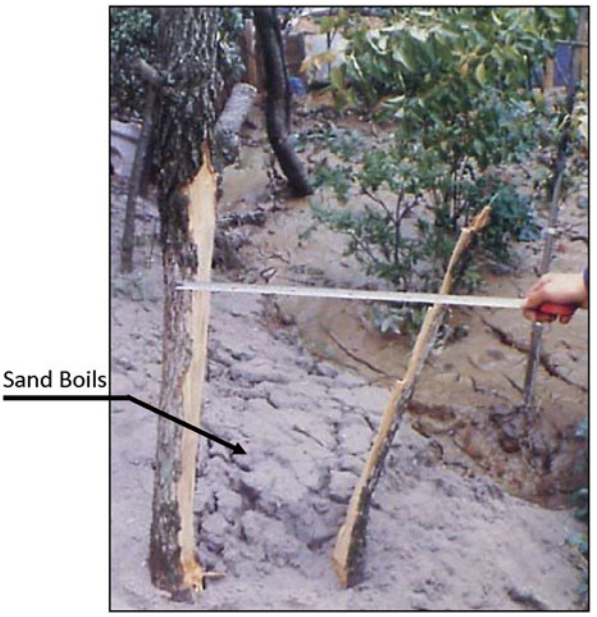

Fig. 4.10 Split tree caused by liquefaction-induced ground displacement (after report from Noshiro city during 1983 Central Japan Sea earthquake)

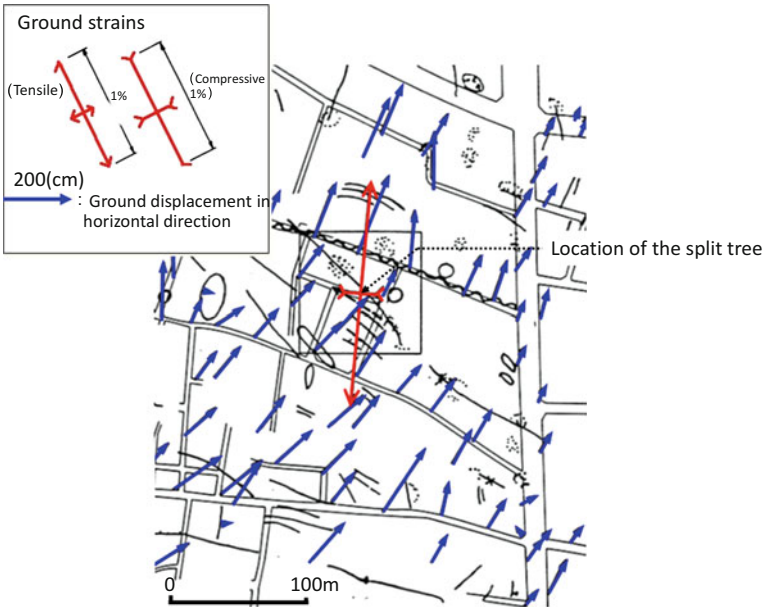

Fig. 4.11 Ground surface displacements and ground strain nearby the split tree (1983 Central Japan Sea earthquake)

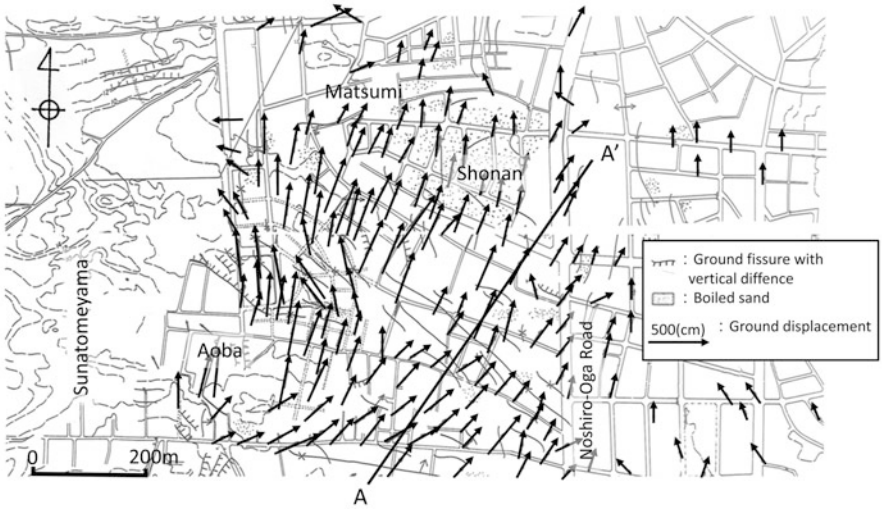

Fig. 4.12 Ground displacements in the north area of Noshiro

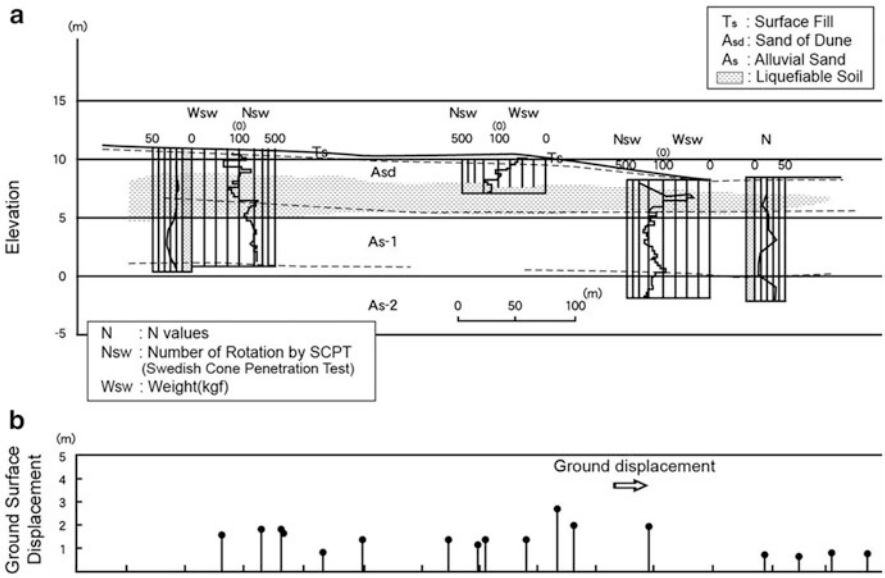

Fig. 4.13 Soil condition, estimation of liquefiable soil and ground displacements in horizontal direction (A–A' Section in Fig. 4.6). (**a**) Soil condition and estimation of liquefaction. (**b**) Horizontal ground displacements (right direction in figure (a) is positive)

The figure also shows estimation of soil liquefaction by the *Specification of Highway Bridges* [4] (cf. Sect. 3.2) under an assumption that maximum acceleration was 200 cm/s^2. Liquefiable soil extended over long distances, with maximum thickness of 4 m. Despite the slight inclination of the surface, the ground displacements reached 2–3 m there, as shown in Fig. 4.13b.

4.1.3 1964 Niigata Earthquake [1, 5–7]

Four types of damage to structures due to soil liquefaction were first recognized at the time of the 1964 Niigata earthquake, namely subsidence and inclination of buildings and bridges, uplift of underground structures such as manholes, sliding failures and collapse of earth structures such as embankments, and inclination and collapse of quay walls and retaining walls. Based on these types of damage, researches have been carried out and countermeasures were developed to prevent such damage. However, the 1983 Central Japan Sea earthquake led to recognition of liquefaction-induced ground displacements, and the research on this subject was initiated nearly 20 years after the Niigata earthquake.

The Niigata earthquake caused severe liquefaction and damage to building and bridge foundations and buried lifeline pipes. It was presumed that ground displacements caused by this earthquake were much larger than those by the Central Japan Sea earthquake. Therefore, measurements were conducted using aerial photos taken before and after the Niigata earthquake, as shown in Fig. 4.14a, b.

Figure 4.15 shows ground displacements in the horizontal direction in Kawagishi area on the left bank of the Shinano River of Niigata. Aerial photos in 1962, 2 years before the earthquake, were used to compare with those immediately after the earthquake. Measurement error is estimated at less than $\pm$72 cm horizontally, and 66 cm vertically. Because ground surface displacement reached more than 11 m, the measurement has adequate precision.

Figure 4.15 shows that the ground along the Shinano River was greatly displaced toward the river center. The large area behind the riverbank, about 800 m wide and 200 m long, moved to the river. The figure also shows fissures and sand boils at the ground surface, as found by a research team from Niigata University [8]. It is clear that soil liquefaction occurred over an extensive area, and that there were numerous fissures along the river bank as a result of large ground displacements toward the river.

Figure 4.14a, b facilitate visual understanding of the ground displacement measurements. By comparing the post-earthquake and pre-earthquake photos, it is seen that the space between two buildings (A: apartment building; B: warehouse), some 100 m away from the river, greatly expanded. The warehouse B was deformed by differential ground displacement of both sides of the building. Furthermore, the riverbank line was curved much more after the earthquake.

Horizontal ground displacements along the riverbank between the Bandai and Yachiyo bridges are shown in Fig. 4.16. The ground on both banks displaced toward

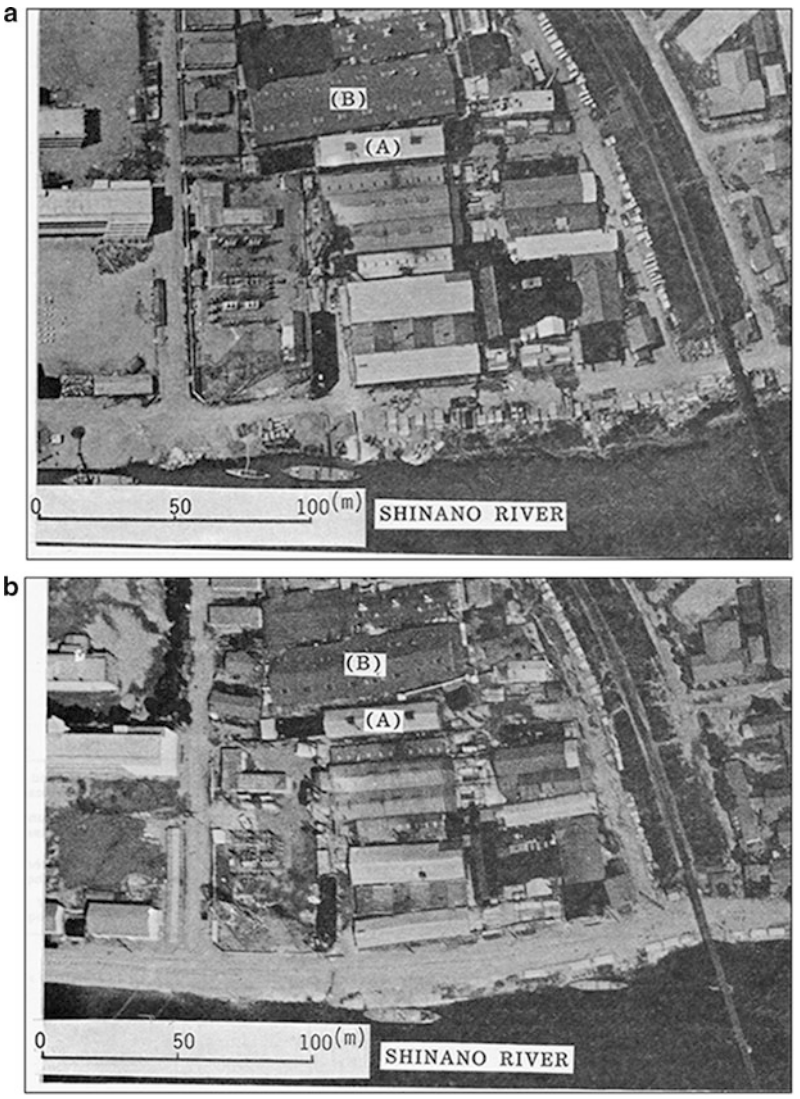

Fig. 4.14 Aerial photos of Kawagishi in Niigata. (**a**) Two years before the earthquake (1962). (**b**) After the earthquake (1964)

the river center. Maximum displacement of the right bank was more than 10 m at downstream side of the Bandai Bridge. However, ground displacements near the bridge abutment were much smaller than those further from the bridge. This shows that the high rigidity of the abutment foundation reduced ground displacements.

The measurements in Fig. 4.16 indicate that the width of the Shinano River narrowed during the earthquake. To quantify reduction of river width, measurements

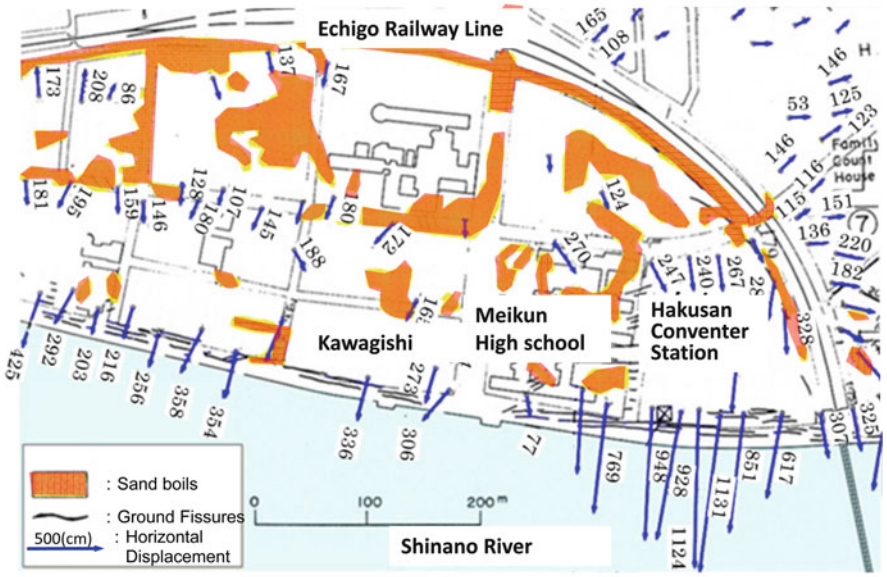

Fig. 4.15 Horizontal ground displacements in Kawagishi along Shinano River in Niigata city (1964 Niigata earthquake)

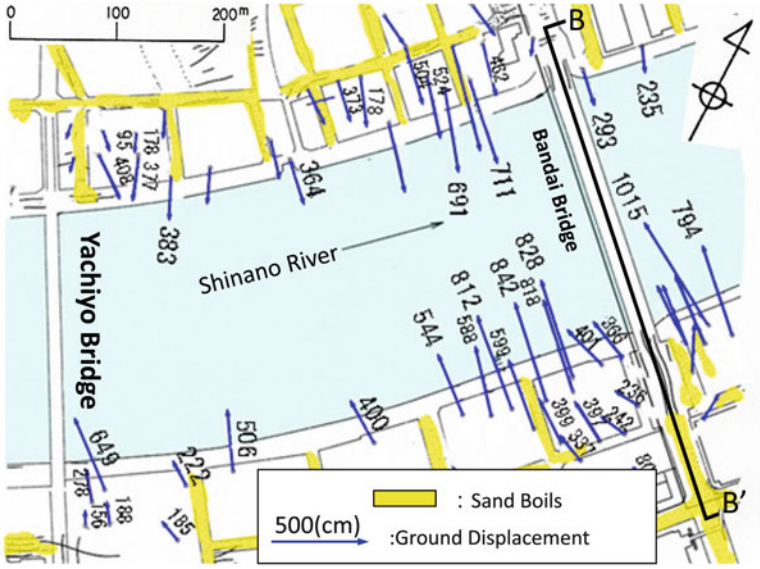

Fig. 4.16 Ground displacements between Bandai~Yachiyo bridges (1964 Niigata earthquake)

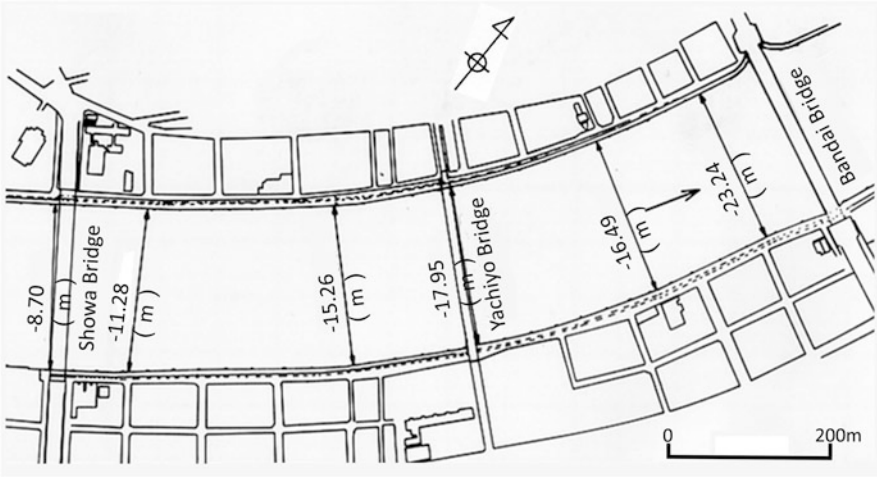

Fig. 4.17 River width reduction by horizontal ground displacements (1964 Niigata earthquake)

were made by using aerial photos taken in 1964, and 1972 when reconstruction of the collapsed riverbanks was completed. Figure 4.17 shows that river width between the Bandai and Yachiyo bridges had decreased by 16–23 m. This indicates that river width decreased by mostly 10 % from the original width of about 200 m.

The narrowing of the Shinano River was quantitatively ascertained 20 years after the earthquake. However, there was a widespread awareness among people living along the river that their land had been expanded by the earthquake. The following are examples of remarks made by residents at a citizen's meeting held on July 26, 1964, 1 month after the earthquake.

A: "My house is about 70 m from the Shinano River, and there hadn't been any significant damage to my house. But when I measured the distance, the land had stretched a good 2.7 m. I thought that both streets and houses were displaced toward the Shinaro River."

B: "I crossed the Yachiyo Bridge to attend this meeting today. I have the unmistakable feeling that the land along the river has extended toward the river."

C: "My house was built close to the hedge in the back, but now I can pass easily through the space between the hedge and house. The street in front of my house also became wider, and there's a greater separation between my house and the neighbor's house. I don't know why. It's all very strange."

The problem is that despite these testimonies, scientists and engineers in the field of earthquake disaster prevention were unaware of what had occurred. Until the Central Japan Sea earthquake in 1983, no research had been done on liquefaction-induced ground displacements. Testimonies of the residents did not arouse the attention of experts, so research was not begun after the Niigata earthquake. However, in the report on the Niigata earthquake by the Japan Society of Civil

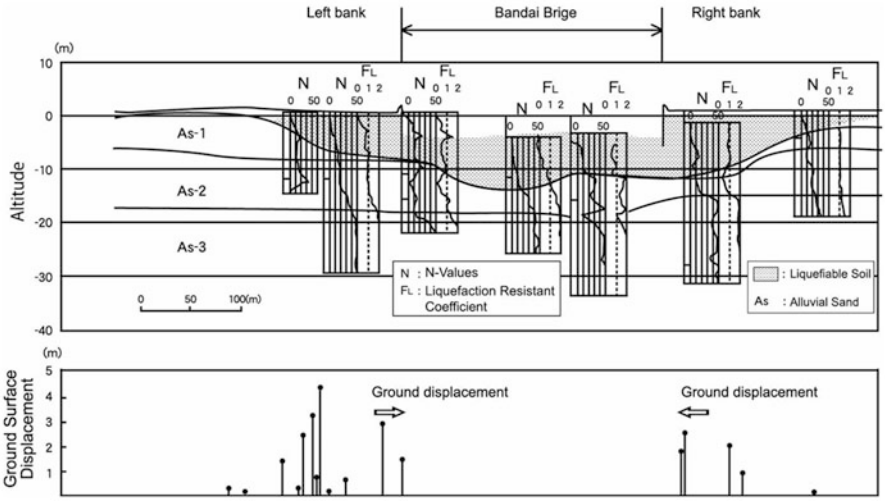

Fig. 4.18 Soil condition, estimation of liquefiable soil and horizontal ground displacements (B–B' Section in Fig. 4.15)

Engineers (JSCE) the term "sand-flow phenomenon" was used [9]. This shows that there was some sense in the scientific community that the ground moved by the flow of liquefied sand. Studies on liquefaction-induced ground displacements began after the 1983 Central Japan Sea earthquake, toward developing methods of earthquake-resistant design and countermeasures. However, the same phenomenon reoccurred during the 1995 Kobe earthquake, causing great and widespread damage to buildings, bridges and lifeline facilities.

Figure 4.18 shows the soil condition, estimation of liquefaction, and horizontal ground displacements along a cross section of the Bandai Bridge (B–B' Section in Fig. 4.16). There is a liquefiable soil layer that broadly extends toward the middle of the river, attaining thickness of up to 10 m. The ground behind both riverbanks displaced considerably toward the river.

The Showa Bridge was collapsed by the 1964 Niigata earthquake as shown in Fig. 4.19. It had been built on a pile bent foundation, which was constructed by driving steel pipe piles in a line at right angles to the bridge axis. Soil liquefaction greatly weakened the ground stiffness, resulting in large deformation of piers and falling of simply supported girders. The Showa Bridge had been constructed to transport audiences of the National Athletic Meet in the same year as the earthquake. Its collapse came just after the meet, only 15 days after completion of the bridge. Figure 4.20 shows horizontal ground displacements, with traces of sand boils and ground fissures on the left bank. However, ground displacements were smaller, with almost no sand boils on the right bank. This was because the left bank was reclaimed from the old river channel, which was liquefiable. The right bank was on original non-liquefiable natural levees with higher elevation.

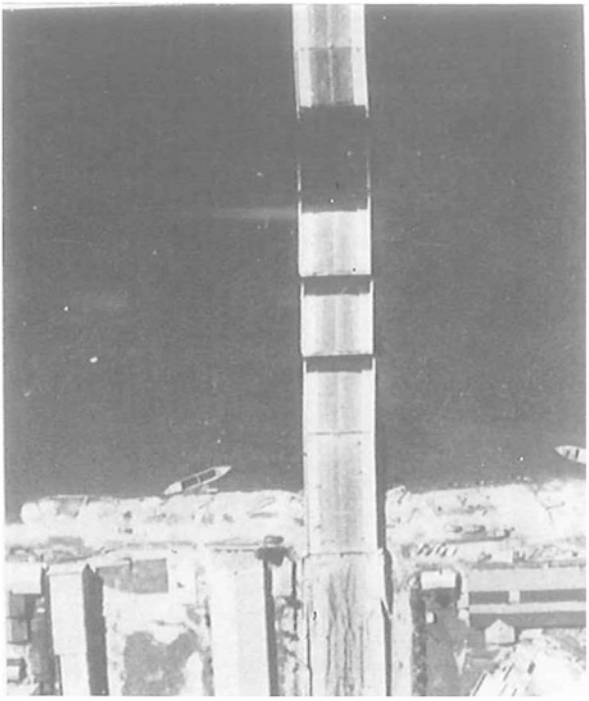

Fig. 4.19 Girders' fall of Showa bridge (1964 Niigata earthquake)

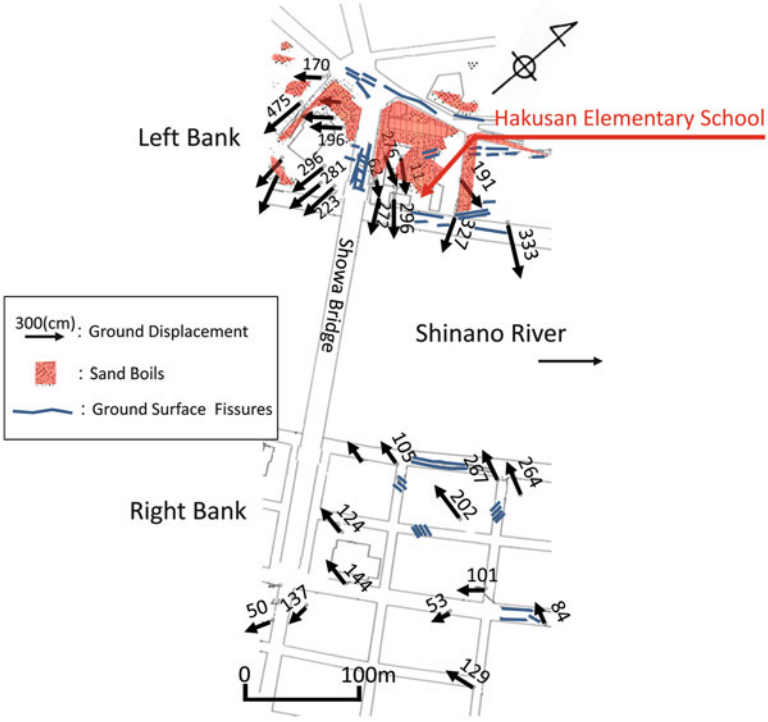

Fig. 4.20 Ground displacements, sand boils and ground fissures on both banks of Showa bridge (1964 Niigata earthquake)

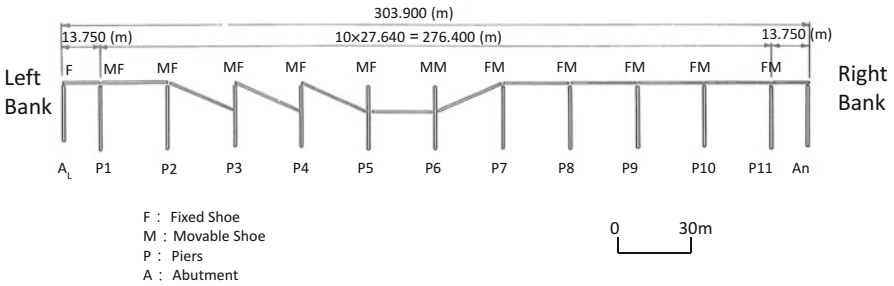

Fig. 4.21 Girders' fall of Showa Bridge by liquefaction-induced ground displacements due to soil liquefaction

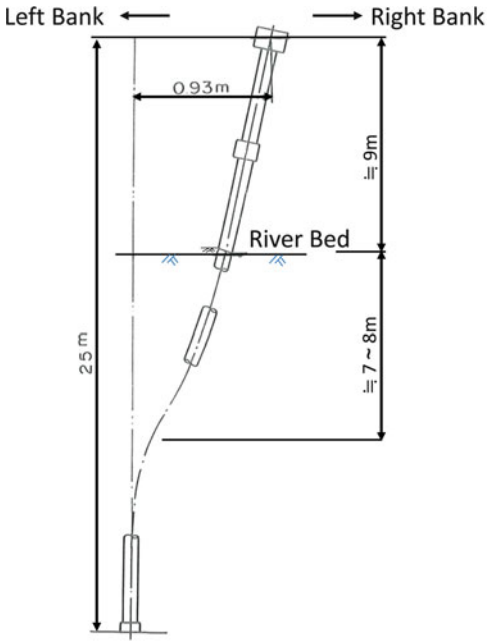

Fig. 4.22 Deformation of a steel pile of the Showa bridge

As seen in Fig. 4.21, the girders on the left bank side had fallen considerably. Figure 4.22 shows the deformation of a steel pipe of a pier that was pulled out of the riverbed after the earthquake [9]. The steel pile was bent toward the right bank, at a depth of 7–8 m from the riverbed. The author inferred the following regarding the cause of the girders' fall. Soil liquefaction occurred in the ground and riverbed mainly on the left bank, and induced ground displacements toward the river center. This deformed the steel piles and increased the span between neighboring piers, resulting in the girder fall.

There is another explanation for the reason of the girder fall, as follows: the bearing capacity of the riverbed greatly decreased owing to soil liquefaction, and

the piers vibrated largely. Furthermore, there was a problem of the structure of the bridge that supported this explanation. Figure 4.21 shows connection between the girders and the piers. In the figure, F represents a fixed shoe, and M is a moveable shoe on which the girders can move freely from the piers. Both girders on pier 6 (P6) were on moveable shoes; on other piers, one girder was on a movable shoe and the other on a fixed shoe. Therefore, the mass on top of P6 was much smaller than that on other girders. The natural period of vibration of P6 was different from those of other piers, so considerable relative displacements were induced between P6 and neighboring piers by earthquake ground motion. Therefore, the fall of the girders was caused by a difference in dynamic response between neighboring piers. However, a counter argument against this explanation was given in the testimony of a taxi driver: [10]

"At the time of the earthquake, I was driving a taxi on the middle of the bridge. Feeling a strong earthquake motion, I stopped the car and waited some time for the shaking to end. Then, abandoning the vehicle, I ran to the left bank, periodically glancing back over my shoulder. I was astonished to see the girders over which I had just passed dropping into the river, one by one."

It is surmised from this testimony that the girders did not begin to fall during the strong vibration, because the taxi driver said that the girders began to fall when he started to run from the bridge, after some time. It may be supposed that several tens of seconds passed before the fall began. This provides strong evidence for the first explanation, which the author supports. Liquefaction-induced ground displacement is a phenomenon whereby liquefied soil flows under the influence of gravity according to the inclination of the ground surface. It takes some time until the end of liquefaction, when excess pore water pressure is dissipated. Because liquefaction persists long after earthquake ground motion has ceased, ground displacements continue. This explains why even after earthquake ground motion had ceased, sand and water boiled up for some time in Urayasu and elsewhere during the 2011 Tohoku earthquake. The assumption is that delayed ground displacements from the left bank toward the river center are the cause of the Showa Bridge collapse.

Figure 4.23 shows ground displacements and the micro-topographic condition in the Ohgata area of Niigata, along the Agano River. As indicated, Ohgata Primary School is on a natural levee, at slightly higher elevation than the lowland area that had been the old Agano River stream (white part in the figure). The ground displaced from the school toward the Tsusen River, an old channel of the Agano River. Figure 4.24a shows a large fissure on the surface of the school playground, and Fig. 4.24b shows the separation of school buildings due to the tensile strain of the ground. Figure 4.24c was taken after 25 years from the 1964 earthquake, and shows a curved road along the playground that had been straight before the earthquake.

The dotted line in Fig. 4.23 shows dislocation of National Highway No. 7. This road was constructed on a natural levee, the surface of which slightly inclined in a southerly direction. As a result of liquefaction-induced ground displacement, the road dislocated southward and curved. The maximum offset displacement in the horizontal direction from the original straight line was 5.6 m, corresponding closely to ground displacement measured by aerial photos.

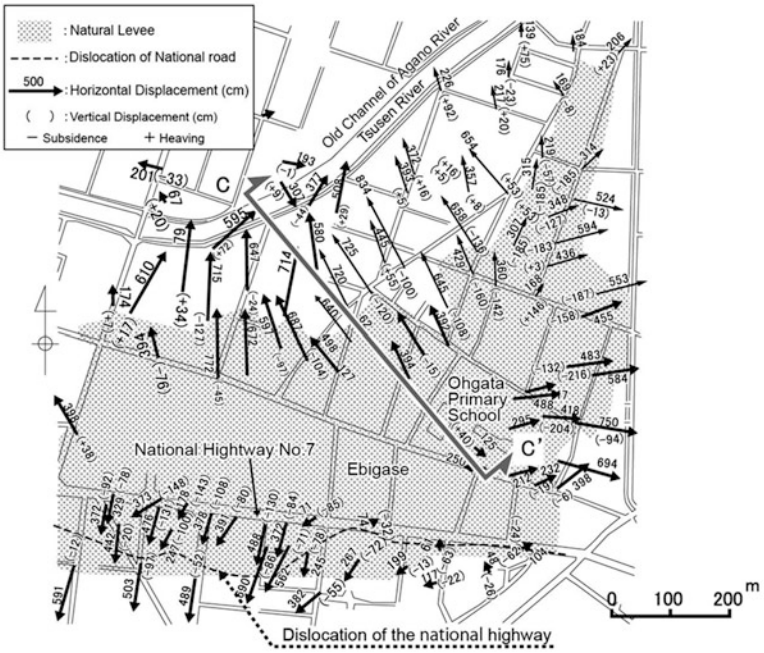

Fig. 4.23 Ground displacements and micro-topographical condition in Ohgata area (1964 Nigata earthquake)

Figure 4.25 shows the soil condition and estimation of liquefaction along the Section C–C' in Fig. 4.23, from the school to the Tsusen River. The ground surface sloped down from the school to the river, but the mean gradient of the surface is less than 1 %. The reduced scale of elevation on the vertical axis of the figure is one-tenth of that on the horizontal axis. There was liquefiable soil continuously from the school to the Tsusen River, with maximum thickness of 7–8 m. Large ground displacements were caused by a flow of liquefied soil from the effect of gravity of the soil.

Liquefaction-induced ground displacement inflicted damage to the foundation piles of buildings, bridges and buried pipes. Figure 4.26 shows ruptured concrete piles discovered after 20 years from the 1964 earthquake, during building reconstruction. All piles of 30 cm diameter were broken at two depth [11]. Figure 4.27a schematically shows rupture of piles and soil conditions, and Fig. 4.27b shows horizontal and vertical displacements at the ground surface nearby the building. The two rupture points of the piles mostly coincided with boundaries between liquefiable and non-liquefiable soil. N values of the ground below the lower rupture point were large (mostly greater than 10), so the ground was presumed not to have liquefied. Likewise, ground above the upper rupture point was unsaturated above the groundwater level, so liquefaction did not occur. The cause of the pile ruptures was stress concentration between liquefied and non-liquefied soil. Residual displacement of the piles (Fig. 4.27a), which is the differential displacement between

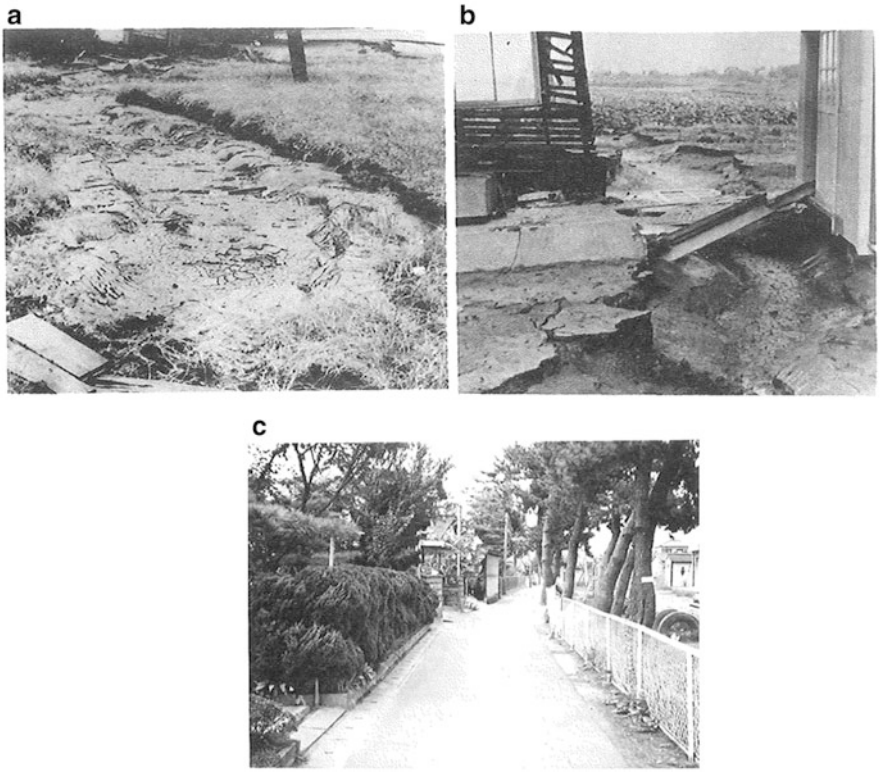

Fig. 4.24 Fissures on the play ground of the primary school, separation of school buildings and curved road (1964 Niigata earthquake). (**a**) Surface fissure of play ground. (**b**) Separation of school building. (**c**) Curved road

the top and tip of the pile was 1.0–1.2 m toward the southeast. Figure 4.27b shows that the ground also displaced about 2 m toward the southeast. The residual deformation of the piles after the rupture is mostly consistent with the ground displacements. Figure 4.28 shows another damage to concrete piles of buildings, such as the Niigata Family Court, Hotel Niigata, and S-Construction Company.

In the city of Niigata, there were numerous reports of damage to buried pipes. Figure 4.29 shows an example of protrusion of a gas pipe above the ground surface. Alignment of the buried pipe, the location of its protrusion, and vectors of horizontal ground displacements in the neighborhood are shown in Fig. 4.30. In the zone surrounded by the broken line, the ground on the northern side of the protrusion displaced about 2 m, mostly toward the pipe axis. However, ground displacement was reduced near the protrusion. The compressive strain determined from ground displacement was about 0.3 % in the axial direction. It is surmised that the compressive strain of the ground caused the pipes to buckle and protrude over the ground surface. Many instances of buckled buried pipes surfacing above the

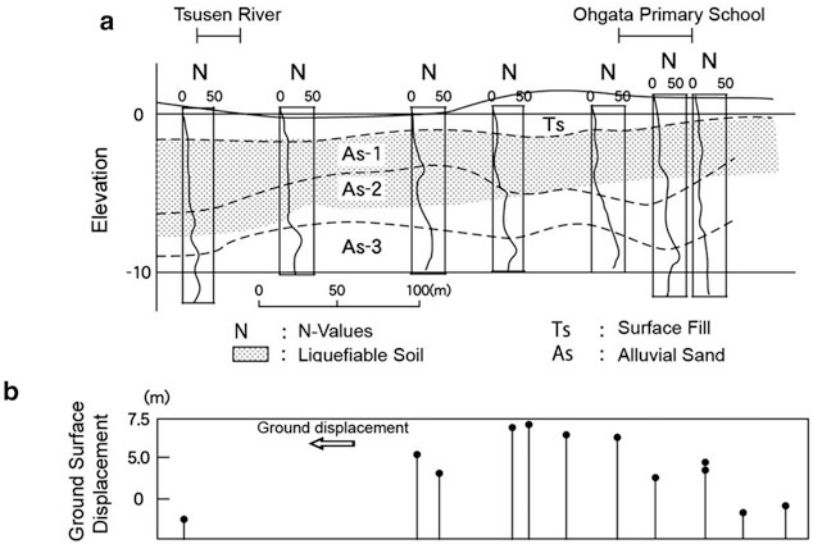

Fig. 4.25 Soil condition, estimation of liquefaction and horizontal ground displacements (C–C' Section in Fig. 4.22). (**a**) Soil condition and estimation of liquefied soil. (**b**) Horizontal ground displacements (along C–C' Section in Fig. 4.23, positive: left direction)

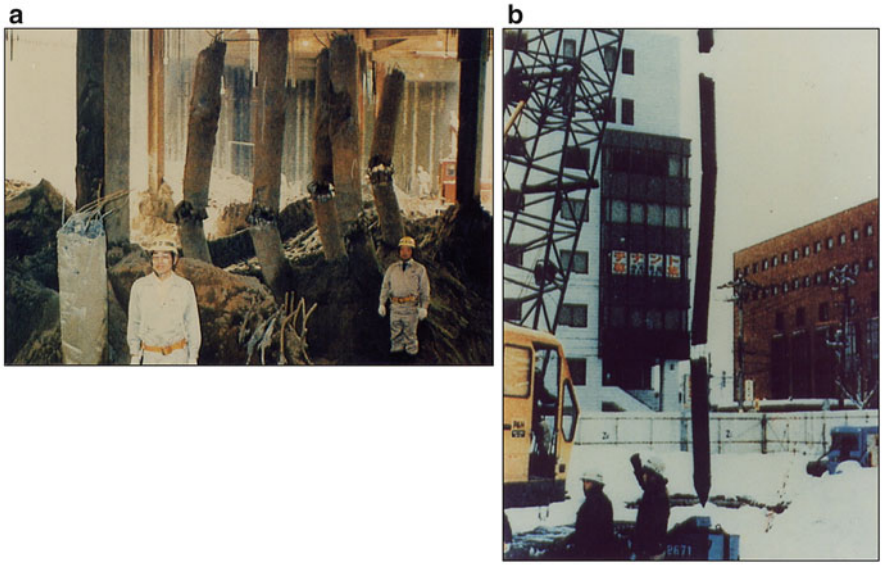

Fig. 4.26 Concrete piles ruptured by liquefaction-induced ground displacements (1964 Niigata earthquake). (**a**) Ruptures of concrete piles found 20 years after the earthquake (after Kawamura [14]). (**b**) Ruptures at two elevations of piles (after Kawamura [14])

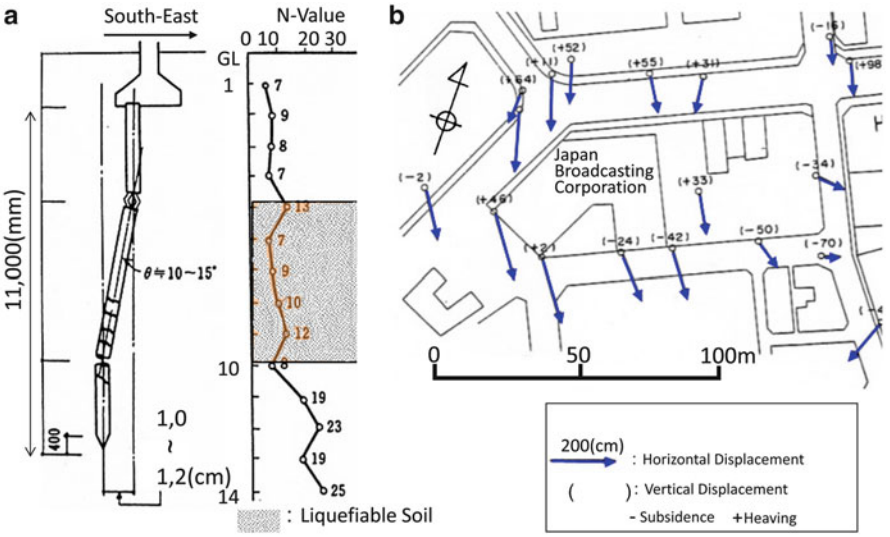

Fig. 4.27 Rupture of piles and ground displacements nearby the inclined building. (**a**) Deformation of a pile and estimation of liquefaction. (**b**) Horizontal and vertical displacements at ground surface nearby the building

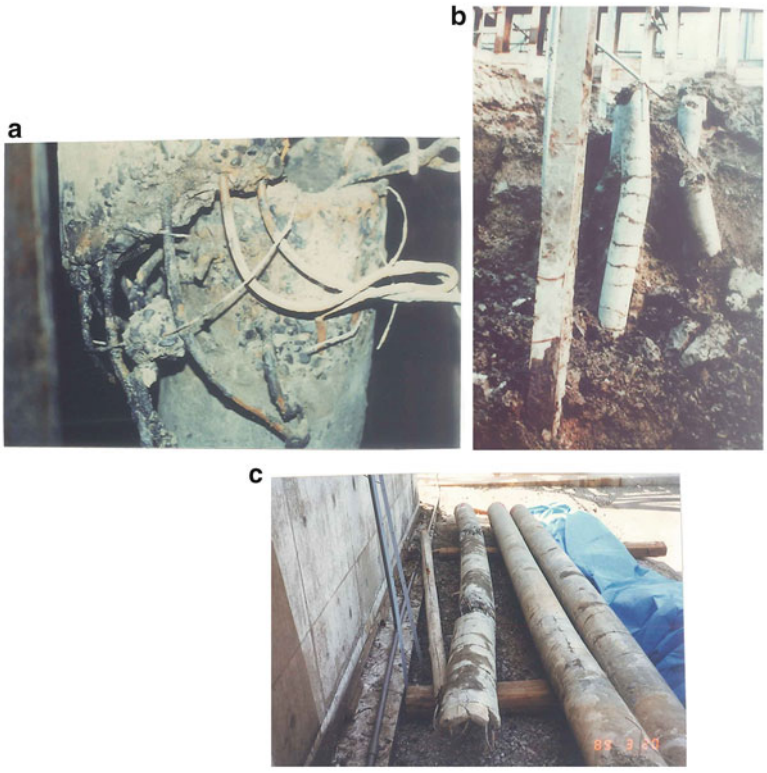

Fig. 4.28 Concrete piles ruptured by liquefaction-induced ground displacements (1964 Niigata earthquake). (**a**) Niigata family court house. (**b**) Hotel Niigata. (**c**) S-construction company building

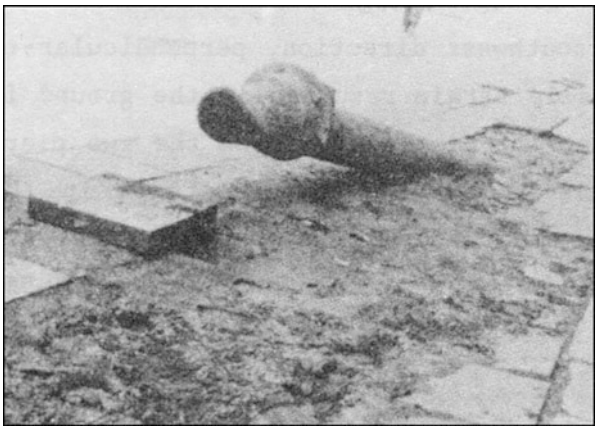

Fig. 4.29 Protrusion of a buried gas pipe above ground surface by liquefaction-induced ground displacements (1964 Niigata earthquake)

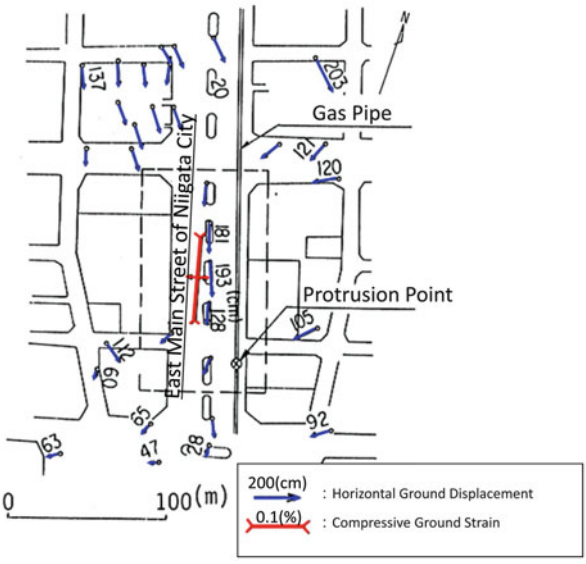

Fig. 4.30 Ground displacements and strain nearby the protrusion of gas pipe

ground could be seen in Niigata. Figure 4.31a, b show gas pipes, and Fig. 4.31c a natural gas pipeline.

There are many reports that previously straight roads were curved by liquefaction-induced displacements in Niigata. Figure 4.32 was taken from point B in Fig. 4.33. This road had been straight prior to the earthquake, but the ground displaced 3–4 m westward (Fig. 4.33). The gradient of the ground surface was very small, about 0.3 %. From Fig. 4.32, however, it is inferred that the ground surface slightly inclines from right to left in a westerly direction.

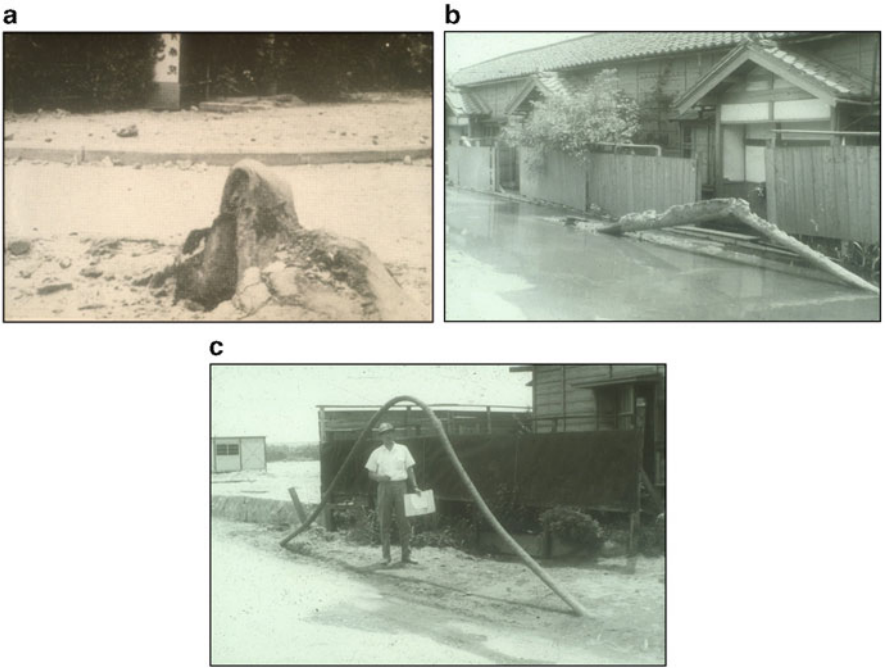

Fig. 4.31 Surfacing of buried pipes by buckling due to liquefaction-induced ground displacements. (**a**) Buried gas pipe. (**b**) Buried gas pipe. (**c**) Natural gas pipe line

Fig. 4.32 Curved road by liquefaction-induced ground displacements (1964 Niigata earthquake)

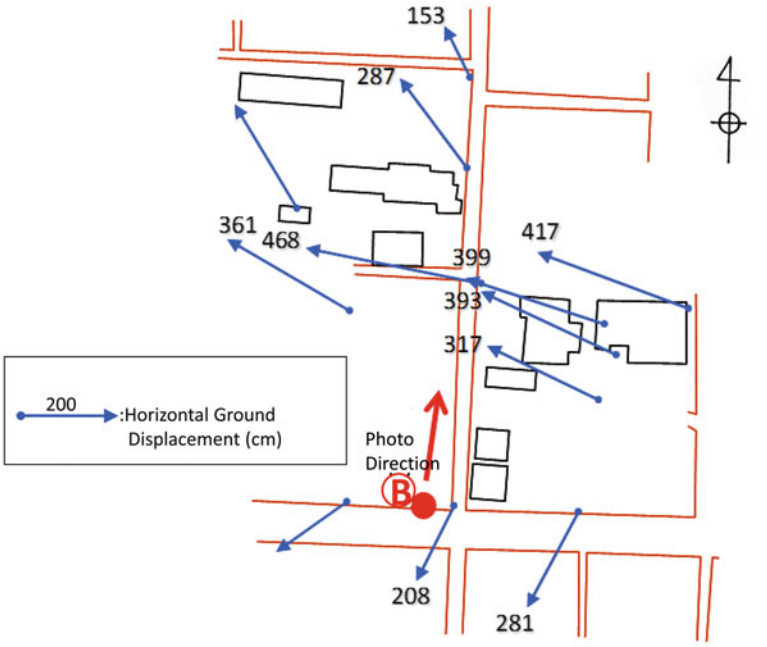

Fig. 4.33 Ground displacements in the vicinity of curved road (1964 Niigata earthquake)

4.1.4 1995 Kobe Earthquake [12–16]

The 1995 Kobe earthquake caused widespread liquefaction, particularly in broad reclaimed lands extending from Kobe to Nishinomiya. Strong earthquake ground motions by an inland fault with moment magnitude Mw = 6.9 and soil liquefaction caused large movement of quay walls. In many cases, such as on Port and Rokko Islands, soil used for reclamation contained large quantities of decomposed granite, including gravel and fine fractions. Before the earthquake, the liquefaction potential of soil containing gravel was believed to be low, because excess pore water pressure could dissipate through the gravel. After the earthquake, methods for estimation of liquefaction potential were revised in various design codes, in which the possibility of soil liquefaction of gravel including sand and fine fractions was considered, based on laboratory tests [4].

Figure 4.34 shows displacements at the ground surface in the horizontal and vertical directions, nearby the northern quay wall of the Rokko Island. The caisson-type quay walls displaced 3–4 m in a northerly seaward direction, and reclaimed lands behind them also moved toward the sea. Point C in Fig. 4.34 marks the location of the fallen railway girder seen in Fig. 4.35. The ground displacements moved the foundation of a bridge pier toward the sea, so with expansion of its span between two neighboring piers, and a simply-supported

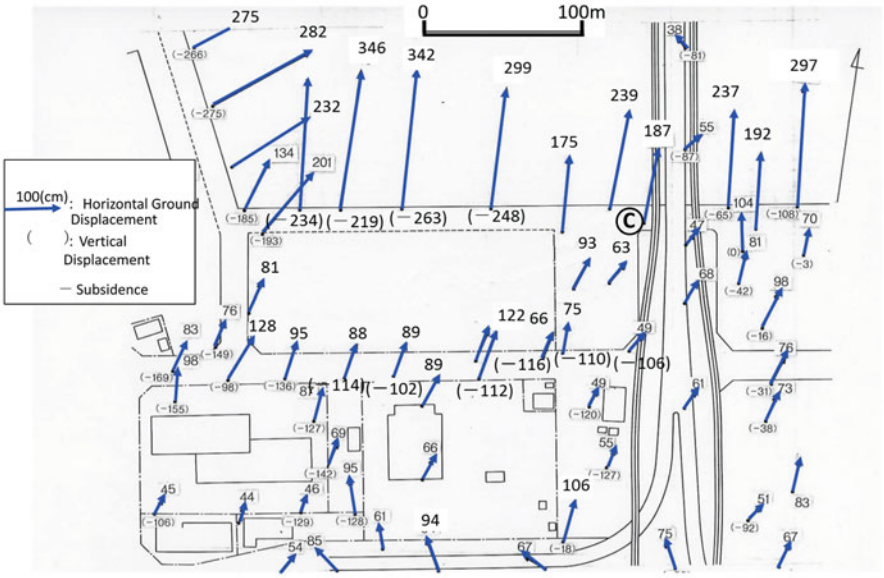

Fig. 4.34 Liquefaction-induced ground displacements (1995 Kobe earthquake, at Rokko Island)

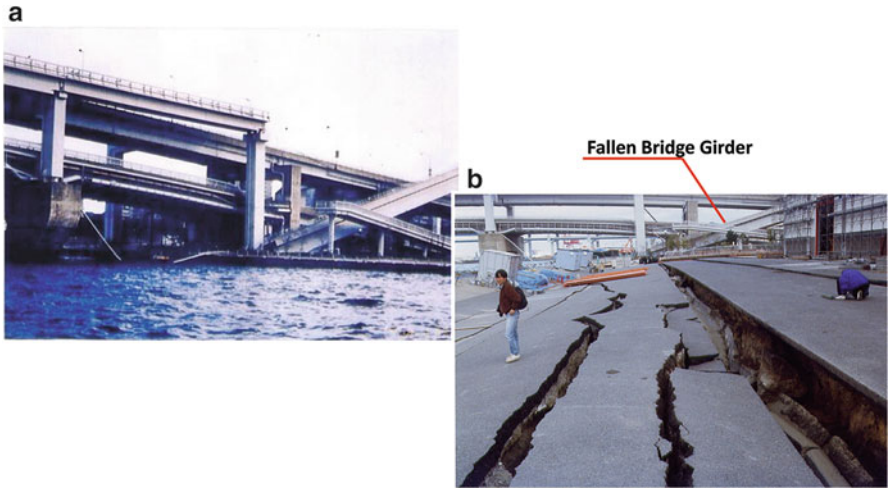

Fig. 4.35 Fall of a bridge girder by liquefaction-induced ground displacements (1995 Kobe earthquake, at Rokko Island). (**a**) Fall of a bridge girder. (**b**) Ground fissures, and inclination and subsidence of ground surface

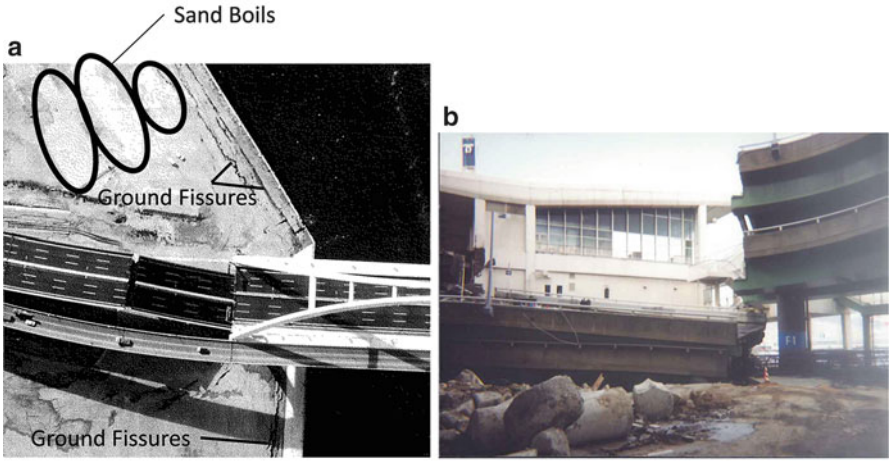

Fig. 4.36 Fall of bridge girders by liquefaction-induced ground displacement (1995 Kobe earthquake). (**a**) Fall of a highway bridge. (**b**) Fall of a ramp of Kobe bridge

girder dropped. According to a post-quake ground survey, the foundation displaced seaward about 1 m.

Figure 4.35 shows the fallen bridge girder and post-earthquake situaton of the ground surface, which had previously been level. The ground inclined toward the sea, with fissures running parallel to the quay wall. The ground surface along the wall sank more than 2 m, and areas as far as 100 m also sank, by over 1 m (Fig. 4.34). Increased span between neighboring piers as the cause of bridge girder fall during the Kobe earthquake was seen elsewhere. A bridge of the Hanshin Expressway Bayshore Line collapsed, as shown in Fig. 4.36a, due to the movement of the pier foundation with a magnitude of about 1 m in the direction of the sea. As an aerial photo shows, the vicinity of the pier was covered by boiled sand due to soil liquefaction, with fissures opening in the ground behind the quay wall. Figure 4.36b shows an approach ramp to the Kobe Bridge, which also collapsed due to the ground displacements in the seaward direction.

Figure 4.37 is an aerial photo taken over a tank yard in Kobe, 2 days after the earthquake. Boiled sand accumulated all over the yard, indicating that its entire area had liquefied (yellow colored part in the figure). The three large tanks in the photo contained LPG (liquefied propane gas). In the aftermath of the earthquake, a large amount of gas leaked because of rupture of a pipeline valve. The threat of a massive explosion of leaked propane gas forced neighborhood residents to be evacuated for about 24 h.

Figure 4.38 shows horizontal and vertical ground displacements of the tank yard, indicating that the quay wall displaced a maximum of 3.6 m seaward. Furthermore, the entire tank yard, with about 400 $\times$ 400 m area, also moved 2–3 m seaward and the ground surface sank more than 1 m. The ground displacement close to the quay

Fig. 4.37 Soil liquefaction in a tank yard (1995 Kobe earthquake, Mikagehama in Kobe city)

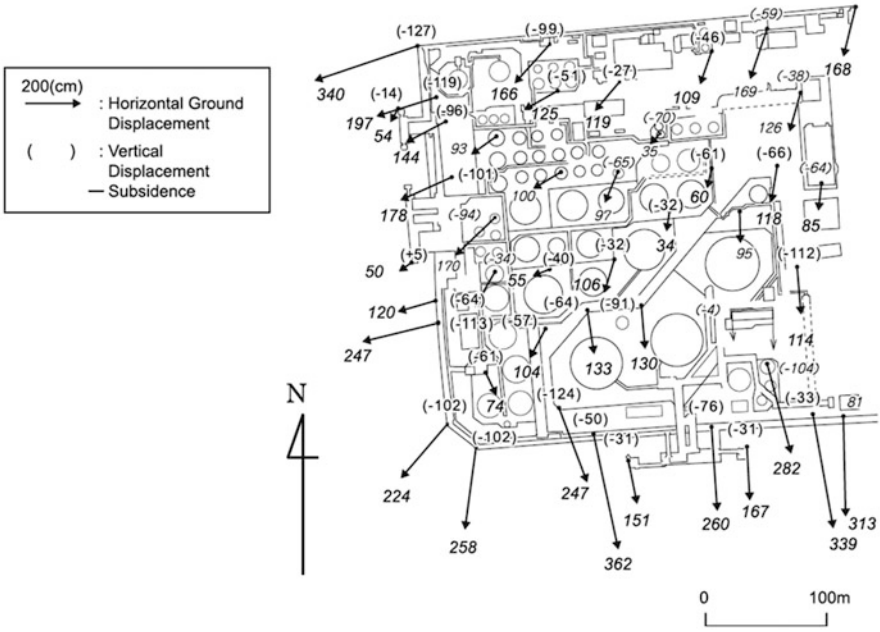

Fig. 4.38 Liquefaction-induced ground displacements in a tank yard (1995 Kobe earthquake, at Mikagehama, Kobe city)

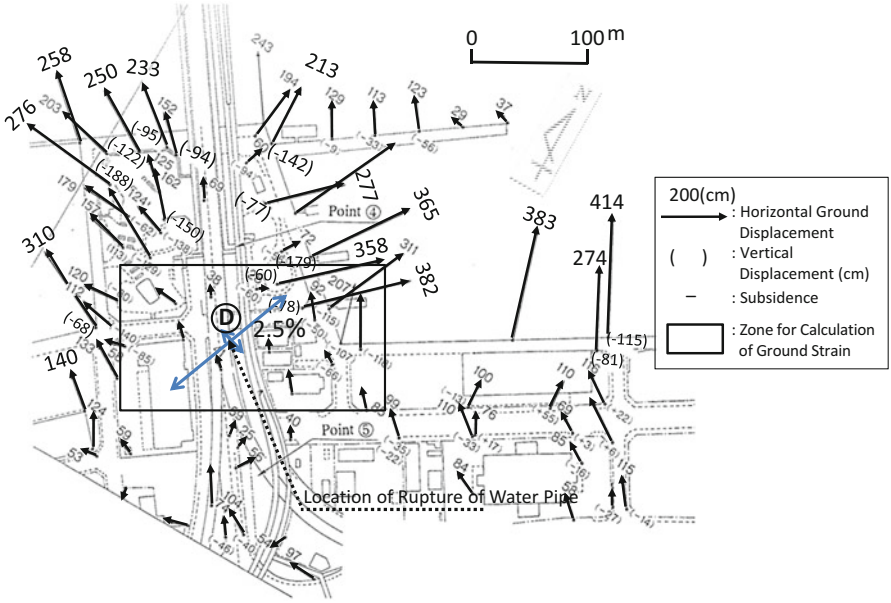

Fig. 4.39 Liquefaction-induced ground displacements (1995 Kobe earthquake, at Port Island)

wall was much greater than that further from the wall, which means that the land expanded. The tensile strain caused by land expansion and large ground surface subsidence ruptured the pipeline valve, resulting in the gas leakage.

Figure 4.39 shows horizontal and vertical ground displacements in a park in northern part of the Island. The park is surrounded by the sea on three sides, and the ground expanded seaward in three directions. Maximum horizontal ground displacement in this area reached more than 4 m. Point D in Fig. 4.39 indicates where a buried pipe of a water trunk line was ruptured. The pipe was broken and separated at the welded joint, as shown in Fig. 4.40. From measured displacements, ground strain was estimated to be tensile with magnitude 2.5 %.

Liquefaction-induced large ground displacements severely damaged structures and facilities of lifeline systems, such as wastewater treatment plants. The Eastern Nada wastewater treatment plant in Kobe was constructed on reclaimed land in front of a small canal, and its quay wall moved substantially toward the canal. Figure 4.41 shows the horizontal displacements of the ground and quay wall. The quay wall displaced a maximum of about 3 m and the whole area of the plant also moved toward the canal. As shown in Fig. 4.42a, foundation piles of the administration building were broken, and the foundation of a pedestrian bridge over the canal moved significantly and inclined (Fig. 4.42b).

Fig. 4.40 Rupture of buried pipe of water trunk line by liquefaction-induced ground displacements (1995 Kobe earthquake, Port Island)

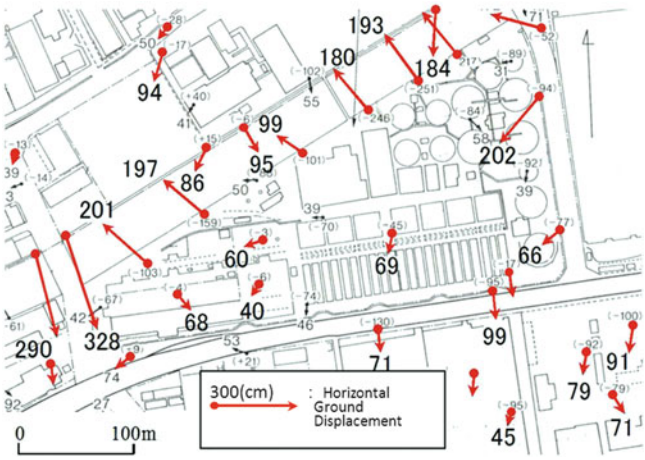

Fig. 4.41 Liquefaction-induced ground displacements (1995 Kobe earthquake, at the Eastern Nada waste water treatment plant)

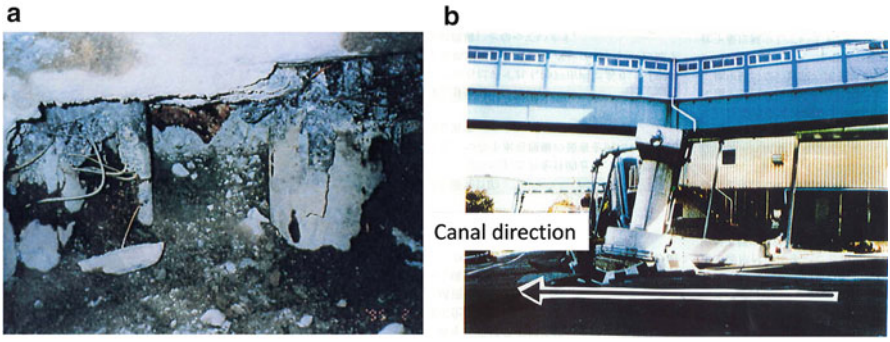

Fig. 4.42 Rupture of foundation piles and movement of foundation of a pedestrian bridge by liquefaction-induced ground displacements. (**a**) Rupture of foundation piles. (**b**) Movement of foundation of a pedestrian bridge (the foundation moved towards the canal)

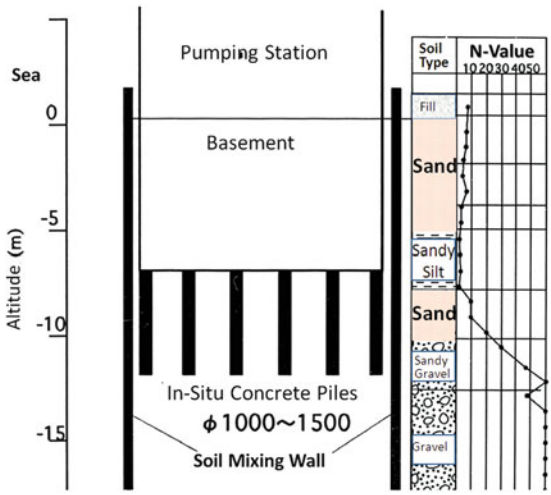

Fig. 4.43 Foundation of a pumping station building

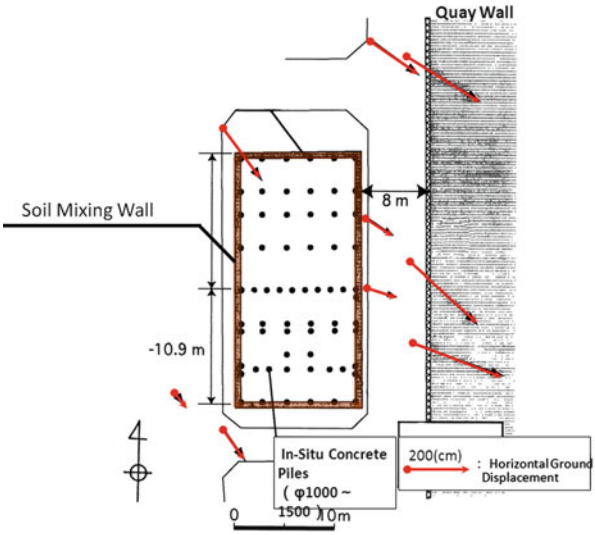

Fig. 4.44 Liquefaction-induced ground displacements around the pumping station (1995 Kobe earthquake)

Nevertheless, there were examples of non-damaged structures against the liquefaction-induced ground displacements. Figures 4.43 and 4.44 show such an example, a sewage pumping station. This building had three characteristics that prevented damage from ground displacements caused by soil liquefaction. One is that the building had a basement; the second is that the retaining wall, made by the soil mixing method for basement excavation, remained after building construction; the third is that the building had in situ concrete piles driven into firm ground.

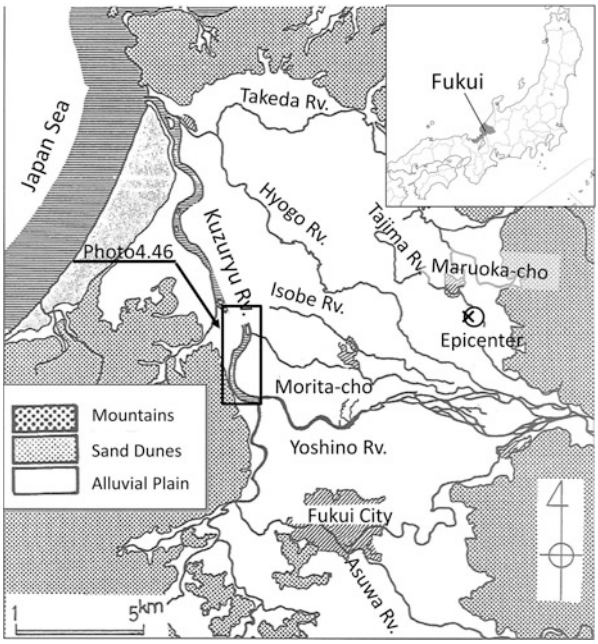

Fig. 4.45 Epicenter of 1948 Fukui earthquake and geological condition of Fukui plain

4.1.5 1948 Fukui Earthquake [17]

There was widespread liquefaction in the 1948 Fukui earthquake, particularly on the alluvial plain along the Kuzuryu River in Fukui Prefecture. Destruction from the inland earthquake of moment magnitude Mw = 7.3 (7.1 on the Japan Meteorological Agency scale) was severe, with a death toll of 3,769; collapsed buildings numbered 36,184. Because it occurred so soon after the end of the Pacific War, there are few precise records of the earthquake and its damage. As indicated in Fig. 4.45, the epicenter was near the town of Maruoka on the Fukui Plain. The seismic intensity (JMA Intensity) was estimated at 6 over the entire plain. Figure 4.46, a photograph taken by the Allied Occupation Forces (GHQ), shows conditions along the Kuzuryu River just after the quake. The whitish parts of the photo, which represent the riverbed and lowlands along the river, reveal sand boils due to liquefaction, indicating liquefaction over a broad expanse of the river alluvial plain.

Figure 4.47 shows liquefaction-induced ground displacements measured by aerial photos at Morita region. Scales of the GHQ-source photos taken before and after the earthquake are 1/12,000 and 1/5,400, respectively, with a horizontal measurement error less than ±87 cm. The Morita region is on the right bank of the Kuzuryu River. A small stream of the Yoshino River flowed parallel to that river, and had been a part of the Kuzuryu until the late nineteenth century. As shown in

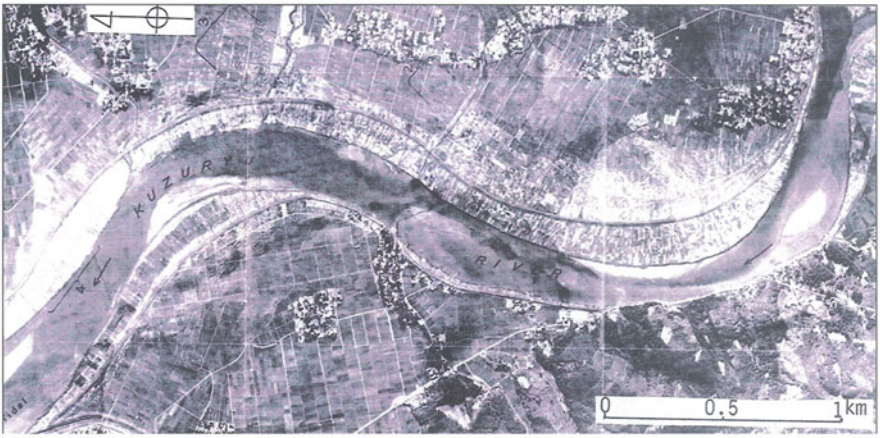

Fig. 4.46 Sand boils along the Kuzuryu River (1948 Fukui earthquake) (*white colored* area is surmised to have liquefied)

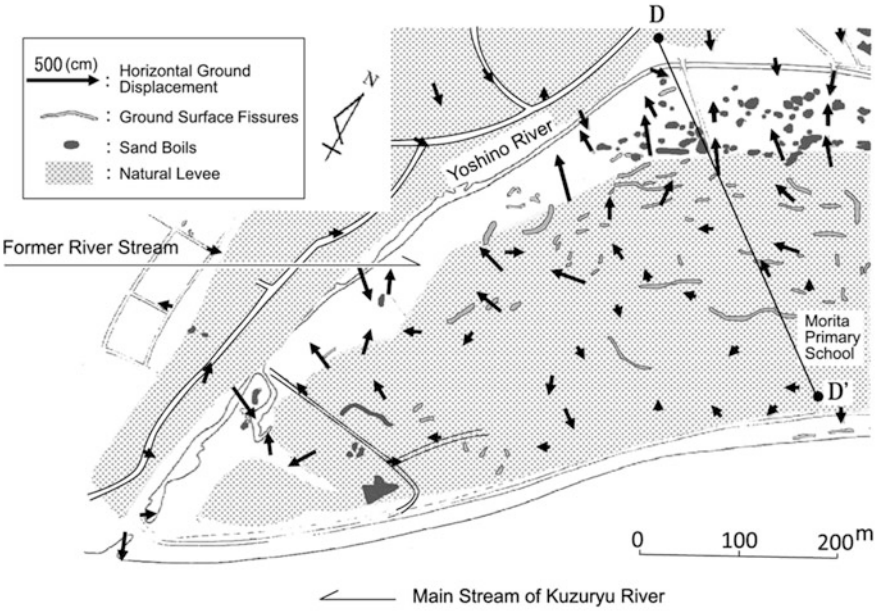

Fig. 4.47 Liquefaction-induced ground displacements (1948 Fukui earthquake, at Morita along Yoshino river)

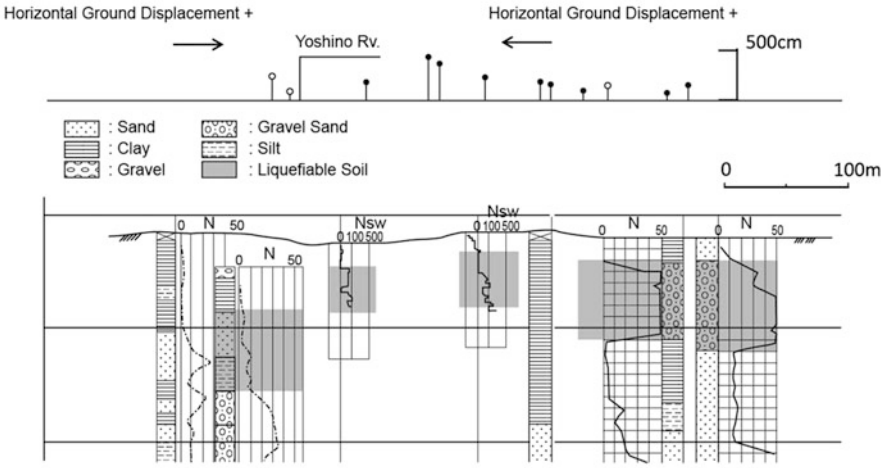

Fig. 4.48 Soil condition along Yoshino River and estimation of liquefaction (D–D' Section in Fig. 4.47)

Fig. 4.47, natural levees formed on both sides of the Yoshino River, with villages established at higher elevations. Between the natural levees and the Yoshino was a former river stream at lower elevation (white part in the figure). The ground displaced from natural levees of higher elevation to the river stream of lower elevation. However, displacement from the levees toward the Kuzuryu River was relatively slight. Morita Primary School was on a natural levee at several meters of elevation, and the ground displaced downward. Many fissures appeared on the levee, with sand boils near the old river stream. According to accounts from local residents, both banks of the Yoshino River moved toward the river center, and the stream narrowed.

Figure 4.48 shows the soil condition and estimation of liquefaction along the Section D–D' in Fig. 4.47. The ground consists of alternate layers of sand, gravel and clay. Liquefaction potential was estimated using results from the standard penetration test and Swedish cone penetration test. It was found that there was liquefiable soil with maximum thickness of 7 m from the natural levee to the old river stream.

4.1.6 1993 Southwest Hokkaido Offshore Earthquake

On July 12, 1993, an earthquake struck a broad area along the coast of Oshima Peninsula in southwest Hokkaido. The moment magnitude was measured at Mw = 7.8 (7.7 on JMA scale). Soil liquefaction occurred over a wide area of southwest Hokkaido. There was especially extensive liquefaction in the lowlands along the Shiribeshi-Toshibetsu River, which flow into the Japan Sea and is close to the epicenter. Ground fissures and sand boils were also sporadically observed along the river.

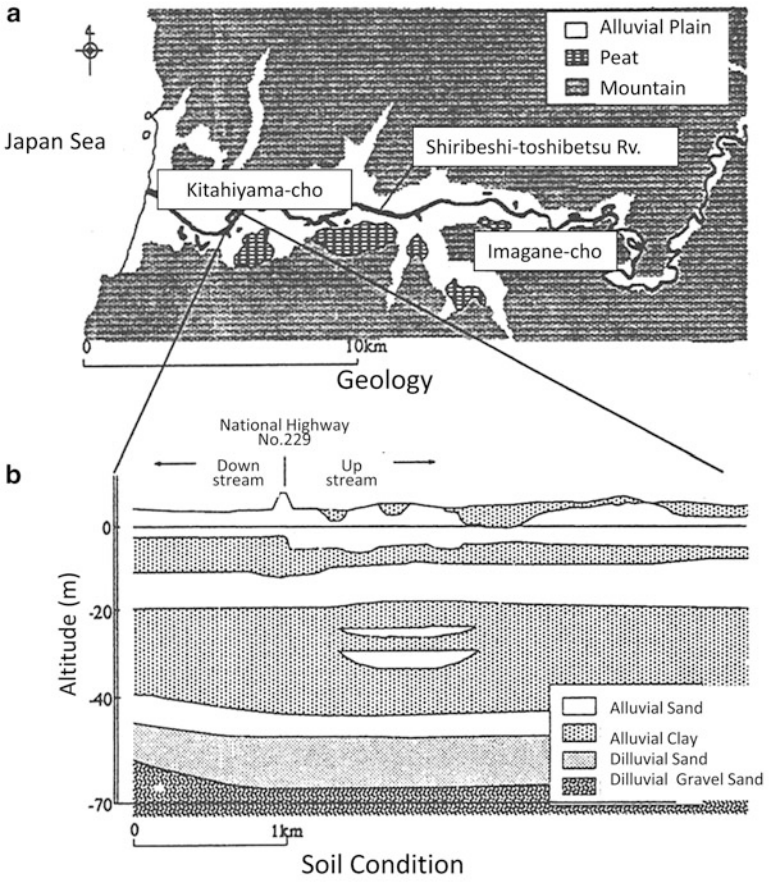

Fig. 4.49 Soil condition and geology along Shiribeshi-toshibetsu River

Seismic intensity along the river was reported at 5 (JMAI). Ground accelerations were not recorded there, but based on acceleration records in the surrounding area, maximum acceleration at the ground surface was estimated at approximately 200–400 cm/s^2.

Figure 4.49 shows that the river originates on the watershed divide between the Japan Sea and Pacific Ocean. The river flows for some 80 km until it passes through the towns of Imagane and Kitahiyama, before emptying into the Japan Sea. As a result of river improvement works during the Meiji Period, the stream now follows a mostly straight course from its middle reaches in Imagane. Because of repeated flooding, the river meanders considerably, as evidenced by its many oxbow lakes and streamlets. Such geological factors were influential in both soil liquefaction and resulting ground displacement.

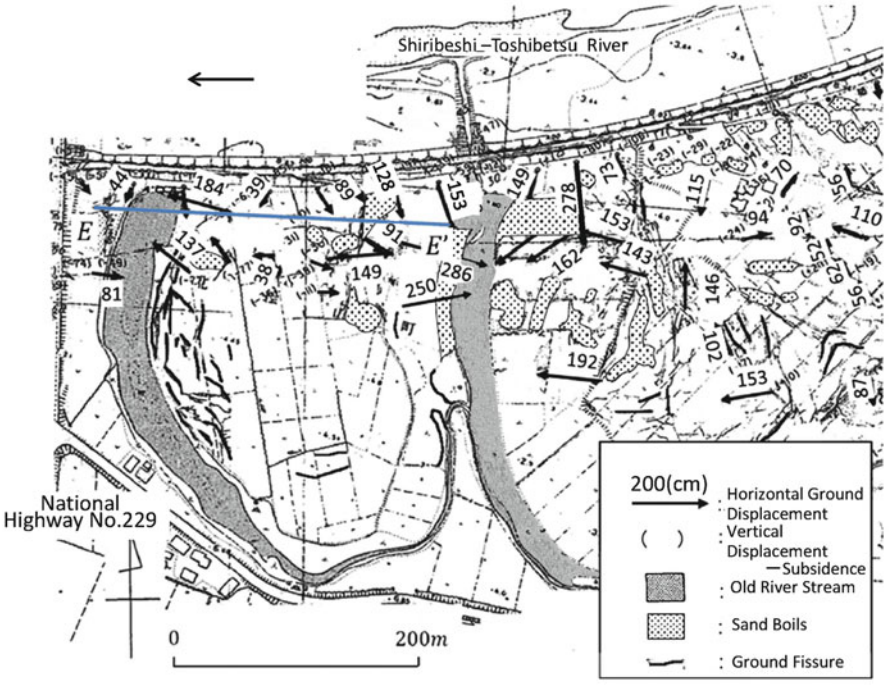

Fig. 4.50 Liquefaction-induced ground displacements, ground fissures and sand boils (1993 Southwest Hokkaido offshore earthquake, along Shiribeshi-Toshibetsu River)

Using aerial photos taken before and after the earthquake (scales 1/4,000 and 1/2,000, respectively), horizontal and vertical ground displacements were measured. Measurement errors are estimated as less than ±22 cm horizontally, and ±20 cm vertically. Figure 4.50 shows ground displacements in the Aichi region on the left bank of the river, approximately 4 km upstream from its mouth. Figure 4.51 is an aerial photo of the area. Ground displacements in the zone surrounded by the solid line in the figure. were measured. The maximum ground displacement was about 3 m, in the direction of low-lying old river streams. Ground fissures were observed mostly along these old streams, and sand boils spread over a large area. Ground displacements from the river embankment toward the south were also observed. These displacements may well have been caused by the sinking of the embankment due to liquefaction of the foundation ground.

The soil condition and estimation of liquefaction along the Section E–E' of Fig. 4.50 are shown in Fig. 4.52. The ground consists of an alluvial clay (AC-1, 2) and alluvial sands (AS-1, 2). According to *Specification of Highway Bridges* [4], under an assumption that the maximum acceleration at the ground surface was 200 cm/s^2, the saturated sandy soil with N value 10 or less to have undergone liquefaction. Thickness of the liquefied soil was about 7 m.

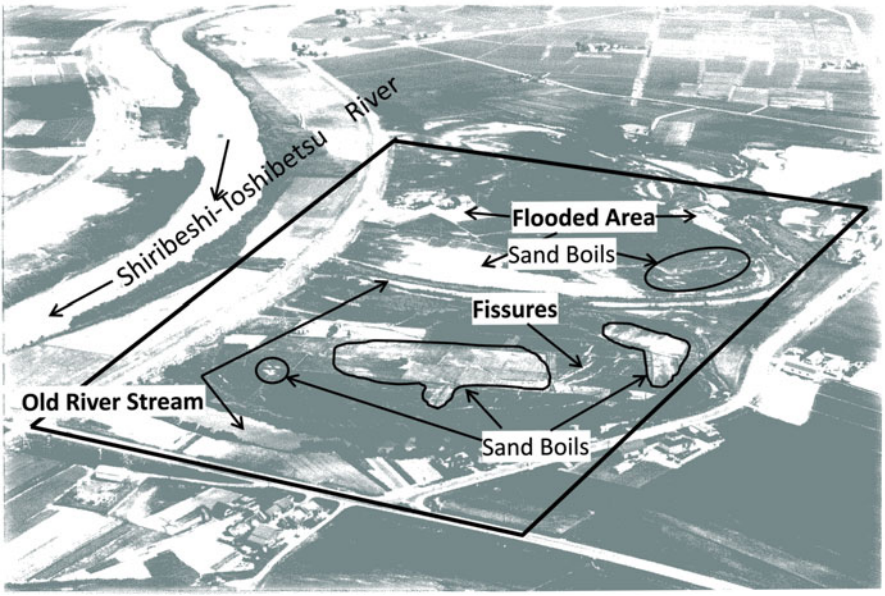

Fig. 4.51 Air photo of the Shiribeshi-Toshibetsu river after the earthquake (*open square box*-: zone of measurement of ground displacement)

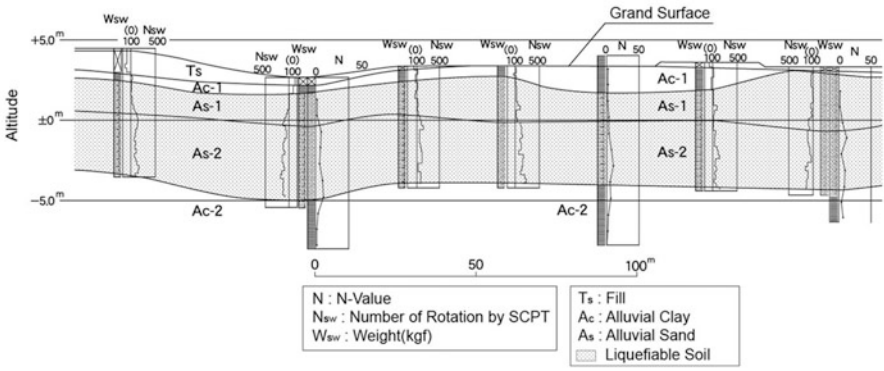

Fig. 4.52 Soil condition and estimation of liquefaction (E–E' Section in Fig. 4.50)

4.1.7 1923 Great Kanto Earthquake [18]

The 1923 Great Kanto earthquake marked the first major disaster to strike the capital region since the beginning of Japan's modern era. A survey on soil liquefaction and resulting ground displacement during the Kanto earthquake is of utmost importance for prevention of future disasters in highly urbanized metropolitan

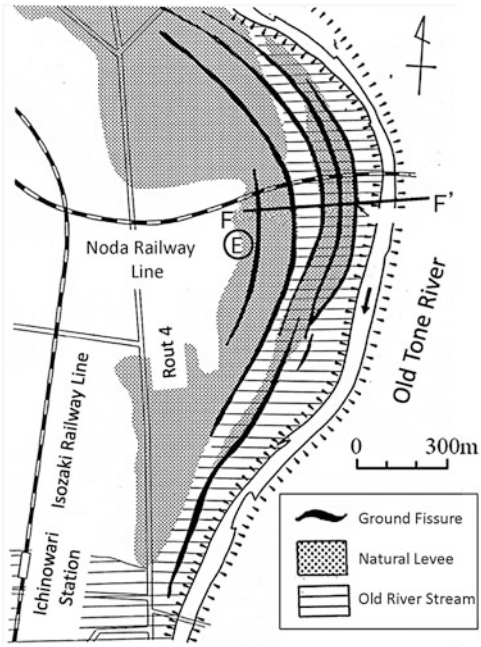

Fig. 4.53 Ground surface fissures along the Old Tone River (1923 Kanto earthquake at Kawakubo, after the report from Japan geological survey) [20]

areas. However, there was a lack of sufficiently accurate aerial photos, so the traces of soil liquefaction and ground displacement were surveyed by documents and interviews with those who experienced the earthquake. Documents [19] report numerous instances of sand and water boils, along with uplift of wooden piles above the ground surface. Based on the documents several locations of intense soil liquefaction were selected for a survey of ground displacement, and interviews with eyewitnesses were conducted. As a result, ground displacements of several meters were confirmed in Nishi-Kameari of Katsushika in Tokyo, Kawakubo in Kasukabo of Saitama Prefecture, and Nakajima in Chigasaki of Kanagawa Prefecture. The case of Kawakubo is described here.

The Kawakubo region is on the right bank of the upper reaches of the old Tone River. The old Tone River was the main stream of greater Tone River until some 370 years ago. Natural levees form a belt along the former riverbed. According to a survey by the Japan Geological Survey, there were numerous parallel ground fissures extending more than 2 km along the old Tone River, as shown in Fig. 4.53, with water and sand boils. The sand boils were particularly severe in the Kawakubo region, which was flooded to 15 cm depth by boiled water. Along the micro-topographic boundary between the natural levees and old riverbed, fissures ran roughly parallel to the old Tone River, with 0.6–0.9 m widths and 1.2 m vertical gaps. According to local residents, houses built over these fissures were pulled apart and collapsed, while the embankment sank and expanded toward the river. Furthermore, as shown in Fig. 4.54, at point E of Fig. 4.53, roadside hedges with a length of

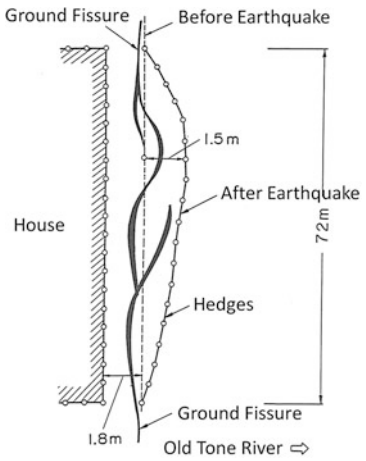

Fig. 4.54 Horizontal movement of hedges along a road [19]

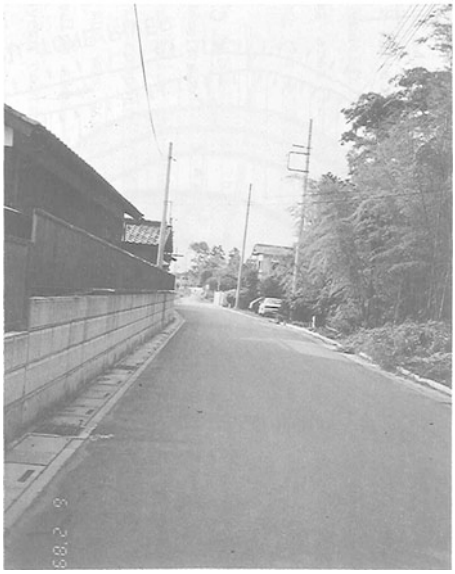

Fig. 4.55 Curved road due to the liquefaction-induced ground displacement (1923 Kanto earthquake at Kawakubo)

72 m displaced a maximum of 1.5 m eastward, toward the old Tone River. A survey by the author confirmed that as seen in Fig. 4.55, the road remains curved. Following the F–F' section of Fig. 4.53, Fig. 4.56 shows the soil condition and estimation of liquefaction under an assumption that ground surface acceleration was 200 cm/s^2. The present ground surface is 5–7 m above sea level and the mean gradient of the ground surface is 0.7 % toward the Old Tone River. The ground under the riverbank consists of a sand deposit, mostly with fine and medium grain-size sand of 5 m thickness. Maximum thickness of the liquefied soil where there were fissures and

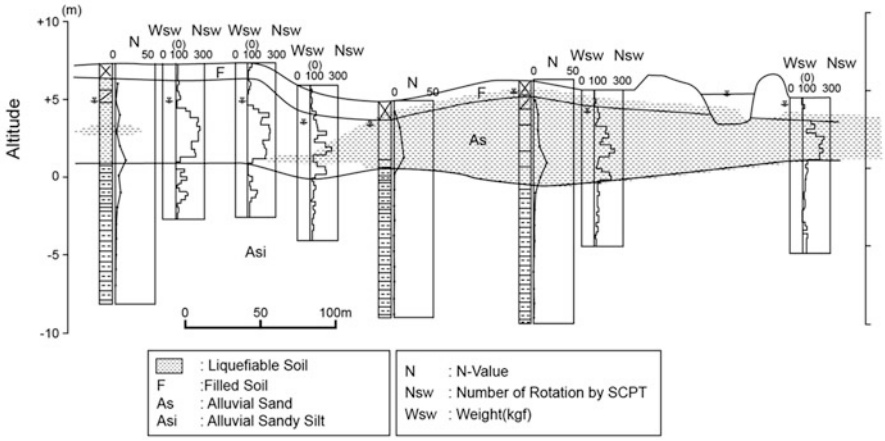

Fig. 4.56 Soil condition and estimation of liquefaction (along F–F' Section in Fig. 4.52)

displaced hedges was estimated at approximately 6 m. The upper part of the liquefiable soil and groundwater level inclined slightly toward the river.

4.1.8 1971 San Fernando Earthquake [20, 21]

The San Fernando earthquake occurred on February 9, 1971, with an epicenter 13 km north-northwest of San Fernando, California. The moment magnitude was Mw = 6.6, and hypocentral depth was estimated at 8–9 km. The quake triggered soil liquefaction, primarily in the city of San Fernando, severely disrupting lifeline systems and having long-lasting deleterious effects on municipal functions.

In the Upper Van Norman Lake region, 10 km west of the city, extensive soil liquefaction and its caused ground displacements were observed. Figure 4.57 shows horizontal and vertical displacements near the lake. Measurement errors by aerial photos are estimated at less than ±47 and ±42 cm in the horizontal and vertical directions, respectively. According to the measurements, there was maximum horizontal displacement 2.3 m southward between the Golden State Freeway and San Fernando Road, toward the lake. There was further horizontal displacement in excess of 2 m near Juvenile Hall, north of San Fernando Road. Based on standard penetration and Swedish cone penetration tests, ground conditions were surveyed. The topographic and ground conditions following the Section G–G' of Fig. 4.57 are shown in Fig. 4.58. It is seen that the gradient of the ground surface is about 1 % from Juvenile Hall toward the lake. The ground consisted of loose alluvial sand, and was estimated to have liquefied, resulting in downward displacement, following the slope.

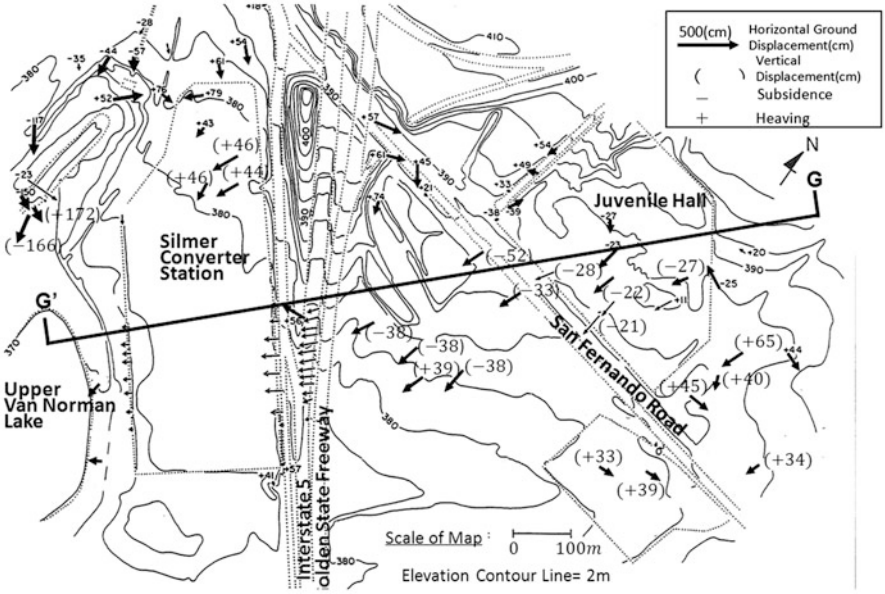

Fig. 4.57 Liquefaction-induced ground displacements (1971 San Fernando earthquake, Van Norman Lake's area [20])

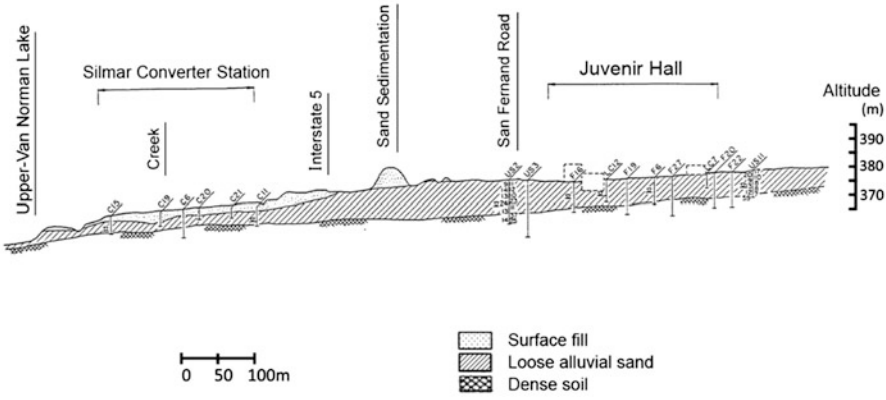

Fig. 4.58 Soil condition and estimation of liquefiable soil (along G–G' Section in Fig. 4.56, [20])

4.1.9 1990 Luzon Island Earthquake

An earthquake occurred on July 16, 1990 in the central mountainous region of northern Luzon Island. The moment magnitude (Mw) is estimated to have been 7.6, with a hypocentral depth of 25 km. The peripheral area of Lingayen Gulf,

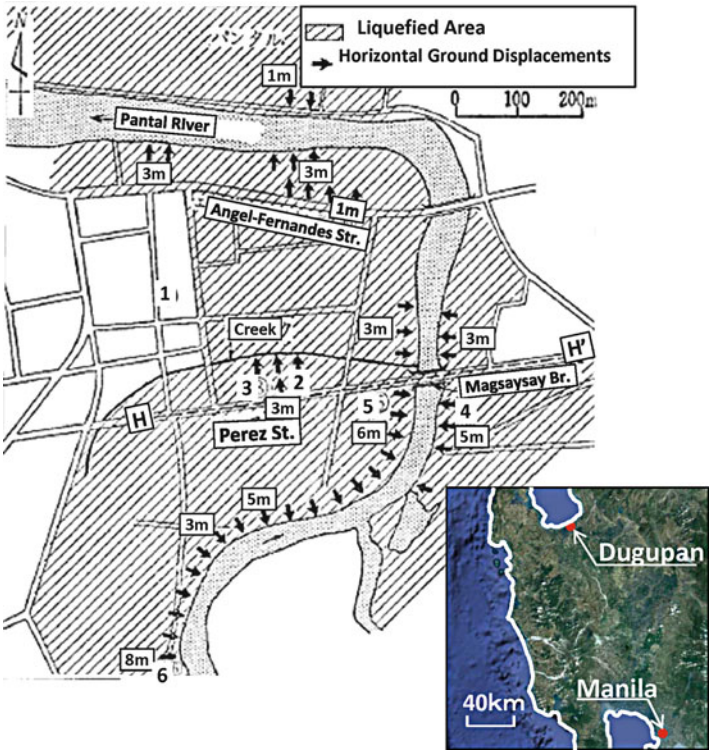

Fig. 4.59 Area of liquefaction and ground displacements (1990 Luzon Island earthquake, Philippine, at Dugupan) (Photo from Google earth)

some 60 km from the epicenter, and the city of Dagupan in particular, suffered damage caused by soil liquefaction and ground displacements. Figure 4.59 indicates the liquefied area, together with estimated ground displacements. A large area of the alluvial sandy ground along the Pantal River liquefied, and displaced toward the water. The horizontal ground displacements shown in the figure were estimated from offset deformations of the straight road and jutting displacement of riverbank revetments. Along the Pantal River, average displacement was estimated at 3–6 m, with a maximum of 8 m. Figure 4.60a shows a building along the riverbank, displaced toward the water. Figure 4.60b shows the collapsed Magsaysay Bridge across the river, the principal cause of which is the liquefaction of the riverbed and the ground displacements. Figure 4.61 shows the soil condition and estimation of liquefaction along the Section H–H' in Fig. 4.59. Nearly 10 m of alluvial sandy soil sediment spread widely along the river, with an N value about 10. The underground water level was shallow, about 2 m. This alluvial sand liquefied and caused ground displacements toward the river.

Fig. 4.60 Liquefaction-induced ground displacements (1990 Luzon Island earthquake, Phillipines, at Dugupan). (**a**) Movement of a building towards the river. (**b**) Collapse of the Magsaysay bridge

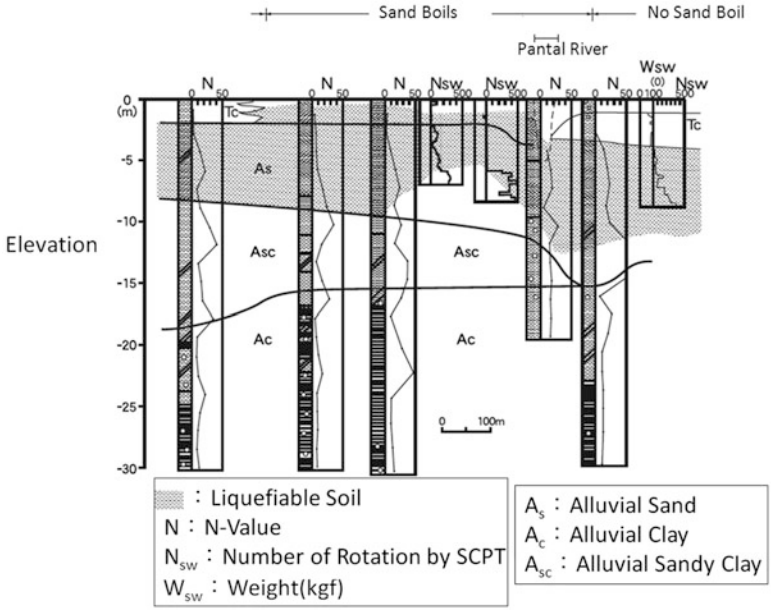

Fig. 4.61 Soil condition and estimation of liquefaction (along H–H' Section in Fig. 4.58)

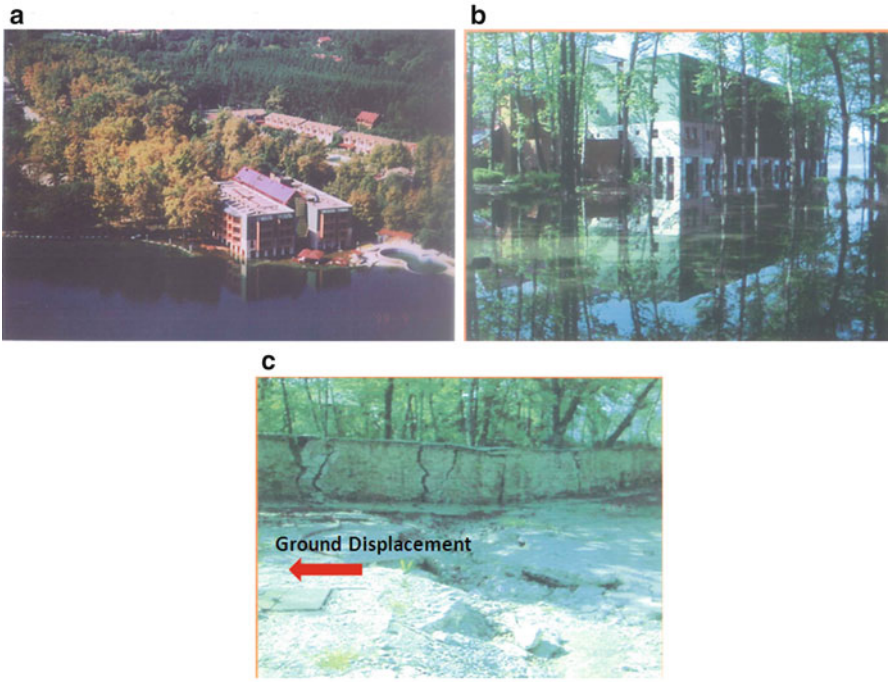

Fig. 4.62 Movement of a hotel building and ground surface fissures (1999 Kocaeri earthquake, Turkey, at Sapancha lake). (**a**) A hotel building moved toward the lake. (**b**) Flood around the hotel. (**c**) Fissure due to ground displacement

4.1.10 1999 Kocaeli Earthquake, Turkey

The Kocaeli earthquake, with moment magnitude Mw = 7.6, struck the province of Kocaeli in the Marmara region of western Turkey, on August 17, 1999 (Sect. 1.2.1). The quake killed more than 15,500 people and caused considerable damage, including destruction of over 170,000 buildings. In this disaster, both soil liquefaction and ground displacements were observed over a large area from Izmit to the city of Adapazari, especially in the coastal area of Sapanca Lake, some 20 km west of the epicenter. Figure 4.62a, b show a lakeside hotel building that was displaced toward the lake and inclined, with the first floor flooded. As seen in Fig. 4.62c, there were many fissures at the surface caused by ground displacement.

Figure 4.63 shows horizontal ground displacements in the area, measured by aerial photos before and after the earthquake. Measurement error is estimated at less than 50–60 cm in the horizontal direction. In the hotel area, maximum horizontal displacement was approximately 3 m.

Figure 4.64 shows the soil condition and estimation of soil liquefaction. The ground consists of surface fill, humus soil, gravel with fine fraction, sand and silt.

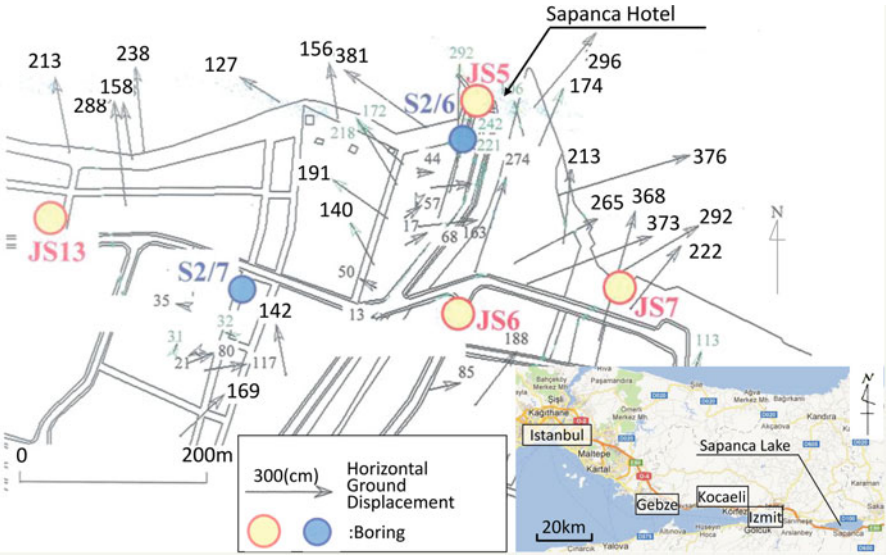

Fig. 4.63 Liquefaction-induced ground displacements around the Sapanca Lake (1999 Kocaeli earthquake, Turkey, unit: cm)

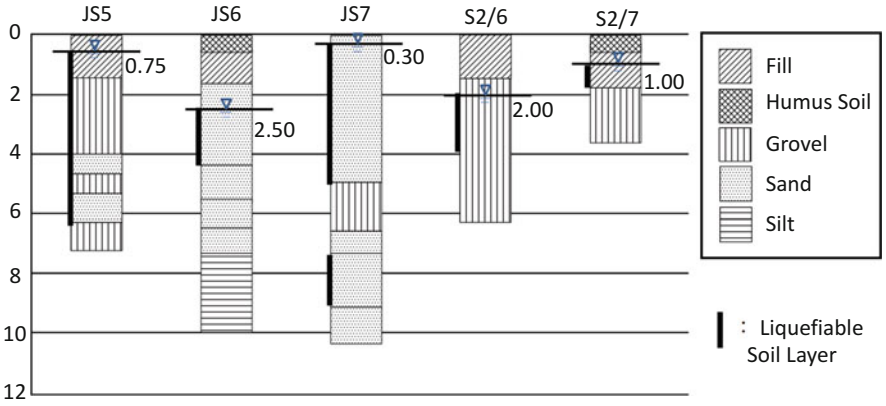

Fig. 4.64 Soil condition around Sapanca lake and estimation of liquefaction (boring points in Fig. 4.39)

At points JS5 and S2/6, where the surface ground consists of gravel, sand and fine fraction, the sand and gravel boils and surface fissures suggests that liquefaction have occurred in this area. There is no record of earthquake ground motion near the lake but in Adapazari, 20 km to the west, maximum acceleration

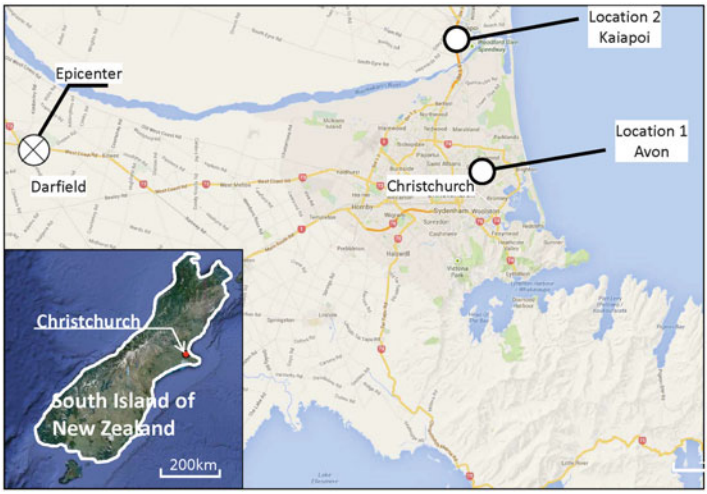

Fig. 4.65 Areas for study on liquefaction and its induced ground displacements (2010 Darfield earthquake, New Zealand) (photo from Google earth)

at the ground surface was 399 cm/s^2 (Fig. 1.10). The thickness of liquefiable soil was estimated about 6 m, under an assumption that ground surface acceleration was 200 cm/s^2.

4.1.11 2010 Darfield Earthquake, New Zealand

An earthquake of moment magnitude Mw = 7.1 struck the city of Christchurch on the South Island of New Zealand on September 4, 2010, with an epicenter some 50 km west in Darfield. The earthquake triggered extensive soil liquefaction and ground displacements in residential suburbs of the city, causing severe damage to houses and lifeline systems, including water and sewage services. Ground displacements were measured by aerial photos before and after the earthquake in two Christchurch suburbs, Avon and Kaiapoi (Fig. 4.65). As indicated in Fig. 4.66, a number of houses suffered from liquefaction-induced ground displacements, and ground fissures and pavement buckling were observed.

In Avon, the Avon River meandered considerably (Fig. 4.67a). Maximum ground surface displacement reached over 2 m. The river's meandering has resulted in loose, sandy soil sedimentation. Figure 4.67b shows surface ground displacement in Kaiapoi. The area was developed by reclamation from swampland, but some water areas were remained. The ground displaced 3.2 m at maximum toward the water area.

Fig. 4.66 Damage to house, ground fissure and buckling of pavement (2010 Darfield earthquake, New Zealand). (**a**) A House damaged by ground displacement. (**b**) Ground fissure and sand boil. (**c**) Buckling of pavement

4.1.12 Joint U.S.–Japan Research on Liquefaction-Induced Ground Displacement and Resulting Damage

As explained at the beginning of this chapter, Japanese research on liquefaction-induced ground displacement and resulting damage to structures began at the same time as studies in the U.S. concerning liquefaction and ground displacement of reclaimed lands during the 1906 San Francisco earthquake. This led to U.S.–Japan joint research on the mechanism of large ground displacements and countermeasures for structures. Eight U.S.–Japan workshops, entitled "Earthquake Resistant Design of Lifeline Facilities and Countermeasures against Liquefaction" have been held to exchange research findings and discuss the direction of the joint research. The first was in Tokyo in 1988, and was followed by workshops in Buffalo, San Francisco, Honolulu, Snowbird (Utah), Tokyo, Seattle, and Tokyo again (Fig. 4.68) [22].

A broad range of topics have been discussed in these workshops: reinforcement of underground lifeline facilities for resistance to liquefaction and ground displacement, development of liquefaction hazard maps, evaluation of lifeline system resistance to earthquakes, evaluation of liquefaction potential via laboratory tests and on-site surveys, and earthquake resistance of pile foundations with respect to soil liquefaction and ground displacements. Findings have been published in the U.S. by the National Center for Earthquake Engineering Research (NCEER) and the

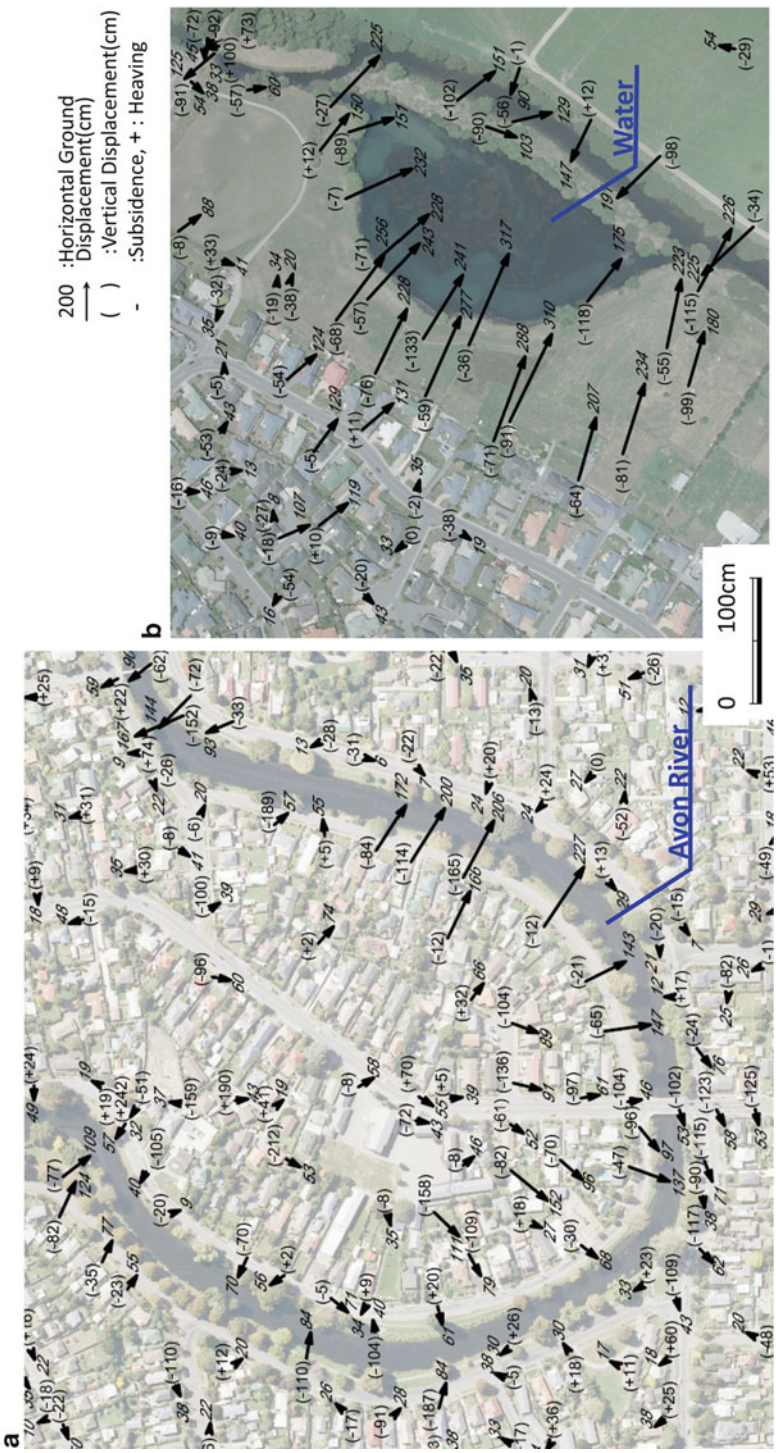

Fig. 4.67 Liquefaction-induced ground displacements (2010 Darfield earthquake, New Zealand). (**a**) Avon area. (**b**) Kaiapoi area

Fig. 4.68 The 8th U.S.-Japan workshop on countermeasures of lifelines against liquefaction

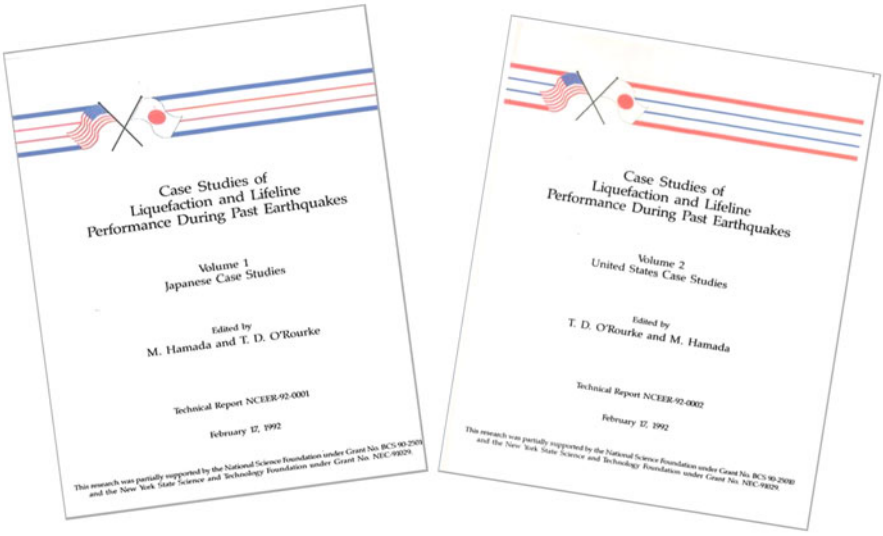

Fig. 4.69 U.S.-Japan Joint Case Studies on Liquefaction, Ground Displacements, and their caused damage to lifelines

Multi-disciplinary Center for Earthquake Engineering Research (MCEER). These workshops provided an opportunity for joint U.S.–Japan experiment, as well as for case studies concerning displacement measurement, as discussed in Sect. 4.1.

Figure 4.69 shows two publications from this joint research: *Case Studies on Liquefaction and Lifeline Performance During Past Earthquakes*, Volume 1:

Japanese Case Studies [2, 5, 16, 18]; and Volume 2: United States Case Studies [20, 23]. The subjects of the Japanese case studies were the 1923 Great Kanto earthquake, the 1948 Fukui earthquake, the 1964 Niigata earthquake, the 1983 Central Japan Sea earthquake, and the 1990 Luzon earthquake. The subjects of the U.S. case studies were the 1906 San Francisco earthquake, the 1964 Alaska earthquake, the 1971 San Fernando earthquake, the Southern California Imperial Valley earthquakes in 1979, 1981 and 1987, and the 1989 Loma Prieta earthquake.

4.2 Mechanism of Liquefaction-Induced Large Ground Displacement

4.2.1 Mechanism of Liquefaction Ground Flow

Liquefaction-induced ground displacements can be classified into two types, as shown in Fig. 4.70. Type 1 ground displacement was observed in Noshiro during the 1983 Central Japan Sea earthquake, where the ground surface was gently sloped and the ground displaced downslope. Type 2 displacements were observed along the Shinano River in Niigata during the 1964 earthquake and in reclaimed islands during the 1995 Kobe earthquake. The ground behind the quay walls displaced toward the river or sea, triggered by large movements of riverbanks and quay walls. In both types 1 and 2, gravity of the liquefied soil was considered as the cause of displacements.

There are three hypotheses for the mechanism of large horizontal ground displacement of several meters, as follows. The first is that under a large decrease of soil stiffness, the ground displaces owing to gravity. The second hypothesis is that large ground displacements are caused by the liquid behavior of liquefied soil. The

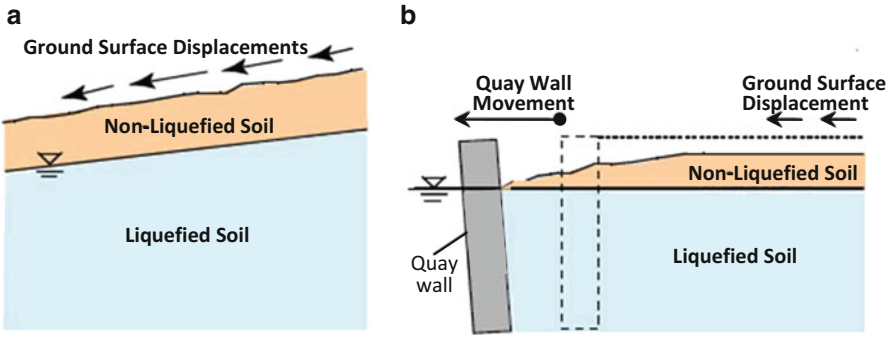

Fig. 4.70 Two types of liquefaction-induced ground displacements. (**a**) Type 1: ground displacement due to inclination of ground surface. (**b**) Type 2: ground displacement due to quay wall movement

third is that the ground slides substantially on a water film that forms at the boundary between permeable and impermeable soil layers, after soil liquefaction.

In the first hypothesis, it is necessary but difficult to estimate the large decrease in soil stiffness due to liquefaction, because liquefied ground is treated as a solid body. In the second concept, properties of liquefied soil must be evaluated as a liquid. Experimental results show that liquefied soil behaves as pseudo-plastic fluid, but there remain many issues to be resolved for using this method in engineering practice. The third hypothesis cannot explain all cases of large ground displacements because, in most cases, the ground was deformed along the entire depth and not at a specific elevation. This was revealed from analysis of damaged foundation piles during earthquakes, such as that mentioned in Sect. 4.1.3 (Fig. 4.27).

To elucidate the mechanism of large ground displacements due to soil liquefaction is essential for reliable assessment of ground displacements during future earthquakes. However, the examples mentioned in Sect. 4.1 show that in some cases, there were large differences among displacement magnitudes at nearby observation points. This variation results from the unstable liquid behavior of liquefied soil. Attention should be paid to this for the assessment of liquefaction-induced ground displacement. This is common to all methods based on the three hypotheses above.

4.2.2 Assessment of Type 1 Ground Displacement (on Sloped Ground Surface)

Estimation of the magnitude of liquefaction-induced ground displacements is important for the design of structure foundations and buried pipes. The author proposed Eq. (4.1) for estimation of ground displacements, based on correlation analysis between measured displacements and various influential factors such as ground surface gradient and liquefiable soil thickness. Displacement data used were from the 1983 Central Japan Sea and 1964 Niigata earthquakes.

$$D = 0.75 \cdot \sqrt{H} \cdot \sqrt[3]{\theta} \tag{4.1}$$

Here,

D: horizontal ground displacement on the surface (m)
H: thickness of liquefiable soil (m)
θ: the larger gradient value between ground surface and lower boundary plane of liquefied soil (%)

Figure 4.71 shows a comparison between observed ground displacements and those estimated by Eq. (4.1). The estimated values largely scatter between twice and one second of observed values. This scattering is reasonable, because liquefaction-induced ground displacements are caused by the liquid behavior of liquefied soil, as mentioned above. Furthermore, the following problems exist in

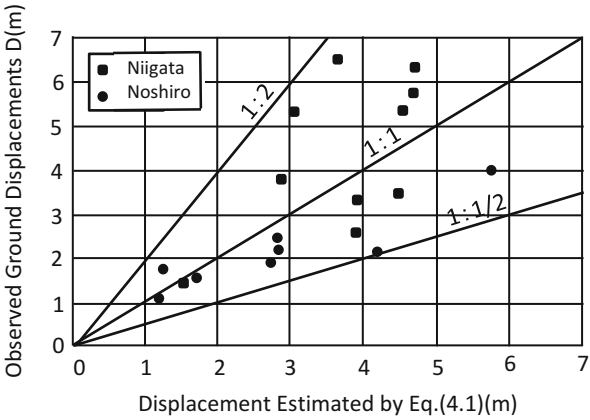

Fig. 4.71 Ground surface displacements by observation and Eq. (4.1) (type1)

Eq. (4.1). The first is that the magnitude of displacement D is proportional to the cubic root of gradient θ, which means that the effect of the gradient on ground displacements is very small. If liquefied soil flow is caused by gravity as mentioned previously, ground displacement should be proportional to the gradient.

The second problem of Eq. (4.1) is that ground displacement at the surface is proportional to the square root of the thickness of liquefied soil H. If ground displacements occur along the depth of liquefied soil under an assumption that the elastic or viscous properties are constant in the direction of the soil depth, displacement at the ground surface should be proportional to the square of H. The fact that the ground surface displacements are proportional to the square root of H suggests that properties of liquefied soil such as shear modulus or coefficient of viscosity change with soil depth.

To resolve these problems of this equation, the author conducted model tests on flow properties of liquefied soil, showing that its flow had two nonlinear characteristics. One is that liquefied soil behaves as a non-linear flow, wherein its coefficient of viscosity increases with ground thickness. Other characteristic is that the liquefied soil behaves as a pseudo-plastic flow, for which the coefficient of viscosity decreases with increased shear strain rate. These characteristic properties of liquefied soil are introduced in Sect. 4.2.4.

Based on the above experimental findings and case study results, the author proposes the following new equation for estimation of horizontal displacement at the ground surface:

$$D \doteq 1.5 \times 10^2 \cdot \frac{\sqrt{H} \cdot \theta}{N} \tag{4.2}$$

where:

D: horizontal ground displacement at the surface (m)
H: thickness of liquefiable soil (m)
θ: gradient of the ground surface (%)
N: mean N values of liquefiable soil

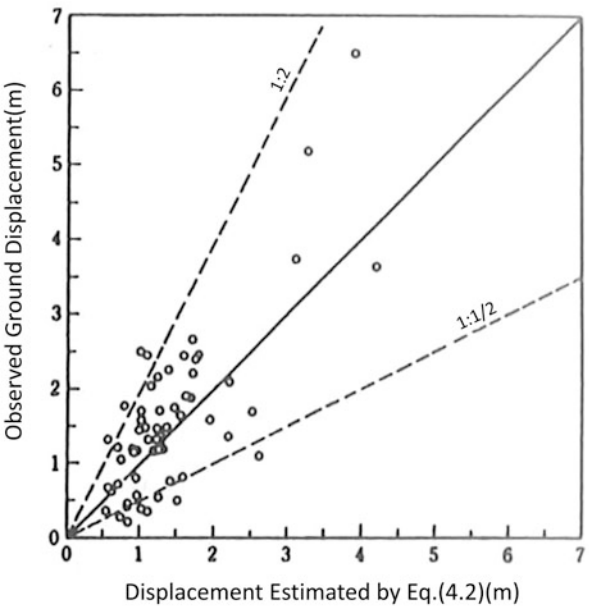

Fig. 4.72 Ground surface displacements by observation and Eq. (4.2) (type 1)

Figure 4.72 shows a comparison between observed ground displacements and those estimated by the newly proposed Eq. (4.2). The estimated values still scatter between twice and one second of the observed displacements. Estimation accuracy of Eq. (4.2) was not improved compared with Eq. (4.1). This again shows that liquefaction-induced ground displacements are caused by unstable liquid behavior of liquefied soil, and that there is a limitation to increasing estimation accuracy.

An estimation of type 1 horizontal ground displacements, based on correlation analysis and using data from Japanese and U.S. case studies, was proposed by Bartlet and Youd [23]:

$$\begin{aligned}\log(D_H + 0.01) = &-15.787 + 1.178M - 0.927\log R - 0.013R \\ &+0.429\log S + 0.348\log T_{15} + 4.527\log(100 - F_{15}) \\ &-0.922D50_{15}\end{aligned} \tag{4.3}$$

Here, D_H is horizontal displacement at the ground surface, M is earthquake moment magnitude, R is epicentral distance (km), S is ground surface gradient (%), T_{15} is total thickness of saturated soil with modified N value $(N_1)_{60}$ less than 15, F_{15} is fine fraction contents in T_{15} (%), and $D50_{15}$ is mean grain size in T_{15}.

Bartlet et al. also proposed the following equation for type 2 ground displacement [23]:

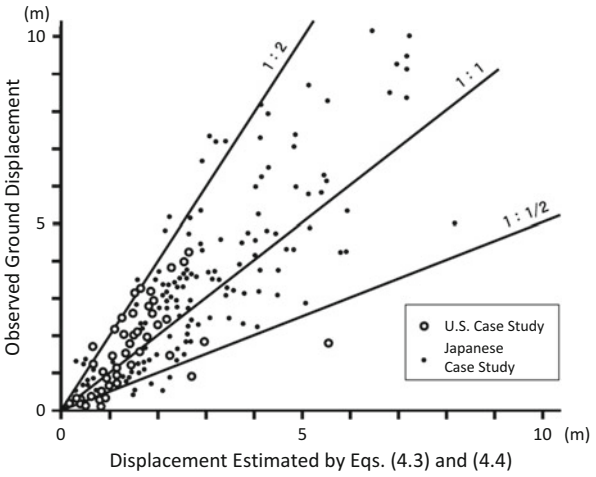

Fig. 4.73 Ground surface displacements by observation and Eqs. (4.3) and (4.4)

$$\begin{aligned}\log(D_H + 0.01) = &-16.366 + 1.178M - 0.927\log R - 0.013R \\ &+0.657\log W + 0.348\log T_{15} + 4.527\log(100 - F_{15}) \\ &-0.922D50_{15}\end{aligned} \quad (4.4)$$

Here, W is the ratio of horizontal distance between a quay wall and the point where ground displacement is estimated to the quay wall height, which indicates the mean gradient at the ground surface.

Figure 4.73 shows a comparison between estimated ground displacements using Eqs. (4.3), (4.4) and observed ones in Japan and the U.S. The estimated values also scatter between twice and one second of the observed ones.

4.2.3 Assessment of Type 2 Ground Displacement (Caused by Quay Wall Movement)

For assessment of liquefaction-induced ground displacements caused by movement of quay walls, Iai et al. proposed a method that has been used in the design of port and harbor structures and high-pressure gas facilities [24].

First, for estimation of horizontal displacement at the top of quay walls, the following was proposed:

$$\Delta = \frac{F_d}{100} \cdot H_W \quad (4.5)$$

Here, Δ is horizontal displacement at the top of the quay wall (m), H_W is quay wall height (m), and F_d is quay wall displacement rate, which is given in Table 4.2, depending on the type of quay wall and degree and extent of soil liquefaction.

Table 4.2 Displacement rate of Quay wall due to soil liquefaction (after Iai et al.)

Type of Quay wall	Ground motion	Soil condition		Displacement ratio Fd (%)
Gravity type	Level 1	Loose sand behind quay wall		5–10
		Loose sand behind quay wall and foundation ground		10–20
	Level 2	Loose sand behind quay wall		10–20
		Loose sand behind quay wall and foundation ground		20–40
Sheet piles type	Level 1	Loose sand behind quay wall	Firm ground around archorage	5–15
			Loose sand around archorage	15–25
		Loose sand behind quay wall, around aechorage and foundation ground		25–50
	Level 2	Loose sand behind quay wall	Firm ground around archorage	15–20
			Loose Sand around archorage	25–40
		Loose sand behind quay wall, around aechorage and foundation ground		50–75

Level 1 ground motion, and level 2 ground motion (see Sect. 2.3.2)

Horizontal ground displacements behind quay wall gradually decrease with the distance from the wall. The following equation is proposed:

$$D/\Delta = \exp(-3.35x/L) \tag{4.6}$$

Here, D is ground displacement at the surface (m), x is distance between the quay wall and point of assessment of ground displacement (m), and L is distance from the quay wall over which ground displacement is caused (m), assumed in practice as 100 m.

The author proposed the following equation for estimation of quay wall displacement rate in Eq. (4.5), based on case studies of quay wall displacements at the Port and Rokko Islands during the Kobe earthquake.

$$F_d = 0.014H + 0.057 \tag{4.7}$$

Here, H is total thickness of liquefied soil at the estimation location of ground displacement (m). The following equation was proposed for attenuation of ground displacements, depending on distance from the quay wall.

$$D/\Delta = \exp(-\alpha x) \quad (\alpha = -0.0007H + 0.0182) \tag{4.8}$$

Here, D is ground surface displacement at distance from the quay wall (m); α is a constant representing attenuation by distance, and is related to thickness of liquefied soil.

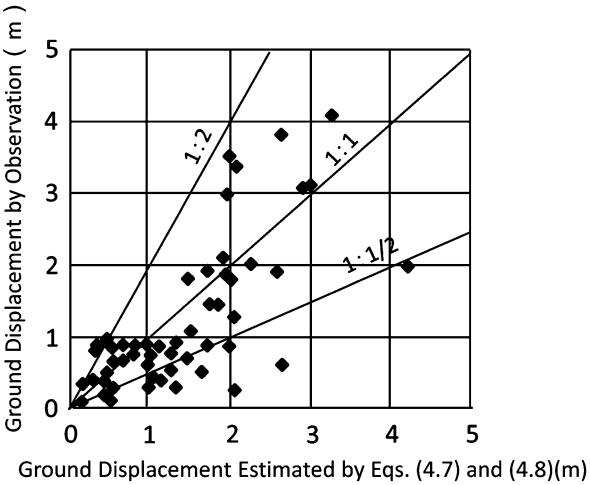

Fig. 4.74 Horizontal ground displacements by observation and Eqs. (4.7) and (4.8)

Figure 4.74 compares ground displacements estimated by Eqs. (4.7) and (4.8) and observed ones. In this case, the estimated displacements also show large scatter, again indicating the difficulty of estimating liquefaction-induced ground displacements with high accuracy.

4.2.4 Fluid Properties of Liquefied Soil [25–27]

The author supports the hypothesis that liquefaction-induced ground displacements are caused by the liquid behavior of liquefied soil. Evidence of this hypothesis is the damaged sewage pipes in Noshiro during the 1983 Central Japan Sea earthquake. Figure 4.75 shows horizontal ground surface displacements at the surface between two neighboring manholes (Fig. 4.75a) and displacement of sewage pipes (Fig. 4.75c). The latter displacements were measured as horizontal offsets from a straight line connecting the two manholes. Figure 4.75b indicates components of ground surface displacement perpendicular to the pipe axis. According to the results in Fig. 4.75b, displacements at the ground surface perpendicular to the pipe axis were 80–110 cm, whereas offset displacements of the sewage pipe were much larger, at 160 cm. This phenomenon can be more easily explained by examining Fig. 4.76, which shows mean displacement at the ground surface, mean displacement of two neighboring manholes, and maximum offset displacement of sewage pipes on a cross section. The figure also shows soil conditions and estimation of liquefaction. Absolute displacement of sewage pipes was 255 cm, as the sum of pipe offset displacement 160 cm and mean displacement of manholes 95 cm. However, average ground surface displacement was only 82 cm. Figure 4.76b shows that the estimated liquefied soil depth was between 1.8 and 4.2 m below

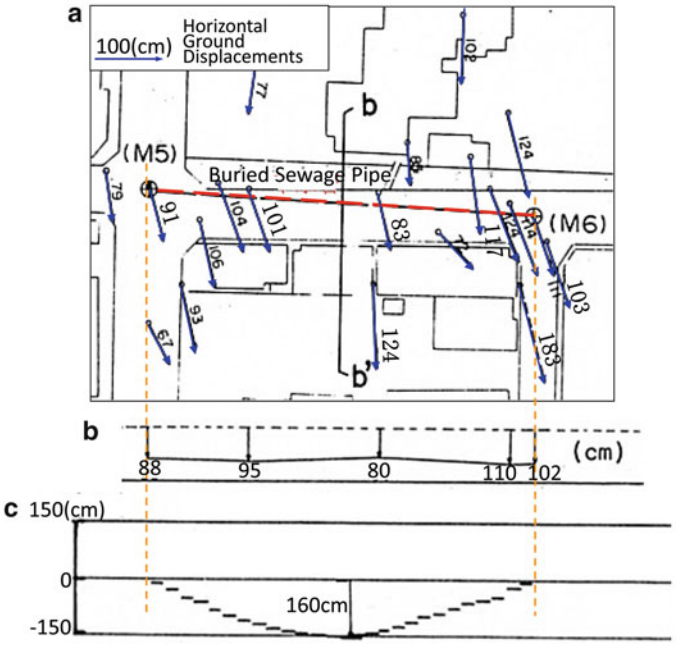

Fig. 4.75 Horizontal movement of buried sewage pipe and ground surface displacements (1983 Central Japan Sea earthquake). (**a**) Horizontal ground surface displacements nearby sewage pipe. (**b**) Horizontal ground surface displacements in the direction perpendicular to pipe's axis. (**c**) Horizontal displacement of the pipe (offset displacement from two manholes)

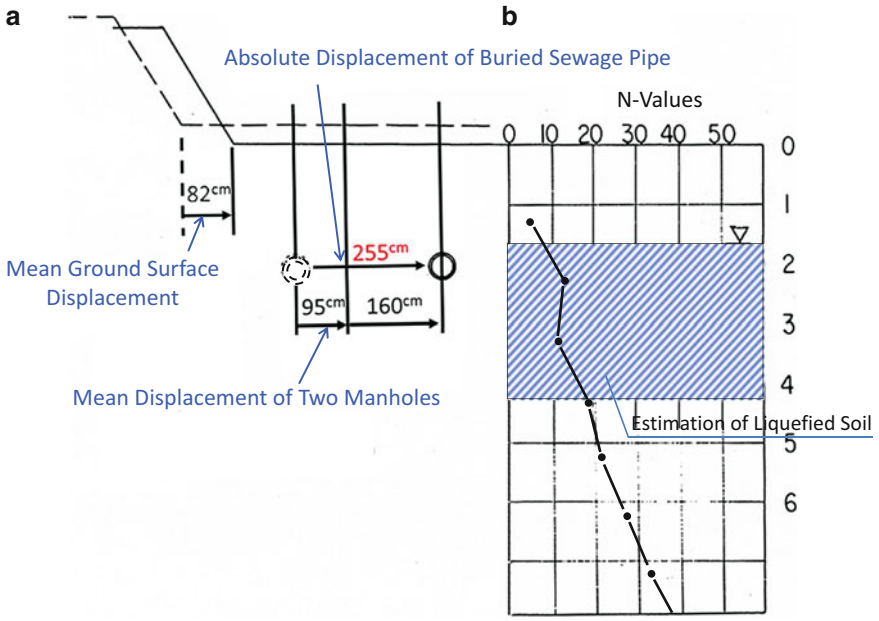

Fig. 4.76 Horizontal displacements at ground surface and of buried sewage pipe, and estimation of liquefied soil. (**a**) Displacements of ground surface and of buried sewage pipe. (**b**) Soil condition and estimation of liquefied soil

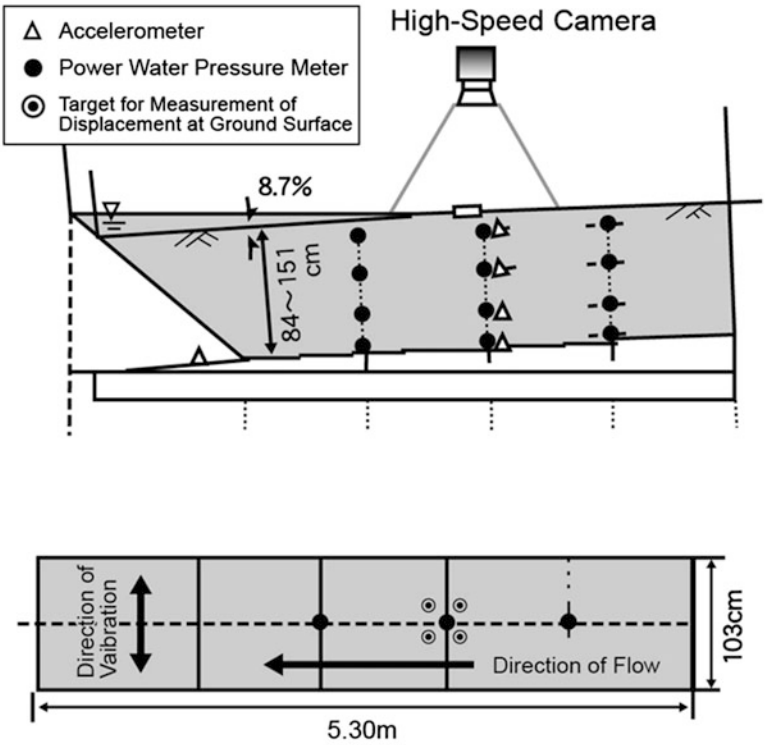

Fig. 4.77 Model ground for flow test of liquefied soil (under 1 g condition)

the ground surface. The sewage pipes were buried in this liquefied soil, and were greatly displaced by the liquefied soil flow.

During the 1964 Niigata earthquake, water pipes were found under roadside ditches. There was a high-pressure gas pipe buried on the left bank of the Shinano River, but it could not be found by excavation after the event. It is believed that the gas pipe was swept into the river by liquefied soil flow.

If liquefaction-induced large ground displacements are governed by the liquid behavior of liquefied soil, it is important to investigate its fluid properties. For this purpose, the author performed a flow test of liquefied soil under 1 g conditions using model ground of thickness and length 84–151 cm and 5.3 m, respectively (Fig. 4.77). The model ground consisted of a mixture of silica sands No. 5 and No. 6. Mean grain size, uniformity coefficient, and relative density were 0.4 mm, 2.5 and 33–35 %, respectively. The surface of the model ground was inclined 8.7 %. Liquefaction was caused by shaking at 600 cm/s^2 acceleration and 6.0 Hz frequency in a direction perpendicular to the surface inclination, and the ground moved downward.

Time histories of the horizontal ground surface displacements were measured by a high-speed camera, and ground surface flow velocity was calculated by differential calculus of time histories of the measured displacements. The velocity of

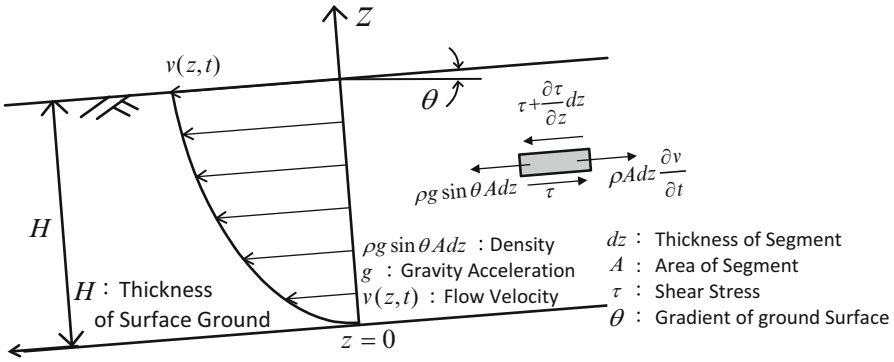

Fig. 4.78 One-dimensional viscous flow

Table 4.3 Cases of flow test of liquefied soil

Case	Thickness of model ground (cm)	Relative density (%)	Gradient of ground surface (%)	Input acceleration (cm/s2)	Input frequency (1/s)
A1	84	34	8.7	597	5
A2	100	33	8.7	590	5
A3	119	33	8.7	679	5
A4	151	35	8.7	619	5

one-dimensional viscous flow at the surface from a stationary condition can be obtained as follows, from the dynamic equilibrium of forces on a small segment of liquefied soil (Fig. 4.78):

$$V(t) = \sum_{i=1,3,\cdots}^{\infty} 16\frac{H^2}{(i\pi)^3}\frac{\rho g \sin\theta}{\mu} \times \left[1 - \exp\left\{-\left(\frac{i\pi}{2H}\right)^2 \frac{\mu}{\rho} t\right\}\right] \sin\frac{i\pi}{2} \tag{4.9}$$

Here, μ, ρ, θ, g , H, t are coefficients of viscosity of liquefied soil, density of liquefied soil, ground surface gradient, gravity acceleration (980 cm/s^2), thickness of liquefied soil and time, respectively. The experiments were conducted under conditions shown in Table 4.3. The thickness of the model ground was varied from 84 to 151 cm, but the relative density of the model ground was mostly constant, and ground surface gradient, acceleration and frequency of input motion were same. The purpose of this experiment was to examine the effect of thickness of the ground on flow characteristics of liquefied ground.

The coefficient of viscosity μ for each time was identified, to satisfy Eq. (4.9) using the time histories of ground surface flow velocity $V(t)$ by the experiment. Figure 4.79 shows the calculated coefficients of viscosity versus shear strain rate, which was obtained by dividing ground surface flow velocity $V(t)$ by model ground thickness H. The shear strain rate expresses a mean value over the depth of the

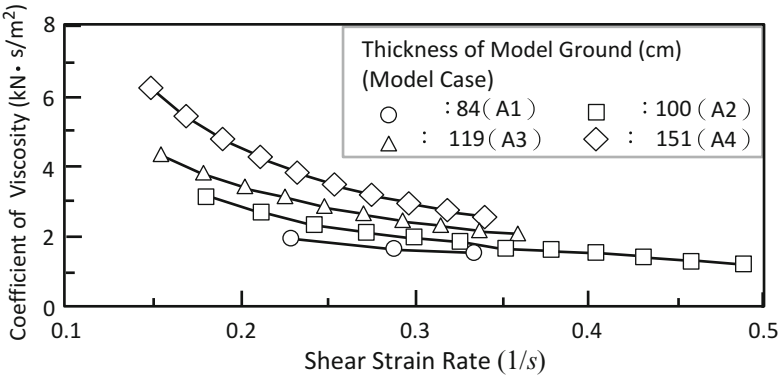

Fig. 4.79 Coefficient of viscosity of liquefied soil (under 1 g)

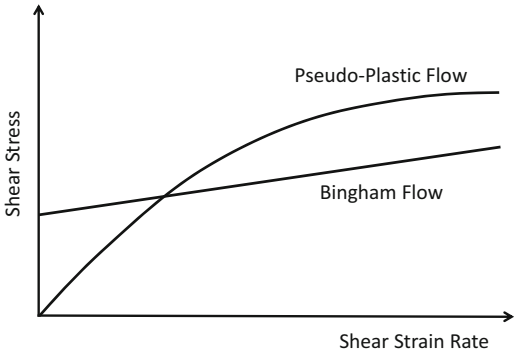

Fig. 4.80 Non-Linear viscosity of liquefied soil (relationship between shear stress and shear strain rate)

ground. According to results shown in Fig. 4.79, the coefficient of viscosity decreased with increasing shear strain rate and increased with increasing model ground thickness. The latter result means that the viscosity of liquefied soil increases with the overburden pressure of soil, such that the ground has greater resistance to flow. The former result means that liquefied soil behaves as non-linear viscous flow, which is called pseudo-plastic flow or Bingham flow (Fig. 4.80).

Similar experiments on the viscosity of liquefied soil were conducted under centrifuge conditions using model ground (Fig. 4.81). In these experiments, centrifuge acceleration was varied from 10 to 40 g with constant 20 cm model ground thickness (Table 4.4). This means that thickness of the prototype ground varied approximately 2–8 m. The coefficient of viscosity was estimated from the time history of ground surface velocity, by the same procedure used in the experiment under 1 g conditions.

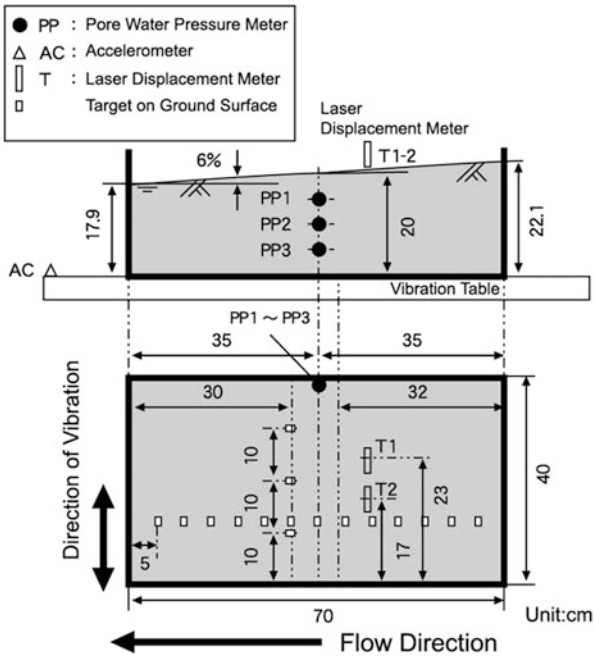

Fig. 4.81 Model ground for flow test of liquefied soil (under centrifuge condition)

Table 4.4 Cases of flow test of liquefied soil (under centrifuge condition)

Case	Thickness of model ground (cm)	Centrifuge acceleration (g)	Relative density (%)	Input acceleration (cm/s^2)	Frequency (1/s)
B1	20	10	35	270 × 10	50
B2	20	20	37	341 × 20	100
B3	20	30	35	373 × 30	150
C1	20	10	36	394 × 10	50
C2	20	10	41	380 × 10	50
C3	20	40	40	270 × 40	200
C4	20	40	39	350 × 40	200

Figure 4.82 shows the test results, in which the coefficient of velocity of liquefied soil decreased with increased shear strain rate. This also means that the liquefied soil behaves as non-linear viscous, pseudo-plastic or Bingham flow. Furthermore, the figure shows that the coefficient of viscosity of liquefied soil increased with centrifuge acceleration with the same model ground thickness. This means that the viscosity of liquefied soil increased with overburden pressure.

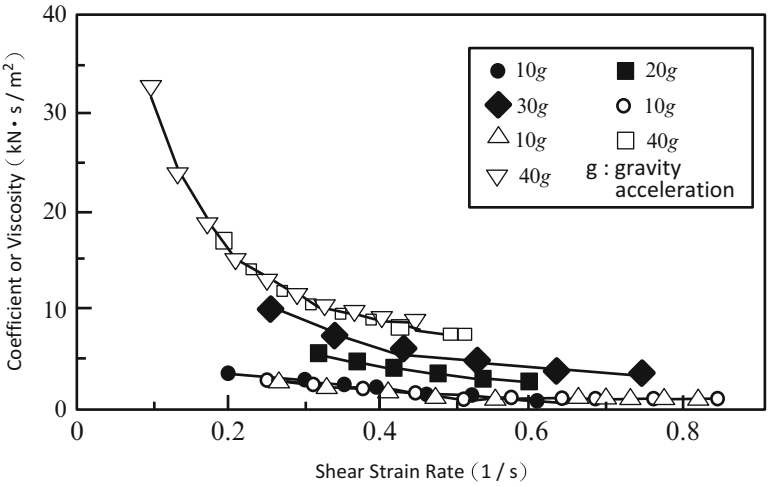

Fig. 4.82 Coefficient of viscosity of liquefied soil (under centrifuge condition)

4.3 Earthquake-Resistant Design of Buried Pipes and Foundations Against Liquefaction-Induced Ground Displacement

4.3.1 Ground Strain and Damage to Buried Pipes

Ground strains due to liquefaction-induced displacements directly affect the integrity of buried pipes of lifeline systems, as mentioned in Sect. 4.1. Ground strains during past earthquakes were calculated for each type of ground displacement (Type 1and 2; Fig. 4.70). For type 1 displacements by inclination of ground surface, data were from case studies in Noshiro during the 1983 Central Japan Sea earthquake. For type 2 displacements by quay wall movement, data from the 1964 Niigata earthquake were used. The procedure for calculation of ground strain is as follows.

(i) The displacement function in quadrilateral areas with side length about 100 m (Fig. 4.83) is defined by

$$\begin{aligned} u(x,y) &= \alpha_1 x + \beta_1 y + \gamma_1 \\ v(x,y) &= \alpha_2 x + \beta_2 y + \gamma_2 \end{aligned} \tag{4.10}$$

Here, u and v are displacements in the x and y directions, respectively.

(ii) The six coefficients α_1–γ_2 of the displacement function are determined from measured displacements in quadrilateral areas, by the least mean square method.

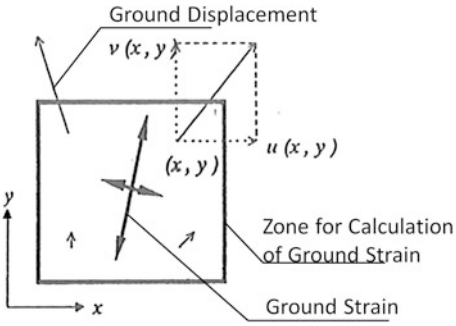

Fig. 4.83 Calculation of ground strains on horizontal plane

(iii) Ground strains on the horizontal (x–y) plane are calculated from the coefficients, as follows:

$$\gamma_{xx} = \frac{\partial u}{\partial x}$$
$$\gamma_{yy} = \frac{\partial v}{\partial y} \tag{4.11}$$
$$\tau_{xy} = \frac{\partial v}{\partial x} + \frac{\partial u}{\partial y}$$

Here, γ_{xx} and γ_{yy} are the normal strains in x and y directions, respectively, and τ_{xy} is shear strain.

An example of ground strains calculated at Port Island in Kobe is shown in Fig. 4.84. Behind the quay walls, there were large tensile strains of more than 2 %. Figure 4.85 shows statistics of compressive and tensile strains in reclaimed land of Kobe, and Fig. 4.86 shows results from sloped ground in Noshiro. According to Fig. 4.85, the mean tensile strain just behind the quay wall (along water in Fig. 4.85) was 0.97 %, which was much larger than that of inland areas at 0.36 %. This large tensile strain was caused by large displacement of the quay wall toward the sea. Similarly, large ground tensile strains were observed behind banks of the Shinano River during the 1964 Niigata earthquake.

According to Fig. 4.86, the magnitudes of tensile strains at the upper part of the sloped ground, and of compressive strains on the lower part, were mostly between 0.5 % and 0.8 %; however, there were some cases of maximum ground strain exceeding 2 %. These results were referenced for ground strain determination during the design of buried water and sewage pipes, as addressed in Sect. 4.3.2.

Figures 4.87 and 4.88 show the relationships between ground strains and damage rate of water and sewage pipes. In these figures, ground strains are the component in the axial direction of the pipes. The damage rate of water pipes is the number of damages per 1 km length, whereas the rate for sewage pipes is the ratio of number of damaged sections between two neighboring manholes to the total number

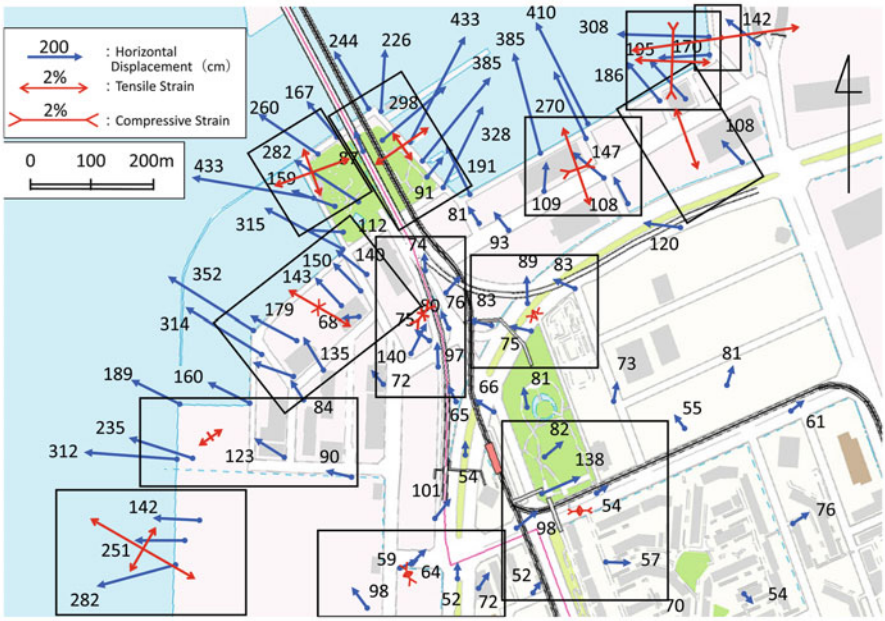

Fig. 4.84 Ground strains from liquefaction-induced displacements (Port Island)

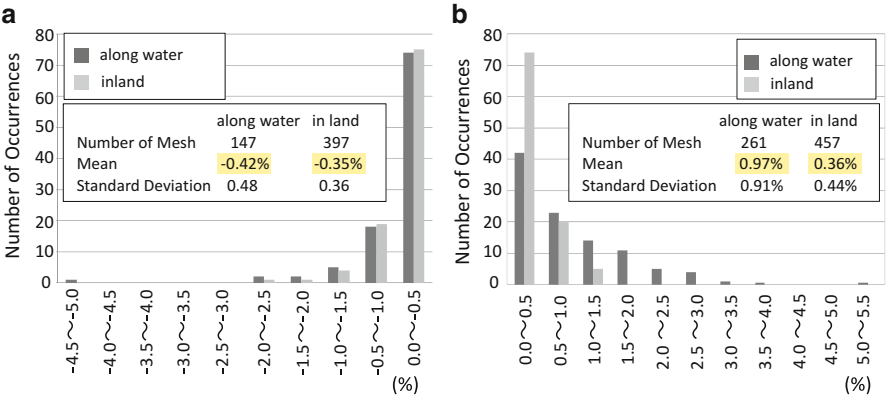

Fig. 4.85 Ground strains behind quay wall in reclaimed land (1995 Kobe earthquake, ground strain due to type 2 displacement in Fig. 4.70b). (**a**) Compressive strain. (**b**) Tensile strain

of sections. Water pipes were ductile pipes without earthquake-resistant joints (A, K and T types). No damage was reported for ductile pipes with earthquake-resistant joints (SS type). The damage to sewage pipes included rupture of pipes and pipe intrusion into manholes. According to the results in the figures, the damage rate to water pipes and sewage pipes proportionally increased with ground strains. About

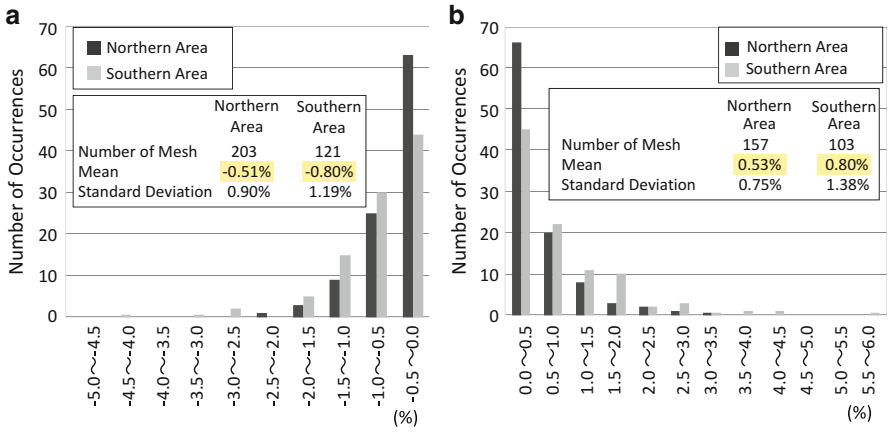

Fig. 4.86 Ground strains due to surface inclination (1983 Central Japan Sea earthquake, ground strain due to type 1 displacement in Fig. 4.70a). (**a**) Compressive strain (*lower part of slope*). (**b**) Tensile strain (*upper part of slope*)

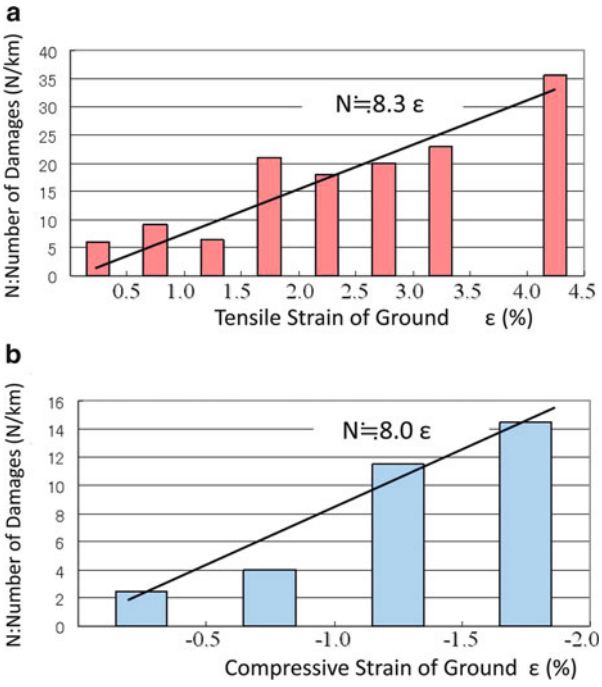

Fig. 4.87 Relationship between damage rate of water pipes and ground strains (Ductile pipe with A, K, type joints). (**a**) Number of damages of water pipes per 1 km and tensile strain of ground. (**b**) Number of damages of water pipes per 1 km and compressive strain of ground

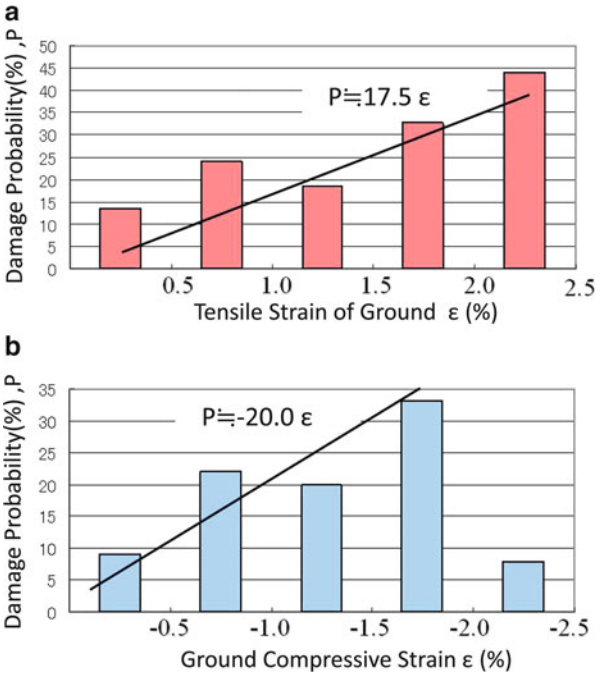

Fig. 4.88 Relationship between damage probability of sewers and ground strains. (**a**) Damage probability of sewers and tensile strain of ground. (**b**) Damage probability of sewers and compressive of ground

35 instances of water pipe damage per 1 km were caused by tensile ground strains of 4.0–4.5 % (Fig. 4.87a), while sewer damages occurred in about 40 % of the total sections from tensile ground strains of 2.0–2.5 % (Fig. 4.88a).

4.3.2 Earthquake-Resistant Design of Buried Pipes

Liquefaction-induced ground displacements in the 1995 Kobe earthquake caused considerable damage to buried water and sewers. Therefore, in *the Guidelines for Earthquake Resistant Measures for Sewage Facilities* (1997 Japan Sewage Association) and *Principles of Earthquake Design and Construction of Water Supply Facilities* (1997 Japan Water Works Association) [28], both of which were revised after the earthquake, ground strains due to liquefaction-induced ground displacements were considered. Two types of ground strains (Fig. 4.89) were considered in the design of water pipes. One is tensile ground strain caused by the movement of quay walls; a maximum ground strain of 1.5 % was adopted, which was determined based on calculated strains shown in Fig. 4.85 at non-exceedance probability 80 %. This was the first time that the concept of non-exceedance probability was taken into the consideration for earthquake-resistant design of structures and facilities.

For sloped-ground tensile and compressive strains, values of 1.3 % were adopted based on calculated ground strains for Noshiro during the 1983 Central Japan Sea

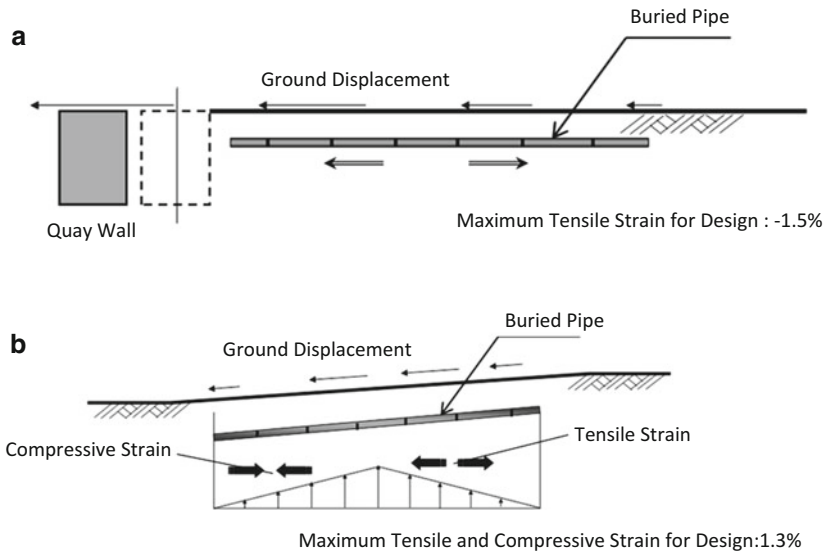

Fig. 4.89 Ground strains for design of water pipes. (**a**) Ground nearby Quay Wall (type 2 ground displacement in Fig. 4.70b). (**b**) Sloped ground (type 1 ground displacement in Fig. 4.70a)

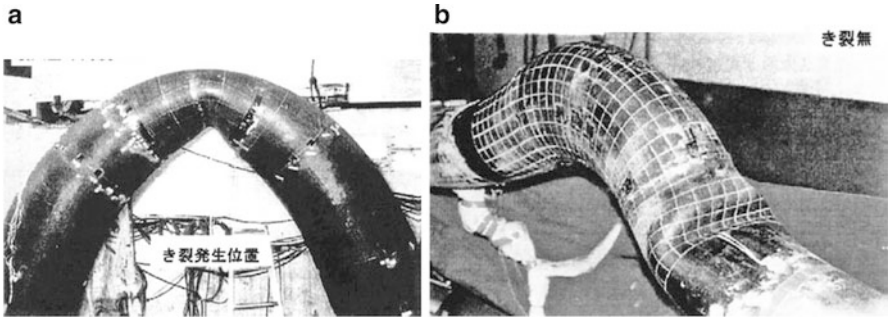

Fig. 4.90 Experiment on large deformation of gas pipes [31]. (**a**) Inner bending (ultimate strain: 30 %). (**b**) Outer bending (ultimate strain: 10 %)

earthquake (Fig. 4.86), at the same non-exceedance probability of 80 %. When ground strains by liquefaction-induced large displacements were considered for buried pipe design, the concept of ultimate strength design was also introduced in *Earthquake Resistant Design of Gas Pipes* (2000 Japan Gas Association) [29]. Design strains for the limit state were determined as 30 % for tensile deformation of straight pipes, and 30 % and 10 % for inner and outer bending deformation of bend pipes, based on ultimate deformation tests shown in Fig. 4.90. These levels of design strains were determined based on the probability of gas leakage during the tests [30, 31].

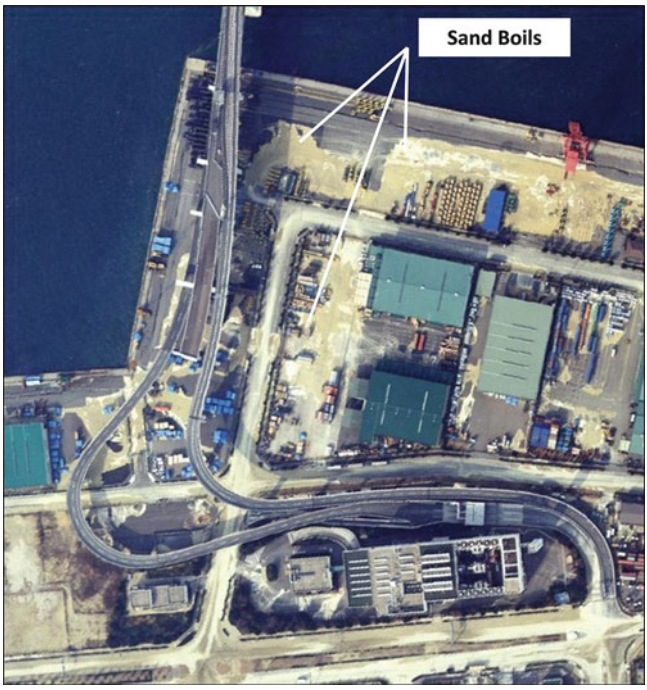

Fig. 4.91 Sand boils around a highway bridge (1995 Kobe earthquake at Rokko island in Kobe)

4.3.3 Earthquake-Resistant Design of Foundations

The 1995 Kobe earthquake caused extensive liquefaction and large ground displacements in reclaimed land, which induced large residual deformation of highway bridge foundations. Among these bridges, some girders fell owing to expansion of spans between neighboring piers.

Figure 4.91 shows an aerial photo of a highway bridge on Rokko Island in Kobe. The yellow colored part on the ground surface indicates sand boils due to soil liquefaction. Figure 4.92 displays horizontal displacements at the ground surface and at the tops of bridge piers, measured by aerial photos before and after the earthquake. The ground surface around the highway displaced 2–3 m seaward, and tops of piers moved a maximum of 90 cm. Based on ground displacement. Through investigation of damage to bridge foundations, the effects of liquefaction-induced ground displacement were taken into the consideration in the revision of earthquake-resistant design of highway bridges and railway bridges after the earthquake. Figure 4.93 illustrates the design method for road bridges (Fig. 4.93a) [4] and railway bridges [32] (Fig. 4.93b). For road bridge design, passive earth pressure from upper non-liquefied soil and earth pressure equivalent to the liquid force generated by liquefied soil flow are considered. The coefficient of equivalent earth pressure from liquefied soil is about 0.3, which was determined by back analyses of the residual deformation of the highway bridge piers after the Kobe earthquake. For the design of

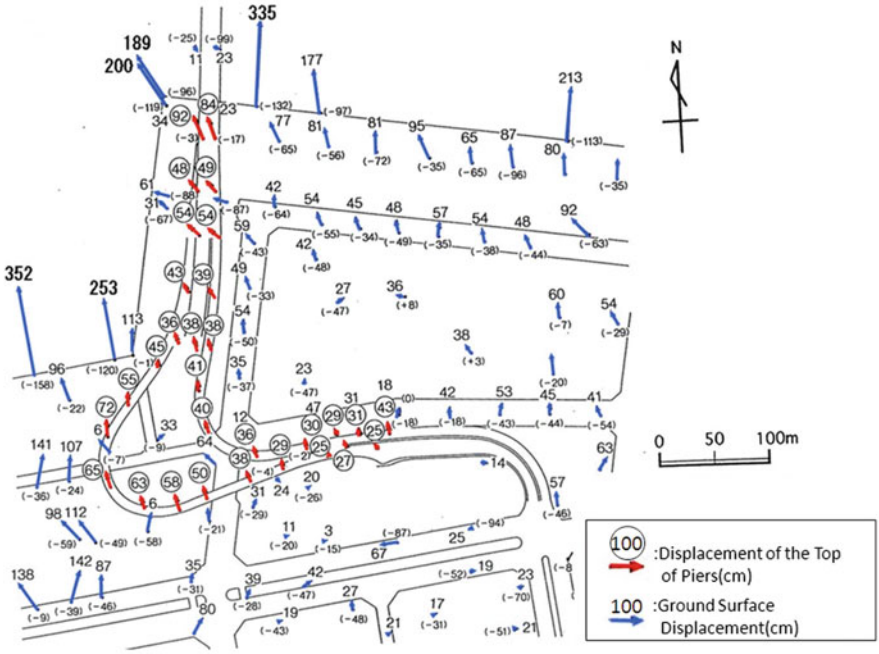

Fig. 4.92 Horizontal displacements at ground surface and the top of bridge piers (1995 Kobe earthquake, Port Island, No. 5 bay shore highway)

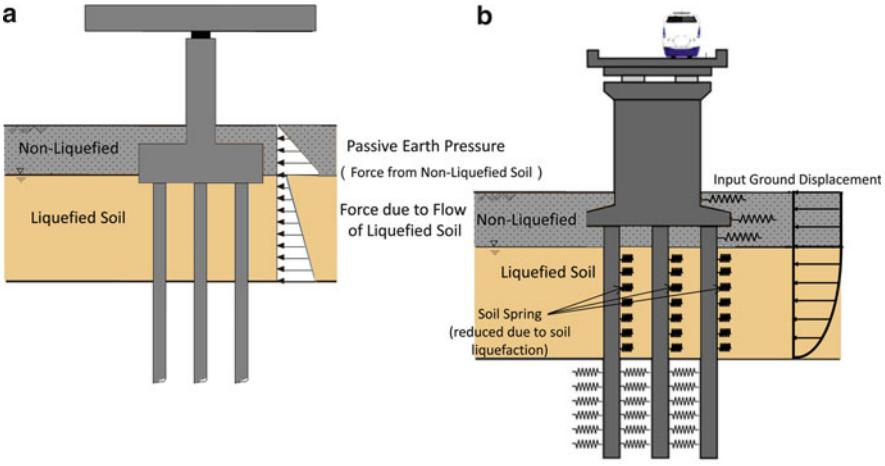

Fig. 4.93 Earthquake resistant design of pile foundation against liquefaction-induced ground displacements. (**a**) Highway bridges [4]. (**b**) Railway bridges [30]

railway bridges, ground displacements are inputted to the foundations through the soil springs. However, the coefficient of soil springs of liquefied soil is reduced from 1/1,000 to 1/10,000, owing to a large decrease in soil stiffness due to liquefaction. The reason for adoption of the different design methods between road and railway bridges is that characteristics of the external forces on the foundations from flowing liquefied soil have not yet been clarified. These methods were tentatively proposed soon after the Kobe earthquake, and should be improved based on future development of research on forces from liquefied soil flow.

4.4 Countermeasures Against Liquefaction-Induced Ground Flow

4.4.1 Countermeasures for Quay Walls

In the 1995 Kobe earthquake, liquefaction-induced ground displacements triggered by large movements of quay walls caused severe damage to foundation piles and buried pipes. Extensive coastal areas around Japanese mega cities such as Tokyo, Nagoya and Osaka had been reclaimed before the experience of soil liquefaction at the time of the Niigata earthquake. On most of these artificial islands, the occurrence probability of soil liquefaction and large ground displacement is very high, because enough countermeasures against ground and quay wall movement have not been implemented. If liquefaction and ground displacement occur on these islands, storage tanks and other industrial facilities on reclaimed ground may be destroyed and large quantities of oil and petrochemical products could flow into the sea, producing a fire threat.

Such accidents could seriously hamper sea transport in bay areas such as Tokyo Bay. This could negatively affect rescue operations, and restoration and reconstruction efforts after an earthquake. Furthermore, various industrial complexes, power generation plants, and facilities for commerce and culture are concentrated in the bay areas of megacities. If these structures and facilities were severely damaged and their functions were lost, social and economic activities of the country would be seriously impacted. The effect of heavy damage to these areas could expand worldwide.

Therefore, effective countermeasures against soil liquefaction and large ground displacement for structures and facilities on reclaimed lands should be developed. Three methods for reinforcement of an existing quay wall are proposed (Fig. 4.94). The existing quay wall (shown in Fig. 6.7) was constructed without any consideration for liquefaction, because it was built before the Niigata earthquake, where the phenomena of soil liquefaction was firstly recognized from engineering standpoint. The tip of existing sheet piles is in liquefiable soil with a liquefaction safety factor (F_L) less than 1.0, and does not reach the lower non-liquefiable clay layer. Figure 4.94a shows a measure to prevent liquefaction-induced ground displacement

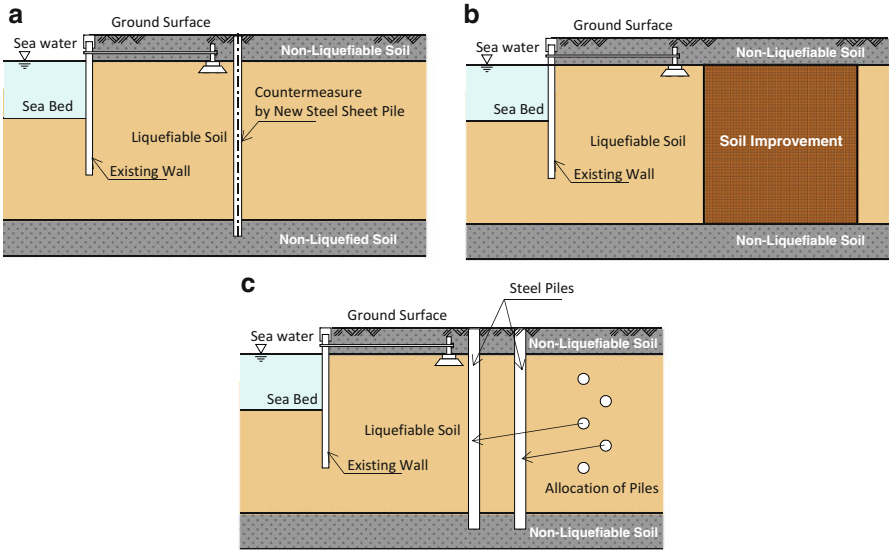

Fig. 4.94 Countermeasures of existing quay walls against flow of liquefiable soil. (**a**) Steel sheet pile. (**b**) Soil improvement. (**c**) Steel piling

by driving new sheet piles into the non-liquefiable layer. Figure 4.94b shows a countermeasure whereby ground behind an existing quay wall is improved using cement-mixing grout materials. Figure 4.94c shows a third approach called the piling method, whereby steel piles of 1.0 m diameter and 25 mm sheet thickness are driven into the lower non-liquefiable layer along two rows, at an interval 4–6 times the pile diameter.

Figure 4.95 shows results of experiments on the effectiveness of the three methods in reducing horizontal ground displacements, which were examined using a 1/50 scale model under 50 g centrifuge condition. The vertical axis of the figure is displacements at each point on the ground surface, and the horizontal axis shows distance from the existing quay wall. It was found that ground displacement was greatly reduced by soil improvement and the piling method. Furthermore, these two methods can reduce deformation of existing quay walls by preventing flow of liquefied soil toward the existing walls, reducing earth pressure on the wall. The effectiveness of construction of a new sheet pile wall behind the existing wall is not very effective compared with the other two measures. The reason for this can be explained as follows. In the case of the sheet pile wall, the external force on the wall from flowing liquefied soil becomes larger than that with the piling method, because soil movement is completely halted by the continuous wall, resulting in greater deformation due to increased external force. On the contrary, in the piling method, some liquefied soil can flow between the piles, resulting in reduction of the external force and less pile deformation.

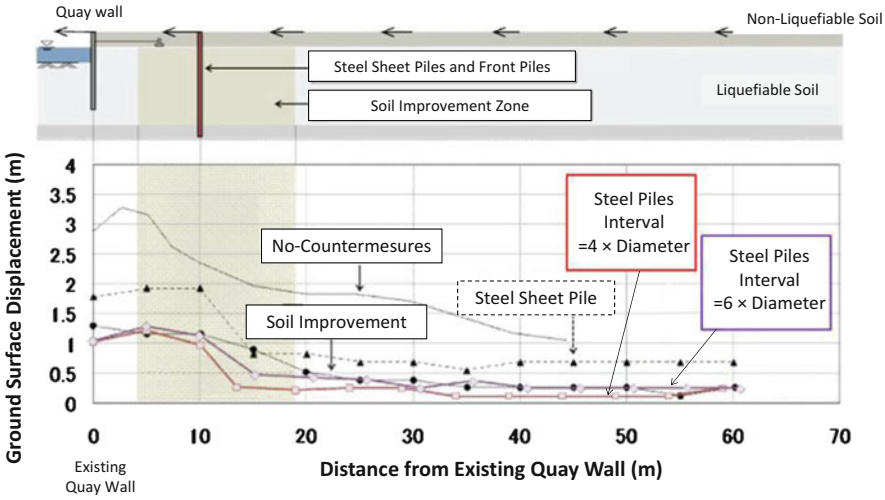

Fig. 4.95 Effectiveness of countermeasures for exiting quay wall (experiment under 50 g centrifuge condition)

4.4.2 Countermeasures for Foundations of Existing Structures

The following countermeasures are proposed for the protection of existing structure foundations:

(i) Driving additional piles around an existing foundation (additional piling method in Fig. 4.96a)
(ii) Construction of an ground wall around an existing foundation (ground wall method in Fig. 4.96b)
(iii) Hardening surrounding ground by grouting (grouting method in Fig. 4.96c)

In addition to the above countermeasures, a method whereby liquefiable soil of upstream side of foundation is replaced by a lightweight soil to reduce the earth pressure (replacement by lightweight soil method) is proposed. In some cases, these methods have been applied for reinforcement of existing foundations of bridges. However, reinforcement has not been extensively applied because of the high construction cost and traffic congestion during construction.

In the 1995 Kobe earthquake, liquefaction-induced large ground displacements damaged highway bridge foundations and lifeline facilities such as wastewater treatment plants. In the revised design codes after the Kobe earthquake, the effects of liquefaction-induced ground displacement were taken into consideration, but there remain many bridge foundations that have no reinforcement. Among these,

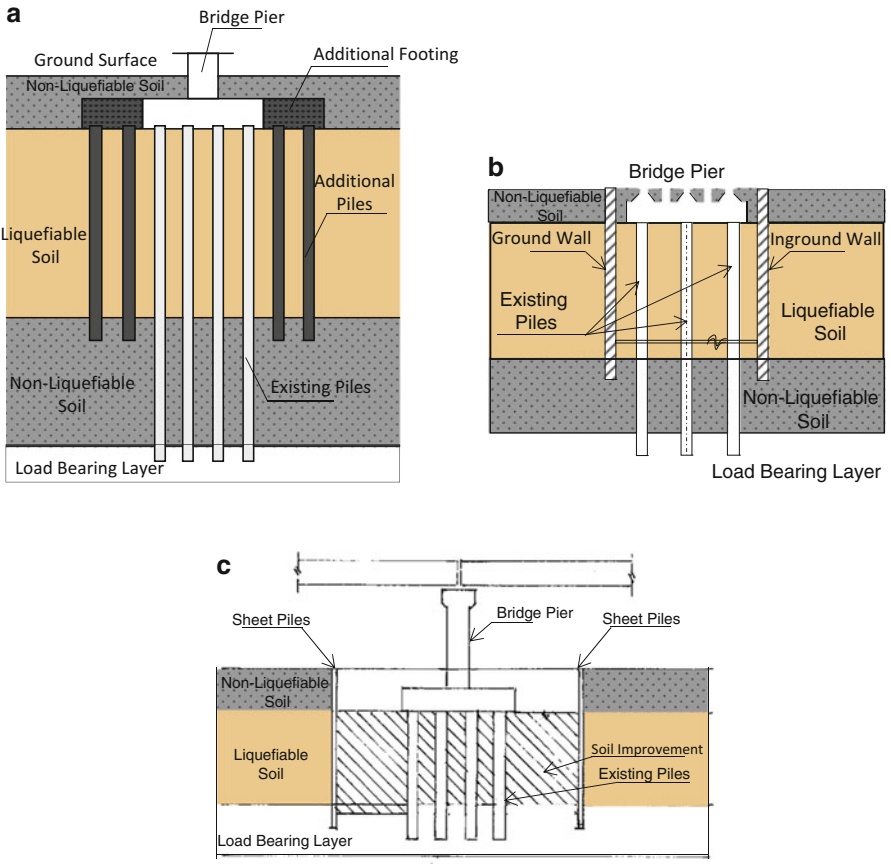

Fig. 4.96 Countermeasures for existing pile foundations against liquefaction-induced ground displacement. (**a**) Additional piles. (**b**) Ground walls. (**c**) Soil improvement by grouting

it is particularly urgent to reinforce foundations of the structures constructed behind quay.

On the artificial islands reclaimed from Tokyo Bay, many high-rise residential and commercial buildings have been constructed, and the area has been newly developed. The effect of soil liquefaction on foundation ground has been considered for earthquake-resistant design of these buildings. However, in many cases, the effect of liquefaction-induced ground displacement was not considered. This is because there is insufficient communication between building designers and engineers engaged in construction of port structures such as quay walls. It is necessary to examine the safety of high-rise buildings in reclaimed lands, to prevent the damage due to large ground displacements.

References

1. Hamada M, Yasuda S, Isoyama R, Emoto K (1986) Study on liquefaction induced permanent ground displacements. Association for the Development of Earthquake Prediction, Japan
2. Hamada M (1992) Large ground deformations and their effects on lifelines: 1983 Nihonkai-Chubu earthquake. Case studies of liquefaction and lifeline performance during past earthquakes. Technical report NCEER-92-0001, vol 1. National Center for Earthquake Engineering Research, USA
3. Noshiro City Government (1983) Report of the 1983 central Japan Sea earthquake. Record of disaster in Noshiro (in Japanese)
4. Japan Road Association (1996) Specification for highway bridges and explanations, part V seismic design/Japan Society Civil Engineers (JSCE) (2000), Earthquake resistant codes in Japan
5. Hamada M (1986) Large ground deformations and their effects on lifelines: 1964 Niigata earthquake. Case studies of liquefaction and lifeline performance during past earthquakes, vol 1. Technical report NCEER-92-001. National Center for Earthquake Engineering Research, USA
6. Hamada M, Saito K, Yasuda S, Isoyama R (1988) Earthquake damage by liquefaction-induced permanent ground displacement. In: Proceedings of 9th world conference on earthquake engineering, pp VII-213-218
7. Hamada M (1994) Case studies on liquefaction-induced ground displacement during past earthquakes in Japan, Prediction versus performance in geotechnical engineering. Balkema, Netherlands, pp 319–326
8. Niigata University and Fukada Geological Research Institute (1964) Map of ground disaster during the Niigata earthquake, Kubota, Japan
9. Japan Society of Civil Engineers (JSCE) (1966) Report on the 1964 Niigata earthquake (in Japanese)
10. Waseda University Research Laboratory (1966) Bulletine of science and engineering research laboratory, No. 34. Special issue of Niigta earthquake
11. Kawamura S, Nishizawa T, Wada K (1985) Damage to foundation piles discovered 20 years after the 1964 Niigata earthquake. Nikkei architecture, pp 130–134, July 1985 (in Japanese)
12. Hamada M, Isoyama R, Wakamatsu K (1995) The 1995 Hyogo-ken (Kobe) earthquake-liquefaction, ground displacement and soil condition in Hanshin area. Association for Development of Earthquake Prediction, Japan
13. Hamada M, Isoyama R, Wakamatsu K (1996) Liquefaction-induced ground displacement and its related damage to lifeline facilities. Special issue of soil and foundations, Japan Geotechnical Society Tokyo, pp 197–205
14. Hamada M, Wakamatsu K (1996) Liquefaction, ground deformation and their caused damage to structures. A special report on the 1995 Hyogoken-nanbu earthquake. Japan Society of Civil Engineers, pp 81–98
15. Hamada M, Wakamatsu K, Ando T (1996) Liquefaction-induced ground deformation and its caused damage during the 1995 Hyogoken-nanbu earthquake. In: Proceedings of 6th Japan-U. S. workshop on earthquake resistant design of lifeline facilities and countermeasures against soil liquefaction. Technical report NCEER-96-0012. National Center for Earthquake Engineering, USA, pp 137–152
16. Hamada M, Yasuda S, Wakamatsu K (1992) Large ground deformation and their effects on lifelines: 1964 Niigata earthquake. Case studies of liquefaction and lifeline performance during past earthquakes, vol 1. Technical report NCEER-92-0001. National Center for Earthquake Engineering Research, USA
17. Hamada M, Yasuda S, Wakamatsu K (1992) Large ground deformation and their effects on lifelines: 1948 Fukui earthquake. Case studies of liquefaction and lifeline performance during past earthquakes, vol 1. Technical report NCEER-92-0001. National Center for Earthquake Engineering Research, USA

18. Hamada M, Wakamatsu K, Yasuda S (1992) Liquefaction-induced ground deformation during the 1923 Kanto earthquake. Case studies of liquefaction and lifeline performance during past earthquakes, vol 1. Technical report NCEER-92-001. National Center for Earthquake Engineering Research, USA
19. Japan Geological Survey (1925) Report of the 1923 great Kanto earthquake (in Japanese)
20. O'Rourke TD, Roth BL, Hamada M (1992) Large ground deformations and their effects on lifeline facilities: 1971 San Fernando earthquake. Case studies of lifeline and lifeline performance during past earthquakes, vol. 2. Technical report NCEER-92-0002. National Center for Earthquake Engineering Research, USA
21. Miura F, O'Rourke TD, Hamada M (1992) Interpretation of high pressure pipeline damage by liquefaction-induced ground movement. In: Proceedings of 10th world conference on earthquake engineering, pp 5453–5457
22. Proceedings of U.S.-Japan Workshop on Earthquake Resistant Design of Lifeline Facilities and Countermeasures against Liquefaction. National (Multidisciplinary) Center for Earthquake Engineering Research USA, 1988, 1988, 1990, 1992, 1994, 1996, 1999, 2002
23. Bartlett SF, Youd TL (1992) Empirical prediction of lateral spread displacement. In: Proceedings from the 4th Japan-U.S. workshop on earthquake resistant design of lifeline facilities and countermeasures for soil liquefaction. Technical report NCEER-92-0019, vol I, pp 351–366
24. Iai S, Ichii K, Morita T, Sato Y (1997) Displacement of quay walls due to soil liquefaction during past earthquakes. In: Proceedings of 2nd symposium on the 1995 Kobe earthquake, vol 2, pp 259–264 (in Japanese)
25. Hamada M, Sato H, Nakamura T (1994) An experimental and numerical study on liquefaction-induced ground displacement. In: Proceedings of 5th national conference on earthquake engineering, vol IV, USA
26. Hamada M (1996) A study on flow characteristics of liquefied soil. In: Proceedings of U.S.-Japan cooperative research on urban earthquake disaster mitigation U.S-Japan joint workshop and 3rd grantees' meeting, pp 89–96
27. Hamada M, Sato H, Kawakami T (1994) A consideration of the mechanism for liquefaction-related large ground displacement. In: Proceedings of the 5th U.S.-Japan workshop on earthquake resistant design of lifeline facilities and countermeasures against soil liquefaction. Technical Report NCEER 94–0026, pp 217–232
28. Japan Water Works Association (2000) Principles of seismic design and construction for water supply facilities/JSCE (2000), Earthquake resistant design codes in Japan
29. Japan Gas Association (2000) Recommended practices for earthquake resistant design of gas pipelines/JSCE. Earthquake resistant design codes in Japan
30. Yoshizaki K, Hamada M, O'Rourke TD (1999) Large deformation behavior of pipelines with elbows. In: Proceedings of optimizing post-earthquake lifeline earthquake engineering, ASCE, pp 302–311
31. Yoshizaki K, O'Rourke TD, Hamada M (2001) Large deformation behavior of buried pipelines with low-angle elbows subjected to permanent ground deformation. Struct Eng/Earthquake Eng, JSCE 18(1):418–528
32. Railway Technical Research Institute (2000) Seismic design of railway structures/JSCE. Earthquake resistant design codes of civil engineering structures in Japan

Chapter 5
Dynamic Behaviors of Underground Structures During Earthquakes and Earthquake-Resistant Design

Abstract Dynamic behaviors of underground structures such as underground tanks, submerged tunnels and rock caverns during earthquakes were observed. The earthquake observation revealed that the deformation of underground structures is governed by relative displacements of the surrounding ground, namely, by ground strain during earthquakes, and that underground structures themselves do not have their own natural period and vibration modes. Based on these observed results, the response displacement method was proposed for the earthquake-resistant design of underground structures such as buried pipes, underground tanks and submerged tunnels. Furthermore, the concept of input ground displacement for the design of buried water, sewer and gas pipes in the current design codes of Japan is introduced.

Keywords Design code • Earthquake resistant design • Ground strain • Response displacement method • Rock cavern • Submerged tunnel • Underground structures • Underground tank

5.1 Analysis with Interaction Model of Ground and Underground Structures

The dynamic behavior of aboveground structures such as bridges and buildings is governed by acceleration of those structures. The seismic coefficient and modified seismic coefficient methods, which apply static external forces to structures as well as dynamic response analysis, are design methods based on inertia forces from seismic acceleration (Chap. 2).

The behavior of underground structures such as tanks and tunnels is expressed differently. Until their behavior was clarified through earthquake observations,

M. Hamada, *Engineering for Earthquake Disaster Mitigation*,
Springer Series in Geomechanics and Geoengineering,
DOI 10.1007/978-4-431-54892-8_5, © Springer Japan 2014

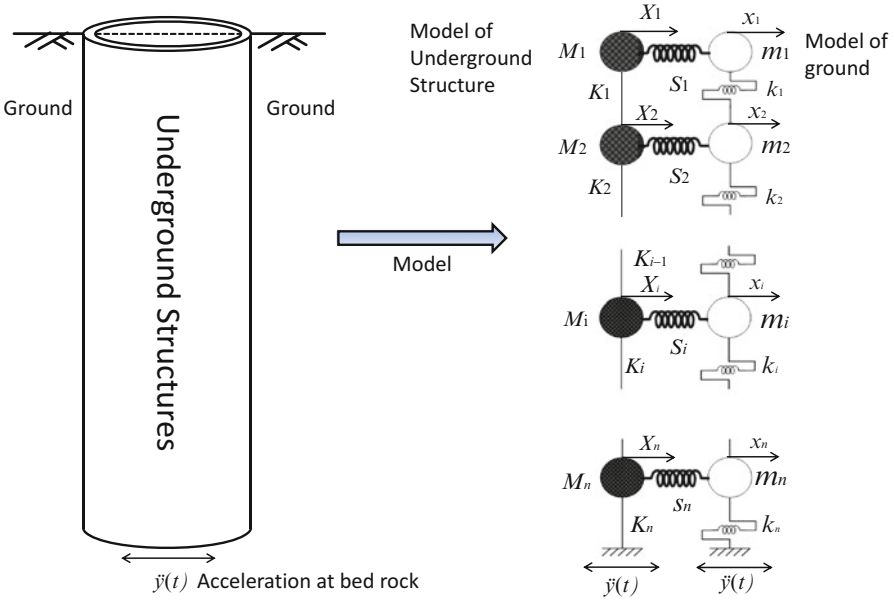

Fig. 5.1 Soil-structure interaction model for dynamic analysis of underground structures

analytical models such as that shown in Fig. 5.1 were used to characterize the interaction of dynamic behavior between the structures and surrounding ground. In this model, the structures and surrounding ground were modeled as multiple masses-springs, with interacting forces through soil springs $s_1 - s_n$ between structures and ground. This is based on the concept in which underground structures have natural frequencies and vibration modes [1].

Vibration in the interaction model for underground structures and ground shown in Fig. 5.1 is determined through Eq. (5.1):

$$\begin{bmatrix} M_1 & & & \\ & \ddots & & \\ & & M_i & \\ & & & \ddots \\ & & & & M_n \end{bmatrix} \begin{Bmatrix} \ddot{X}_1 \\ \vdots \\ \ddot{X}_i \\ \vdots \\ \ddot{X}_n \end{Bmatrix} + \begin{bmatrix} & & C_{ij} & & \end{bmatrix} \begin{Bmatrix} \dot{X}_1 \\ \vdots \\ \dot{X}_i \\ \vdots \\ \dot{X}_n \end{Bmatrix} + \begin{bmatrix} & & K_{ij} & & \end{bmatrix} \begin{Bmatrix} X_1 \\ \vdots \\ X_i \\ \vdots \\ X_n \end{Bmatrix}$$
$$= - \begin{bmatrix} M_1 & & & \\ & \ddots & & \\ & & M_i & \\ & & & \ddots \\ & & & & M_n \end{bmatrix} \begin{Bmatrix} 1 \\ \vdots \\ 1 \\ \vdots \\ 1 \end{Bmatrix} \ddot{y} + \begin{bmatrix} s_1 & & & \\ & \ddots & & \\ & & s_i & \\ & & & \ddots \\ & & & & s_n \end{bmatrix} \begin{Bmatrix} x_1 - X_1 \\ \\ x_i - X_i \\ \\ x_n - X_n \end{Bmatrix} \tag{5.1}$$

Equation (5.2) is for ground vibration:

$$\begin{bmatrix} m_1 & & & & \\ & \ddots & & & \\ & & m_i & & \\ & & & \ddots & \\ & & & & m_n \end{bmatrix} \begin{Bmatrix} \ddot{x}_1 \\ \vdots \\ \ddot{x}_i \\ \vdots \\ \ddot{x}_n \end{Bmatrix} + \begin{bmatrix} & & \\ & l_{ij} & \\ & & \end{bmatrix} \begin{Bmatrix} \dot{x}_1 \\ \vdots \\ \dot{x}_i \\ \vdots \\ \dot{x}_n \end{Bmatrix} + \begin{bmatrix} & & \\ & k_{ij} & \\ & & \end{bmatrix} \begin{Bmatrix} x_1 \\ \vdots \\ x_i \\ \vdots \\ x_n \end{Bmatrix}$$
$$= - \begin{bmatrix} m_1 & & & & \\ & \ddots & & & \\ & & m_i & & \\ & & & \ddots & \\ & & & & m_n \end{bmatrix} \begin{Bmatrix} 1 \\ \vdots \\ 1 \\ \vdots \\ 1 \end{Bmatrix} \ddot{y} + \begin{bmatrix} s_1 & & & & \\ & \ddots & & & \\ & & s_i & & \\ & & & \ddots & \\ & & & & s_n \end{bmatrix} \begin{Bmatrix} X_1 - x_1 \\ \\ X_i - x_i \\ \\ X_n - x_n \end{Bmatrix} \tag{5.2}$$

In both equations, the second term on the right side shows the interaction between underground structures and surrounding ground. Terms 1, 2, and 3 on the left side indicate the inertia forces, damping forces, and restoring force of the structure and ground, respectively.

If the seismic motion $\ddot{y}(t)$ input to the bedrock is known, it is possible to calculate the ground response $x_1(t) - x_n(t)$ and underground structure response $X_1(t) - X_n(t)$ by the method shown in Sect. 2.4.3.

In Eq. (5.1), $M_1 - M_n$ indicate masses of the underground structures, and C_{ij} and K_{ij} show the damping matrix and mass matrix elements, respectively. $s_1 - s_n$ are soil springs expressing interaction between the underground structures and ground. $m_1 - m_n$ are ground masses, and l_{ij} and k_{ij} indicate the damping matrix and stiffness matrix elements related to ground vibrations.

Before the response displacement method (described in Sect. 5.6) was developed for earthquake-resistant design of underground structures, dynamic analysis was generally performed using Eqs. (5.1) and (5.2). Beginning in the 1970s, there was substantial construction of submerged tunnels, large underground tanks for storage of liquefied natural gas (LNG), and rock caverns for oil reserves. These are all critical structures that support transportation, energy, and industries. Considering these were built in earthquake-prone areas, the earthquake resistance of these types of large underground structures became an important topic in the field of earthquake engineering.

Based on earthquake observations, Sakurai and others stated that the dynamic deformation of buried pipelines was governed by ground strain [2]. The author also conducted earthquake observations of the behavior of underground tanks, undersea tunnels, and rock tunnel, to develop a rational earthquake-resistant design method for underground structures.

5.2 Behavior of Underground Tanks During Earthquakes

5.2.1 *Earthquake Observation of Underground Tanks and Surrounding Ground [3]*

Dynamic behavior of a reinforced concrete underground tank (24.0 m diameter and about 10 m depth; Fig. 5.2) was observed during earthquakes. The purpose of this tank was to temporarily store drainage from a factory during rainfall, so it does not normally contain water. Therefore, there was no need to consider effects of added mass and sloshing vibration of contained water on tank deformation behavior. A concrete ground wall of depth approximately 21.0 m and thickness 60 cm was constructed and, after the interior was excavated, inner concrete was cast with a thickness of 30 cm. The reinforced concrete base slab of the tank with a thickness of 20 cm was structurally separated from the side wall.

Soil conditions of the reclaimed land in which the tank was constructed are shown in Fig. 5.3. The surface ground consists of filled soil (E.L. + 4.50 ± 1.70 m) and original seabed sand (E.L. + 1.70 − 1.30 m), and below these soil layers sand, silt, and clay exist alternatively. Sand rock is found approximately 55 m below the surface, and this can be considered as the bedrock. The velocity of S wave of surface ground above the bedrock is generally 130–200 m/s.

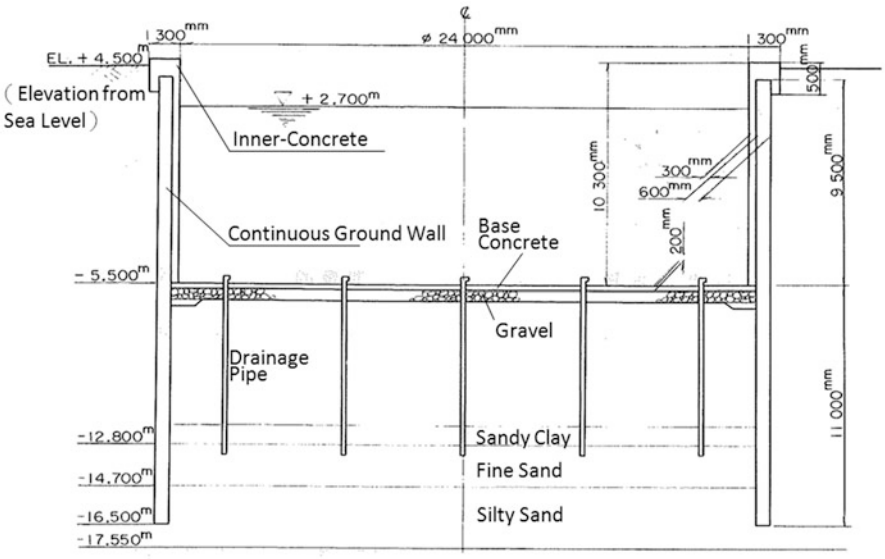

Fig. 5.2 Structure of the underground tank

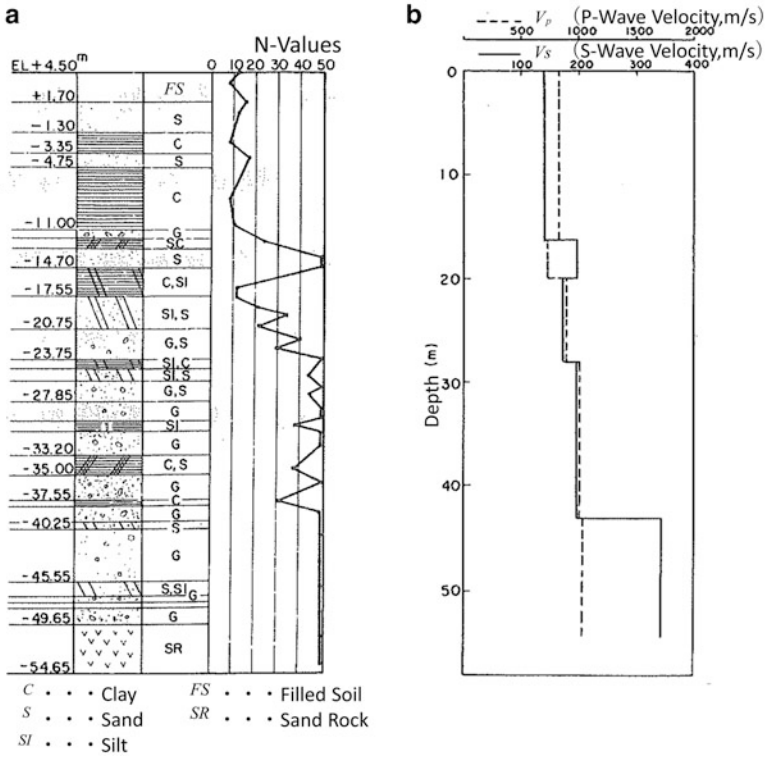

Fig. 5.3 Soil condition and wave velocities. (**a**) Soil condition. (**b**) Wave velocities

Figure 5.4 shows the placement of measuring instruments for observation of the underground tank behavior during earthquakes. Here, A denotes accelerometers, and S represents strain gauges. Earth pressure gauges are indicated by P, but no usable measurements were obtained. Acceleration was measured at the upper surface of the bedrock (A9), ground surface (A1, A3 and A4), and on the tank (A2 and A7). To study tank deformation behavior during earthquakes, strain gauges were placed on the inner surface of the tank side wall. Circumferential and vertical strains were measured. As shown in Fig. 5.5, the strain gauges are steel bars, 1.0 m in length, with one end attached to the concrete surface of the inner tank wall and the other end to a differential transformer. Resolution of strain measurement was confirmed by testing at 0.1×10^{-6}.

5.2.2 *Dynamic Behavior of Underground Tanks During Earthquakes*

Figure 5.6 shows accelerations in the horizontal direction (the *X* direction is horizontal and parallel to the plane of Fig. 5.6) and their power spectra. The moment magnitude

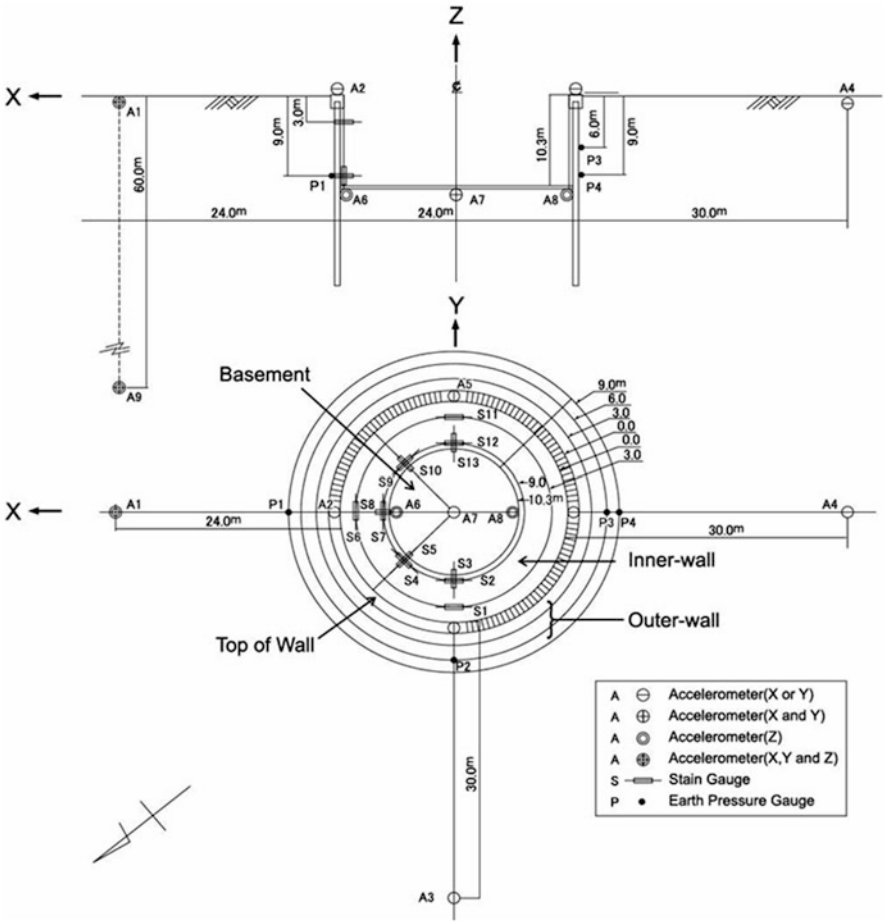

Fig. 5.4 Placement of measuring instruments

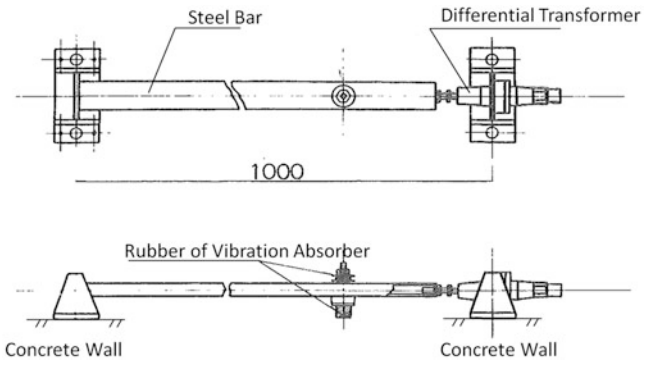

Fig. 5.5 Strain gauge

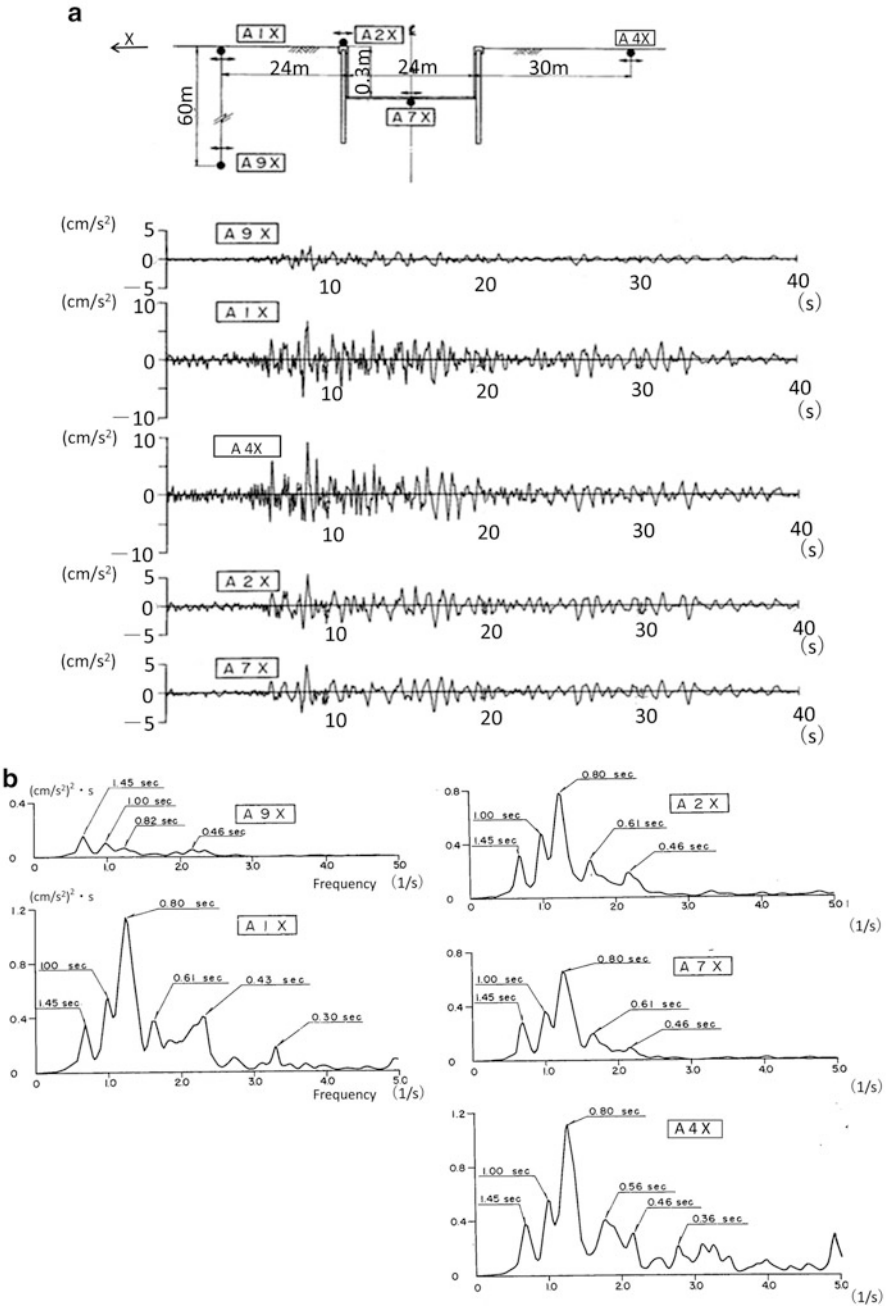

Fig. 5.6 Accelerations observed in the tank and the ground, and power spectra (epicenter: Yamanashi Prefecture, Mw: 5.7, June, 16, 1976). (**a**) Observed accelerations. (**b**) Power spectra of accelerations

of the earthquake which occurred in Yamanashi Prefecture on June 16, 1976 is 5.7. Figure 5.6a indicates that accelerations at the ground surface (A1 and A4) are amplified in comparison with acceleration at the bedrock (A9). Accelerations on the tank (A2: top of side wall; A7: base slab) are of smaller amplitude but of the same phases as the accelerations at the ground surface. Motion of the underground tank is basically the same as that of the surrounding ground. The reason for the smaller amplitude of acceleration on the tank is that motion was suppressed by its rigidity. According to the power spectra of acceleration shown in Fig. 5.6b, the dominant periods of tank acceleration are the same as those at the ground surface; the tank did not show any unique dominant period and vibration mode. These observational data indicate that the tank did not vibrate at its own natural period, but at the same dominant period as the ground, albeit with smaller amplitude. Accelerations at the ground surface and on the tank have a dominant period of nearly 0.8 s, which is the primary natural period of the surface ground.

Figures 5.7 and 5.8 are strains in the circumferential direction of the inner surface of the tank side wall. These strain records indicate the following regarding the underground tank deformation behavior during the earthquake. Strain measurement points S2, S7, and S12 are points at intervals of 90° to the central angle. The strain records at S2 and S12 have the same phases, whereas phase of the strain at S7 is reversed from those at S2 and S12. In other words, the positive and negative of their strain time histories are practically inverted. Considering the side wall of the underground tank as a circular beam, the measurement data suggest that the tank was deformed elliptically with X and Y as the short and long axes, respectively, as shown in Fig. 5.9a.

Figure 5.7a also shows the time history of relative displacement in the X direction, which denotes normal strain of ground γ_{xx}, obtained by double integration of the acceleration records at two measurement points (D1X and D4X) on the ground surface. Depending on the relationship of the positive direction along measurement axis X, this expresses compressive strain when the relative displacement is positive, and expresses tensile strain when the relative displacement is negative. When the ground is in a compressive state in the x direction, circumferential strain at S2 on the sidewall is compressive, while strain at S7 is tensile (for strain, tensile is positive). This indicates elliptical deformation, with the short axis in the x direction and long axis in the y direction. Conversely, during times when the ground is in a tensile state, S2 is positive and S7 is negative, indicating elliptical deformation with the long axis in the x direction and short axis in the y direction.

Similarly, Fig. 5.8 shows circumferential strain records at measurement points S4 and S9, at an interval of 90° to the central angle. Phases of these two strain time histories are also mostly reversed (positive and negative inverted), indicating elliptical deformation. However, in this case, the long and short axes of the ellipse are oriented at 45° to the x and y axes, as shown in Fig. 5.9b.

Figure 5.8 shows the time history of relative displacement in the y direction at two measurement points (D3 and D4) on the ground surface, along with strain records.

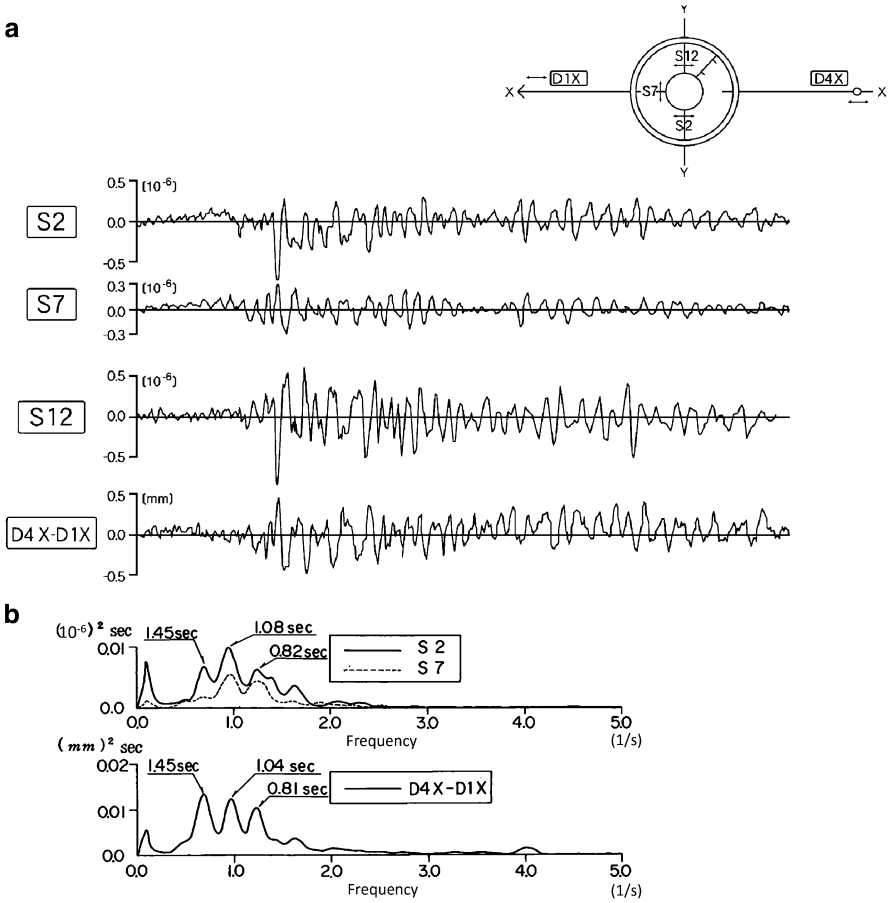

Fig. 5.7 Strains in the circumferential direction on inner surface of tank wall (S2, S7, S12) and relative ground displacement (X direction). (**a**) Strains in the circumferential direction of inner tank wall and relative displacement of ground (X direction). (**b**) Power spectra of circumferential strains of tank and relative ground displacement

This relative displacement can be considered to express shear strains γ_{xy} in the $x - y$ plane of the ground surface. The time history of circumferential strain of the tank at S4 and S9 is similar to that of ground shear strain. This indicates that the tank has been deformed by the ground shear strain into an ellipse with its short and long axes oriented 45° from the x and y axes at the central angle, as shown in Fig. 5.9b.

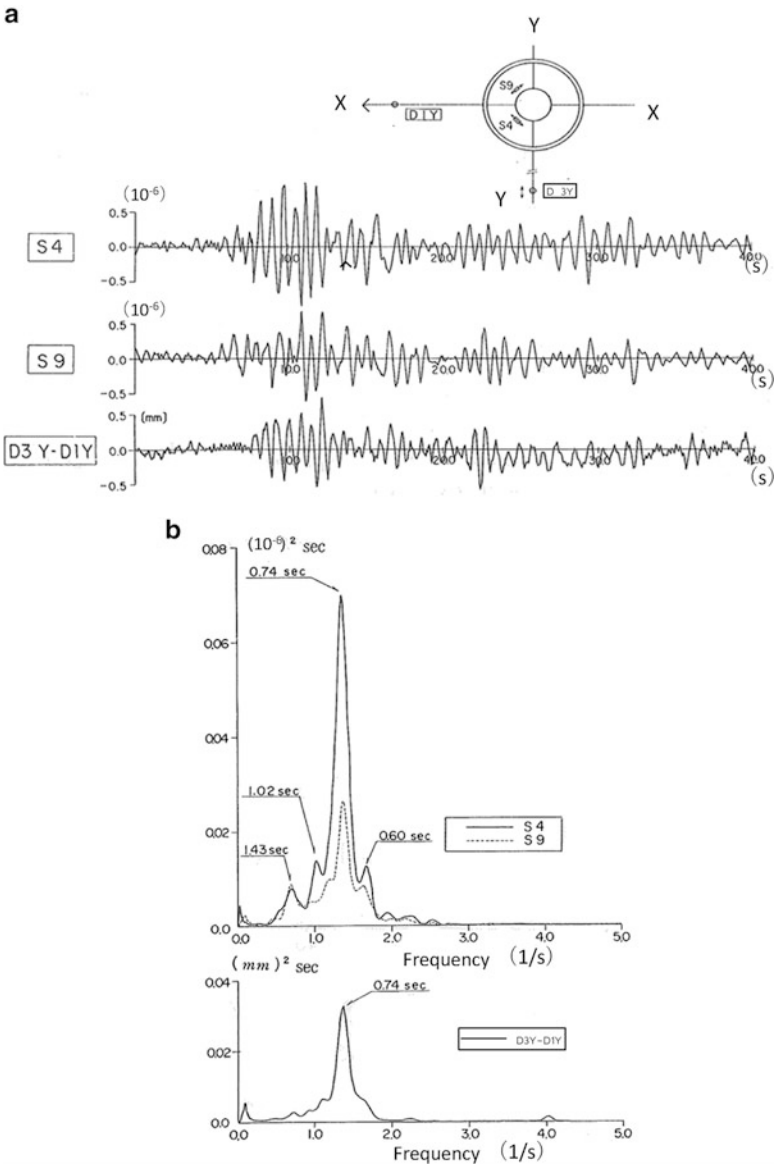

Fig. 5.8 Strains in the circumferential direction on Inner tank wall (S4, S9) and relative ground displacement (Y direction). (**a**) Circumferential strains of inner tank wall and relative ground displacement. (**b**) Power spectra of circumferential strains of inner tank wall tank and relative ground displacement

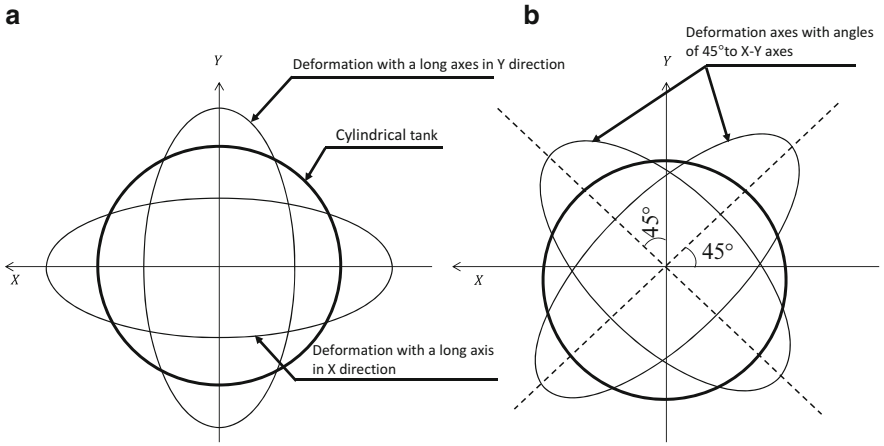

Fig. 5.9 Elliptical deformation of the underground tank. (**a**) Elliptical deformation of the tank in X-Y direction. (**b**) Elliptical deformation of the tank in directions with angle of 45° to X-Y axes

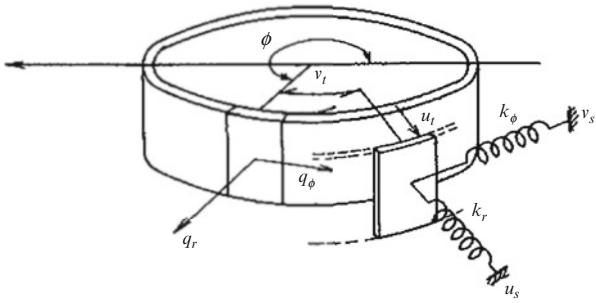

Fig. 5.10 Ring beam model of underground tank

5.3 Discussion of Underground Tank Deformation [4]

Observations of dynamic behaviors of the underground tank during earthquakes have shown that tank deformation is dominated by the ground strains. This section addresses the deformation of underground tanks using an analytical model. Given that the side wall and base slab are structurally separated, the tank is modeled as a ring beam per unit length in the depth direction, as shown in Fig. 5.10. Here, k_r and k_ϕ are soil spring coefficients (per unit length) in the radial and circumferential directions, respectively; u_t and v_t indicate tank displacement in the radical and circumferential directions; and q_r and q_ϕ are distributed loads per unit length in the circumferential direction of the tank.

q_r and q_ϕ are interaction forces between the ground and the tank. When ground displacement in the radial and circumferential directions is expressed as u_s and v_s, the result is

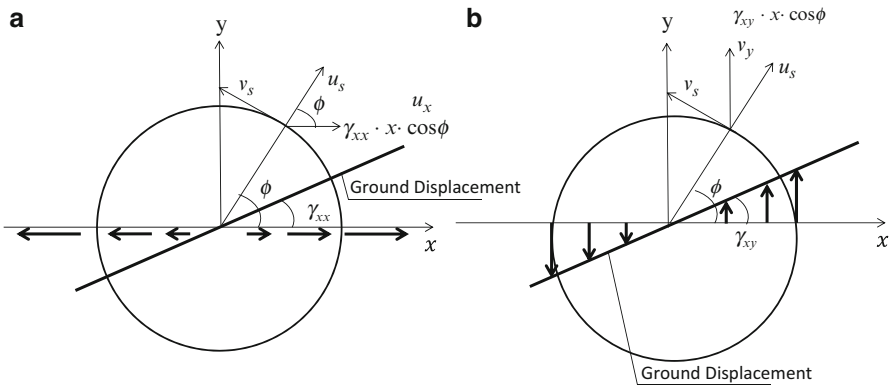

Fig. 5.11 Expression of ground displacements by cylindrical coordinates. (**a**) Ground displacement by normal strain of ground γ_{xx}. (**b**) Ground displacement by shear strain of ground γ_{xy}

$$q_r = k_r(v_s - v_t) \tag{5.3}$$

$$q_\phi = k_\phi(u_s - u_t) \tag{5.4}$$

When ground displacement has linear distribution only in the x direction, as shown in Fig. 5.11a, that is, when normal strain γ_{xx} in the x direction is constant, ground deformation u_x in that direction at central angle ϕ is

$$u_x = \gamma_{xx} \cdot x \cdot \cos\phi \tag{5.5}$$

and ground displacement at position ϕ at the central angle in the radial and circumferential directions u_s and v_s is determined as

$$u_s = \frac{1}{2}\gamma_{xx} \cdot r(\cos 2\phi + 1) \tag{5.6}$$

$$v_s = -\frac{1}{2}\gamma_{xx} \cdot r \cdot \sin 2\phi \tag{5.7}$$

The following equations express deformation of the ring beam under distributed loads per unit length q_ϕ and q_r in the circumferential and radial directions.

$$q_\phi = \frac{EI}{r^4}\left(\frac{\partial^3 u_t}{\partial\phi^3} + \frac{\partial u_t}{\partial\phi}\right) - \frac{EA}{r^2}\left(\frac{\partial^2 v_t}{\partial\phi^2} + \frac{\partial u_t}{\partial\phi}\right) \tag{5.8}$$

$$q_r = \frac{EI}{r^4}\left(\frac{\partial^4 u_t}{\partial\phi^4} + \frac{\partial^2 u_t}{\partial\phi^2}\right) + \frac{EA}{r^2}\left(\frac{\partial v_t}{\partial\phi} + u_t\right) \tag{5.9}$$

In the above equations, u_t and v_t are displacements of the ring beam in the radial and circumferential directions, respectively. E, I, A, and r indicate Young's modulus of the tank concrete, moment of inertia per unit length in the depth direction, sectional area, and radius, respectively. Taking Eqs. (5.6) and (5.7) as input displacement and substituting Eqs. (5.3), (5.4), (5.6), and (5.7) in Eqs. (5.8) and (5.9), ring beam deformation u_t and v_t are determined by the following, using orthogonal relation of the trigonometric functions.

$$u_t = \frac{1}{2}\gamma_{xx} \cdot r(e_0 + e_2 \cos 2\phi) \tag{5.10}$$

$$v_t = \frac{1}{2}\gamma_{xx} \cdot r \cdot f_2 \sin 2\phi \tag{5.11}$$

Coefficients of the above equations are as follows:

$$\begin{aligned} e_0 &= \frac{1}{1 + \dfrac{E}{k_r}\dfrac{A}{r^2}} \\ e_2 &= \frac{1}{\alpha_2}\left(1 + 4\frac{E}{k_\phi}\frac{A}{r^2} + 2\frac{E}{k_r}\frac{A}{r^2}\right) \\ f_2 &= \frac{1}{\alpha_2}\left(1 + \frac{E}{k_r}\frac{A}{r^2} + 2\frac{E}{k_\phi}\frac{A}{r^2} + 6\frac{E}{k_\phi}\frac{I}{r^4} + 12\frac{E}{k_r}\frac{I}{r^4}\right) \\ \alpha_2 &= 1 + \frac{E}{k_r}\frac{A}{r^2} + 4\frac{E}{k_\phi}\frac{A}{r^2} + 12\frac{E}{k_\phi}\frac{A}{r^2} + 36\frac{E}{k_\phi}\frac{E}{k_r}\frac{I}{r^4}\frac{A}{r^2} \end{aligned} \tag{5.12}$$

Similarly, as shown in Fig. 5.11b, with linear distribution of ground displacement in the y direction and taking γ_{xy} as ground shear strain in the $x - y$ plane, ground displacement in the y direction at central angle ϕ is

$$v_y = \gamma_{xy} \cdot x \cdot \cos\phi \tag{5.13}$$

Ground displacement u_s in the radial direction and v_s in the circumferential direction can be expressed by

$$u_s = -\frac{1}{2}\gamma_{xy} \cdot r \cdot \sin\phi \tag{5.14}$$

$$v_s = \frac{1}{2}\gamma_{xy} \cdot r(1 - \cos\phi) \tag{5.15}$$

Equations (5.14) and (5.15) can be used to determine ring beam deformation u_t and v_t, as shown in the following equations:

$$u_t = -\frac{1}{2}\gamma_{xy} \cdot r \cdot e_2 \sin 2\phi \tag{5.16}$$

$$v_t = \frac{1}{2}\gamma_{xy} \cdot r(1 - f_2 \cos 2\phi) \tag{5.17}$$

Coefficients e_2 and f_2 in the above equations are as indicated in Eq. (5.12).

Bending stress σ_M at the inner and outer edge of the ring beam and axial stress σ_N caused by axial force are determined by the following, with d the thickness of the ring beam:

$$\sigma_M = \pm\frac{E}{r^2} \cdot \frac{d}{2}\left(\frac{\partial^2 u_t}{\partial \phi^2} + u_t\right) \tag{5.18}$$

$$\sigma_N = \frac{E}{r}\left(\frac{\partial v_t}{\partial \phi} + u_t\right) \tag{5.19}$$

Based on ring beam calculations described above, Fig. 5.12 shows an example of tank deformation and stress at the inner and outer edges of the side wall. The tank is deformed by ground normal strain γ_{xx} into an ellipse, with x and y as the long and short axes; stress is also distributed elliptically. In addition, the tank is deformed by ground shear strain γ_{xy} into an ellipse with axes oriented 45° to the x and y axes.

Time histories of analytically determined strains are compared with those of observed strains in Fig. 5.13. The soil spring coefficients per unit area (coefficients of subgrade reaction K_r in the radial direction and K_ϕ in the circumferential direction) were taken as 4.90×10^3 kN/m^3 (0.5 kgf/cm^3) and 2.45×10^3 kN/m^3 (0.25 kgf/cm^3), respectively, and Young's modulus of concrete is 3.4×10^7 kN/m^2 (3.5×10^5 kgf/cm^2). Input ground strain was determined by dividing relative displacements at two observation points on the ground surface (shown in Figs. 5.7a and 5.8a) by the distance between those points. The time histories of analytically determined circumferential strains on the inner surface of the tank side wall agree well with observed values, demonstrating the validity of modeling the underground tank as a ring beam.

Figure 5.14 shows the ratios of circumferential strain on the inner surface of the tank side wall to ground strains, which are the strain transmission rates from the ground to the tank. These ratios can be expressed by the following non-dimensional parameters.

$$\beta = \frac{K_r}{E}\frac{r^2}{d}, \frac{d}{2r}, \frac{K_\phi}{K_r} \tag{5.20}$$

Here, K_r and K_ϕ are the coefficients of subgrade reaction in the radial and circumferential directions; r is tank radius; d is thickness of the tank side wall; and E is

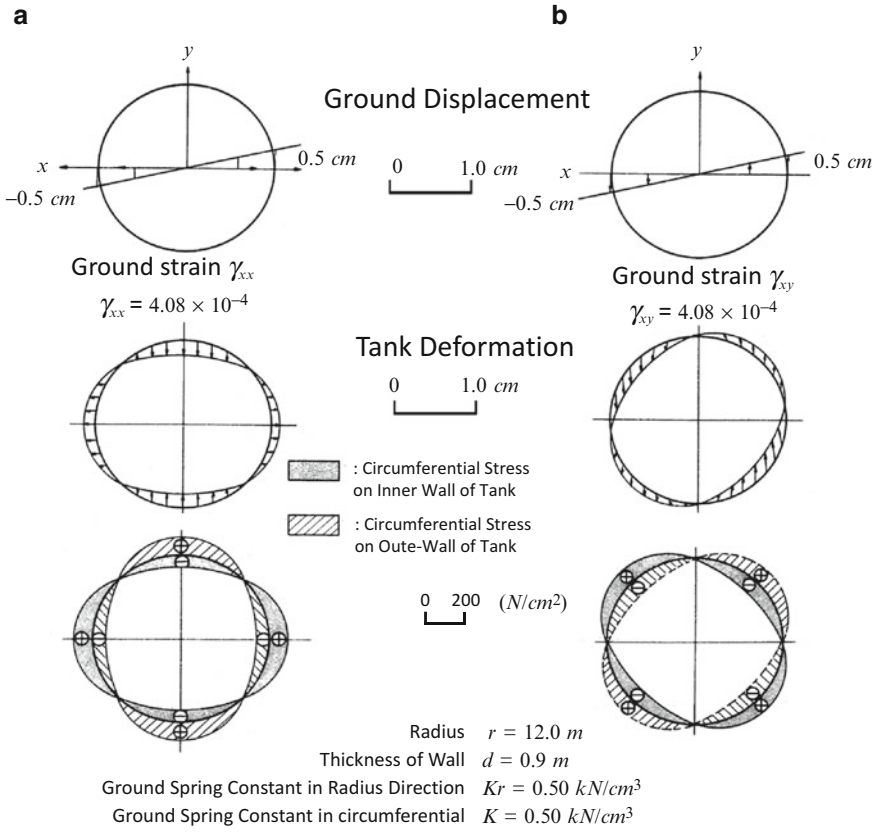

Fig. 5.12 Deformation and stress of tank caused by uniform ground strain. (**a**) Deformation and stress of tank by ground normal strain γ_{xx}. (**b**) Deformation and stress of tank by ground shear strain γ_{xy}

Young's modulus of concrete. If the ground strains γ_{xx} and γ_{xy} are known, stresses on the tank side wall can be determined by Fig. 5.14a, b.

Based on the measurement data and analytical results described above, it is possible to eliminate the terms for the dynamic effects of inertia and damping forces from Eq. (5.1). The following equation is used to obtain the deformation of underground structures:

$$\begin{bmatrix} & & \\ & K_{ij} & \\ & & \end{bmatrix} \begin{Bmatrix} X_1 \\ \vdots \\ X_i \\ \vdots \\ X_n \end{Bmatrix} = \begin{bmatrix} s_1 & & & \\ & \ddots & & \\ & & s_i & \\ & & & \ddots \\ & & & s_n \end{bmatrix} \begin{Bmatrix} x_1 - X_1 \\ \vdots \\ x_i - X_i \\ \vdots \\ x_n - X_n \end{Bmatrix} \tag{5.21}$$

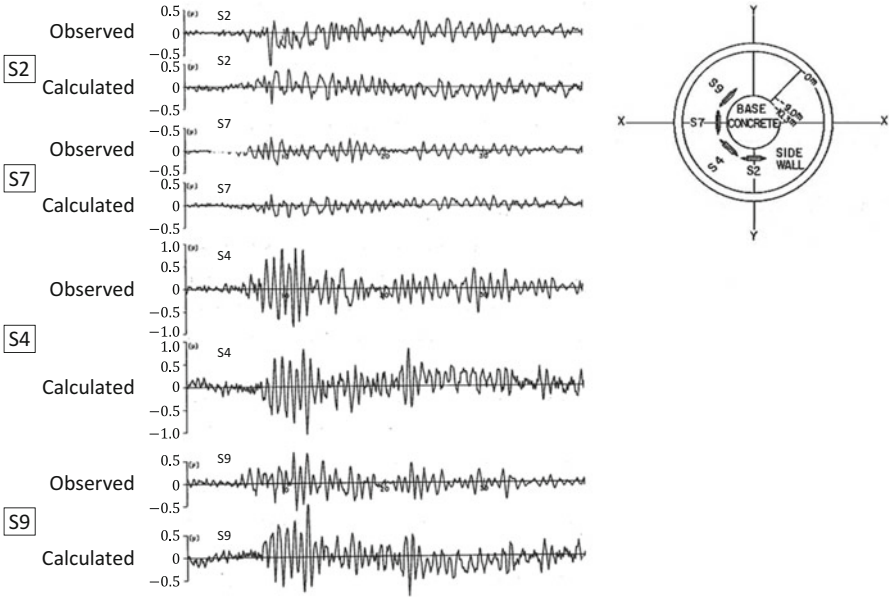

Fig. 5.13 Calculated circumferential strains of the tank under comparison with the observed strains

In addition, assuming only a small effect of the second term on the right side of the ground vibration of Eq. (5.2), the following ensues.

$$\begin{bmatrix} m_1 & & & & \\ & \ddots & & & \\ & & m_i & & \\ & & & \ddots & \\ & & & & m_n \end{bmatrix} \begin{Bmatrix} \ddot{x}_1 \\ \vdots \\ \ddot{x}_i \\ \vdots \\ \ddot{x}_n \end{Bmatrix} + \begin{bmatrix} & & & & \\ & & & & \\ & & l_{ij} & & \\ & & & & \\ & & & & \end{bmatrix} \begin{Bmatrix} \dot{x}_1 \\ \vdots \\ \dot{x}_i \\ \vdots \\ \dot{x}_n \end{Bmatrix} + \begin{bmatrix} & & & & \\ & & & & \\ & & k_{ij} & & \\ & & & & \\ & & & & \end{bmatrix} \begin{Bmatrix} x_1 \\ \vdots \\ x_i \\ \vdots \\ x_n \end{Bmatrix}$$

$$= - \begin{bmatrix} m_1 & & & & \\ & \ddots & & & \\ & & m_i & & \\ & & & \ddots & \\ & & & & m_n \end{bmatrix} \begin{Bmatrix} 1 \\ \vdots \\ 1 \\ \vdots \\ 1 \end{Bmatrix} \ddot{y}(t) \tag{5.22}$$

The deformation of underground structures can be determined by inputting ground displacements through the soil springs. This concept is the basis of the response displacement method, which will be described later.

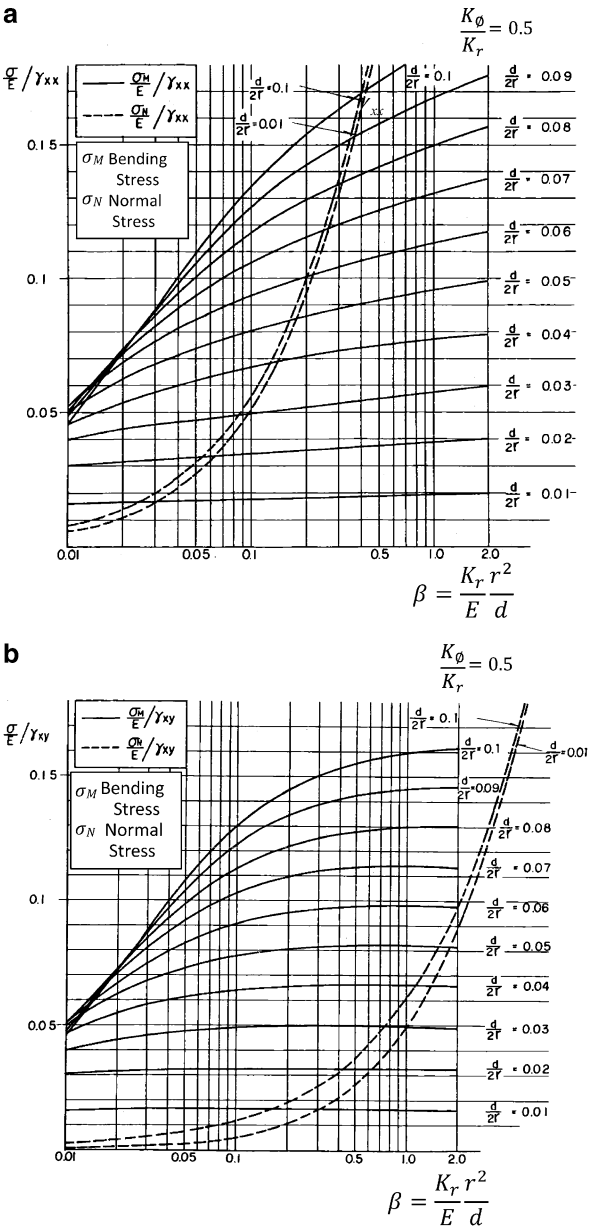

Fig. 5.14 Ratio of tank strains to ground strains γ_{xx}, γ_{xy}. (**a**) Ratio of tank strain to ground normal strain γ_{xx}. (**b**) Ratio of tank strain to ground strain γ_{xy}

5.4 Observation of the Dynamic Behavior of Submerged Tunnels

5.4.1 Structures of Submerged Tunnels and the Ground Condition [5]

Deformation behavior during earthquakes was observed in two submerged tunnels in Tokyo Port, as shown in Fig. 5.15 (referred as Tunnels A and B). Total lengths of these tunnels are 1,035 and 744 m, respectively, and each consists of submerged elements having flexible joints: nine 110 m elements in Tunnel A, and six 124 m elements in Tunnel B. As shown in Fig. 5.16, the cross section of a submerged element is rectangular. Tunnel A has a large cross section of 37.4 m width with a six-lane roadway, and Tunnel B has a medium cross section of 28.4 m with a four-lane roadway.

Figure 5.17 shows that the joints of Tunnel B consist of PC cable, making them highly flexible compared with those of Tunnel A, which consists of steel shear keys and concrete mortar.

Figure 5.18 shows soil conditions along the tunnels. Most of Tunnel A is within a soft alluvial clay layer (Ac) with shear wave velocity about 150 m/s, and Tunnel B is within a diluvial clay layer (Dc) with shear wave velocity approximately 200 m/s. Thus, Tunnel B was constructed in ground that is somewhat harder than that of Tunnel A. At both tunnel locations, a tertiary layer with shear wave velocity more than 600 m/s is found at depths 50–60 m beneath the ground surface. There are ventilation towers at both ends of the tunnels, and joints between these ventilation

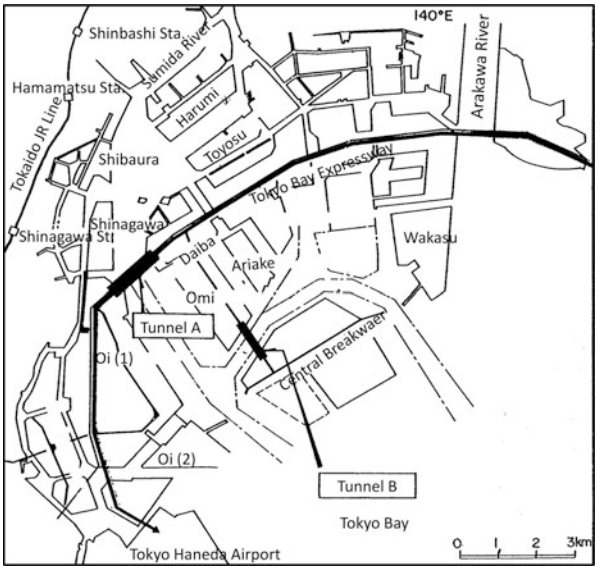

Fig. 5.15 Two submerged tunnels for earthquake observation in Tokyo Port

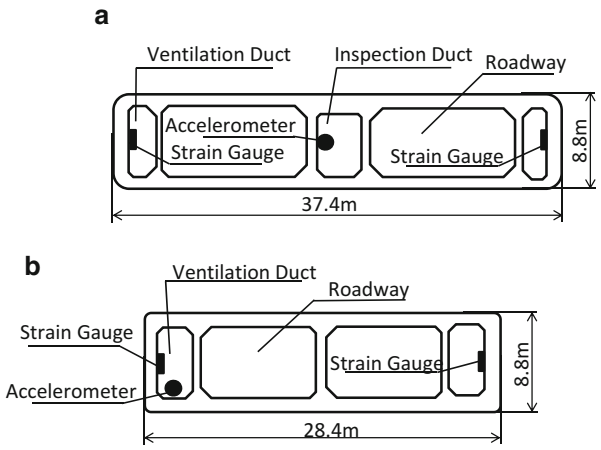

Fig. 5.16 Cross section of submerged elements. (**a**) Tunnel A. (**b**) Tunnel B

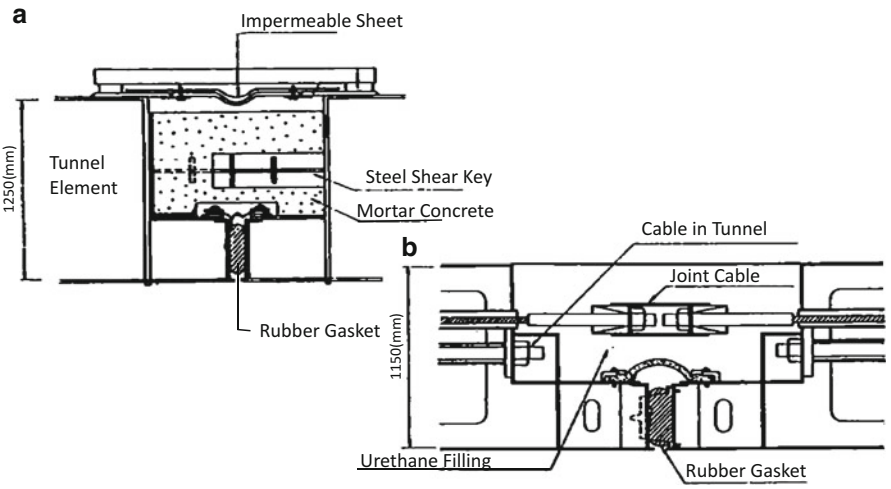

Fig. 5.17 Joints between tunnel elements. (**a**) Tunnel A. (**b**) Tunnel B

towers and tunnel elements are extremely flexible, making them free ends in structural terms.

Accelerations were observed at the ground surface, bedrock, and in both tunnels, at the points A1-A4 in Fig. 5.18. Strains in the axial direction were measured on side walls of ventilation ducts on both sides of the roadways, denoted by S points in the figure. Axial strain caused by deformation of the tunnels in the axial direction can be determined by calculating average strains on both side walls; strain caused by bending deformation of the tunnels around the vertical axis can be determined by taking the difference between strains on both side walls.

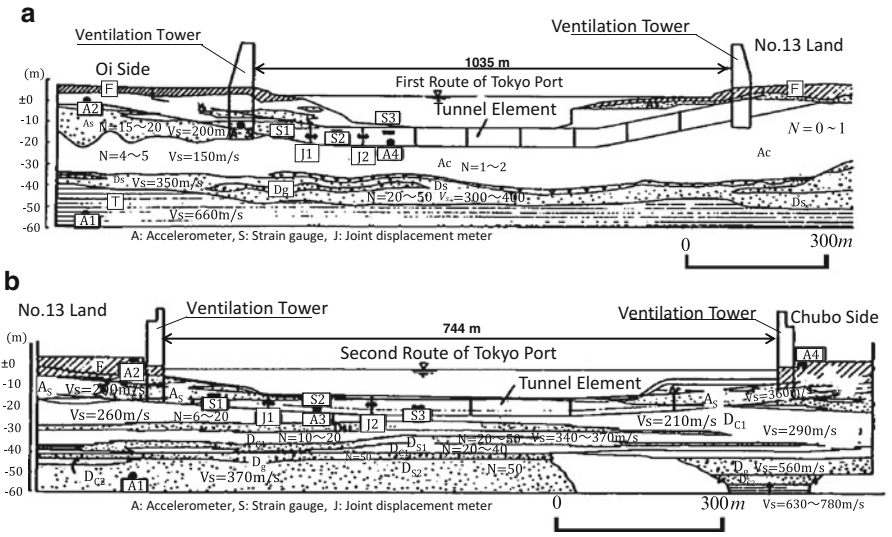

Fig. 5.18 Soil conditions along two tunnels. (**a**) Tunnel A. (**b**) Tunnel B

5.4.2 *Deformation Behavior of Submerged Tunnels During Earthquakes [6]*

Figure 5.19 shows acceleration (*x*: tunnel axis direction, *y*: horizontal direction, perpendicular to tunnel axis), strains by axial deformation, and strains by bending deformation around the vertical axis of Tunnel B during an earthquake on May 9, 1974 off Izu Peninsula (moment magnitude Mw = 6.9, epicentral distance 80 km, focal depth 10 km). These data indicate the following regarding characteristics of strain in the tunnel. The principal motion of accelerations (A2x, A2y) occurred over an interval of 0–30 s, but strains by axial deformation (S1, S3 in Fig. 5.19b) were large in the later period of earthquake motion (after about 60 s). However, bending strains (S1, S3 in Fig. 5.19c) were predominant during the principal motion of accelerations. These observational results indicate that axial deformation of the tunnel is not dependent on the acceleration of earthquake motion, and strain by bending deformation is correlated with that acceleration. In addition, the amplitude of strains by axial deformation was two to three times larger than that by bending deformation.

Figure 5.20 shows a time history of Tunnel A velocity of in the axial direction (V4*x* in the figure), and strain by axial deformation of tunnel element 1 (S1) during an earthquake on September 25, 1980 in Chiba Prefecture (moment magnitude Mw = 6.1, epicentral distance 40 km, focal depth 80 km). The velocity (V4*x*) and axial strain (S1) had very similar time histories and the same phases. Figure 5.21 shows velocity in the axial direction at the ground surface (V2x) and strain by axial deformation of tunnel element 3 (S3) of Tunnel A during the Izu Peninsula offshore earthquake mentioned above. The axial strain time history was similar to the velocity, but their phases were mostly reversed.

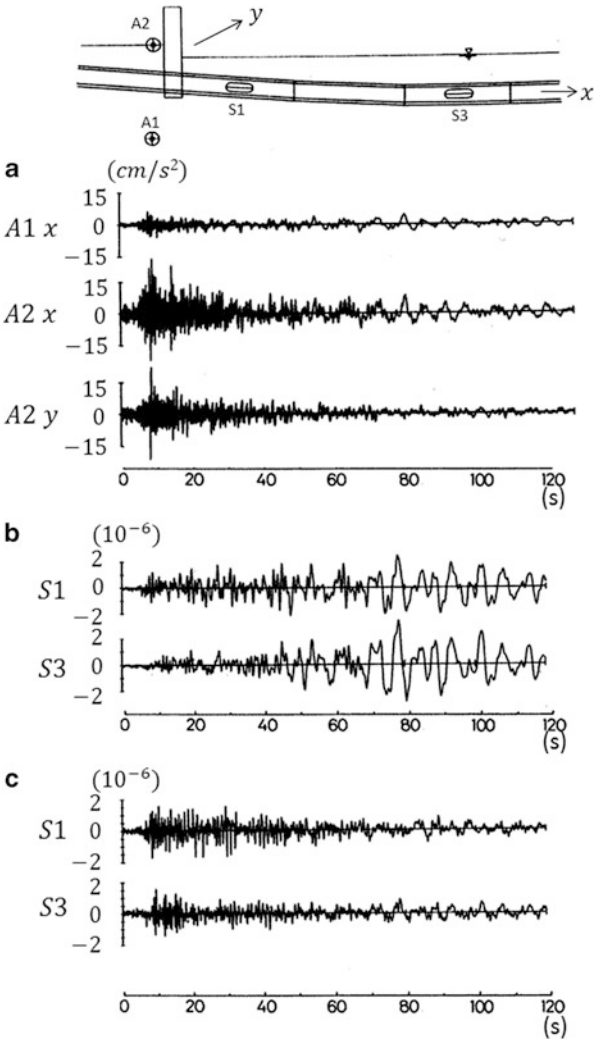

Fig. 5.19 Accelerations and strains by axial and bending deformations (1974 Off-Izu Peninsula earthquake). (**a**) Accelerations. (**b**) Strains by axial deformation. (**c**) Strains by bending deformation

The observational data above can be interpreted as follows. As shown in Fig. 5.22, ground displacement by seismic wave propagation is indicated by V_G for displacement in the axial direction, and U_G for displacement perpendicular to the tunnel axis. In each case, by indicating the wave propagation velocity along the tunnel axis as c_v and c_u, the respective wave motions can become

$$V_G = f\left(t - \frac{x}{c_v}\right) \tag{5.23}$$

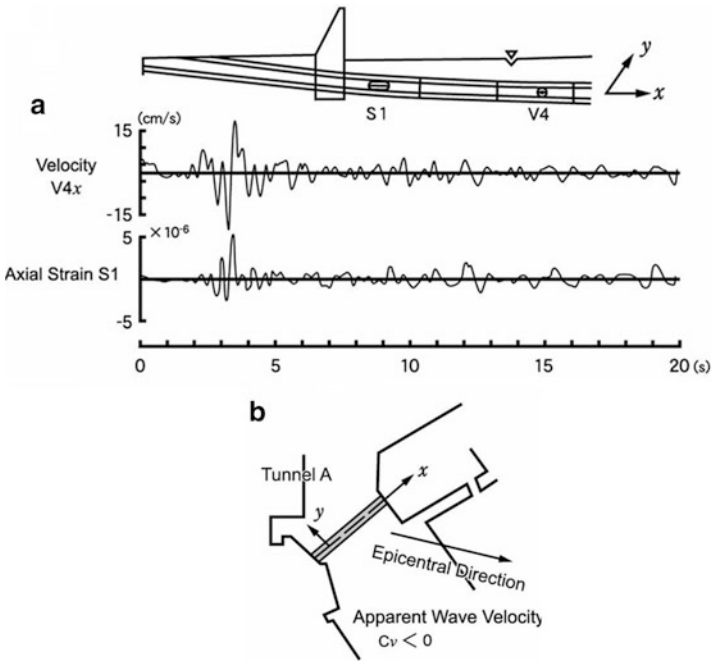

Fig. 5.20 Velocity in the axial direction and strain by axial deformation of Tunnel A (1980 Chiba prefecture earthquake). (**a**) Velocity and axial strain. (**b**) Location of tunnel A and epicentral direction

$$U_G = g\left(t - \frac{x}{c_u}\right) \tag{5.24}$$

Here, x is the coordinate along the tunnel axis (indicated by x in observational data); for Tunnel A, the direction shown in Figs. 5.20b and 5.21b is taken as positive. c_v and c_u indicate apparent propagation velocity along the tunnel axis of vibration components parallel and perpendicular to that axis, respectively. Based on Eq. (5.23), normal strain γ_{xx} of ground in the X-direction is expressed as

$$\begin{aligned} \gamma_{xx} &= \frac{\partial V_G}{\partial x} \\ &= -\frac{1}{c_v}\frac{\partial V_G}{\partial t} \end{aligned} \tag{5.25}$$

Based on Eq. (5.24), the rate of curvature ρ of bending deformation of ground rotation around the vertical axis is expressed as

$$\begin{aligned} \rho &= \frac{\partial^2 U_G}{\partial x^2} \\ &= \frac{1}{c_u^2}\frac{\partial^2 U_G}{\partial t^2} \end{aligned} \tag{5.26}$$

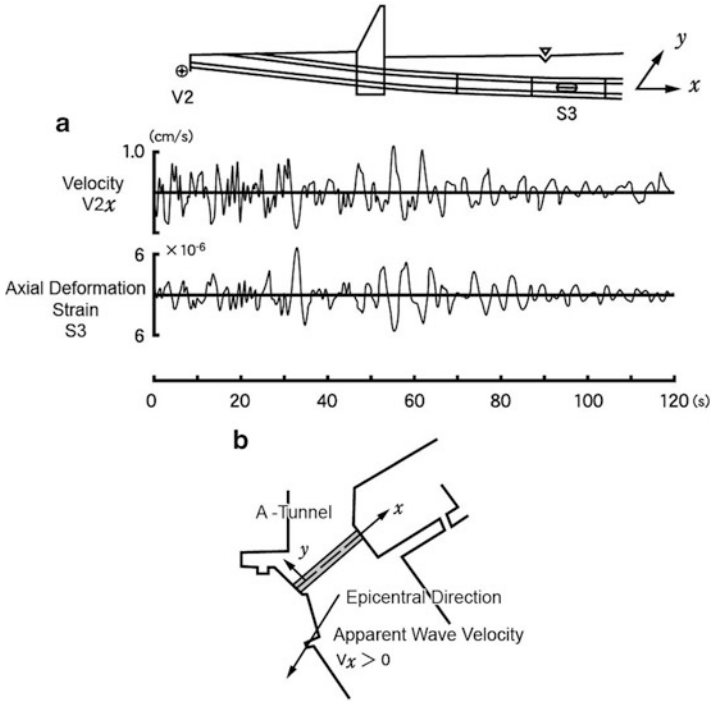

Fig. 5.21 Velocity in the axial direction at ground surface and strain by axial deformation of Tunnel A (1974 Off Izu Peninsula earthquake, Tunnel A). (**a**) Velocity and strain. (**b**) Location of tunnel A and epicentral direction

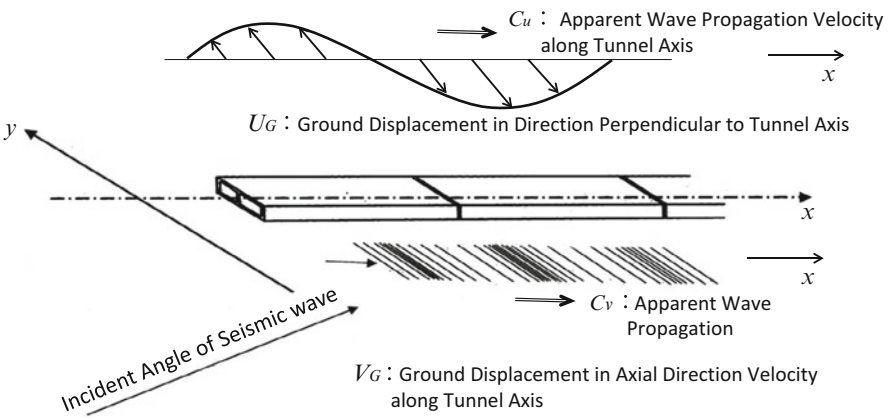

Fig. 5.22 Seismic wave propagation along tunnel axis

Equation (5.25) indicates the similarity between seismic motion velocity in the x direction $\frac{\partial V_G}{\partial t}$ (called particle velocity) and normal strain γ_{xx} of the ground in the x direction. When apparent propagation velocity c_v is positive, phases of the velocity and ground strain are inverted, and they have the same phases when c_v is negative. Equation (5.26) indicates the similarity between the rate of curvature of bending deformation of ground and acceleration perpendicular to the tunnel axis.

As shown in Figs. 5.20 and 5.21, because of the relationship of Tunnel A to the epicenter, apparent propagation velocity was positive in the Izu Peninsula offshore earthquake and negative in the Chiba Prefecture earthquake. The observational data represented in Figs. 5.20 and 5.21 can be understood by considering that strain by deformation in the tunnel axial direction was induced by ground strain. In addition, as shown in Fig. 5.19c, strain by bending deformation of the tunnel was predominant during the principal part of the acceleration. This indicates that strain owing to bending deformation is governed by acceleration. Eq. (5.26) supports this deduction.

5.5 Dynamic Behavior and Analysis of Rock Caverns [7, 8]

5.5.1 Earthquake Resistance of Rock Caverns

There has been little attention paid to the stability of caverns excavated from rock during earthquakes, such as underground power stations and mountain tunnels. This is because the inherent seismic stability of rock caverns has been considered empirically guaranteed as long as the excavation work is performed safely, and seismic motion within rock has generally been smaller than that of quaternary ground strata such as alluvial layers. Indeed, for underground caverns such as power stations constructed within hard rock, there have been no reports of major damage similar to that of aboveground structures. Although earthquakes have caused damage to tunnels, most such damage has occurred at portals in deposits of talus and at intersections with faults or weak strata. No damage has occurred in hard rock.

Compared with conventional rock caverns, a higher level of earthquake resistance is required in rock caverns for storage of oil and high-level radioactive waste, which are being planned for construction. Therefore, it is necessary to study the stability of rock caverns during earthquakes.

5.5.2 Behavior of Mountain Tunnels During Earthquakes

Figure 5.23 shows the tunnel where earthquake observation was conducted, along with the placement of strain gauges and accelerometers. The tunnel has a horseshoe-shaped cross section for a railway track, and thickness of the concrete lining is about

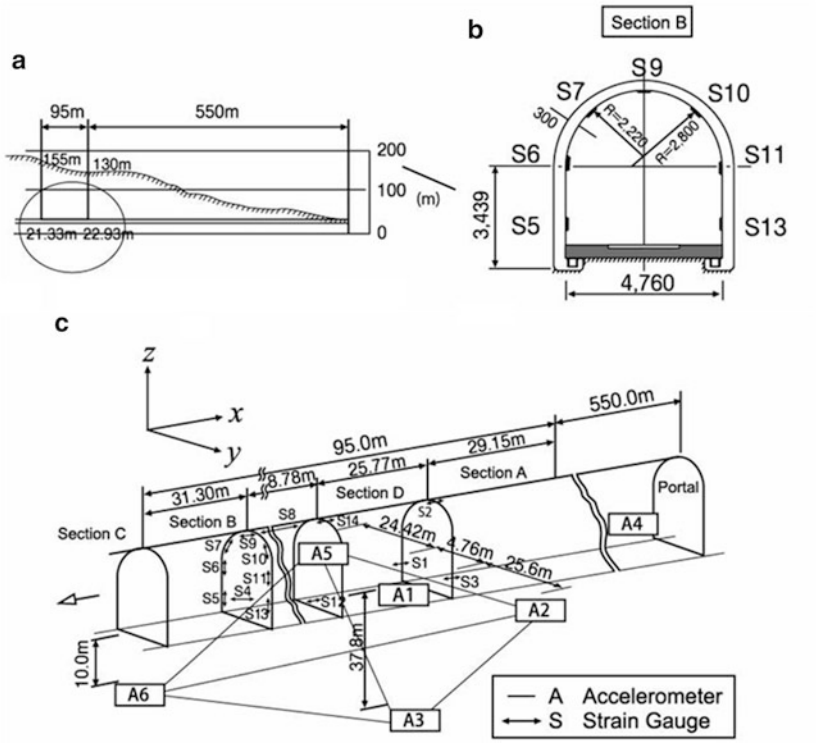

Fig. 5.23 Allocation of measurement instruments for observation of dynamic deformation of a tunnel during earthquakes. (**a**) Zone for observation. (**b**) Cross-section of the tunnel. (**c**) Allocation of measurement instruments

30 cm, the design value. The ground consists of stable slate without major groundwater flow; based on indoor rock testing, its shear wave velocity is 2.7–3.6 km/s and unconfined compressive strength is 49–225 MPa (500–2,300 kg/cm^2).

Total length of the tunnel is 4,600 m. A segment 550 m inward from the portal was observed. Tunnel depth at the observation segment is 110–130 m, and talus and topsoil cover the surface to a depth about 10 m.

Accelerations in three directions were observed at the portal (A4), in the tunnel (A1) and within the rock (A2, A3, A5 and A6). Four accelerometers within the rock were placed in horizontal and vertical boreholes from the tunnel, and these were arranged at the vertices of a triangular pyramid. The size of the rock in this pyramid was 66 m in the axial direction, 55 m in the horizontal, and 41 m in the vertical.

Strains in the direction of the tunnel axis and in the cross-sectional direction were measured along the tunnel axis and perpendicular direction by 13 strain gauges (S1–S13) situated on the inner surface of the concrete lining. Relative displacement in the axial direction was measured (S14) at joints of the concrete lining, at 12 m intervals. The strain gauges were made of 50 cm steel bars and

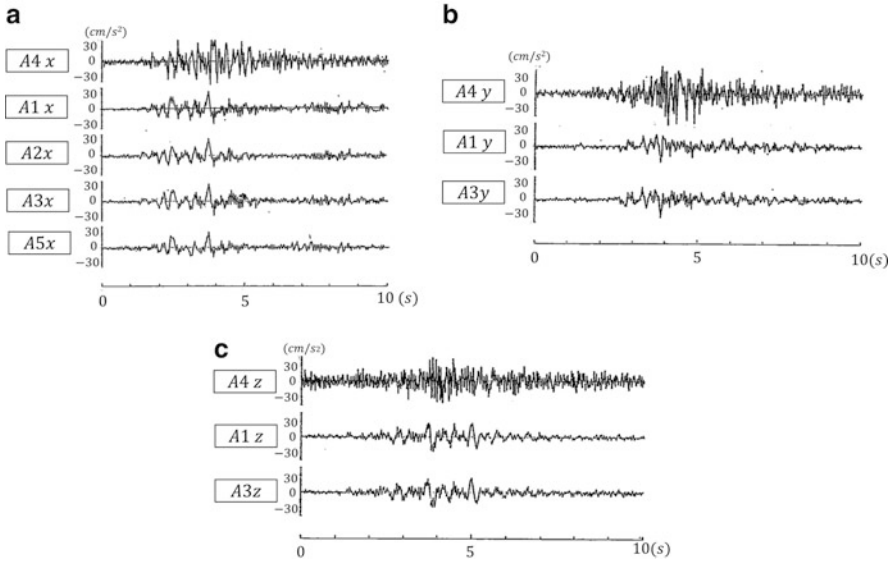

Fig. 5.24 Accelerations observed at the portal *A*4 and in the rock (*A*1, *A*2, *A*3, *A*5): (**a**) *x* direction (axial direction), (**b**) *y* direction (the direction perpendicular to tunnel axis), and (**c**) *z* direction (vertical direction)

differential transformers, and laboratory testing verified that the gauges were capable of measuring strain of 0.2×10^{-6} (Fig. 5.5).

During an observation period of approximately 4 years, there were 11 observed earthquakes with JMA seismic intensity of 2 or more. Figure 5.24 shows acceleration from an earthquake that produced the largest strain (June 1, 1982; Kesennuma offshore earthquake, moment magnitude Mw = 6.3, focal depth 40 km, epicentral distance 65 km). *x*, *y*, and *z* in the figure indicate the tunnel axis direction, horizontal direction perpendicular to the tunnel axis, and the vertical direction, respectively.

The accelerations in the axial direction (Fig. 5.24a) reveal very similar waveforms at each of the four measurement points in the rock (A1, A2, A3 and A5), indicating that seismic motion was practically uniform within this region. The same results are obtained from accelerations in the *y* and *z* directions (Fig. 5.24b, c). These results demonstrate that the reflection and scattering of seismic waves on the surface of the rock cavern did not affect motions at three observation points in the rock (A1 and A3), which were distant from the cavern by as much as 5–6 times the cavern width.

Figure 5.25 shows maximum acceleration at portal (A4) in relation to that at a measurement point in the tunnel (A1). The amplification factor of acceleration at the portal is 1.5–3.0 times in both horizontal directions, and 1.0–3.0 times in the vertical. One reason for this amplification at the portal is the fact that it is a free surface, and another is the fact that the rock surface is covered by talus and topsoil to about 10-m depth.

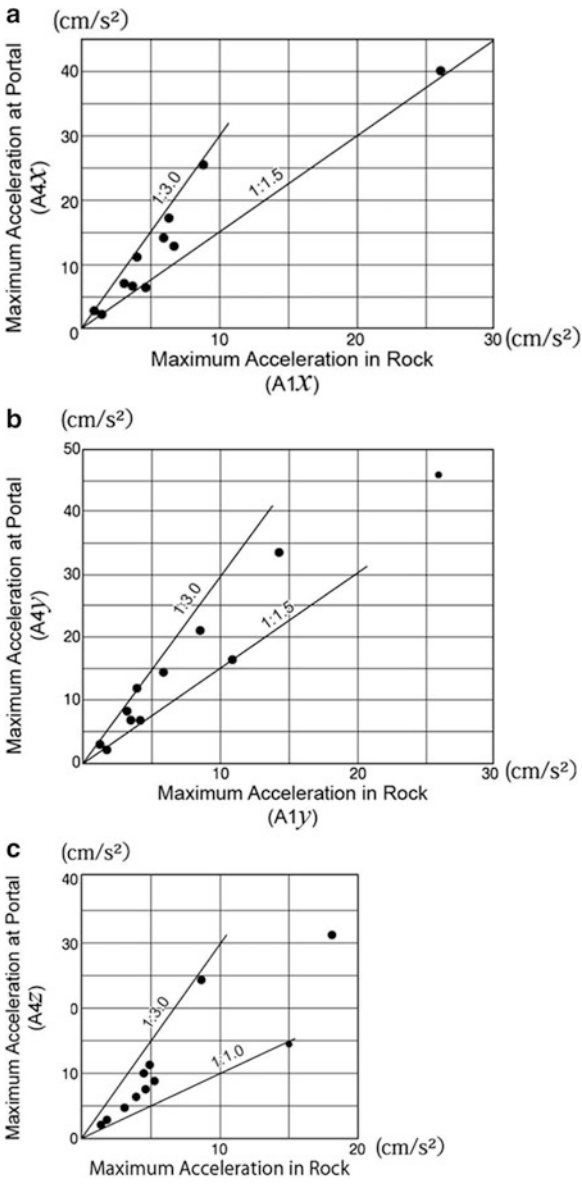

Fig. 5.25 Amplification of acceleration at portal: (**a**) *x* direction (axial), (**b**) *y* direction (lateral), and (**c**) *z* direction (vertical)

In earthquake observations of underground power stations, Komada and Hayashi [9] reported that the amplification factor of acceleration at the ground surface was 1.0–3.0 in the horizontal direction, while that in the vertical was somewhat less, close to 1.0. Observations by Okamoto [10] also indicated that the ratio of maximum acceleration at the ground surface to maximum acceleration in the rock ranges from 1.0 to 3.0, with an average value near 2.0. These findings suggest that seismic

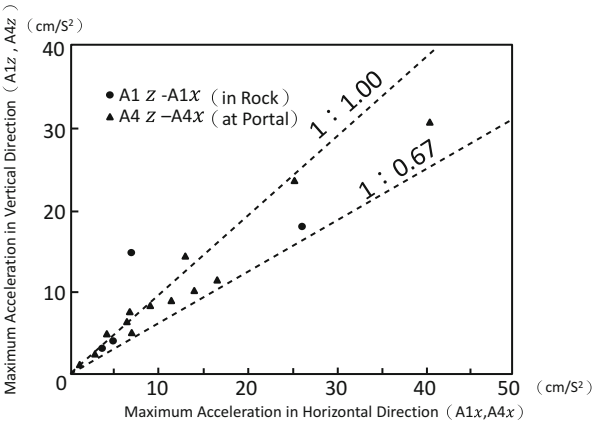

Fig. 5.26 Maximum accelerations in vertical and horizontal directions

intensity used in earthquake-resistant design for underground structures within rock can be somewhat lower than that for aboveground structures.

Figure 5.26 shows the ratio of maximum vertical acceleration to maximum horizontal acceleration. This ratio does not differ greatly between the portal and regions within the rock, and the distribution is about 0.7 or higher. As mentioned above, Komada and Hayashi reported that the ratio of maximum acceleration in the vertical to horizontal was 1:2 or more. Noda and Uwabe [11] indicated that the ratio of maximum acceleration in the vertical to horizontal was 1:2 or less, on average. A reason for this difference may be that most of the records used by Noda and Uwabe were observed on relatively flat ground, whereas those by Komada and Hayashi were obtained in complex topography.

5.5.3 *Deformation Characteristics of Mountain Tunnels During Earthquakes*

Figure 5.27 shows strain records of an aftershock of the 1978 Miyagi Prefecture offshore earthquake (June 21, 1978; off Kesennuma, moment magnitude Mw = 5.8, focal depth 50 km, epicentral distance 110 km). Fig. 5.27a shows strains in the axial direction (S1 and S4) and relative displacement at a concrete construction joint (S14). S1 and S4 indicate strains at two points approximately 35 m distant, and S14 indicates relative displacement of the joint within this section. These three time histories are all similar in shape, showing that tensile and compressive deformation was basically uniform in this part of the tunnel.

Figure 5.27b shows strains in the cross-sectional direction at the arch crown (S9) and side walls (S5, S6 and S11). Time histories of strains at these four points are very similar. However, the phase of the strain at the arch crown (S9) is reversed to those of the strains on the side walls (S5, S6 and S11). Strains on both side walls

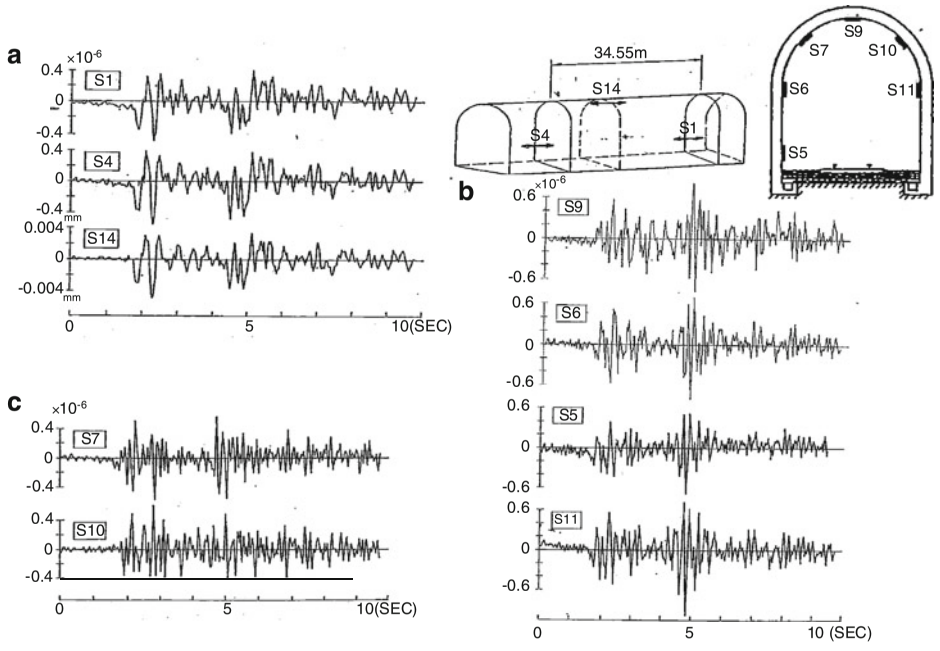

Fig. 5.27 Strains of concrete lining of the tunnel and joint displacement (1978 Miyagi prefecture offshore earthquake, Mw: 5.8, epicentral distance: 50 km, focal depth: 110 km). (**a**) Axial strains and joint displacement. (**b**) Circumferential strains of tunnel in cross section (S9, S5, S6, S11). (**c**) Circumferential strains of tunnel in cross section (S7, S10)

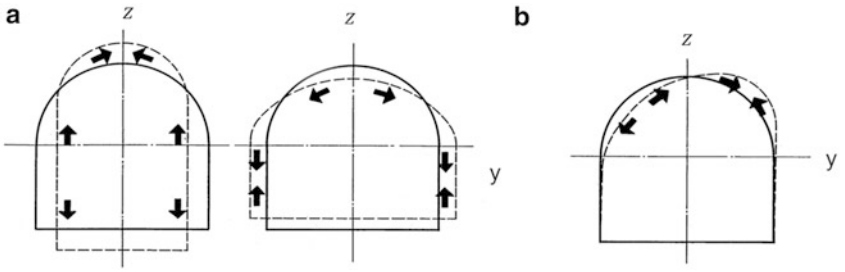

Fig. 5.28 Deformation modes of cross section of the tunnel during earthquakes. (**a**) Symmetrical deformation with respect to z axis. (**b**) Asymmetric deformation with respect to z axis

facing each other (S6 and S11) was of the same phase. Figure 5.27b reveals that the deformation mode that caused the strains on the side walls and the strain at the arch crown appeared symmetric with respect to the vertical axis z, as shown in Fig. 5.28a.

Figure 5.27c shows strains in the cross-sectional direction at two observation points at a 45° angle (S7 and S10) to the horizontal axis y. Time histories of the strains at these two points were similar, but their phases were mostly reversed. Therefore, the deformation mode that induces strains appears asymmetrical with respect to the z axis, as shown in Fig. 5.28b.

Observation of the behaviors of the underground tank and submerged tunnels during earthquakes shows that the deformation and strains of underground structures during earthquakes is dominated by the relative displacements of surrounding ground, or by ground strains. Deformation of the lining of the tunnel, which was excavated within hard rock, also appears dominated by surrounding ground strains. Based on this, four accelerometers (A2, A3, A5 and A6) were arranged in the rock as shown in Fig. 5.23c to detect relative displacements of the surrounding rock during earthquakes, namely, dynamic strains. However, the distance between measurement points was only several dozens of meters, and this was not distant enough to detect strains with sufficient accuracy.

Therefore, the time histories of strains generated in the rock were estimated by the following procedure.

(i) Identifying the incident angle of seismic waves:
Data on three components of acceleration (x, y, z) observed in the tunnel (at point A1) were used to determine the principal axes of ground motion and identify the incident angle of seismic waves.

(ii) Calculating incident P wave, SV wave, and SH wave:
P wave (wave of motion at the incident angle), SV wave (wave of motion perpendicular to the incident angle, in the vertical plane), and SH wave (wave of motion perpendicular to the incident angle, in the horizontal plane) were calculated by the three-dimensional components (x, y, z) at the observation point A1.

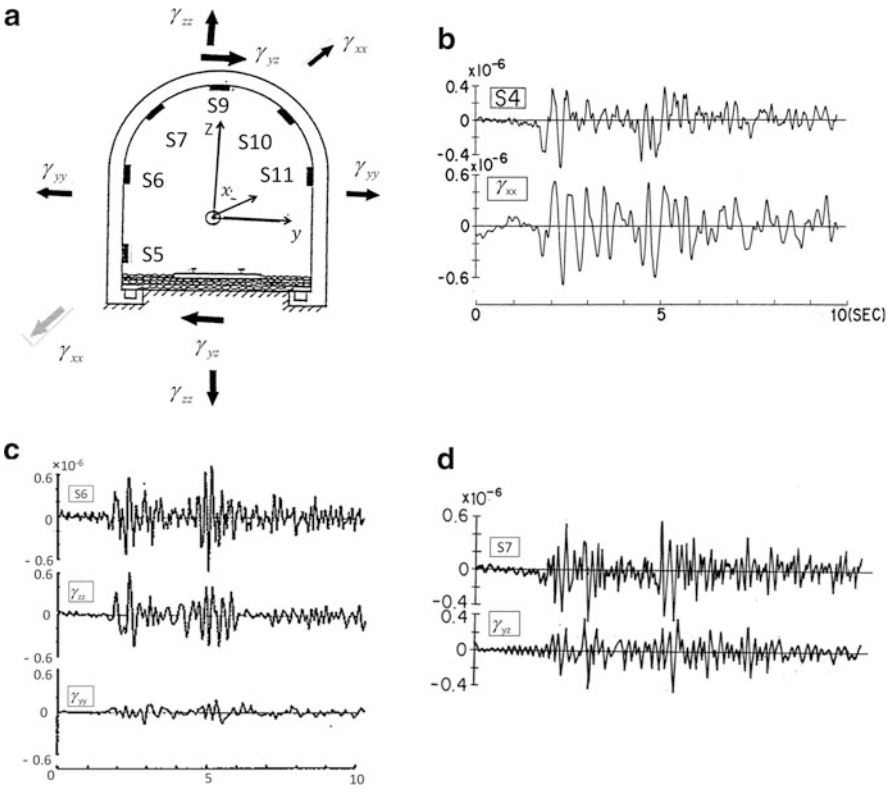

Fig. 5.29 Strains of rock and the tunnel. (**a**) Four-dimensional components of rock strains. (**b**) Axial strain of tunnel (S4) and normal strain of rock γ_{xx}. (**c**) Strain in cross-sectional direction (S6) and normal strains of rock (γ_{yy}, γ_{zz}). (**d**) Strain in cross-sectional direction of tunnel (S7) and shear strain of rock (γ_{yz})

(iii) Calculating the time histories of reflection waves from the ground surface, and of six components of strain in three-dimensional space in the rock:
The reflection waves of the P, SV and SH waves from the ground surface were determined (the ground surface was assumed horizontal, and depth of the measurement point from that surface was assumed to be 130 m); these were combined with the incident waves to determine the six components of strain in three-dimensional space.

Figure 5.29 shows rock strains based on the above procedure, in comparison with strains in the tunnel lining. Figure 5.29b shows that strain in the axial direction (S4) was very similar to normal strain γ_{xx} in the x direction of the rock. Axial strain on the tunnel (S4) was relatively small at 60–70 % of strain γ_{xx} on the rock. The reason seems to be that some of the rock strain was absorbed by the concrete construction joints placed every 12 m.

Based on the symmetry of deformation about the z axis, strains on the arch crown (S9) and side walls (S6 and S11) appear to be dominated by normal strain γ_{yy} and γ_{zz}

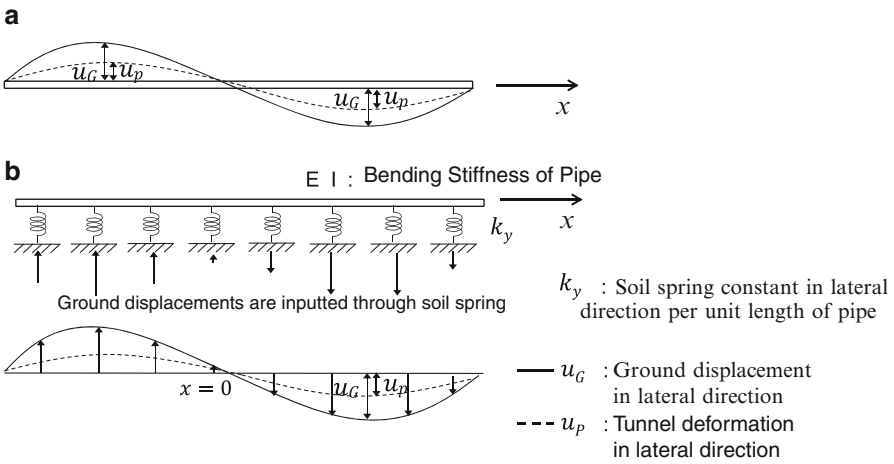

Fig. 5.30 The concept of response displacement method and beam model on elastic foundation. (**a**) Ground displacement and pipe deformation. (**b**) A beam model on elastic foundation

on the cross section (planes y and z in Fig. 5.29a). Normal strain γ_{yy} in the y direction was much less than the rock strain γ_{zz}, because the incident angle of ground motion was approximately perpendicular to the y axis. Therefore, in this earthquake, normal strain γ_{zz} in the z direction governed the symmetrical deformation of the cross section. Figure 5.29c reveal strong correlation between strain on the side walls (S6) and normal strain γ_{zz} in the vertical. Strain observed in the tunnel was somewhat greater than that in the rock, indicating that the cavity shape had an amplifying effect on strain.

Strains in the cross-sectional direction at the point of the arch at a 45° angle (S7 and S10) were caused by shear strain γ_{yz} in planes y and z, because the deformation causing the strains at these two points was asymmetrical about the z axis. This conclusion is supported by the similarity of strain in the lining (S7) and rock strain γ_{yz}, as shown in Fig. 5.29d. Again, strain observed in the tunnel lining was greater than that in the rock, indicating that the rock strain was amplified by the cavity.

5.6 Response Displacement Method

5.6.1 Concept of the Response Displacement Method

Based on the observation of dynamic behaviors of an underground tank, undersea tunnels, and a rock tunnel during earthquakes, it has become clear that the deformation of underground structures is governed by strain in the surrounding ground. The response displacement method has been proposed based on this observational result.

The concept behind this method is shown in Fig. 5.30a, using the example of a buried pipe. Here, $u_G(x)$ is ground displacement perpendicular to the pipe axis at

a given time, and x is a coordinate indicating the axial direction. Deformation of the pipe $u_p(x)$ when subjected to ground displacement depends on the following relationships.

When the buried pipe has sufficiently high stiffness and ground stiffness is low:

$$u_p(x) \rightarrow 0$$

If pipe stiffness is very low, but the ground has sufficiently high stiffness:

$$u_p(x) \rightarrow u_G(x)$$

A model of a beam on an elastic foundation (Fig. 5.30b) can be used to appropriately express the relationship between ground displacement and buried pipe deformation. The pipe is modeled as a beam with bending stiffness and the ground as a spring. The soil spring constant is determined by stiffness of surrounding ground. Ground displacement $u_G(x)$ is inputted though the soil spring to determine deformation $u_p(x)$. This procedure satisfies the characteristics of buried pipe deformation in accord with the stiffness of the buried pipe and the ground, as described above.

The deformation $u_p(x)$ can be derived from

$$EI\frac{d^4u_P}{dx^4} + k_y u_P = k_y u_G \tag{5.27}$$

In this equation, EI is bending stiffness of the pipe, and k_y is the soil spring constant perpendicular to the pipe axis per unit length of the pipe.

That equation can be modified as

$$\frac{d^4u_P}{dx^4} + 4\beta_y^4 u_P = 4\beta_y^4 u_G \tag{5.28}$$

in which

$$\beta_y = \sqrt[4]{\frac{k_y}{4EI}} \tag{5.29}$$

The general solution to Eq. (5.28) can be obtained as

$$\begin{aligned} u_P(x) = {} & \exp(\beta_y x)\left(C_1 \cos\beta_y x + C_2 \sin\beta_y x\right) \\ & + \exp(-\beta_y x)\left(C_3 \cos\beta_y x + C_4 \sin\beta_y x\right) \end{aligned} \tag{5.30}$$

C_1–C_4 are integration constants derived from boundary conditions. Now, taking ground displacement $u_G(x)$ as a sinusoidal wave of wave length L and amplitude $\overline{u}_G$:

$$u_G(x) = \overline{u}_G \cdot \sin\frac{2\overline{u}}{L}x \tag{5.31}$$

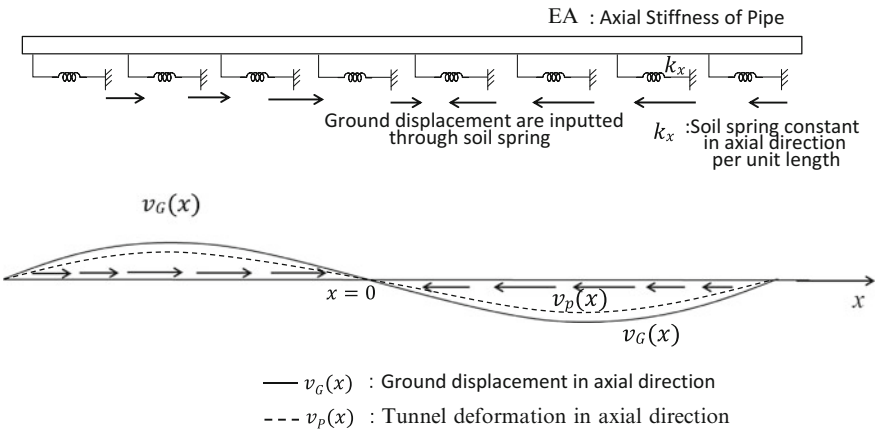

Fig. 5.31 Model for numerical analysis of deformation of buried pipe in axial direction

All the integral constants $C_1 - C_4$ of Eq. (5.30) equal zero, and the particular solution of $u_p(x)$ can be determined by

$$u_P(x) = \frac{4\beta_y^4}{4\beta_y^4 + \left(\frac{2\pi}{L}\right)^4} \overline{u}_G \cdot \sin \frac{2\pi}{L} x \tag{5.32}$$

Bending moment $M(x)$ generated in the buried pipes is obtained by

$$\begin{aligned} M(x) &= -EI \frac{d^2 u_P}{dx^2} \\ &= EI \left(\frac{2\pi}{L}\right)^2 \frac{4\beta_y^4}{4\beta_y^4 + \left(\frac{2\pi}{L}\right)^4} \overline{u}_G \cdot \sin \frac{2\pi}{L} x \end{aligned} \tag{5.33}$$

Similarly, deformation $v_P(x)$ in the axial direction of the pipe can be modeled by a bar on an elastic foundation (Fig. 5.31).

$$EA \frac{d^2 v_P}{dx^2} - k_x v_P = -k_x v_G \tag{5.34}$$

In this equation, $v_G(x)$ is ground displacement in the direction of the pipe axis, EA is pipe stiffness with regard to axial deformation, and k_x is the soil spring constant in the axial direction per unit length of the pipe.

Equation (5.34) can be modified as

$$\frac{d^2 v_P}{dx^2} - \beta_x^2 v_P = -\beta_x^2 v_G$$
$$\beta_x = \sqrt{\frac{k_x}{EA}} \tag{5.35}$$

The general solution of the above equation can be obtained as

$$v_P(x) = C_1 \exp(-\beta_x x) + C_2 \exp(\beta_x x) \tag{5.36}$$

Taking ground displacement $v_G(x)$ as a sinusoidal wave form of wave length L and displacement amplitude $\overline{v}_G$, integration constants C_1 and C_2 of Eq. (5.36) equal zero, and the particular solution of $v_P(x)$ can be determined by

$$v_P(x) = \frac{\beta_x^2}{\beta_x^2 + \left(\frac{2\pi}{L}\right)^2} \overline{v}_G \cdot \sin \frac{2\pi}{L} x \tag{5.37}$$

The axial force $N(x)$ owing to deformation in the axial direction of the buried pipe can be expressed as

$$N(x) = EA \left(\frac{2\pi}{L}\right) \frac{\beta_x^2}{\left(\frac{2\pi}{L}\right)^2 + \beta_x^2} \overline{v}_G \cdot \cos \frac{2\pi}{L} x \tag{5.38}$$

5.6.2 *Deformation of Buried Pipes with Joints*

In many cases, pipelines for water and sewer systems have flexible joints. First, deformation of a buried pipe connected with joints infinitely is examined, in which ground strain in the axial direction of the pipe is constant. Thus, ground displacement is expressed in linear form, as shown in Fig. 5.32. Displacement $v_G(x)$ of the ground in the axial direction is as follows, using constant ground strain γ_{xx} in that direction:

$$v_G(x) = \gamma_{xx} \cdot x \tag{5.39}$$

Taking the pipe length as l and joint stiffness as 0, the boundary condition for solving Eq. (5.36) is

$$\begin{aligned} x &= 0 \qquad v_P(0) = 0 \\ x &= l/2 \qquad \frac{dv_p(0)}{dx} = 0 \end{aligned} \tag{5.40}$$

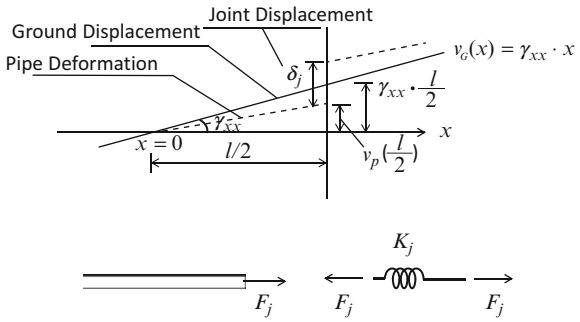

Fig. 5.32 Deformation of buried pipes with joints

Using this, the solution of Eq. (5.35) can be derived as

$$v_P(x) = \gamma_{xx}\left(x - \frac{\sinh\beta_x x}{\beta_x \cosh\frac{\beta_x l}{2}}\right) \tag{5.41}$$

The maximum axial strain $\varepsilon_{\max}$ in the pipe is generated at its central point ($x = 0$)

$$\varepsilon_{\max} = \gamma_{xx}\left(1 - \frac{1}{\cosh\frac{\beta_x l}{2}}\right) \tag{5.42}$$

The value in parentheses in the above equation indicates the transmission rate of strain from the ground to the buried pipe, and equals 1.0 if l is infinitely large. Joint displacement δ_j is obtained by

$$\delta_j = \gamma_{xx}\left(\frac{l}{2} - \frac{1}{\beta_x}\tanh\frac{\beta_x l}{2}\right) \tag{5.43}$$

If the joint has stiffness, taking its spring constant of the joint as K_j, the boundary condition for a general solution of Eq. (5.36) is as follows. The boundary condition and equilibrium are shown in Fig. 5.32.

$$\begin{aligned} x = 0 \quad & v_P(0) = 0 \\ x = 1/2 \quad & EA\frac{dv_P}{dx} = F_j \\ & \delta_j = \frac{F_j}{K_j} \\ & v_P\left(\frac{l}{2}\right) + \frac{\delta_j}{2} = \gamma_x \cdot l \end{aligned} \tag{5.44}$$

Here, F_j is the axial force acting on the joint, and δ_j is joint displacement. The general solution for deformation $v_P(x)$ in the pipe axial direction is determined

Table 5.1 Axial strains and joint displacements observed in two tunnels

Tunnel	Tunnel A (l = 110 m)		Tunnel B (l = 124 m)	
$\beta_\chi \imath = \sqrt{\frac{k_x}{EA}} \cdot \imath$	0.42–0.94		0.51–1.12	
Earthquake	Chiba	Izu-osuhima	Chiba	Izu-osuhima
Maximum tunnel strain ε_{T}	5.4×10^{-6}	5.0×10^{-6}	4.4×10^{-6}	2.5×10^{-6}
Maximum joint displacement δ_j (mm)	0.061	0.053	1.04	–
Maximum velocity at A2 Vx (m/s)	2.9	1.1	6.7	4.8
Apparent wave velocity along tunnel axes ν_s (m/s)	2,800	1,720	4,200	2,200
Maximum ground stains γ_{xx}	10.4×10^{-6}	6.4×10^{-6}	16.0×10^{-6}	21.6×10^{-6}
Transfer ratio of strains $\varepsilon_T/\gamma_{xx}$	0.52	0.78	0.28	0.22
Maximum joint displacement $\sigma_j/\gamma_{xx}l$	0.03	0.078	0.53	–

using the above boundary condition, and axial strain $\varepsilon_P(x)$ of the pipe is obtained as follows.

$$\varepsilon_P(x) = \gamma_{xx}\left\{1 - \frac{\cosh\beta_x x}{\cosh\frac{\beta_x l}{2}}\left(1 - \frac{2\frac{\tanh\frac{\beta_x l}{2}}{\beta_x l}}{\frac{EA}{K_j l} + \frac{2\tanh\frac{\beta_x l}{2}}{\beta_x l}}\right)\right\} \tag{5.45}$$

Joint displacement δ_j is obtained as

$$\delta_j/l = \gamma_{xx}\frac{\frac{2}{\beta_x l}\tanh\frac{\beta_x l}{2}}{1 + \frac{K_j l}{EA}\cdot\frac{2\tanh\frac{\beta_x l}{2}}{\beta_x l}} \tag{5.46}$$

5.6.3 *Verification of the Analytical Model by Earthquake Observation in Submerged Tunnels*

The above analytical model for buried pipe deformation can also be applied for the two submerged tunnels described in Sect. 5.4. Although these tunnels consist of nine and six tunnel elements, an infinite chain of tunnel elements is assumed. Maximum strain in axial direction ε_T, maximum joint displacement δ_j, ground strain γ_{xx}, the ratio of tunnel strain to ground strain, and non-dimensional joint displacement were determined for the Chiba Prefecture and Izu Peninsula offshore earthquakes. In each case, the maximum values during the time history were used (at the same time), as shown in Table 5.1. Accelerations in the axial direction at observation point A2 (Fig. 5.18a, b) were integrated to obtain the velocities, and these was divided by the apparent propagation velocity of the earthquake waves to

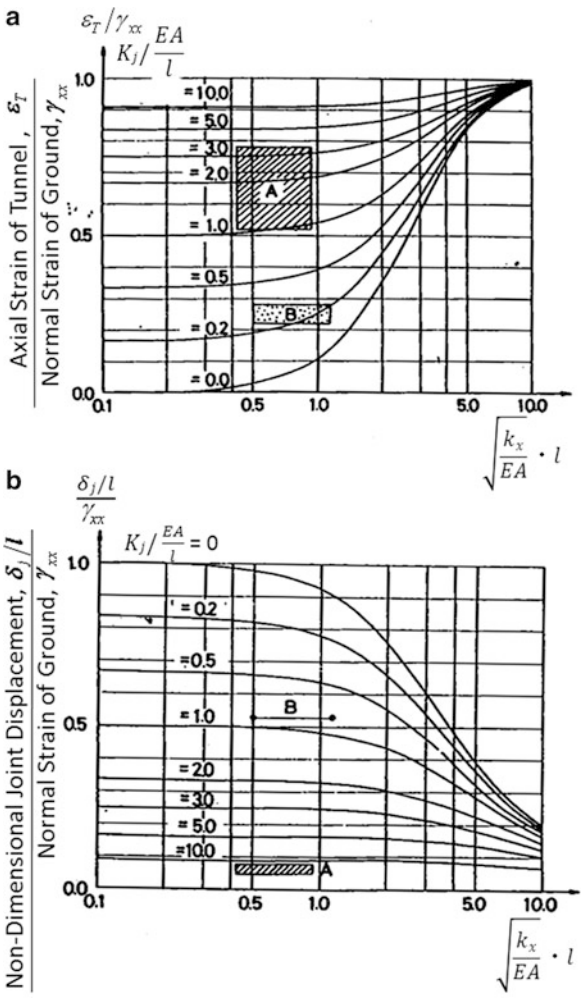

Fig. 5.33 Axial strain and joint displacement by non-dimensional paraments. (**a**) Ratio of tunnel strain to ground strain (strain transfer ratio). (**b**) Non-dimensional joint displacement

evaluate the ground strain γ_{xx} e. As shown in Table 5.1, the apparent propagation velocity was 1,700 to 4,200 m/s from the cross-correlation functions of acceleration at measurement points on land and inside the tunnel. These values vary according to the incident angle of earthquake wave motion relative to the tunnel axis.

It is difficult to accurately assess the soil spring constant acting on a large structure such as an undersea tunnel. Nevertheless, considering the range of values ordinarily used in the design of pile foundation and caissons and size of the tunnel cross section, the coefficient of subgrade reaction was assumed here to be 0.98–4.91 kN/m^3 (0.10–0.50 kgf/cm^3). With the soil spring acting on both side walls and base slab, non-dimensional parameter $\beta_x l$ was calculated at 0.42–0.94 for Tunnel A and 0.5–1.12 for Tunnel B. By plotting the non-dimensional joint displacement $\delta_j/\gamma_{xx}l$ and ratio of tunnel strain to ground strain $\varepsilon_\tau/\gamma_{xx}$ shown in Table 5.1, the regions shown in Fig. 5.33 is obtained. Based on Fig. 5.33, the strain transmission

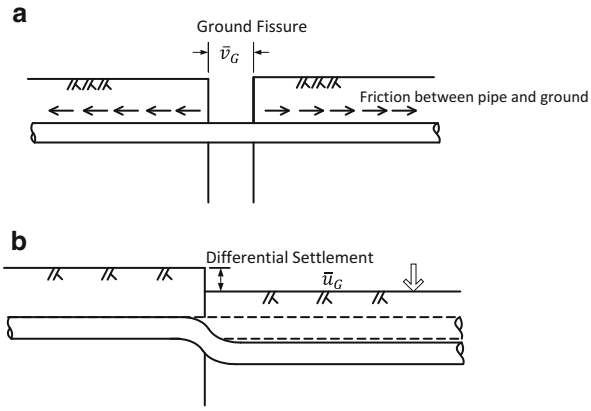

Fig. 5.34 Buried pipe deformation due to ground fissure and differential settlement. (**a**) Ground fissure. (**b**) Differential settlement

rate of Tunnel A is greater than that of Tunnel B. Furthermore, the non-dimensional joint displacement of Tunnel A is smaller than that of Tunnel B. The reason is that joint stiffness in Tunnel A (Fig. 5.17a) is greater than that of Tunnel B (Fig. 5.17b). Figure 5.33 indicates the ratio of the ground tunnel strain to that of the ground strain, and displacement of the joints is greatly dependent on joint stiffness.

5.6.4 Deformation of Buried Pipes by Ground Fissures and Ground Differential Settlement

According to the *Guidelines for Earthquake Resistant Design* [12] issued by the Japan Gas Association in 1980, consideration must be given to ground fissures and differential settlement of the ground surface in earthquake-resistant design of gas pipes, as shown in Fig. 5.34. This was determined after many gas pipes were damaged by ground fissures and differential settlement at boundaries between cut and filled soil in residential areas of hilly suburbs of Sendai and other cities during the 1978 Miyagi Prefecture offshore earthquake. In addition, many buried pipes of lifeline systems have been damaged during past earthquakes by differential settlement and horizontal relative displacement between buildings and ground where such pipes enter buildings.

Axial deformation of pipes for horizontal ground fissures of width $\bar{v}_G$ (Fig. 5.35a) was analyzed. The general solution for axial deformation of a buried pipe in such a case is given by Eq. (5.36). The boundary condition is

$$x = 0 \quad v_p(0) = 0$$

$$x \Rightarrow \infty \quad v_p \Rightarrow \frac{\bar{v}_G}{2}$$

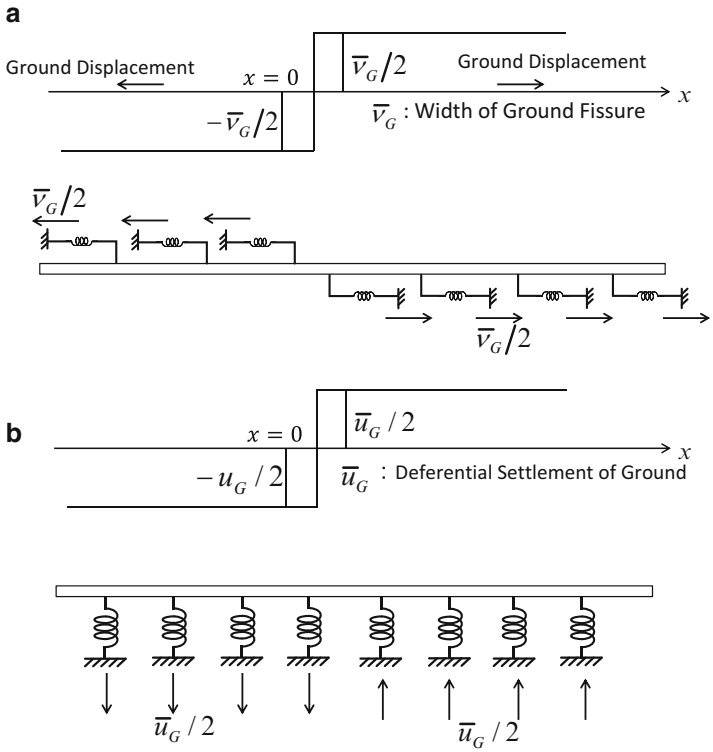

Fig. 5.35 Deformation of buried pipe caused by ground fissure and differential settlement. (**a**) Deformation by ground fissure (in axial direction). (**b**) Deformation by differential settlement (in direction perpendicular to the pipe axis)

Deformation of the buried pipe is

$$v_p(x) = \frac{\overline{v}_G}{2}\{1 - \exp(-\beta_x x)\} \tag{5.47}$$

Axial stress $\sigma_x(x)$ in the buried pipe is

$$\begin{aligned}\sigma_x(x) &= E \cdot \frac{dv_p}{dx} \\ &= E\frac{\overline{v}_G}{2}\beta_x \exp(-\beta_x x)\end{aligned} \tag{5.48}$$

Maximum axial stress $\sigma_{\max}$ occurs at $x = 0$, or the central point of a ground fissure.

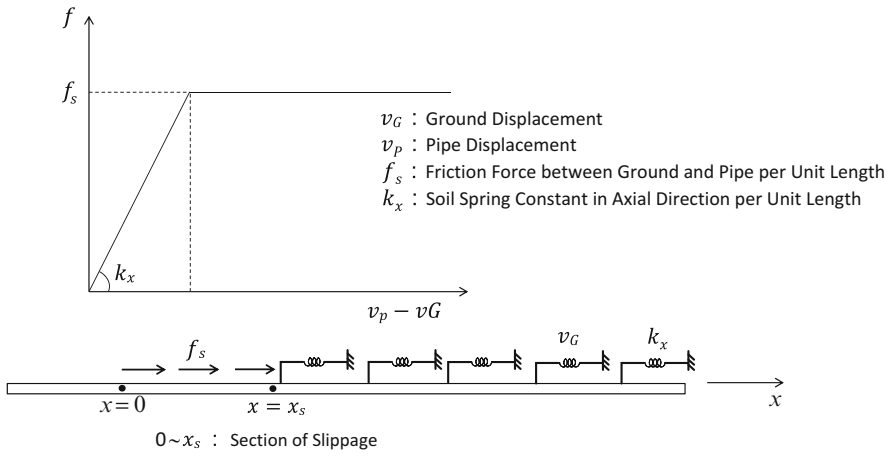

Fig. 5.36 Slippage between ground and buried pipe

Deformation of a buried pipe in the case of differential settlement (Fig. 5.35b) can be obtained using the general solution indicated in Eq. (5.30). The boundary condition in such a case is

$$x = 0 \quad u_p(0) = 0, \quad x \Rightarrow +\infty \quad u_p = \frac{1}{2}\overline{u}_G, \quad \frac{d^2 u_p}{dx^2} = 0$$

Pipe deformation perpendicular to its axis is

$$u_p(x) = \frac{\overline{u}_G}{2}\left\{\left[1 - \exp\left(-\beta_y x\right)\right] \cdot \cos\beta_y x\right\} \tag{5.49}$$

When the amount of relative displacement between buried pipe and ground exceeds a certain level, there is slippage between pipe and ground, as shown in Fig. 5.36. With f as the friction force per unit length of pipe between pipe and ground, the maximum axial force $N_{\max}$ (at $x = 0$) is

$$N_{\max} = f_s \cdot x_s + \int_{x_s}^{\infty} k_x \cdot \frac{\overline{v}_G}{2} \exp(-\beta_x x) dx \tag{5.50}$$

In the above equation, k_x is the soil spring constant per unit length of pipe, and x_s is distance where the slippage occurs, which is the solution of

$$\frac{\overline{v}_G}{2}\exp(-\beta_x x_s) = \frac{f_s}{k_x} \tag{5.51}$$

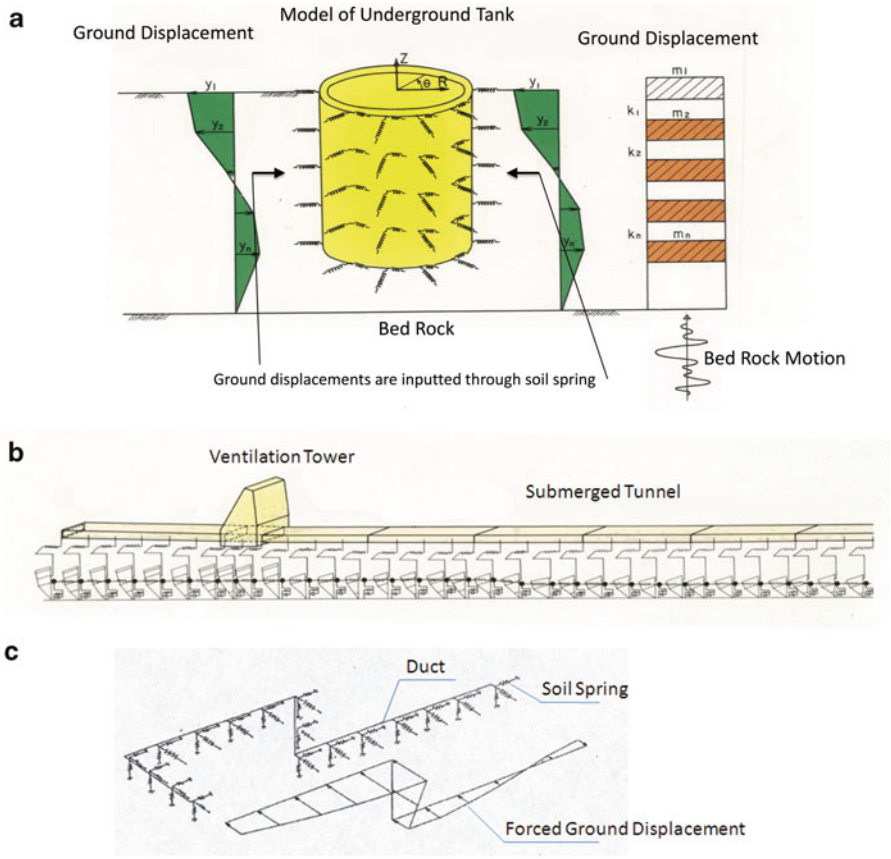

Fig. 5.37 Model of underground structures by response displacement method. (**a**) Underground tank. (**b**) Submerged tunnel. (**c**) Underground duct

5.6.5 Earthquake-Resistant Design of Underground Structures by the Response Displacement Method

The response displacement method is used for earthquake-resistant design of underground tanks, undersea tunnels, underground ducts and others. Figure 5.37 illustrates the analytical model for the response displacement method of underground structures. Underground tanks are modeled as a cylindrical body supported by a soil spring as shown in Fig. 5.37a, and ground displacements are inputted through the soil spring to determine tank deformation, stress, and strain. Analysis is conducted using the finite element method, aforementioned ring beam model, and others. The multiple mass-spring model is used for the surface ground, and ground displacement calculated by this model is used as the input.

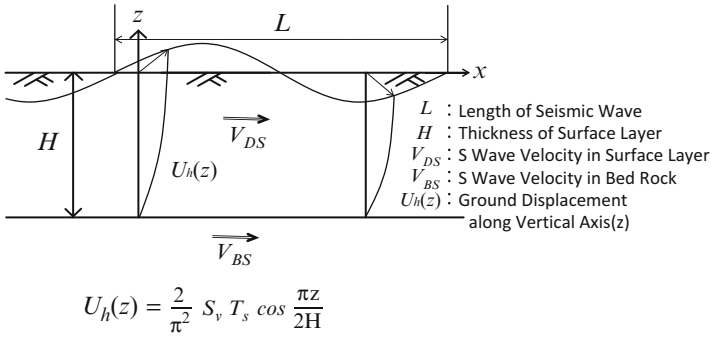

Fig. 5.38 Ground displacement for earthquake resistant design of buried pipe

Submerged tunnels and underground ducts are modeled as beams and bars on an elastic foundation. Either relative displacement from earthquake wave propagation or response displacement of surface ground along the tunnel or duct may be used as the input ground displacement. Figure 5.37b shows an example of the model used in earthquake-resistant design of submerged tunnels [13]. In this model, ground along the tunnel axis is modeled by multiple single-mass- spring systems. Ground displacement is determined from the response of mass points to the bedrock input, and this displacement is inputted to the submerged tunnel. The multiple single-mass-spring models are linked in the tunnel axis direction by a soil spring that expresses their interaction.

Figure 5.37c shows model for underground ducts of three-dimensional distribution. The ducts are modeled as beams and bars on the elastic foundation of the ground. The input ground displacement is calculated with consideration of earthquake wave propagation or surface ground response.

5.6.6 *Input Ground Displacement*

In most of the design codes for buried pipes, the input ground displacement is specified as shown in Fig. 5.38. The distribution of ground displacement along the vertical axis is given by

$$U_h(z) = \frac{2}{\pi^2} S_V T_S \cos \frac{\pi z}{2H} \tag{5.52}$$

Here, $U_h(z)$ is of ground displacement (cm) in the horizontal direction at depth z (m) from the ground surface; T_S is the first natural period (s) of surface ground; H is thickness (m) of surface ground. S_V is the velocity response spectrum (cm/s), using the spectra shown in Fig. 5.39 with respect to earthquake ground motions of Levels 1 and 2 [14].

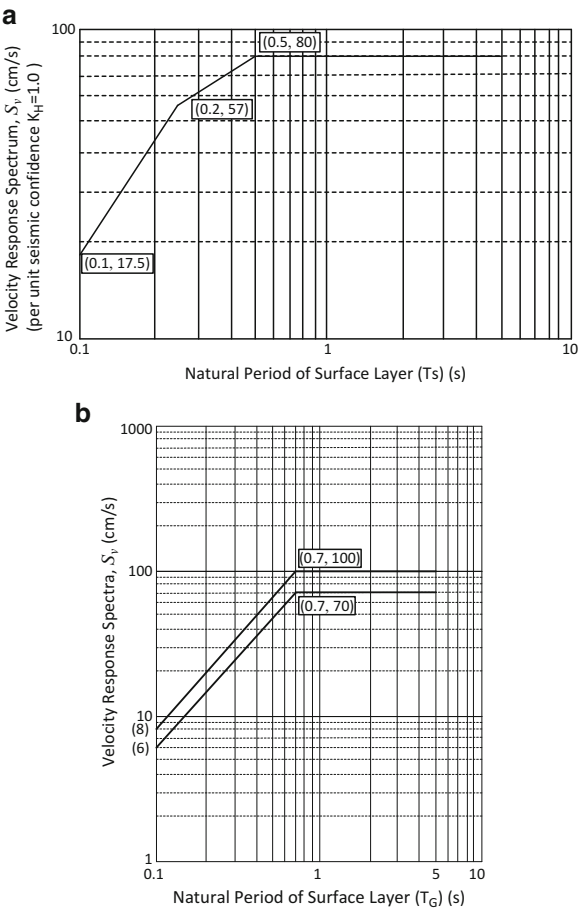

Fig. 5.39 Velocity response spectrum for earthquake resistant design of water pipe. (**a**) Level 1 ground motion. (**b**) Level 2 ground motion (velocity spectra is determined based on the regional seismic activity from the values between two *solid lines*)

The coefficient $2S_V T_S/\pi^2$ in Eq. (5.52) indicates amplitude of ground surface displacement. This can be determined by substituting $\omega_0 = 2\pi T_s$ into Eq. (2.18) and $i = 1$ into the right side of Eq. (2.37).

The following method has been proposed regarding wave length L in the horizontal direction. It is used in standards and guidelines for petroleum pipelines, water pipes, and underground conduits. The harmonic mean value of wave lengths in the surface ground L_1 and in the bed rock L_2. The wave length for the design L is evaluated by

$$L = \frac{2L_1 L_2}{L_1 + L_2}$$
$$L_1 = V_{DS} T_S = 4H, \quad L_2 = V_{BS} T_S \tag{5.53}$$

Here, V_{DS} and V_{BS} are shear wave velocities (m/s) of the surface ground and bedrock, respectively; T_S and H are the natural period (s) and thickness (m) of surface ground, respectively.

References

1. Penzien J (1969) Earthquake engineering, chapter 14. In: Soil-pile foundation interaction. Prentice Hall, Englewood Cliffs
2. Sakurai A, Takahashi T, Kurihara C, Yajima H (1970) Earthquake resistance of buried pipelines based on the observation of strains during earthquakes, Central Research Institute of Electric Power Industry, Research Report No. 69087 (in Japanese)
3. Hamada M, Izumi H, Soto S (1975) Behavior of underground tanks during earthquakes. In: The 4th Japan earthquake symposium, pp 583–590
4. Hamada M, Yokoyama M, Sugihara Y (1980) Earthquake observation of underground structures and aseismic design. In: The 7th world conference on earthquake engineering, vol 6, pp 485–492
5. Hamada M, Akimoto T, Izumi H (1975) Dynamic stresses of submerged tunnel during earthquakes. In: The 4th Japan earthquake symposium, pp 647–654
6. Hamada M, Shiba Y, Ishida O (1982) Earthquake observation on two submerged tunnels at Tokyo Port. In: The 1st international conference on soil dynamics and earthquake engineering, vol 2, pp 723–935
7. Hamada M, Izumi H, Sugihara Y, Iwano M (1983) Earthquake resistant design of rock oil tanks. In: The American Society of Mechanical Engineers, international symposium on earthquake behavior and safety of oil and gas storage facilities, PVP-vol 77, pp 94–101
8. Hamada M, Nakagawa K, Muranishi Y (1985) Earthquake observation and BIE analysis on dynamic behavior of rock cavern. In: The 5th international conference on numerical method in geomechanics, vol 3, pp 1525–1532
9. Komada H, Hayashi M (1979) Earthquake observation in underground power station. In: Report of Electric Power Institute, No. 379013 (in Japanese)
10. Okamoto S (1971) Introduction to earthquake engineering. University of Tokyo Press, Tokyo
11. Noda S, Uwabe T (1976) A study on vertical component of earthquake strong ground motion. In: Proceedings of 14th symposium of earthquake engineering, JSCE
12. Japan Gas Association (1980) Guidelines for earthquake resistant design of gas pipelines, Tokyo, Japan
13. Tamura C, Okamoto S, Hamada M (1975) Dynamic behavior of a submerged tunnel during earthquake. In: Report of Institute of Industrial Science, vol 24, No 5. The University of Tokyo, Tokyo
14. Japan Water Works Association (2000) Basic principles of seismic design and construction for water supply facilities/JSCE (2000), Earthquake resistant design codes in Japan

Chapter 6
Mitigation Measures Against Future Natural Disasters

Abstract Reasons for the worldwide increase in the number of natural disasters, such as earthquakes, tsunamis, rainfalls and floods, are discussed, and the basic concept for mitigation of large-scale disasters is introduced. Earthquakes and tsunamis are predicted to occur in the near future in Japan, and the probable damage caused by such earthquakes is addressed. The strategies and organization of the Japanese government for disaster mitigation are introduced. Also introduced are recommendations to the Japanese government by the Science Council of Japan, for the creation of a safer country against increasing natural hazards and societal vulnerability, and for international cooperation in the mitigation of natural disasters.

Keywords Earthquakes predicted beneath Tokyo area • Increase of natural disasters • International cooperation • Recommendations by SCJ • Strategies for mitigation of natural disasters

6.1 Predicted Damaging Earthquakes

6.1.1 Failed Earthquake and Tsunami Predictions and Subsequent Confusion [1]

After the 2011 Tohoku earthquake (Great East Japan Earthquake and Tsunami Disaster), the Japanese people lost confidence in the science and technology of disaster prevention. Public mistrust for science and technology has been intensified by the failure of earthquake and tsunami prediction, serious nuclear power plant accidents, collapse of tsunami barrier walls and other failures of disaster prevention infrastructure, damage to numerous homes due to liquefaction, fires and explosions in coastal industrial zones, and other losses. Trust in science and technology is one of the cornerstones for "developing a safe society", but that trust was damaged by the tragic disaster.

M. Hamada, *Engineering for Earthquake Disaster Mitigation*,
Springer Series in Geomechanics and Geoengineering,
DOI 10.1007/978-4-431-54892-8_6, © Springer Japan 2014

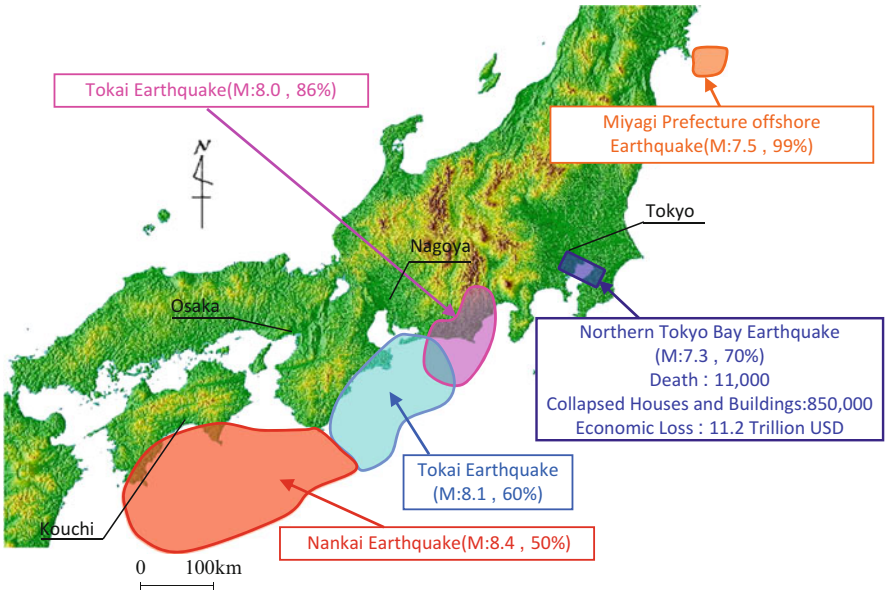

Fig. 6.1 Earthquakes predicted before Tohoku earthquake (Central Disaster Management Council, M: magnitude on Japan meteorological agency scale, probability of occurrence within next 30 years)

Prior to the 2011 Tohoku earthquake, the Central Disaster Management Council (CDMC) had predicted a risk of five earthquakes in the near future: Tokai, Tonankai, and Nankai earthquakes along the Nankai Trough, inland earthquakes directly beneath the Tokyo area such as the Northern Tokyo Bay earthquake, and a Miyagi Prefecture offshore earthquake (Fig. 6.1) [1]. Each of the three earthquakes along the Nankai Trough was forecast to be of magnitude 8.0 or more, with a very high probability of occurrence within the next 30 years (50–86 %). The northern Tokyo Bay earthquake is forecast to be of medium scale, magnitude 7.3. A high probability of 70 % was also indicated for inland earthquakes directly beneath the Tokyo area, such as a northern Tokyo Bay event. The Miyagi Prefecture offshore earthquake was forecast to be magnitude 7.5. This is considered a near certainty by seismologists, with a 99 % probability of occurrence within the next 30 years. One of the bases for this estimation is that earthquakes of magnitude 7.5 class have occurred repeatedly off Miyagi Prefecture, with a return period of approximately 50 years. An earthquake occurred here in 1978, so if the return period of 50 years is accurate, it is very likely that another will occur in the near future.

In fact, when the massive magnitude 9.0 Tohoku earthquake occurred off the Pacific coast on March 11, 2011, it had 180 times the energy of the offshore earthquake predicted for Miyagi Prefecture. Its focal region was also enormous, extending far beyond that prefecture, from Iwate Prefecture to Ibaraki Prefecture. In addition to the Miyagi Prefecture offshore earthquake that had been predicted by

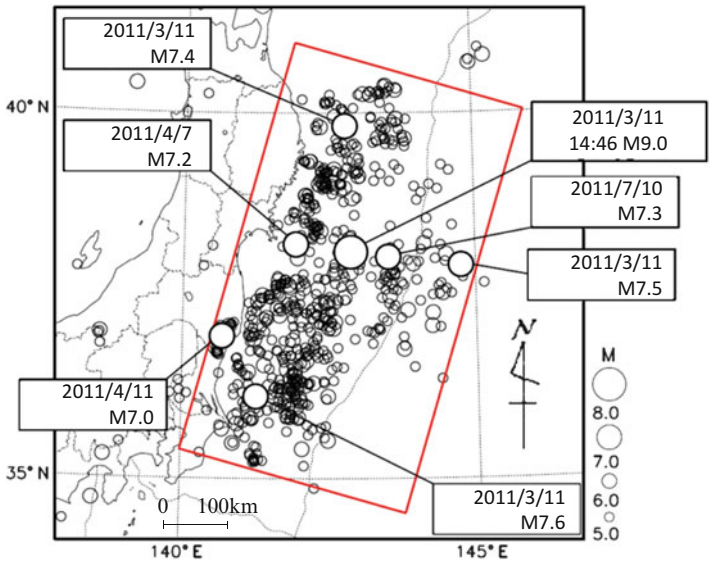

Fig. 6.2 Epicenters of the main shock and after shocks of The 2011 Tohoku earthquake (Japan Meteorological Agency, Data until 2012, 6.8)

the CDMC, a magnitude 7.7 earthquake in the seabed close to the Japan Sea Trough had also been predicted by the Headquarters for Earthquake Research Promotion of the Ministry of Education, Culture, Sports, Science and Technology (MEXT). This organization had forecast that if both these earthquakes occurred continuously, the magnitude would be 8.0. However, that was only 1/32 of the earthquake that actually took place.

The reasons for this serious failure of earthquake prediction must be thoroughly investigated. Based on the findings of such inquiry, it will be necessary to make fundamental changes in approaches to future earthquake prediction research, the forecasting system, and its organization. It has been noted that earthquake prediction in Japan is excessively dependent on recorded historical facts. Instead of depending solely on historical documentation of extremely low-frequency natural disasters that may occur only once in several thousand years, it is necessary to perform investigations from a geological viewpoint and make predictions on that basis.

Figure 6.2 shows epicenters of foreshocks and aftershocks of the Tohoku earthquake that have occurred as of June 8, 2012. The map shows that nearly all foreshocks and aftershocks have occurred at boundaries between the Pacific Ocean and North American plates and inside the plates, within a range of 600 km from north to south and 300 km from east to west. With the eastward movement of the Pacific Plate on the ocean side and the northward movement of the Philippine Plate, compressive stress is believed to be predominant in the Japanese archipelago on the North American and Eurasian plates. However, because there was widespread rupture at plate boundaries in the Tohoku earthquake, it appears that significant

changes are occurring in stress conditions of the Japanese archipelago. This may affect the occurrence probability of the earthquakes shown in Fig. 6.1, which had been predicted before the Tohoku earthquake. Changes of the stress conditions must be carefully monitored in the future through GPS measurements of crustal movements and detailed earthquake observations. On that basis, it will be necessary to comprehensively examine earthquakes that had been predicted previously and those that can be expected in the future.

Here, I am not unilaterally condemning researchers and others involved in the field of earthquake prediction. I myself must also take responsibility for this failure of prediction, as one who has worked to reduce the damage of natural disasters from the standpoint of civil engineering. When I visited Banda Aceh at the northern end of Sumatra about 1 month after the Indian Ocean tsunami of 2004, I witnessed a tragic scene in which approximately 70,000 lives had been lost by the tsunami, about a quarter of the population of the city. At the scene of devastation, I was thinking that surely an extraordinarily large earthquake of magnitude 9.0 would never happen in Japan, and that my country would never experience such a massive tsunami.

However, the plate structure of the west coast of Sumatra is very similar to that of the Pacific coast of Japan. In fact, the Japanese location at a complex juncture of several plates seems even more unstable. Considering this, I realize that there was no scientific basis to the belief that a magnitude 9.0 earthquake would not occur in our country. As one who has been involved in the study of earthquake disaster prevention for many years, I cannot deny my responsibility.

About a year after the Tohoku earthquake, a committee on large earthquakes along the Nankai Trough, organized by the Cabinet Office [2], issued a new prediction of earthquake source areas from Tokai to Kyushu. Along with the previously predicted Tokai, Tonankai, and Nankai earthquakes, this prediction adds a Hyuga-nada earthquake offshore of Miyazaki Prefecture. It also indicates that the focal region of these four earthquakes will expand to an area near the Nankai Trough, and estimates that the magnitude would be 9.0 if they occur simultaneously. This earthquake would produce a tsunami at least 20 m in height that would strike an area from Shizuoka to Tokushima. In Kochi Prefecture, the maximum height would be 34 m. In the Izu Islands, the predicted height is 20 m. However, until now, the government's committee made no mention of the occurrence probability of such a megaquake or about the reliability of this prediction. Following the experience of the Tohoku earthquake, the CDMC has indicated the policy of taking the maximum class of potential earthquakes and tsunamis into consideration for future disaster reduction strategies, but the meaning of "maximum class" is not clear. My interpretation of the earthquake source areas shown in Fig. 6.3 is that they indicate the greatest earthquake potential that could occur along the Pacific coast of Japan. However, the predicted earthquake can be applied to reduce the loss of life. However, it cannot be directly incorporated into national disaster prevention measures, such as the development of disaster prevention infrastructure and national or urban planning. We cannot assume a maximum class of possible or conceivable earthquakes and tsunamis for the sake of urban or national planning in terms of structure and facility construction. In such a case,

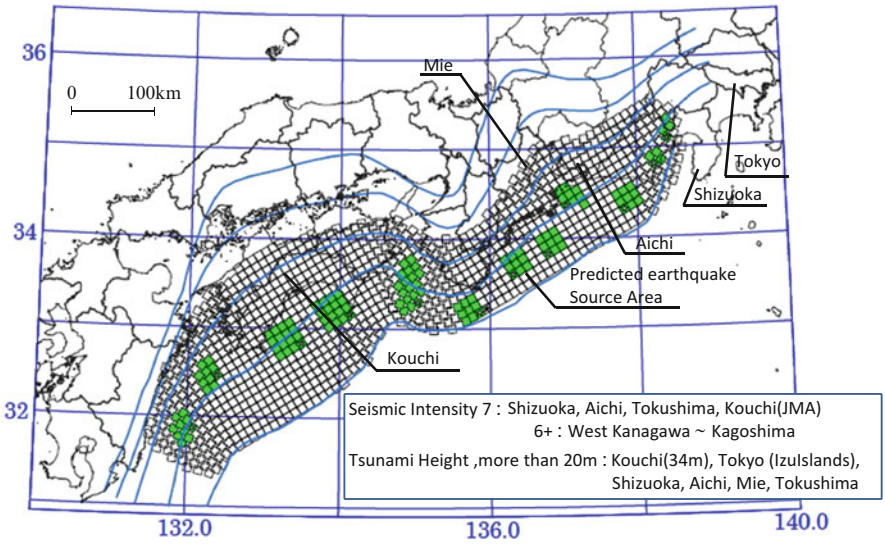

Fig. 6.3 Predicted earthquake source area along the Nankai Sea Trough (2013/3/31) (a committee organized by Cabinet Office of Japanese government)

national planning itself would become impossible. Although there has been no thorough debate concerning the probabilities of hazards that should be considered in infrastructure development or the reliability thereof, the council has continued to issue statements on this "maximum class" of hazards. Thus, the current state of prediction of future earthquake and tsunami hazards is confusing.

6.1.2 Tokyo Area Earthquakes

When considering a future earthquake in the greater Tokyo area (Tokyo, Kanagawa, Chiba, and Saitama Prefectures), the earthquake that struck this region in 1923 (called the Great Kanto earthquake) first comes to mind. This was a large earthquake of magnitude 7.9 (Japan Meteorological Agency (JMA) magnitude) with the epicenter in Sagami Bay, and it left 105,000 people dead or missing and 370,000 buildings destroyed, partially destroyed, or burned down in the greater Tokyo area [3]. This was the greatest natural disaster of the twentieth century in Japan. Because the population of greater Tokyo has grown to approximately 36 million and political, economic and cultural activities are all concentrated here, the possibility of another Kanto earthquake causes the greatest anxiety. However, in the view of the CDMC, there is still time before recurrence of a Kanto-type earthquake. As shown in Fig. 6.4, earthquakes of magnitude 8-class centered in Sagami Bay have occurred at intervals of approximately 200 years. The last earthquake of this class before the Great Kanto earthquake was the Genroku

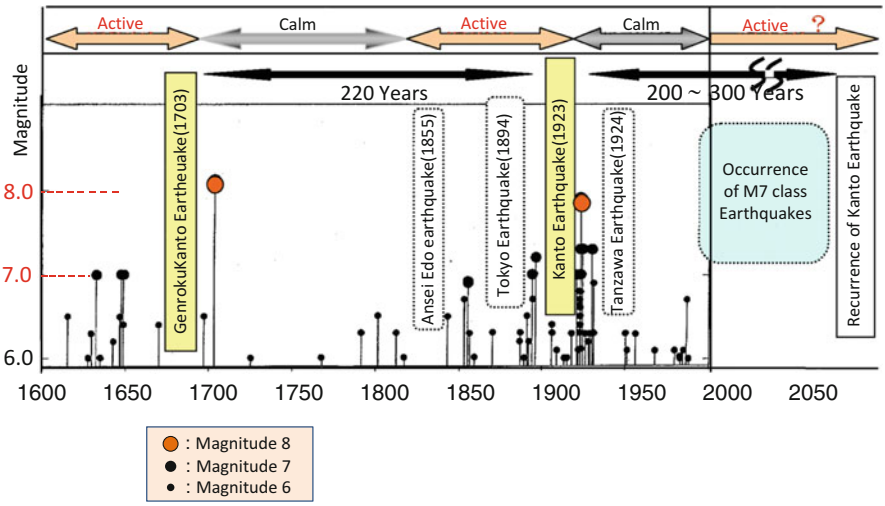

Fig. 6.4 Earthquakes in past in the greater Tokyo area and prediction of future earthquakes (white note on nature disaster prevention, Cabinet office [4])

Kanto earthquake of 1703. The CDMC believes that we still have more than 100 years until the next earthquake on the same scale as the Great Kanto event, assuming that the interval around 200 years holds.

However, when we examine the period of about two centuries between the 1703 Genroku Kanto and 1923 Great Kanto earthquakes (Fig. 6.4), it is important to note that the first of those centuries was a calm period with scarcely any earthquakes, whereas the second was an active period with increased occurrence of medium-scale earthquakes of magnitude 6–7. Some hold the view that these increasingly frequent small and medium earthquakes eventually led to the Great Kanto earthquake. According to that perspective, the greater Tokyo area may now have entered an active seismic period, 90 years after that earthquake. One of the medium-scale earthquakes is expected to be a northern Tokyo Bay earthquake of magnitude 7.3. As described above, because the Tohoku earthquake has changed the stress conditions of the Japanese archipelago, there is concern that such an earthquake may come earlier.

Regarding preparedness for inland earthquakes in the greater Tokyo area, the CDMC has issued hypothetical epicenters of earthquakes that could occur anywhere in the area [1]. Their reasoning is that some earthquakes of magnitude 7 or less may not have left traces of fault ruptures at the ground surface; that is, earthquake surface faults may not be observable, so there may be hidden faults underground even if no corresponding surface faults have been discovered.

As shown in Fig. 1.69, the Niigata-Chuetsu earthquake of 2004 occurred where no active fault was known to exist prior to the earthquake. As shown in Fig. 1.90, the Iwate-Miyagi inland earthquake of 2008 also had its epicenter where no active fault was previously known to exist.

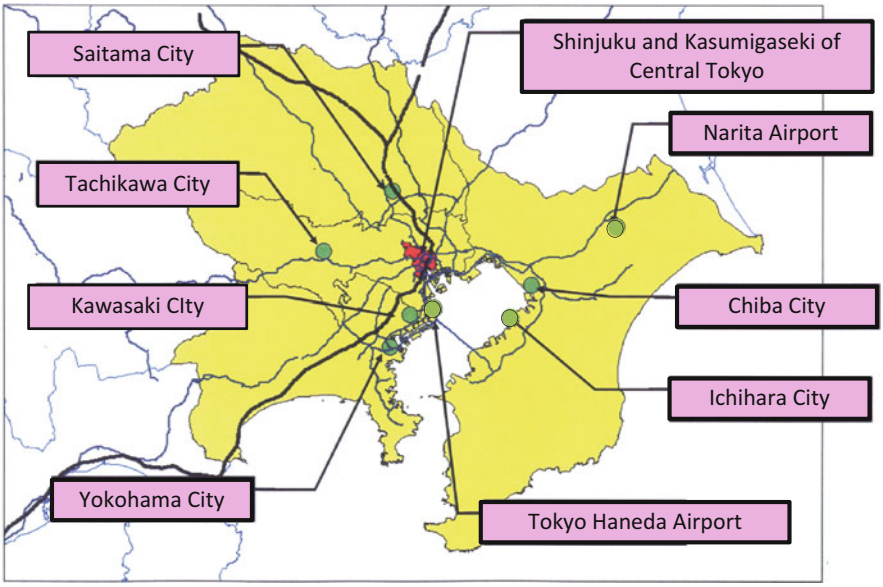

Fig. 6.5 Epicenters of hypothetical inland earthquakes in the greater Tokyo area [4]

There is another factor that makes it difficult to discover active faults below the greater Tokyo area. This is because the entire area is covered by sedimentary soil to depths of 2–3 km. Even if there are active faults in the bedrock below, it would be practically impossible to detect them from the ground surface. Therefore, the CDMC assumed locations where earthquakes could occur, as shown in Fig. 6.5. Each is a location of concentrated political and economic activity, a densely populated area, or an airport or concentration of various industries. As shown in the figure, an earthquake directly beneath Shinjuku, the western part of central Tokyo, would impact the newly developed city center, and an earthquake directly beneath Kasumigaseki, the eastern part of central Tokyo, would affect the political and administrative center. Other hypothetical earthquakes would directly impact the densely populated cities of Yokohama, Kawasaki, Chiba or Saitama, or the major airports of Narita and Haneda. Debate arose within the CDMC concerning the scale of earthquakes anticipated at these locations. As stated in Chap. 1, the magnitude of the Iwate-Miyagi inland earthquake of 2008 was 7.2 (JMA magnitude), and that of the 2004 Niigata-Chuetsu earthquake was 6.8; both were caused by previously unknown active faults. The Western Tottori earthquake of 2000, also at a previously unknown active fault, had magnitude 7.3. Based on these cases, the CDMC had to establish a hypothetical magnitude of an earthquake directly striking the greater Tokyo area with unknown epicentral location. Ultimately, a special committee organized by the CDMC decided to adopt magnitude 6.9 for damage predictions. There is no scientific basis for this magnitude. Some of the special

committee felt that the magnitude should be at least 7, while others asserted that it should be 6.5, which has been adopted for many years in earthquake-resistant design of nuclear power plants, directly beneath the reactor building. That magnitude was based on reasoning that investigation of active faults in surrounding areas has been performed much more meticulously in earthquake-resistant design of nuclear power plants than in the same design for ordinary structures, but there is still a possibility that an active fault may have been missed. Magnitude 6.9 was the result of compromise within the special committee.

6.2 Measures Against Earthquakes Beneath the Tokyo Area

6.2.1 Damage Prediction and Related Issues

The CDMC and Headquarters for Earthquake Research Promotion of MEXT have predicted magnitude 7.3 for a northern Tokyo Bay earthquake. As of 2004, they considered the probability of a magnitude 7 class earthquake within the next 30 years in the greater Tokyo area, including northern Tokyo Bay, to be 70 % [4].

Table 6.1 shows CDMC damage predictions for a northern Tokyo Bay earthquake. The estimates are that if such an earthquake occurred at 6 p.m., about 850,000 homes would be destroyed by ground motion, fire and slope sliding. This is approximately seven times the number destroyed in the Kobe earthquake of 1995,

Table 6.1 Prediction of damage by the Northern Tokyo Bay earthquake (based on the data from central disaster management council Japan [4]) (wind spread: 15 m/s)

	Occurrence time of earthquake	5AM	6PM	Kobe earthquake
Collapse of buildings and houses	Ground motion	150,000	150,000	110,000
	Slope sliding	35,000	35,000	46
	Tsunami	0	0	0
	Fire	160,000	650,000	7,000
	Total	360,000	850,000	117,000
Dead	Collapse of buildings and houses	4,200	3,100	4,915
	Tsunami	0	0	0
	Fire	400	6,200	550
	Slope sliding	1,000	900	37
	Brick wall falling objects	0	800	0
	Total	5,600	11,000	5,520

Number of People who cannot go home: 6.5 million in greater Tokyo(Tokyo: 3.9 million)
Refugees: 7 million at Maximum. Number of people who need temporary houses: 4.6 million
Economic loss: direct loss 66.6 Trillion yen,in-direct loss 45.2 Trillion yen (total 111.2 Trillion yen)

which was 117,000. The prediction of 11,000 fatalities is approximately double the 5,520 directly caused by the Kobe event. The total predicted economic losses are 112 trillion Yen, including 67 trillion Yen in direct losses from the destruction of public and private property and 45 trillion Yen in indirect losses from economic stagnation following the earthquake.

Another major problem caused by The Northern Tokyo Bay earthquake would be the number of stranded commuters and displaced persons. If this earthquake occurred at noon, it is predicted that 6.5 million people in the greater Tokyo area would be unable to return to their homes on the same day. It was reported that 3.52 million people remained in Tokyo after the 2011 Tohoku earthquake. However, many were successful in returning home, although it took them much longer than usual. There was lighting along streets, and people were able to buy water and other necessities at convenience stores. In The Northern Tokyo Bay earthquake, electric power would be cut off and enormous numbers of commuters would be returning home on foot in the dark, without food or water supplies. It is anticipated that many would be stranded in central Tokyo and that they would need to remain there for long periods. It would be necessary to supply these stranded commuters with food and water for long durations, as well as with heaters if it were winter. Although the CDMC has made the damage predictions shown in Table 6.1, it has not yet indicated any specific solutions.

It has been predicted that 4.6 million people in the greater Tokyo area would need temporary houses. This is approximately 15 times the number of people (300,000) who moved to temporary houses after the Kobe earthquake. Even if all national homebuilders and construction materials could be brought to the greater Tokyo area, it would still take considerable time to build temporary housing for all these victims. The concept of group evacuation has been proposed as part of the debate on housing for disaster victims. Specifically, the idea is that group evacuation housing would be constructed in advance in the Tomakomai-East area of Hokkaido, which has vast tracts of state-owned land. Disaster victims would be transported there from the greater Tokyo area by ferries or other means. However, following the Kobe earthquake, it was difficult to obtain the consent of disaster victims who had lived in central Kobe to relocate even to temporary housing on Kobe's Port Island, and the idea of long-distance group evacuation was shelved. Considering the reality that many victims of the 2011 Tohoku earthquake are still leading lives of hardship in distant temporary housing, the option of group evacuation after an earthquake in the greater Tokyo area must be kept on the table as a possible measure.

Table 6.2 shows anticipated disruptions of lifeline utility services in a northern Tokyo Bay earthquake, based on reports from utility companies. Restoration of electricity, telecommunications and gas is forecast to take about the same number of days as the Kobe earthquake, but the predicted recovery time for water and sewage services is much shorter. To determine whether it would be possible to restore services in such a short time if lifeline utilities were damaged to a much greater extent than in the Kobe earthquake, it will be necessary to inspect and

Table 6.2 Damage prediction of lifeline systems by the Northern Tokyo Bay earthquake and recovery days

	Number of affected households	Number of affected households by Kobe earthquake
Water	39,000,000 (30)	1,265,000 (70)
Sewage	15,000 (40)	– (140)
Electricity	1,600,000 (6)	2,600,000 (14)
Telephone (number of damaged lines)	1,100,000 (14)	285,000 (14)
Gas	1,800,000 (55)	857,000 (54)

( ): recovery days

reassess the vulnerabilities of these systems and facilities and take necessary measures, such as seismic retrofitting.

The following are some of the issues that must be addressed with regard to future solutions and countermeasures for an earthquake in the greater Tokyo area.

(i) Earthquake and tsunami resistance of industrial complexes on reclaimed land around Tokyo Bay
(ii) Safety of land along rivers at elevations below sea level
(iii) Building collapse and fires in densely populated residential areas with high proportions of wood construction
(iv) Earthquake resistance of residential areas in hilly suburbs
(v) Safety of high-rise buildings and their residents

6.2.2 Safety of Industrial Complexes Around Tokyo Bay

The 2011 Tohoku earthquake caused a great deal of damage in industrial zones around Tokyo Bay, including explosions and fires involving 17 spherical liquefied propane gas tanks of an oil refinery plant. The main reasons for the damage were the long duration of earthquake ground motion, long-period component of ground motion, and soil liquefaction of reclaimed ground. Accidents such as overflowing of tank contents also occurred in industrial zones along the coast of the Sea of Japan in the Tohoku region, in addition to Tokyo Bay. This is described in Sect. 1.3.9 on the 2011 Tohoku earthquake. Figure 6.6 shows the history of land reclamation around Tokyo Bay [5]. The reclamation from the bay began in the Edo period, and projects are still underway to reclaim ground by landfilling. This reclaimed land includes large areas of ground constructed prior to the 1964 Niigata earthquake. Soil liquefaction and its damage came to be understood from an engineering standpoint for the first time after the 1964 Niigata earthquake.

Several years after the Niigata event, research and development on liquefaction countermeasures for ground and structures resulted in practical measures that have been put in place. No liquefaction countermeasures have been taken for land

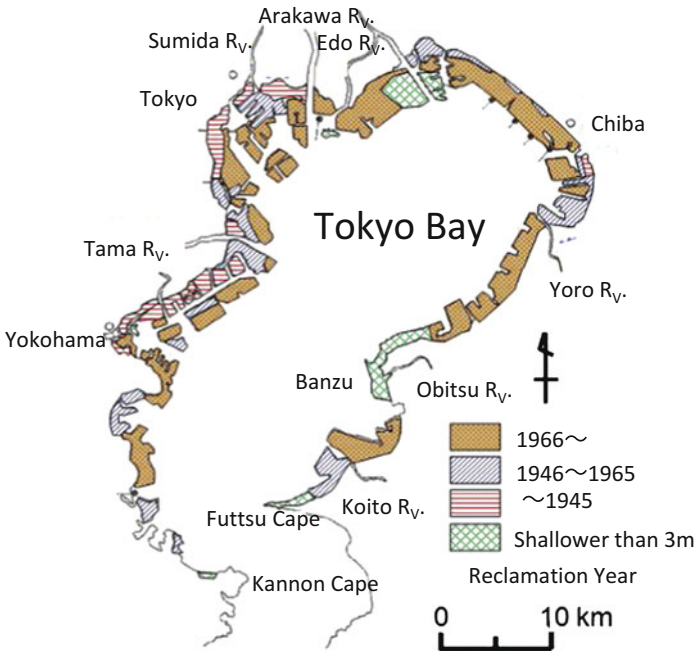

Fig. 6.6 History of reclamation of Tokyo Bay (after Kaizuka [5])

reclaimed prior to that time or for the many structures and facilities built on such land.

Figure 6.7 shows a quay wall of land reclaimed from Tokyo Bay and soil liquefaction predicted to be caused by The Northern Tokyo Bay earthquake. Reclamation began in this area around 1930 and was completed about 1960; it is now an industrial zone of petroleum and chemical plants and steel mills. As shown in the figure, there are steel sheet pile walls with an anchorage, and the ground is composed of sandy soil of the former seabed (*N* values are 10 to 15) and a layer of sandy fill (*N* values are about 5). In predictions of liquefaction in a northern Tokyo Bay earthquake, it is believed that there would be liquefiable ground to a depth approximately 14 m below the ground surface, and that ends of steel sheet piles would not reach the lower non-liquefiable clayey soil. It is anticipated that the foundation ground of anchors would also be liquefied. If liquefaction occurs, it is likely that there would either be significant displacement of the steel sheet pile quay walls or, in the worst case, that they would collapse. If they were to collapse, the reclaimed land behind the quay walls would move seaward substantially and greatly subside.

Based on the prediction method in Sect. 4.2 for the movement of quay walls and horizontal displacement of the ground, it is anticipated that these walls would move up to 7 m in the seaward direction and that the reclaimed land would also be horizontally displaced (Fig. 6.8). Thickness of the liquefiable layer is predicted to

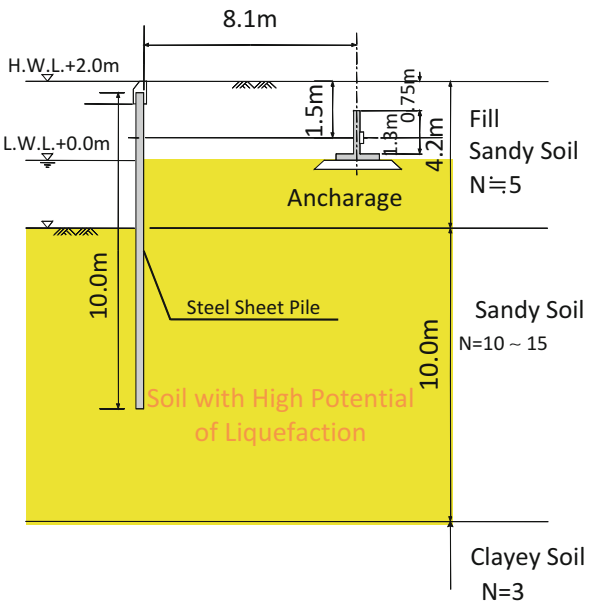

Fig. 6.7 Quay wall of an artificial island reclaimed from Tokyo Bay and estimation of liquefaction

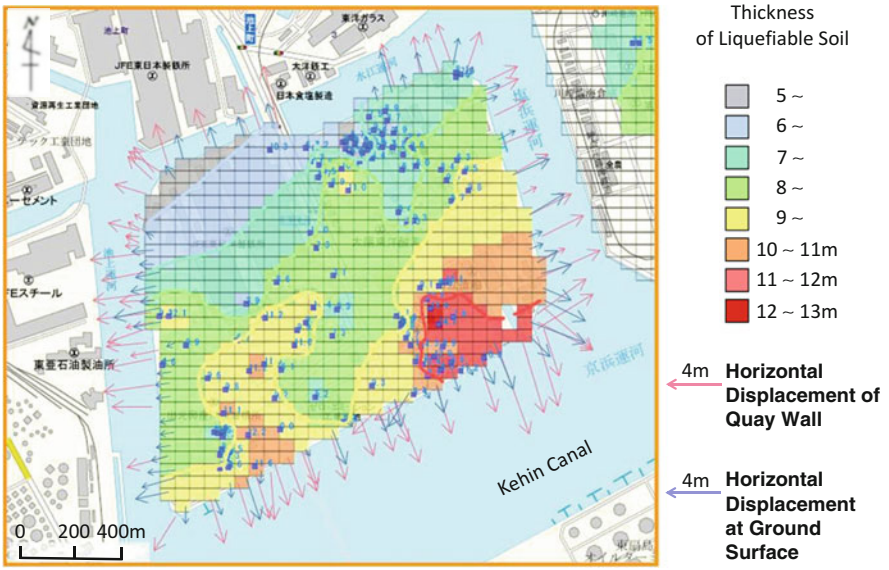

Fig. 6.8 Estimation of soil liquefaction of the an artificial island and horizontal displacements of the quay walls and the ground

Fig. 6.9 Petro-chemical complexes around the Tokyo Bay

be more than 10 m. However, many petroleum product storage tanks are still in the vicinity of these quay walls.

Measures for long-period earthquake ground motions are another issue in earthquake disaster prevention, for coastal reclaimed land around Tokyo Bay and elsewhere. As stated in Sect. 1.3, these ground motions in the 2003 Tokachi offshore earthquake caused sloshing vibration of the liquid contents of floating roof-type tanks, causing two tanks to be destroyed by fire. In Japan, tank fires due to sloshing vibration of crude oil also occurred in the 1964 Niigata and 1983 Central Japan Sea earthquakes. There are many reports of fire and collapse of floating roof-type tanks by long-period components of earthquake ground motions, as mentioned in Sect. 1.2.1 on the 1999 earthquake in Kocaeli, Turkey.

Figure 6.9 shows examples of floating roof-type tanks in an oil industry around Tokyo Bay. It is reported that more than 600 floating-roof-type tanks are on reclaimed land around the bay. These tanks contain crude and heavy oil. Figure 6.10 shows earthquake ground motions and velocity response spectra that have been calculated for coastal areas along the bay, on the assumption of continuous occurrence of Tokai and Tonankai earthquakes. Long-period earthquake ground motions of 9–10 s in the Chiba area and 6–7 s in the Kawasaki area would be predominant. The thickness of sedimentary soil in the Chiba area is about 3 km, larger then 2 km in the Kawasaki area. Based on analysis of sloshing vibration of oil in tanks, it is estimated that the contents of 64 tanks, approximately a tenth of the 600 total, would overflow (Table 6.3). It is expected that some of these incidents would involve fires, as experienced in the Tokachi offshore earthquake. With large ground displacement from the lateral flow of liquefied ground, along with sloshing vibration of tank contents, it is believed that large amounts of crude and heavy oil would spill into Tokyo Bay and become widely diffused on the water. It is certainly possible that this oil could catch fire, causing a large-scale fire on the sea surface. Figure 6.11 shows results of a simulation of the diffusion of crude oil in a case where 12,000 kl of crude oil spills into the ocean from the Kawasaki industrial zone. In the summer season, the crude oil would reach the Chiba area in about 3 days with southwesterly winds of speed 5.0 m/s, drifting and diffusing over a wide area of the bay. In winter, the crude oil would drift toward the mouth of the bay with

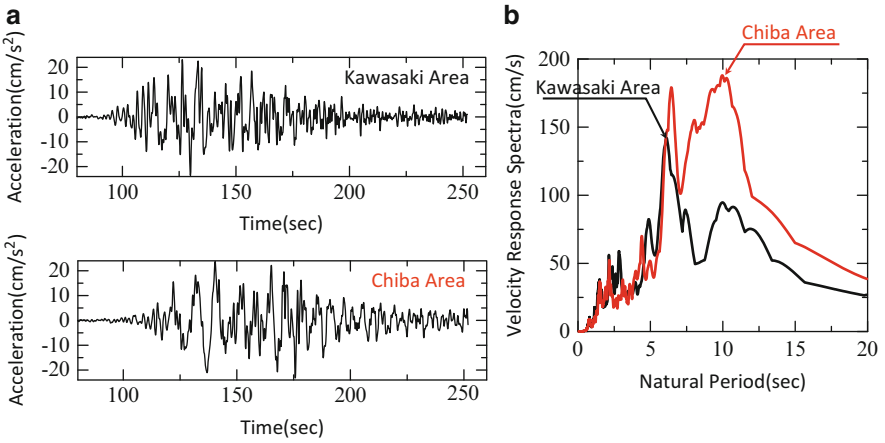

Fig. 6.10 Ground motions with long period component and their spectra (continuous occurrence of Tokai and Tonankai earthquakes, estimated by Furumura). (**a**) Ground accelerations. (**b**) Velocity response spectra

Table 6.3 The number of floating roof type tanks and of overflowing tanks

Diameter of tanks (m)	Total number of tanks	Number of overflowing tanks
~24	203	13 (6.4 %)
24–34	136	27 (19.9 %)
34–64	118	18 (15.3 %)
~60	159	6 (3.8 %)
Total	616	64 (10.4 %)

northwesterly winds, also diffusing over a wide area. Figure 6.11 includes a chart of daily wakes of medium and large ships (thin lines in the figure), excluding fishing and leisure boats. About 200 ships navigate Tokyo Bay every day. If an oil spill spreads over the sea area shown in the figure, it would have prevented all ships from coming into or going out of the bay for safety reasons.

The Japanese government has constructed a central disaster management base on Higashiogi Island, Kawasaki (the location is shown in Fig. 6.11). In the event of a natural disaster in the greater Tokyo area, emergency relief supplies and emergency response personnel from other prefectures and foreign countries would gather there for transport by small craft to affected areas. However, if large amounts of hazardous materials leak into the sea from storage tanks as described above, maritime traffic in Tokyo Bay would be halted. Ships would be prohibited from navigating the bay until the spilled heavy and crude oil are recovered. A disaster impact study committee for the Tokyo Bay area organized by the Ministry of Land, Infrastructure and Transport has estimated that recovery of this crude oil would take approximately 2 months. If this situation ensues, it would not be possible to gather

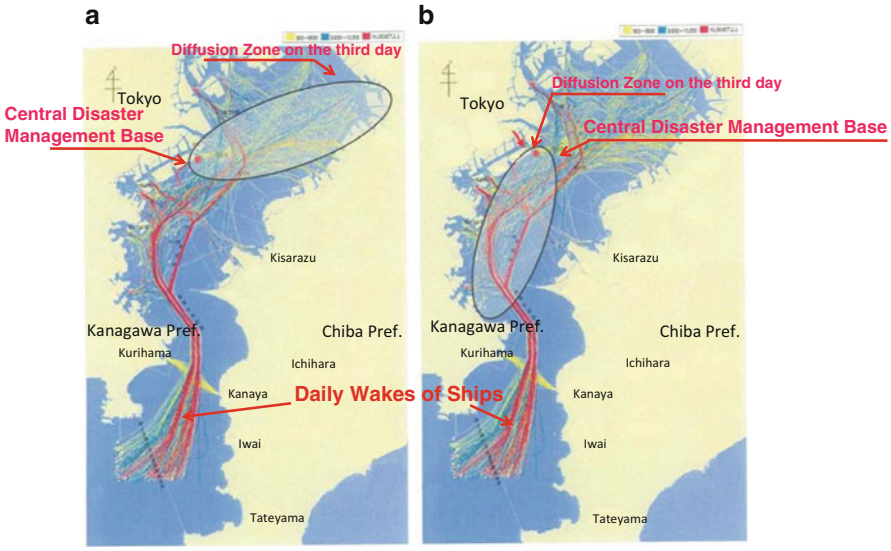

Fig. 6.11 Diffusion of crude oil on Tokyo Bay (committee on earthquake Damage to Bay area, ministry of Land, infrastructure and transport). (**a**) Summer season. Outflow point;Keihin Canal. (**b**) Winter season. Volume of crude oil;12,000 kl

supplies or personnel at the central disaster management base, and this would pose a serious obstacle to post-disaster emergency response as well as restoration and recovery.

Twelve thermal power plants on reclaimed land along Tokyo Bay are currently in operation. Now, all nuclear power generation has been halted after the 2011 Tohoku earthquake, and thermal power plants around Tokyo Bay are supplying at least 80 % of total electric power usage in the greater Tokyo area (as of July 2012). The supply of liquefied natural gas and crude oil imported from overseas would be cut off in a case of the diffusion of crude oil, resulting from liquefaction, large ground displacement, and ruptures of oil tanks. Combined with the stoppage of nuclear power generation, this would result in a critical shortage of electric power in the greater Tokyo area.

In the 2011 Tohoku earthquake, liquefaction occurred in residential districts of Urayasu and other locations, but there was no serious liquefaction in industrial zones because the earthquake ground motion was small. The greatest acceleration observed on reclaimed land around Tokyo Bay was about 100–150 cm/s^2. In a northern Tokyo Bay earthquake, ground surface acceleration along the coast of the bay is predicted around 400–700 cm/s^2, much higher than that in the Tohoku event. Liquefaction would also occur to a much greater extent than in the Tohoku earthquake, and this combined with sloshing vibration of the liquid contents of tanks is anticipated to cause severe damage. Therefore, it is urgently necessary to verify earthquake resistance of thermal power plants and petroleum, chemical and

other industrial facilities in coastal areas along the bay, and take necessary measures for reinforcement.

Earthquake resistance of coastal industrial zones in large cities cannot be improved merely by assigning responsibility to industrial businesses. Damage incurred by one plant extends to others, resulting in many simultaneous losses in the industrial zone. This is clear from the example of 11 accidents around Tokyo Bay during the 2011 Tohoku earthquake (Sect. 1.3.9). All the plants are connected to each other by the bay waters. Even if one plant increases its disaster resistance, it does not reduce the overall risk. To prevent catastrophic damage to the industrial zones around the bay areas of large Japanese cities such as Tokyo, Nagoya and Osaka during future earthquakes, a social framework involving central and local government, industrial businesses, local residents, and concerned engineers and researchers, should be organized for the development and implementation of countermeasures.

6.2.3 Improving Earthquake Resistance of Hilly Land Developed for Residential Use

Given the population growth in Tokyo and other large cities, much hilly suburban land has been excavated and reclaimed for residential use. However, past earthquakes have resulted in sliding and collapse of filled portions of such hilly residential land. Figure 6.12a, b shows examples of slope failures in hilly land reclaimed for residential use from the 1978 Miyagi Prefecture offshore earthquake and the 2011 Tohoku earthquake, respectively. In general, when hills are developed for residential use, ridges are excavated and the resulting soil is used to fill in valleys. This results in balanced amounts of soil for reclamation work. The former Ministry of Construction specified that soil from excavation of ridges must be prepared by removing trees and other foreign matter and then subjected to adequate rolling compaction. However, there are many housing developments where land was reclaimed without thorough compliance with these rules. The damage in residential areas shown in Fig. 6.12 appears to be an example of this problem.

Figure 6.13a shows a boring survey of reclaimed hilly land in Kanagawa Prefecture. When inclination and subsidence caused damage to a house built on land reclaimed by filling in valleys, boring was done for the sake of restoration work, revealing this situation. The boreholes were not dug into soil, but rather revealed timber in a fresh state. This indicated that trees and the like were not removed from the soil before it was used for reclamation in the valleys. Figure 6.13b shows steps built on reclaimed residential land in a valley, with white traces where rainwater had burst through during heavy rainfall. It is thought that rainwater flowed from the ridge into the valley, creating the water flow that emerged from these steps.

Where land has already been reclaimed and towns have been built, seismic reinforcement of the ground itself would be very difficult. Depending on the

Fig. 6.12 Slope failures of residential areas. (**a**) 1978 Miyagi prefecture offshore earthquake (Shiroishi city). (**b**) 2011 Tohoku earthquake (Sendai city)

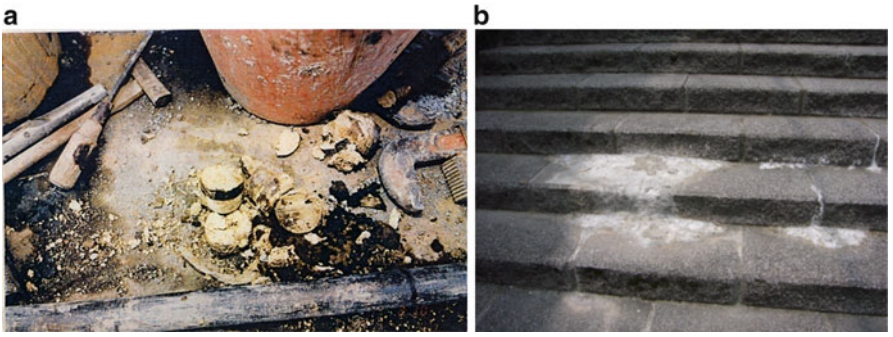

Fig. 6.13 Boring test in the residential area and eruption of water due to rain fall. (**a**) Boring test (wooden fragments were excavated by boring). (**b**) Traces of water eruption from stairs

methods used, this could also be extremely expensive. One proposed method is to bury horizontal drainage pipes into the ground in valleys where rainwater tends to accumulate, as a means of improving drainage. This measure has already been implemented in some reclaimed areas.

It is not easy to improve earthquake resistance of ground that has been artificially made. Conscientious work by construction companies is required. It is also important for residents to thoroughly inspect any such land before purchasing. Adequate information that is easy to understand must be disclosed for this purpose, by both construction companies and related agencies.

Land reclamation, including the preparation of housing sites in hilly areas, is done by construction companies. The construction industry has a multi-layered structure of subcontracting and sub-subcontracting. Construction management does not always appropriately handle every detail of construction project organization. Construction companies must maintain high ethical standards, based on the understanding that unsound work during land development will have a direct impact on the safety of local residents.

6.3 Earthquake Resistance of Abandoned Lignite Mines [6]

There are many rock caves throughout Japan such as abandoned coal mines, caverns abandoned after stone excavation, and air raid shelters excavated before and during World War II. It has been noted that such caverns amplify earthquake ground motion, and that there is risk of collapse if columns and walls remaining in the caves are unable to withstand seismic forces. It is expected that collapse during earthquakes of such caves under urban areas could significantly damage homes and buildings on the surface, as well as lifeline utilities such as water supply and sewer lines. Lignite is a low-quality type of coal. There were 326 collapses or cave-ins of abandoned lignite mines during the 2011 Tohoku earthquake in Ichinoseki and surrounding area. There were 28 failures of cave-ins during the 2005 southern Miyagi Prefecture earthquake, centered on the epicentral area of Yamoto in that prefecture.

Substantial lignite mining took place before, during and after World War II, primarily in the Tokai and Tohoku regions, as part of national policy for addressing the national energy shortage. In parts of Mitake in Gifu Prefecture, there are abandoned lignite mines in more than 80 % of the total area of the central urban district. The column method was used in Mitake; that is, portions of the lignite were left in place as columns to stabilize the mine. Figure 6.14 shows an example of a room-and-column mining cavity. These columns and ceilings can deteriorate if they are repeatedly subjected to dry conditions and then flooding from rainfall, and cave-in accidents are frequent. Figure 6.15 shows locations of cave-ins since 1959. An average of six cave-in failures have occurred annually, with nearly 250 in all. A particularly large cave-in occurred on October 20, 2010, as shown in Figs. 6.15 and 6.16. The cave-in area measured approximately 50×60 m, and caused

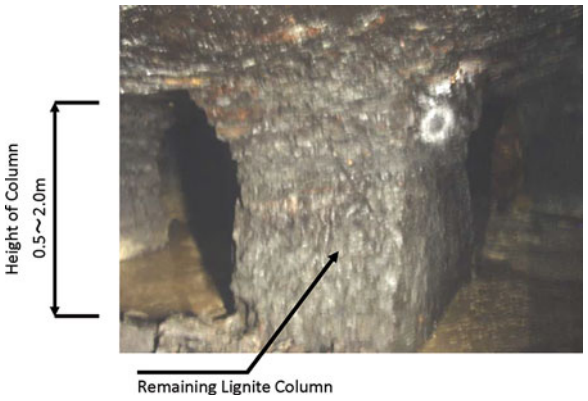

Fig. 6.14 Column in abandoned lignite mine (Mitake in Gifu Prefecture)

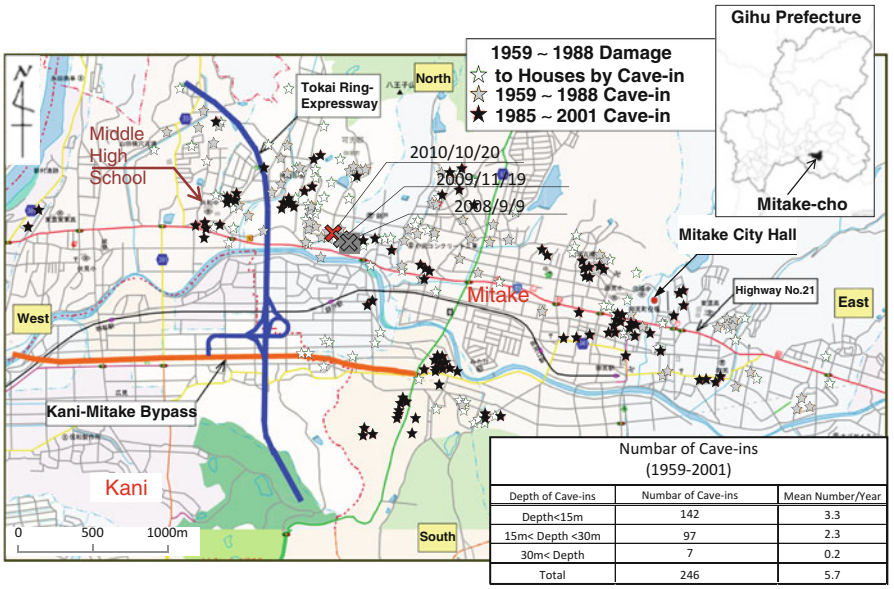

Depth of Cave-ins	Numbar of Cave-ins	Mean Number/Year
Depth<15m	142	3.3
15m< Depth <30m	97	2.3
30m< Depth	7	0.2
Total	246	5.7

Fig. 6.15 Cave-ins by abandoned lignite mine (since 1959)

destruction or partial destruction of six homes. Figure 6.16 shows a view of that cave-in. Large-scale cave-ins have occurred repeatedly over the past few years in Mitake. The reason appears to be that the columns and mine ceilings have deteriorated over the period of more than 60 years since the lignite mines were excavated.

At a Tokai earthquake committee of the CDMC in March 2002, the source area of the earthquake was revised on the basis of updated seismological information. The revised earthquake source area was slightly expanded and moved westward.

Fig. 6.16 Cave-in due to collapse of lignite mine

Revisions were thus made at the same time to the areas for intensified measures against Tokai earthquake, and the city of Nagoya and other locations were added to this list of areas for earthquake-resistance enhancement. The CDMC estimated that seismic intensity in the Mitake area would be from 5 to 6 (JMAI), so this area was not included in the aforementioned area.

However, with abandoned mines under the central part of the town, earthquake ground motion by the Tokai earthquake could collapse the lignite columns and ceilings of abandoned mines over a wide area, resulting in devastating loss of life and property as well as serious effects on the livelihoods of residents after the earthquake. Considering this situation, the author has performed a series of investigations concerning the risk level of abandoned lignite mines in Mitake, in relation to the Tokai earthquake. Because of the broad extent of lignite mines in the town, we surveyed the entire town for the presence of abandoned mines and effects of amplification of earthquake ground motion from such caves. The results of this study are being used in regional disaster management planning of the town.

Figure 6.17 is a map showing locations where lignite was mined in Mitake (an old map of lignite mine caves), from the archives of the Bureau of Mines of the former Ministry of International Trade and Industry. Lignite is classified into three layers at levels numbered from 2 to 4 in increasing order with depth, and the map is a planar representation of locations where there are now caves. This map does not show the depth of each cave. As shown in the figure, levels 2–4 of the three layers of lignite were mined.

To obtain information on depths of these caverns, 427 boring cores were collected within the town of Mitake and construction sites of the Tokai Ring Expressway and Kani-Mitake Bypass, as shown in Fig. 6.17. Based on boring surveys, it was found that the lignite layers are inclined from north to south, with lignite deposits to the north having shallower depths from the surface.

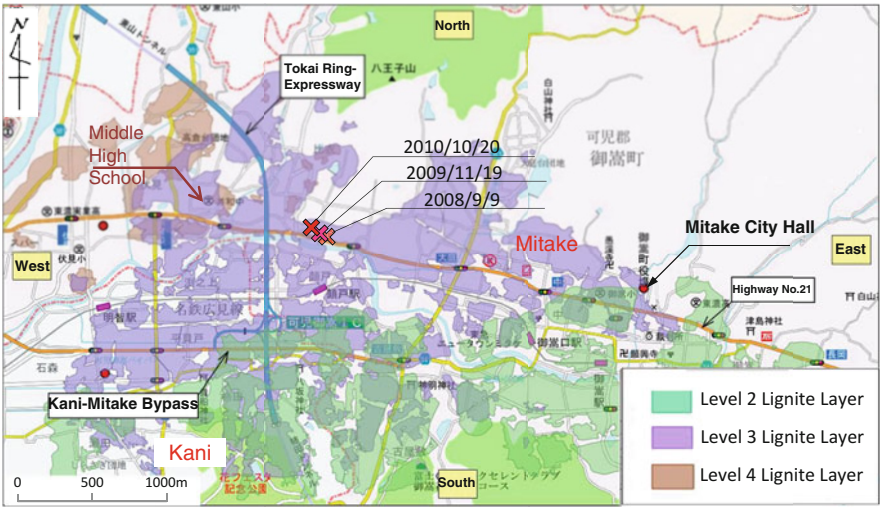

Fig. 6.17 Planar locations of abandoned lignite mine

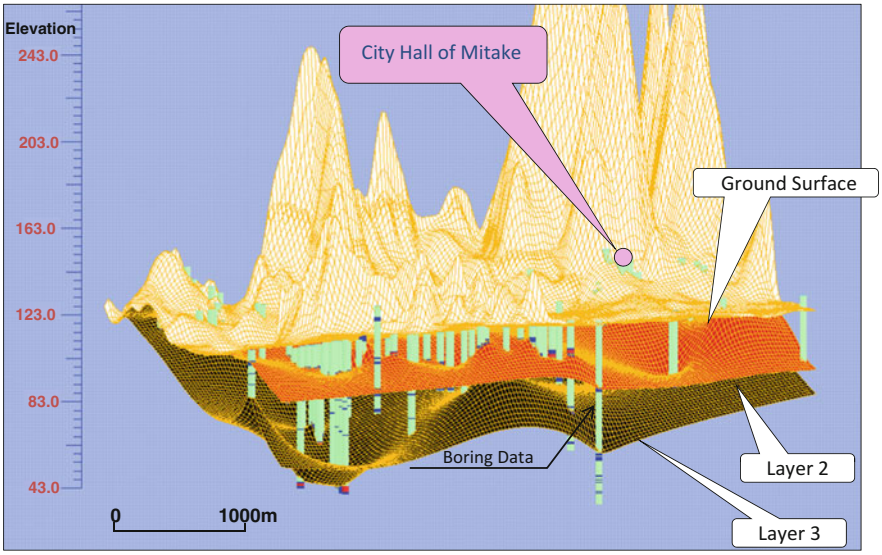

Fig. 6.18 Three-dimensional distribution of the lignite mine

Using information on the planar locations and depths of lignite deposits based on the boring data, the three-dimensional distribution of lignite layers was determined throughout the urban area of Mitake via three-dimensional interpolation. The results are shown in Fig. 6.18. By combining this with information from the old map of lignite mine caves mentioned above, a map with the horizontal distribution

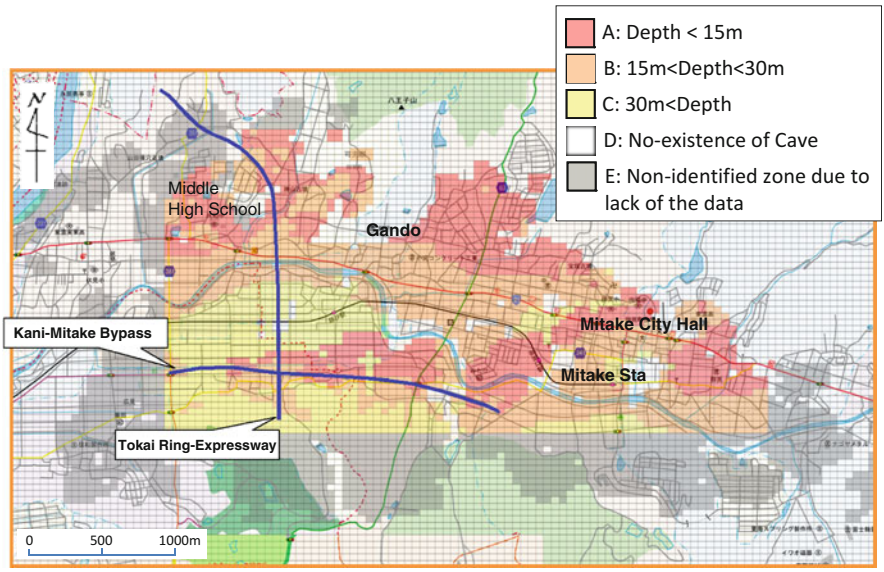

Fig. 6.19 Horizontal distribution and depth of abandoned lignite mine caves

and the depth of the abandoned lignite caves was drawn using a 50 m square mesh, as shown in Fig. 6.19. Caves are at depths 5 m to more than 30 m from the surface over a wide area, which encloses many public facilities such as the town office, public hall, and elementary and high schools.

In the event of the Tokai earthquake, there is concern that buildings and lifeline facilities in Mitake could be severely damaged by cave-ins from the collapse of lignite caves throughout the town. Therefore, studies were done on seismic intensity in the town from the Tokai earthquake and possible cave collapse.

Figure 6.20 shows a prediction of seismic intensity based on an earthquake source model for simultaneous occurrence of the Tokai and Tonankai earthquakes, which was issued by the CDMC in 2002. According to predictions, seismic intensity in JMAI would be from 5 higher (5+) to 6 lower (6−) if there were no underground caves, but the presence of these caves would increase seismic intensity to 6 larger (6+) over an expanded area.

There are underground caves all over Japan and the world, including abandoned coal mines, abandoned stone excavation caverns and air raid shelters, in addition to abandoned lignite mines. For the sake of earthquake disaster mitigation, it is important to assess the situation of these underground caves and take necessary precautions.

In addition to direct methods that use boring to probe for the presence of caves, there are also indirect methods that can be performed from the ground surface to determine cave presence and depth. Proposed indirect methods include geological radar, artificial vibration source, acoustic prospecting, and gravity change measurement. However, no definitive method has been found.

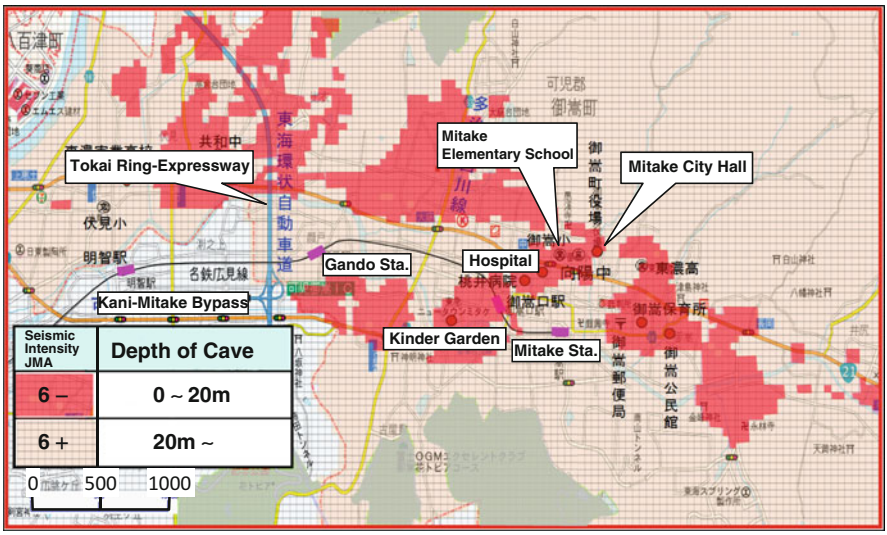

Fig. 6.20 Predicted seismic intensity (JMA intensity)

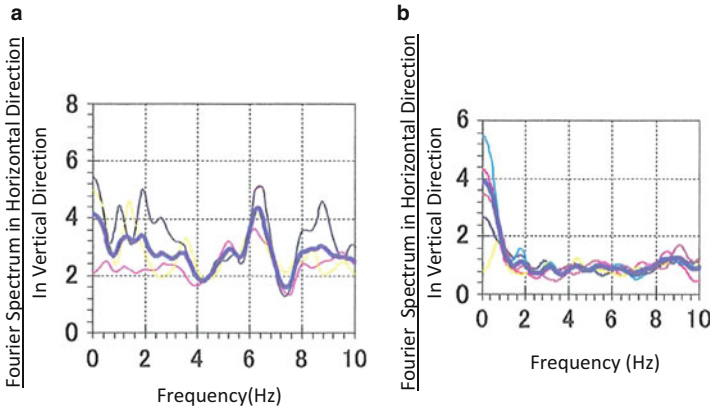

Fig. 6.21 Influence of cave on micro-tremour at the ground surface. (**a**) Cave presence. (**b**) Cave absence

For estimating presence and depth of underground caves over a wide area, from the standpoint of cost and time, it is desirable to conduct investigations from the ground surface. The potential of using micro-tremor observations from the surface is being studied.

Micro-tremor observations were conducted at about 30 locations in Mitake, where boring data and other documents have been used to determine cave presence and depth. Figure 6.21 shows examples of micro-tremor spectra at locations of cave presence or absence. The vertical axis in the figure indicates the ratio of horizontal to vertical tremor spectra, and the horizontal axis indicates frequency. This shows

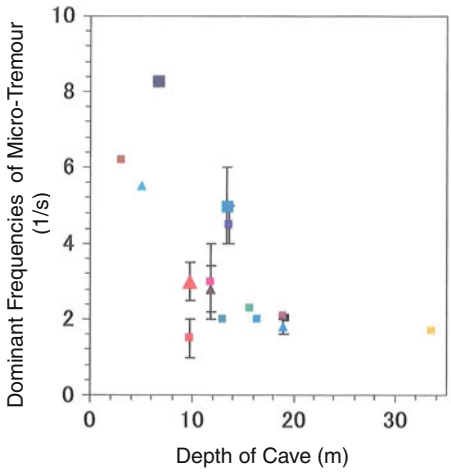

Fig. 6.22 Relationship between dominant frequencies of micro-tremour and depth of cave

that at places where caves exist, there are clear peaks of spectra ratio between 4 and 7 Hz. In contrast, the spectra are basically flat at locations of cave absence, with no dominant period. The reason for emergence of a dominant period at cave locations is that rock and earth above the lignite columns are supported by those columns, forming a vibration system.

Figure 6.22 shows the relationship between the dominant period of the micro-tremor and cavern depth, which was confirmed by borings. When a cavern is present, the trend is that the deeper the cavern, the shorter the dominant frequency; that is, the dominant period lengthens. The apparent reason is that with a deeper cave, there is increased mass of rock and earth above the columns, so mass of the vibration system is greater. However, with cave depth from 10 to 20 m, the dominant frequency scattered, and the relationship between cave depth and dominant frequency is somewhat unclear. Further study is needed, including what types of wave motions produce micro-tremors within ground where cave exist. In any event, the findings here show that micro-tremor observation is a potentially promising method of surveying underground caves.

6.4 Natural Disaster Mitigation

6.4.1 Global Increase of Natural Disasters

In addition to earthquake disasters, there has been an increase of wind and flood disasters by large storms and heavy rains, which are considered related to climate change on a global scale. Figure 6.23 shows the number of wind and flood disasters

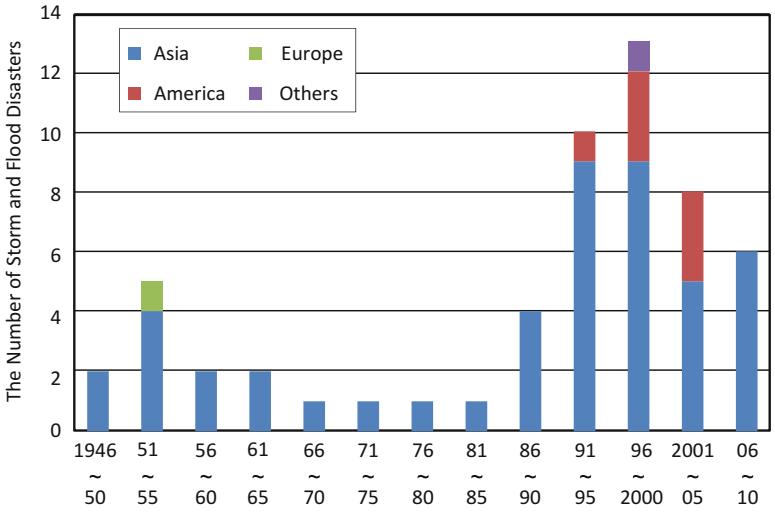

Fig. 6.23 Storm and flood disasters in the world (with more than 1,000 causalities by large storms and heavy rains)

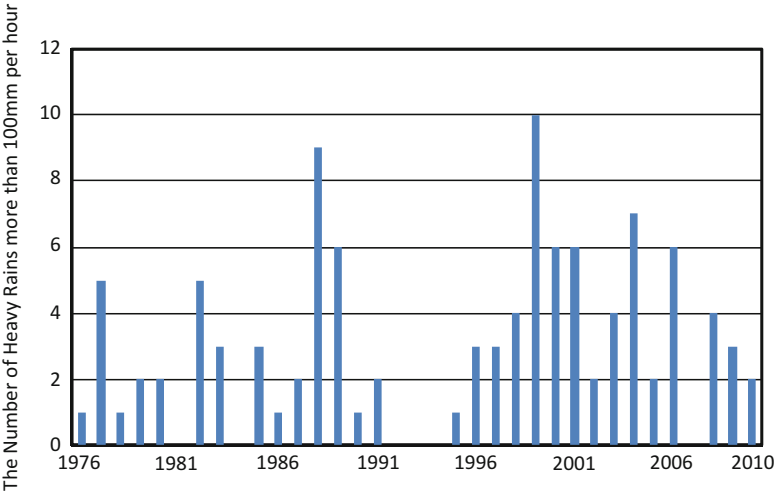

Fig. 6.24 Heavy rains with more 100 mm per hour in Japan (Japan Metrological Agency)

causing more than 1,000 fatalities and missing persons in each 5-year period over the past 65 years. Clearly, there has been a rapid increase in the number of wind and flood disasters over the past quarter century. Most of these disasters have concentrated in Asia.

Figure 6.24 shows the number of heavy rains with more than 100 mm per hour in Japan. Such events, which are also called anomalous heavy downpours, have increased in recent years.

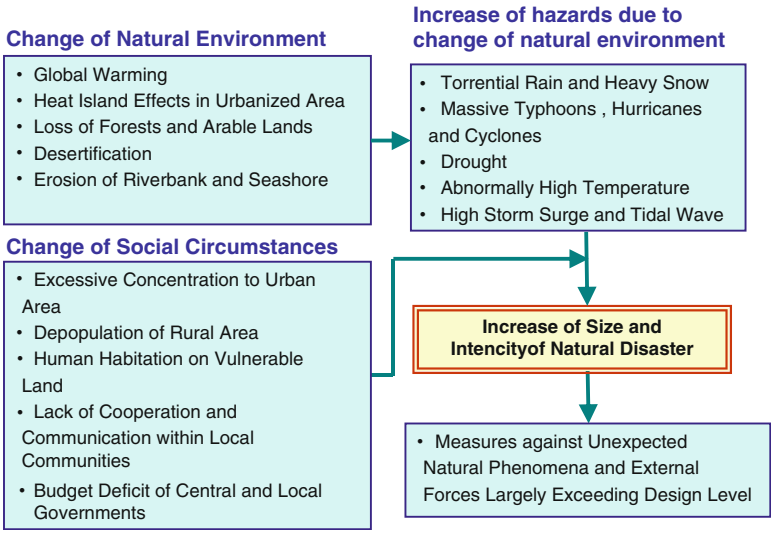

Fig. 6.25 Increase of natural hazards due to changes of natural environment and social circumstances

The reasons for more frequent natural disasters, including earthquakes, are believed to be from changes in the natural environment on a global scale and society's increasing vulnerability to disasters (Fig. 6.25). The natural environment is changing rapidly, including global warming, heat island effects in urbanized areas, loss of forests and arable land, desertification, and erosion of riverbanks and seacoasts. These changes are believed to be a contributing factor to torrential rains, heavy snowfall, massive typhoons, hurricanes, and cyclones, as well as droughts and abnormally high temperatures. Rises in sea level from climate change are also heightening risks of storm surge and tidal wave disasters. These trends are expected to become even more pronounced in the future.

Vulnerability to natural disasters is also increasing as a result of changes in social structures and land use, including dwindling birthrates, aging societies, increasing concentration of population in urban regions, and depopulation of rural areas. Other factors that increase vulnerability to disasters include a decline in cooperation within local communities, failure to fully transfer past disaster experiences to the younger generation, and a lifestyle that is increasingly separated from nature and overly reliant on technology. There is also concern that the worsening finances of national and regional governmental organizations may delay efforts to build disaster prevention infrastructure. In addition, decline of the regional construction industry is casting a shadow over regional disaster preparedness. Regional construction companies and their employees have made important contributions to disaster prevention and emergency activities following disasters, but the number and size of such companies have continued to decline yearly from significant contraction of the construction industry. In developing Asian nations, poverty magnifies the effects of disasters and those disasters worsen poverty, forming a vicious cycle.

There is concern regarding the strong potential for a massive earthquake caused by changes in crustal stress conditions from the Tohoku earthquake, as well as an increasing external load of rainfall from changes in the natural environment. Coupled with weakened social structures, this could result in an enormous disaster. The issue is how to reduce disaster severity regarding natural phenomena that is greater than anticipated levels and external loads that greatly exceed design standards. The 2011 Tohoku earthquake was an alert that measures based on disaster prevention infrastructure and other "hardware" alone cannot adequately mitigate natural disasters. It is important to use a combination of hardware and software measures to reduce the extent of disasters with very low frequency of occurrence but serious damage.

6.4.2 Development of Anti-Tsunami Science and Engineering Plus Promotion of Tsunami Measures

The term "earthquake engineering" has been in use for many years. This is the academic field that deals with the design and construction of safe infrastructure for earthquake motion. In addition, anti-tsunami science and engineering should be developed and, based on research from this field, tsunami measures should be promoted.

The goal of tsunami science has been to study the mechanisms of tsunami occurrence and wave propagation and to predict sea level rise along coastlines and tsunami arrival times. In contrast, the important purpose of anti-tsunami engineering hereafter is to design and construct infrastructure that can withstand tsunamis and urban planning that minimizes the loss of human life.

This concept was suggested based on the investigation of damage to buildings, bridges, and other structures after the 2004 Sumatra and 2011 Tohoku earthquake and tsunami events. As shown in Fig. 1.95 (Sect. 1.3.9 on the Tohoku earthquake), the tsunami was as high as a five-story reinforced concrete apartment building near the coast in Rikuzen-Takata. The tsunami flowed through the entire building but caused no structural damage to it or its concrete foundation piles. Furthermore, as shown in Fig. 1.35 (Sect. 1.2.5 on the Sumatra offshore earthquake and tsunami), a mosque along the coastline in Banda Aceh was structurally unharmed even though the tsunami passed through the prayer hall on its first floor.

In addition, as shown in Fig. 1.96, the tsunami reached the top of a concrete road viaduct constructed on the coastline in Kamaishi, but there was no damage to the concrete pier. The same was reported for a concrete bridge in Banda Aceh.

These cases indicate that it is possible to build structures that can fully withstand a tsunami. The following are the main topics of anti-tsunami science and of engineering and promotion of anti-tsunami measures.

(i) Geological survey of worldwide tsunami traces: One reason for the failure to predict the tsunami of the Tohoku earthquake is an excessive emphasis on written documents in the prediction of earthquakes and tsunamis. In Japan and

the world, there is a need to study the accretion history of sediment deposited by tsunamis that have occurred repeatedly on the order of a thousand to several thousand years, by boring surveys and observation of outcrops.

(ii) Construction of tsunami-resistant infrastructure and buildings: As mentioned above, many buildings and infrastructure survived from the tsunami of the Tohoku earthquake. It is important to develop an appropriate methodology for evaluation of tsunami forces and to apply it to design and construction of anti-tsunami infrastructure.

(iii) Tsunami-resistant urban planning: There is a need for simulations to predict tsunami wave run-up onto land and for promotion of tsunami-resistant urban planning on that basis. This can contribute to residential area selection, street design, locations of artificial hills for emergent evacuation, and construction of evacuation shelters.

(iv) Construction of tsunami-resistant lifeline systems and early restoration: The tsunami of the Tohoku earthquake severely damaged sewage facilities and many other lifeline systems. It is important to promote measures that allow such systems to maintain their function against tsunami wave forces, collisions with drifting objects, and inundation.

(v) Information collection and transmission systems for early detection of wide-area disasters: In a disaster affecting wide area such as the Tohoku earthquake, a system to collect and transmit damage information is extremely important for rescue operations, emergency response and immediate recovery activities, and it is necessary to rebuild the information collection and transmission systems.

(vi) Enhancement of disaster education and training: In the Tohoku earthquake, the lives of many children were saved by disaster education. As shown in Table 1.4, the death rate of children in Kamaishi and Kesennuma was 1/10 less than that of the general population. This is an example of disaster education that was highly effective in saving lives. It is necessary to verify the effects of disaster education and study approaches for future disaster education and training.

To develop anti-tsunami science and engineering and to promote tsunami measures as described above, it is essential to have multidisciplinary cooperation that involves not only earth science and engineering, but also the fields of social science, information science and medical science. This is elaborated in Sect. 6.4.6 on multidisciplinary cooperation for natural disaster mitigation.

6.4.3 Japanese Disaster Prevention Systems and Organizations

Figure 6.26 shows the disaster prevention system and organization in Japan. The Disaster Countermeasures Basic Act of 1962 specifies this system and organization, as well as the roles of each agency in case of disaster. This law specifies that the role

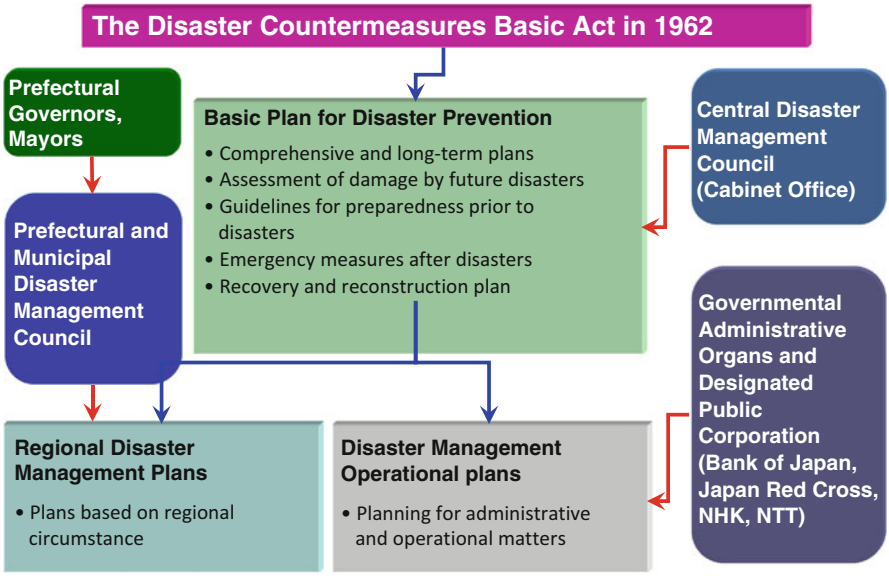

Fig. 6.26 Natural disaster prevention system and organization in Japan

of the national government is to organize the CDMC and develop the *Basic Plan for Disaster Prevention*, as follows:

(i) Comprehensive and long-term national disaster prevention plan
(ii) Assessment of damage by future disasters
(iii) Guidelines for preparedness prior to disasters
(iv) Emergency response after disasters
(v) Recovery and reconstruction plan

Prefectural governors and mayors organize prefectural and municipal disaster management councils, and these councils are in charge of developing regional disaster management plans. Governmental administrative organs and designated public corporation, such as the Bank of Japan, Japan Red Cross, Japan Broadcasting Corporation (NHK), Nippon Telegraph and Telephone (NTT) are required to prepare disaster management operational plans including emergency response procedures, in accordance with the *Basic Plan for Disaster Prevention*.

Figure 6.27 shows the framework of the government's emergency response after a disaster. When a large-scale disaster occurs, the Cabinet Office collects information from the JMA, local government offices and agencies, media organizations and others, and ascertains the scope of damage, reports its findings to the Prime Minister, and consults with the liaison conference of concerned ministries and agencies. In response, a Headquarters for Major Disaster Countermeasures is established under the leadership of the Prime Minister. A government investigation team is dispatched to the affected area, and an onsite disaster management headquarters is established in the affected prefecture or municipality.

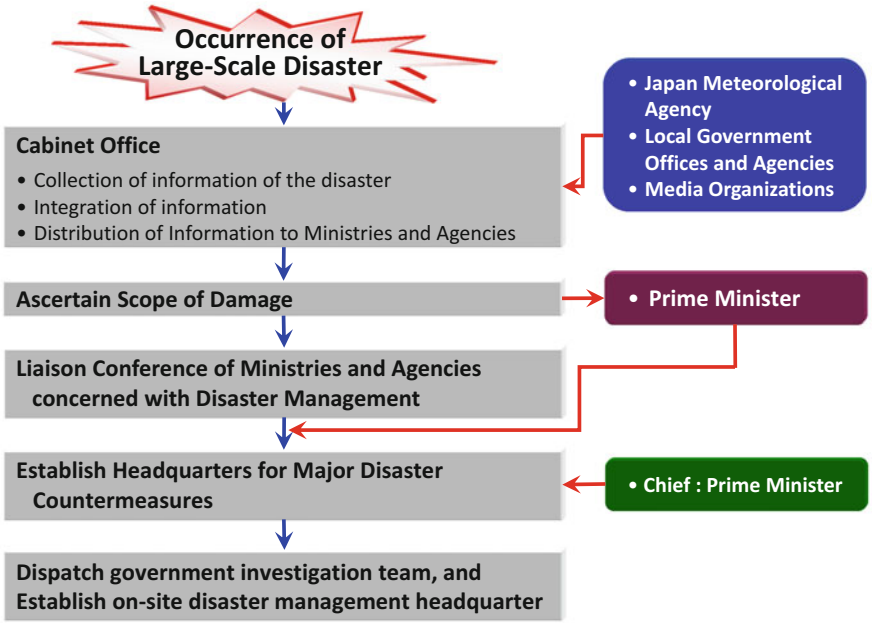

Fig. 6.27 Government emergency response against disaster

6.4.4 Earthquake Disaster Mitigation Strategies of the National Government

The government of Japan has developed and issued disaster mitigation strategies regarding future earthquakes that are believed imminent, including a northern Tokyo Bay earthquake and massive earthquakes along the Nankai Sea Trough. For example, in reference [7] issued in April 2006 (Fig. 6.28), the disaster reduction goals are to reduce the loss of human life by half and economic losses by approximately 40 % within the next 10 years. This means reducing the number of fatalities by the northern Tokyo Bay earthquake from an estimated 11,000 to approximately 5,600 lives, and reducing economic losses, including indirect ones, from an estimated 112 trillion yen to 70 trillion yen. In the northern Tokyo Bay earthquake, collapsed buildings and fires would be the cause of practically all fatalities. Therefore, the most important step is seismic retrofitting of homes and buildings with low earthquake- resistance. There are about 47 million homes and buildings in Japan and about 25 % of the total number, approximately 12 million, do not satisfy current earthquake-resistance standards. The government's goal is to reduce the proportion of existing noncompliant homes and buildings from 25 % to 10 % over a 10-year period. Seven years have already elapsed since the government announced its strategies in April 2006, and the seismic reinforcement of older and single-family homes has not been proceeding as planned.

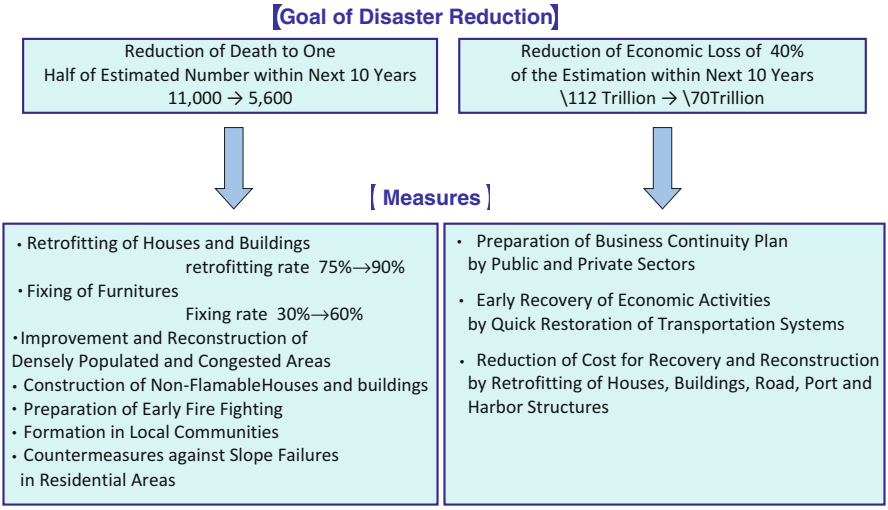

Fig. 6.28 Strategies for disaster mitigation against the Northern Tokyo Bay earthquake (Central Disaster Management Council, 2006)

Although some regional governments have programs that offer loans for seismic reinforcement of homes at very low interest rates, few residents take advantage of these programs. One reason is that most homes with inadequate earthquake-resistance are older, and their inhabitants tend to be elderly persons. With the declining birthrate, aging population and trend toward nuclear family households, the tendency is for one elderly person or couple to be living in an older home with low earthquake resistance. This is an example of how social changes such as these demographic trends can increase vulnerability to future disasters. After the Kobe earthquake, public funds were used for seismic reinforcement of public infrastructure such as roads, harbors, and schools. Japan Rail, Nippon Expressway Company, and electric power companies conducted seismic reinforcement with financial backing, but little progress has been made in improving earthquake resistance of individually owned homes and private buildings. To maintain overall regional disaster resistance, it is important to provide institutional means such as raising the subsidy rate of public support for seismic reinforcement of private homes that face routes and roads used for emergency transportation after a disaster.

6.4.5 Recommendations from the Science Council of Japan for Natural Disaster Mitigation [8]

In light of the frequent worldwide occurrence of natural disasters in recent years, in February 2006 the Science Council of Japan (SCJ) established the Committee on Creation of Safe and Secure Society against the Global Increase of Natural Disasters. This is an issue-specific committee, consisting of practitioners and researchers

in various fields including science, engineering, life sciences, and the humanities. This committee issued the following 13 recommendations to the Japanese government for mitigation of future natural disasters, based on the latest available information and scientific knowledge regarding natural disasters.

6.4.5.1 Recommendations for Policies and Measures to Reduce Damage from Natural Disasters

(i) Paradigm shift for creation of a safe and secure society: Because the natural environment is changing and vulnerability is increasing in land utilization and social systems, the government should pursue a paradigm shift in policies for natural disaster mitigation, away from a short-term perspective that stresses economic growth and toward creation of a safe and secure society as the highest priority.

(ii) Development of a suitable level of infrastructure: Tax revenues should be suitably allocated over the long term to develop infrastructure for natural disaster mitigation. In determining an appropriate level of infrastructure development, evaluation should include not only loss of life and property but also negative effects on national capabilities, landscapes and culture, as well as human psychological trauma.

(iii) Adjustment of national land utilization: Utilization of national land must be better balanced from a long-term perspective to reduce damage from future natural disasters. This will require dispersion of risk through decentralization of population and assets, more appropriate land use, and suitable residence selection by residents. There should be consideration of the risks of disaster-vulnerable areas in light of future population decline, establishment of backup systems for political and economic functions, and developing transportation networks for recovery and reconstruction activities.

(iv) Combining hardware and software measures: It is necessary to pursue software measures such as disaster education, information transfer of past disaster experiences, development of systems for evacuation, emergency response, recovery and reconstruction, improvement of disaster information systems, and strengthening emergency medical systems. At the same time, it is important to promote hardware measures such as construction of disaster prevention infrastructure to reduce damage from large-scale natural disasters. In addition, for earlier recovery, it is important to perform studies and take action in advance to create facilities that will reduce the scope and extent of damage and facilitate reconstruction.

(v) Assessment and recognition of vulnerability in depopulated and isolated areas: On isolated islands and in coastal zones and mountainous areas, where disaster response capabilities have declined because of depopulation, there is a need to assess disaster vulnerability and develop emergency relief and rescue systems.

(vi) Policy integration among national and regional government agencies: Integrated natural disaster mitigation policies should be established and implemented in close cooperation with all related government ministries and agencies, based on clearly defined roles. Regional governments should establish disaster management organizations, systems and measures, while cooperating with other regional government organizations in relation to natural disasters. The national government should support disaster prevention efforts of regional governments, including financial assistance, and should take the leading role when a disaster causes catastrophic losses over a wide area.

(vii) Development of disaster awareness among the general public: Detailed hazard maps should be provided in a form that is readily accessible to the public to improve the availability of hazard information. To promote the development of proper disaster awareness among the general public, the government should evaluate the effects on natural disaster vulnerability of factors such as the declining birthrate and aging population, trend toward nuclear family households, excessive reliance on technology, and social and economic internationalization. The government should make this information widely available to educate the public in disaster awareness, with the goal of improving the "disaster resistance of society", based on cooperation and collaboration with citizens and regional organizations.

(viii) Improving basic education on disaster management: Basic education on disaster management should be improved, including curriculum changes in areas such as geology and geography, to help students develop basic knowledge of the mechanisms of natural disaster occurrence and an understanding of natural phenomena and disaster predictions.

(ix) Promotion and support of non-profit organizations (NPOs) and non-governmental organizations (NGOs): NPOs and NGOs have an important role to play regarding mutual aid within local communities in popular movements, toward reducing damage from natural disasters through public works, community collaboration and individual efforts. Such activities include disaster education, transfer of disaster experiences, and emergency response activities. National and regional government organizations should promote the development of suitable NPOs and NGOs and actively support their activities.

6.4.5.2 Recommendations on the Promotion of Research and Surveys

(i) Improvement of monitoring systems to predict disaster-related natural phenomena: Observation and monitoring systems should be continuously enhanced for the prediction of natural phenomena related to disasters, such as earthquakes, tsunamis, volcanic eruptions, typhoons, local downpours, and floods. Basic research in this area should also be promoted. In addition, the impacts and characteristics of large-scale, low-frequency disasters that may

occur once in several hundreds or thousands of years should be studied by geological surveys and other types of research.

(ii) Improved modeling for natural disaster prediction and recognition of uncertainty: Worldwide satellite monitoring and computer simulations should be continuously implemented and studied to improve the accuracy of predictions. It is important to distinguish the differences between signals of natural environmental variability and changes from human activities with respect to climate change and global warming. At the same time, scientific uncertainties should be identified and taken into account in disaster prevention measures.

(iii) Research and development to improve disaster resistance in land use and social structures: Public and private research institutes and universities should collaborate to conduct research and surveys on methods to overcome disaster vulnerabilities in land use and social structures, as well as on social systems for disaster mitigation. These endeavors should be based on a comprehensive and integrated approach. The government should provide organizational, administrative, and financial support for such efforts.

(iv) Communicating information on research and survey findings and developing human resources: Public and private research institutes and universities should communicate results of their research and development related to natural disaster mitigation to the public and related organizations in an understandable form. These organizations should promote the development of human resources to reduce damage from natural disasters, both within Japan and internationally.

6.4.6 Multidisciplinary Cooperation for Natural Disaster Mitigation

It is clear that multidisciplinary cooperation is indispensable in preparedness for large-scale future disasters, including mega earthquakes along the Nankai Sea Trough and a northern Tokyo Bay earthquake. As shown in Fig. 6.29, cooperation is needed among fields including the cultural and social sciences, informatics and medicine, in addition to science and engineering. Within the field of engineering, natural disaster preparedness must involve nuclear, petroleum and chemical engineering as well as the areas of civil engineering and architecture. The cultural and social sciences should analyze the effects of disasters on people and societies and study ways in which social systems can mitigate risks. Meanwhile, the role of informatics should be to investigate how to properly and quickly collect disaster information, based on the development of advanced information technologies.

The CDMC estimates that more than 200,000 people would be injured in a northern Tokyo Bay earthquake. Communities will be faced with the task of providing relief and medical care for large numbers of displaced and injured people.

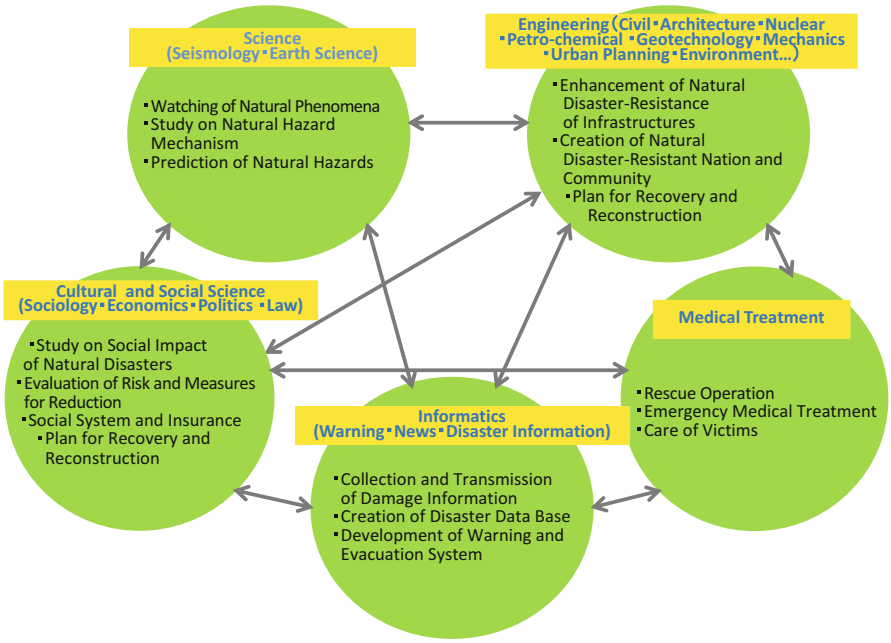

Fig. 6.29 Multidisciplinary joint action for natural disaster mitigation

Universities and other educational institutions will have an important role in their communities. In addition to ensuring the safety of their own students and staffs during a disaster, they will need to find ways to contribute to local relief and rescue activities.

To promote multidisciplinary cooperation for disaster management after the Tohoku earthquake, the SCJ Civil Engineering and Architecture Committee called on 20 academic societies related to natural disasters, and formed the Joint Conference of Academic and Engineering Societies for a Comprehensive Response to the Great East Japan Earthquake and Tsunami Disaster. As of December 2011, 24 academic societies are participating in this committee, representing a wide range of fields from science and engineering to economics and agriculture, forestry, and fisheries. These societies are, in alphabetical order:

Architectural Institute of Japan; Association for Children's Environment; Atomic Energy Society of Japan; City Planning Institute of Japan; Geographic Information Systems Association of Japan; Institute of Electrical Engineers of Japan; Institute of Social Safety Science; Japan Association for Earthquake Engineering; Japan Association for Regional Economic Studies; Japan Concrete Institute; Japan Society for Disaster Information Studies; Japan Society for Natural Disaster Science; Japan Society of Civil Engineers; Japan Society of Engineering Geology; Japan Society of Material Cycles and Waste Management; Japan Society of Mechanical Engineers;

Japan Society on Water Environment; Japanese Geotechnical Society; Japanese Institute of Landscape Architecture; Japanese Society of Fisheries Science; Japanese Society of Irrigation, Drainage and Rural Engineering; Seismological Society of Japan; Society of Environmental Instrumentation, Control and Automation; and Society of Heating, Air Conditioning and Sanitary Engineers of Japan.

This committee has two primary roles. One is to develop a comprehensive, multidisciplinary overview and understanding of the overall damage of the Tohoku earthquake, and the other is to identify and cooperatively address issues requiring multidisciplinary efforts to reduce future damage from natural disasters. It has long been realized that a multidisciplinary approach is indispensable for disaster mitigation, but barriers separating academic fields and professional associations prevented this from becoming a reality. It is hoped that this joint conference organized by SCJ will succeed in facilitating the multidisciplinary approach by taking a central role in research and surveys for disaster prevention in Japan.

The joint conference has issued the following basic policy recommendations on protecting people and property from massive earthquakes and tsunamis.

Basic policy: The basic policy of Japan for future earthquake and tsunami measures shall be to prevent large numbers of fatalities and extreme difficulty for its people in the event of major earthquake and tsunami disasters like the 2011 Tohoku earthquake.

The committee also recommended the following as measures to reduce damage from future natural disasters.

6.4.6.1 Emergency Measures After Disasters

(i) Establishing means of collecting, communicating and transmitting information for early determination of disaster situations, and creating mechanisms for use of various types of information including geospatial data
(ii) Improving wide-area stockpiles and transportation systems to supply food, water and medical supplies for emergency response
(iii) Establishing wide-area systems for the protection and support of disaster victims

6.4.6.2 Recovery and Reconstruction

(i) Minimizing loss of functionality and ensuring rapid restoration of lifeline systems (roads, railways, electric power, water supply and sewage services, waste disposal, gas, and telecommunications)
(ii) Developing wide-area support systems for regional recovery and restoration
(iii) Measures to restore industry, including recovery and restoration of agriculture, forestry, and fisheries

6.4.6.3 National and Urban Planning for Earthquake and Tsunami Resistance

(i) Construction and functional enhancement of disaster prevention infrastructures
(ii) Urban planning for tsunami resistance with consideration for local characteristics (enhancement of tsunami monitoring systems, construction of tsunami evacuation facilities, selection of residential areas, tsunami-resistant urban design, and others)
(iii) Improving capabilities of large cities for restoration and recovery
(iv) Developing support systems for the cooperation of diverse experts with regional and municipal governments

Research, surveys, and education

(i) Cooperation among academic and engineering societies in addressing multidisciplinary issues
(ii) Developing comprehensive understanding of the Tohoku earthquake and transferring this knowledge to the next generation
(iii) Promoting anti-tsunami science and engineering (evaluation of the characteristics of tsunami forces and construction of tsunami-resistant structures)
(iv) Promoting research on earthquake resistance of buildings, infrastructures, industrial facilities, and ground (including resistance to strong earthquake ground motions of long duration and long-period earthquake ground motions)
(v) Promoting disaster education, furthering the transfer of disaster experience, and improving evacuation drills
(vi) Support for formulation and implementation of business continuity plans for local organizations (government, businesses, schools, hospitals and others), as well as district continuity plans

6.5 International Cooperation in Disaster Prevention

6.5.1 Support for Disaster Prevention, Recovery and Restoration

The tsunami of the Tohoku earthquake and the accident at the Fukushima Daiichi Nuclear Power Plant had a severe impact on Japan, and it will take many years for the affected areas to recover and overcome the effects of the nuclear accident. Faced with natural disasters since ancient times, the Japanese people have worked ceaselessly to build safer communities, gaining a variety of knowledge and skills throughout history. Therefore, I am convinced that we will overcome this national crisis.

As shown in Fig. 1.4 (Sect. 1.1), statistical records since 1986 indicate that the world has experienced 60 natural disasters causing more than 1,000 fatalities over

Fig. 6.30 Damage to Muzoi bridge due to soil liquefaction (2005 Nias Island earthquake, Indonesia)

the past quarter century. The loss of life has been approximately 1.27 million. Along with the increasing vulnerability of human social structures to natural hazards such as massive storms and extreme weather events, which are believed related to global climate change, the extent of damage by disasters has been growing rapidly worldwide, especially in Asia. To build sustainable societies and create a safe, secure and peaceful world, not only scientists but all people must work together to mitigate natural disasters in a spirit of close cooperation and friendship. I believe that even the painful experiences of the Tohoku earthquake will prove useful for decrease of damage from natural disasters around the world, and Japan must take a leading role in the international community to mitigate these disasters. This will also help build international respect and a reputation for Japan, for its positive contributions around the world.

In the following, the support for recovery and restoration that has been provided by organizations such as the Japan Society of Civil Engineers (JSCE) and the NPO Engineers Without Borders Japan (EWBJ) is introduced, and the role that Japan should play in disaster mitigation around the world is discussed.

In Sect. 1.2.5, the damage by the Sumatra offshore earthquake and tsunami that struck off the coast of Sumatra, Indonesia on December 16, 2004 was described, as well as the technical support provided by the JSCE in rebuilding roads along the west coast of Sumatra. The following year, on March 28, 2005, a Mw = 8.6 earthquake struck again off Sumatra, causing damage mainly on Nias Island.

Nias is an island with a population of approximately 700,000 people, measuring about 150 km from north to south and 50 km from east to west. Significant damage occurred on Nias because part of the ruptured fault was directly under the island. The earthquake caused 847 deaths and 6,279 injuries and damaged buildings, bridges, slopes, port and harbor structures, and others. The piers of Muzoi Bridge in the northern part of the island were tilted and subsided owing to soil liquefaction, as shown in Fig. 6.30. Inclination and subsidence from soil liquefaction also affected many buildings in the capital of Gunung Sitoli, as shown in Fig. 6.31.

Fig. 6.31 Subsided and Inclined building due to soil liquefaction (2005 Nias Island earthquake, Indonesia)

Fig. 6.32 International technical assistance for restoration of buildings and bridges damaged by soil liquefaction. (**a**) Training of soil survey by Swedish cone penetration test. (**b**) Conference on restoration method of the damaged bridge

The JSCE dispatched a reconstruction support team for recovery of Nias Island. In close consultation with the local government, this team provided advice on bridge reconstruction methods. A large part of their technical assistance focused on liquefaction, including soil survey methods and techniques for estimation of liquefaction potential. The methods they recommended for this estimation were suitable for local conditions, ranging from the simplified method based on topography and soil conditions described in Sect. 3.2 to those using boring and cone penetration tests. In Fig. 6.32a, team members are showing local engineers how to use the Swedish cone penetration test apparatus that they brought from Japan. Figure 6.32b shows a joint meeting with local engineers to discuss how to restore the inclined and subsided bridge piers by liquefaction.

On May 12, 2008, there was a moment magnitude 7.9 earthquake in the central Longmenshan fault zone, which is at the boundary between the Sichuan Basin of inland China and the Tibetan Plateau. In the area near the epicenter, earthquake

Fig. 6.33 Damage to reinforced concrete building (2008 Wenchuan earthquake in Shichuan province, China)

ground motions were even stronger than those of the Kobe earthquake, damaging vast numbers of buildings and civil engineering structures. Because the earthquake was in a steep mountain region with weathered surface rock, there was large-scale slope sliding. Damage from the earthquake is summarized in Sect. 1.2.7 on the 2008 Wenchuan earthquake.

After this earthquake, I was a member of the Sichuan Earthquake Restoration Technical Assistance Liaison Committee, which was organized by eight Japanese academic and engineering societies that had been dispatched to China. The JSCE, Architectural Institute of Japan, Seismological Society of Japan, Japanese Geotechnical Society, Seismological Society of Japan, City Planning Institute of Japan, Geographic Information Systems Association of Japan, and Institute of Social Safety Science. Joint symposia were held with engineers of Sichuan Province concerning reconstruction methods, and specific ways to restore damaged structures such as bridges, buildings and tunnels were discussed.

Figure 6.33 shows a six-story apartment building in Dujiangyan that was damaged by the earthquake. Connections between columns and beams on the first floor were damaged, causing major deformation. In consultation with the local government, the team from the Japanese committee proposed several ways to reinforce the columns. Figure 6.34a illustrates a restoration method used in Japan for seismic retrofitting of buildings and bridges, involving use of steel plates to enclose damaged concrete columns. Figure 6.34b illustrates a method for restoration using earthquake-resistant shear walls that are constructed on the first-floor level, after correcting residual deformation of the building.

Figure 6.35a shows a concrete bridge of an expressway under construction linking Chengdu with Wenchuan, in the epicentral region. On the bridge over a reservoir, there was a simple girder of span length approximately 50 m. Bridge piers were about 100 m in height and the tops of the piers showed residual displacement of approximately 70 cm, suggesting that the piers had been damaged to some extent. Figure 6.35b shows a workshop with Chinese engineers regarding bridge pier damage assessment and reconstruction methods.

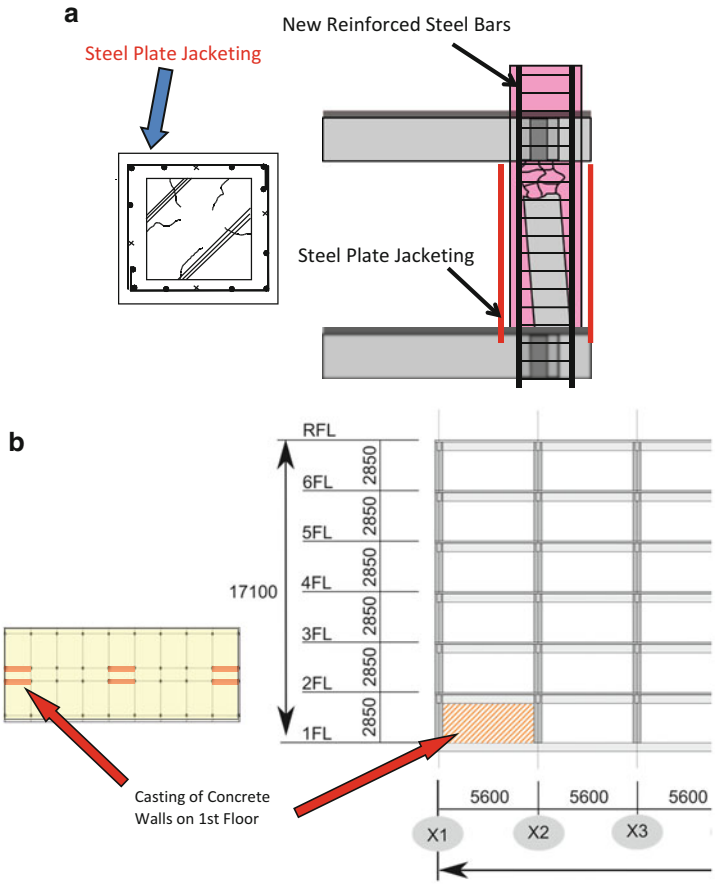

Fig. 6.34 Proposal of restoration methods for damaged concrete buildings. (**a**) Steel plate jacketing of concrete column. (**b**) Casting of earthquake-resistant concrete wall

Special lectures in seismology and earthquake engineering were prepared for engineers, junior faculty and graduate students in Sichuan Province (Fig. 6.36) by the Assistance Liaison Committee composed of Japanese academic and engineering societies, with support from the Japan Bank for International Cooperation. These lectures covered the following nine topics.

(i) Faults, earthquakes, and earthquake ground motion
(ii) Earthquake-resistant design and seismic reinforcement of buildings
(iii) Earthquake-resistant design and seismic reinforcement of civil engineering structures
(iv) Earthquake-resistant design and retrofittings of railway structures
(v) Earthquake-resistant design and retrofittings of road structures
(vi) Ground and slope stability during earthquakes

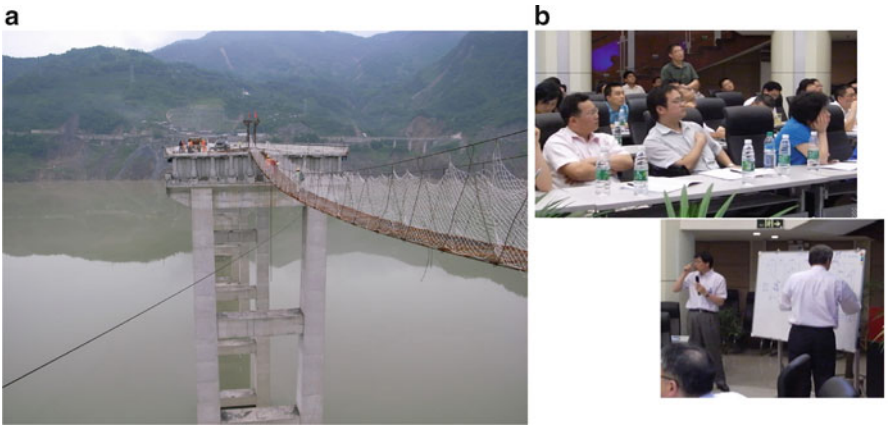

Fig. 6.35 Fall of a expressway bridge ginder (2008 Wenchuan earthquake in Shichuan province, China). (**a**) Falled span and scaffold work. (**b**) Conference for restoration of the damaged bridge

Fig. 6.36 Special lectures on seismology and earthquake engineering in Shichuan province, China

(vii) Social systems for natural disaster mitigation
(viii) Urban planning for disaster resistance
(ix) Utilization of geographic information systems for natural disaster mitigation

Following the earthquake, the Sichuan provincial government at Southwest Jiaotong University in Chengdu established the Sichuan Province Key Laboratory of Earthquake Engineering and Technology. The purpose of this laboratory is to study disaster recovery methods and ways to improve earthquake resistance of civil engineering and architectural structures. Consideration is given to the geographical, topographical and geological conditions of mountainous regions of western China, as well as to training of people and promotion of international exchange in the field of earthquake engineering. The Assistance Liaison Committee agreed to provide

Fig. 6.37 Subsided and inclined concrete building with five stories due to soil liquefaction (1990 Ruzon island earthquake, Phillippines, at Dugupan). (**a**) Damaged building. (**b**) Subsidence and inclination (Max. subsidence: 1.5 m,inclination 3°)

ongoing support for the research activities of this key laboratory. Joint studies have been planned regarding topics such as the following.

(i) Diagnosis and reinforcement techniques for buildings with low earthquake resistance in mountainous areas
(ii) Techniques for functional assessment and reinforcement of road transportation facilities in mountainous areas
(iii) Techniques for prevention of ground-failure disasters, such as slope failure and soil liquefaction
(iv) Techniques for mapping and monitoring of slopes using remote sensing

As described in Sect. 4.1.9, a magnitude 7.7 earthquake occurred in central Luzon, Philippines on July 16, 1990, causing damage by soil liquefaction and ground flow over a wide area in Dagupan. Liquefaction caused subsidence and inclination of a five-story reinforced concrete building of a private university along the banks of the Pantal River in Dagupan, as shown in Fig. 6.37. The building's maximum subsidence was approximately 1.5 m, and maximum inclination approximately 3°. About 1 month after the earthquake, the JSCE sent a team for an onsite investigation and technical cooperation. University officials had requested technical cooperation regarding building restoration methods. The JSCE sent 20 jacks from Japan and dispatched an engineer specializing in restoration of building inclination, and the building was restored. Local construction engineers

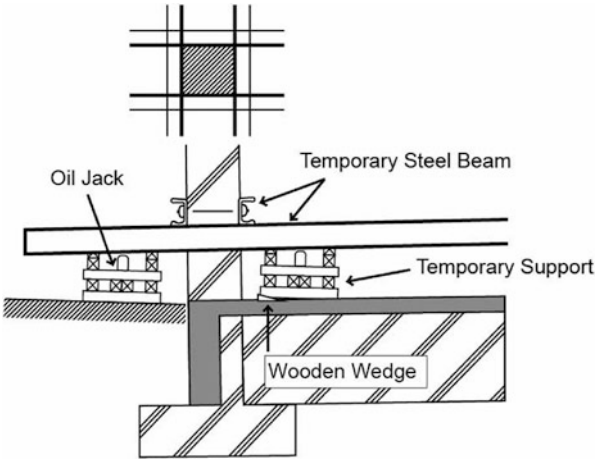

Fig. 6.38 Restoration method for the inclined concrete building

participated in this reconstruction project, ensuring the transfer of reconstruction technology.

Figure 6.38 illustrates the reconstruction method. The procedures were as follows.

(i) All concrete columns on the first floor were cut and detached, and temporary beams were installed on the cut columns to bear the reaction force of the jacks.
(ii) Thirty jacks were arranged between the first-floor foundation and the temporary beams, and these were used to lift the settled side.
(iii) In gaps created by jacking up the building, reinforcing bars were assembled and concrete was cast.

6.5.2 Engineers Without Borders, Japan [9]

After the 2004 Indian Ocean tsunami disaster, when I visited an orphanage in Banda Aceh in Sumatra, Indonesia, a little girl who had lost her family in the tsunami asked me, "Japan has experienced so many earthquake and tsunami disasters. Why didn't you teach us how to prepare for disasters before this even happened?" I could not answer her. This led to the establishment of EWBJ. Sadly, Japan then had the same kind of tragic experience in the Tohoku earthquake.

Both in Japan and internationally, earthquakes, storms, river flooding and other disasters are frequent, causing great loss of life and property and severe difficulties for residents of affected areas. EWBJ was founded as an organization of civil and architectural engineers, to provide technical assistance to people and regions affected by natural disasters such as earthquakes, storms and floods.

As shown in Fig. 6.39, EWBJ has a wide range of participation and support from the JSCE, the Architectural Institute of Japan, and other academic societies, public

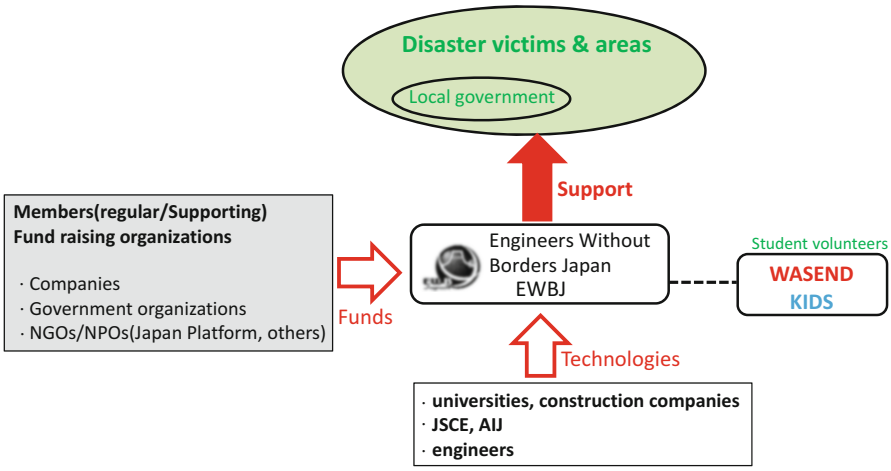

Fig. 6.39 Organization and activities of engineers without border, Japan

institutions and companies. Its basic philosophy is to contribute to the creation of a safe, secure, and peaceful world by engaging in a wide range of activities in close cooperation with other nongovernmental organizations. Activities include support for reconstruction and restoration of affected areas, technology transfer for natural disaster mitigation, and promotion of disaster education and international disaster prevention research.

EWBJ has continuously engaged in activities such as building shelters after the 2005 floods in Bangladesh, and the provision of technical assistance for a seismic isolation system in building construction in Padang, Sumatra. After the Tohoku earthquake, the organization became heavily involved in activities within Japan. It has dispatched senior engineers for recovery and restoration efforts under an agreement with the cities of Ofunato (Fig. 6.40) and Rikuzentakata. Each of these construction engineers is a senior engineer with substantial practical experience in the construction industry and related fields, and they have worked on projects including the planning of tsunami evacuation routes and reconstruction of elementary schools and fish markets. "The Waseda Student Organization for Education of Natural Disasters" was established under EWBJ in July 2005. Science and engineering students of Waseda University took the lead in forming this group, which provides disaster education services mainly for elementary and middle school students throughout Japan and in Indonesia (Fig. 6.41). Kyoto University has also formed a student group for disaster education, which has been active in promoting grassroots activities for disaster prevention among the younger generation.

With the Tohoku earthquake, Japan experienced the same kind of tragedy as the 2004 Indian Ocean tsunami. The accident at Fukushima Daiichi Nuclear Power Plant has raised serious questions concerning the safety of nuclear power generation in relation to earthquakes and tsunamis. Instead of slowing technical cooperation in

Fig. 6.40 Contract between Ofunato city and Engineers without Borders, Japan (*Right*: Mayer Mr. Toda, *Left*:author)

Fig. 6.41 Disaster education in Indonesia by Waseda student organization WASEND

the area of disaster prevention with other countries because of disasters in our own country, we must take even greater initiative in communicating the experience of the Tohoku earthquake and lessons learned from this disaster to the rest of the world.

6.5.3 Recommendations from the Science Council of Japan

International cooperation by Japan in the area of disaster prevention has been supported by funding and human resource assistance from public institutions including the Ministry of Foreign Affairs, the Ministry of Land, Infrastructure and Transport, and the Japan International Cooperation Agency; individual aid projects are also implemented by various private organizations including NPOs and NGOs.

In May 2010, the SCJ organized the Committee on International Cooperation for Natural Disaster Mitigation. This committee issued the following recommendations

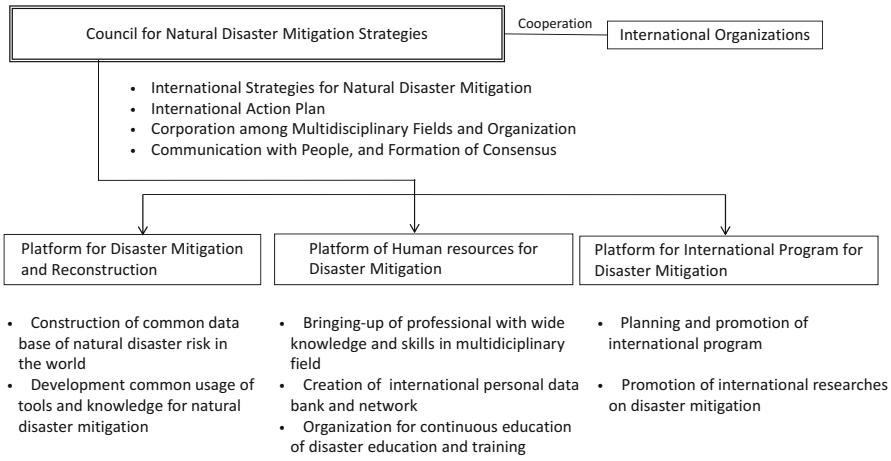

Fig. 6.42 Proposal of an organization for international natural disaster mitigation strategies

concerning basic strategies for international cooperation by Japan in the field of disaster prevention, the approach to providing technical cooperation and aid to affected areas, measures for training people, developing interpersonal networks for international cooperation, and directions for Japanese participation in international organizations and programs.

(i) Basic strategies for international cooperation: The primary goal of Japanese international cooperation is to contribute to worldwide natural disaster mitigation, and this should be pursued through collaboration between national and regional government organizations, industry groups, academia, NPOs, and others. A council on international disaster mitigation strategies should be established with participation by a wide range of agencies and groups involved in international cooperation in disaster prevention. This council should promote collaboration and integration among Japanese efforts toward international cooperation. Figure 6.42 shows the structure and main activities of the proposed council.

(ii) Cooperation for disaster prevention and aid to affected areas: A unified platform for disaster mitigation and reconstruction should be established with participation by government, academia, industry, and the private sector. The aim is to ensure coordination, continuity, and consistency in efforts toward natural disaster prevention, emergency relief after disasters, and recovery and restoration assistance. Steps should be taken to ensure that disaster prevention information is shared, and to clarify the roles of organizations and agencies. Therefore, the council proposed to establish a platform for disaster mitigation and reconstruction.

(iii) Human resource training and networking: One of the important objectives of Japan's international cooperation in the field of disaster prevention has been staff training, primarily at universities and research institutes.

To further promote such training within Japan and abroad, and to build an international human resource network for natural disaster mitigation, an integrated human resource training platform should be established.

(iv) Working with international programs: National and regional government organizations, universities, research institutes, industry groups, NPOs, and others should create an integrated platform for working with international programs, along with a central base for joint international research projects. The aim is to select international programs in which Japan should actively participate or take a leading role in the program operation.

References

1. Cabinet Office of the Japanese Government (2011) Disaster management in Japan
2. Committee on Huge Earthquake Models along The Nankai Trough, Cabinet office of Japan (2012) Seismic intensity and tsunami height by huge earthquakes along the Nankai trough (in Japanese)
3. Usami T (1975) Compendium of earthquakes in Japan and their caused damage (in Japanese)
4. Cabinet Office of the Japanese Government (2008) White note on natural disaster prevention (in Japanese)
5. Kaizuka S (1993) Geology and water of the Tokyo Bay (in Japanese)
6. Hamada M, Kida K, Iwadate T, Miwa S (2003) Study on danger of abandoned lignite mines in Mitake against the Tokai earthquake, Juuten No. 44 (in Japanese)
7. Cabinet office of Japan (2006) White note of disaster prevention (in Japanese)
8. Science Council of the Japan (2008) Proposals to the Japanese government on policies for the creation of a safe and secure society in the light of increasing natural disasters around the world
9. Non-profit organization, Engineers Without Borders Japan, protecting citizens, rehabilitating communities, rebuilding countries. http://www.ewb-japan.org/

Index

M. Hamada, *Engineering for Earthquake Disaster Mitigation*,
Springer Series in Geomechanics and Geoengineering,
DOI 10.1007/978-4-431-54892-8, © Springer Japan 2014